

NIST  
PUBLICATIONS

A11102 966626

NATL INST OF STANDARDS & TECH R.I.C.



A1102966626

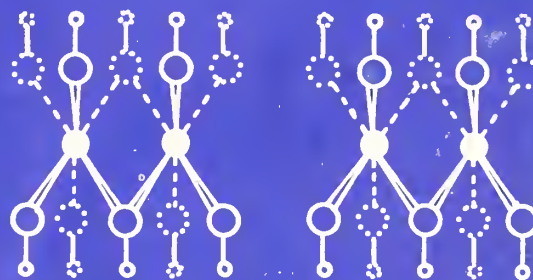
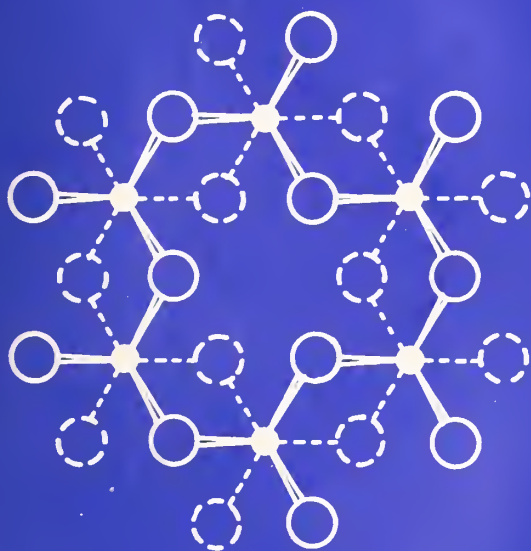
Gates, Richard S/Ceramic tribology : me  
QC100 .U57 NO.758 1988 V1988 C.2 NIST-PU

U.S. DEPARTMENT OF COMMERCE  
National Institute of Standards and Technology  
(formerly National Bureau of Standards)

*NIST Special Publication 758*

# *Ceramic Tribology: Methodology and Mechanisms of Alumina Wear*

*Richard S. Gates, Stephen M. Hsu, and E. Erwin Klaus*



QC  
100  
.U57  
#758  
1988  
C.2

**DOE ECUT Tribology Program**



NISTC 8C 100 .057 NO. 758 1208 5.2

***NIST Special Publication 758***

---

# ***Ceramic Tribology: Methodology and Mechanisms of Alumina Wear***

---

Richard S. Gates and Stephen M. Hsu

Ceramics Division  
Institute for Materials Science and Engineering  
National Institute of Standards and Technology  
(formerly National Bureau of Standards)  
Gaithersburg, MD 20899

E. Erwin Klaus

Department of Chemical Engineering  
The Pennsylvania State University  
University Park, PA 16802



**NOTE:** As of 23 August 1988, the National Bureau of Standards (NBS) became the National Institute of Standards and Technology (NIST) when President Reagan signed into law the Omnibus Trade and Competitiveness Act.

September 1988

U.S. Department of Commerce  
C. William Verity, Secretary

National Institute of Standards and Technology  
(formerly National Bureau of Standards)  
Ernest Ambler, Director

Research Information Center  
National Institute of Standards  
and Technology  
Gaithersburg, Maryland 20899

---

Library of Congress  
Catalog Card Number: 88-600582  
National Institute of Standards  
and Technology  
Special Publication 758  
229 pages (Sept. 1988)  
CODEN: XNBSAV

U.S. Government Printing Office  
Washington: 1988

For sale by the Superintendent  
of Documents,  
U.S. Government Printing Office,  
Washington, DC 20402



## FOREWORD

This report is born out of a cooperative effort between the Chemical Engineering Department, at the Pennsylvania State University (PSU), the Tribology Group of the National Bureau of Standards, and the partial support of the DOE ECUT Tribology Program. For years, the NBS has encouraged and sponsored graduate cooperative programs in which promising young scientists (some of them NBS staff members) come to NBS to conduct research, part of which often becomes the graduate's thesis. While it is not the objective of NBS to teach and train graduate students, such a program often furthers NBS programmatic goals by attracting high caliber scientists working on areas where NBS mission lies. Many excellent research papers have resulted and many students, upon graduation, have chosen to stay at NBS to continue their research careers. Such programs also draw many first rate university professors to NBS through the participation of these students in NBS research programs and projects, thus fostering NBS-university interactions and enhancing the scientific caliber of the work and reputation at NBS and the participating university. At the same time, through the frequent contacts that NBS has with industries, a natural university/government lab/industry relationship evolves, bringing a team focus on many research projects of significant economic and technological impact.

In 1984, primarily through the interactions of Dr. Stephen M. Hsu of NBS and Professors Elmer Klaus and Larry Duda of PSU, a cooperative program in Tribology was started. Three graduate students: Mr. Richard Gates ( a NBS staff member), Mr. Jeffrey Yellets, and Mr. Douglas Deckman were enrolled at the Chemical Engineering Department at PSU. Three reports have been prepared to describe the fruit of their relentless efforts in the last three years. These studies were conducted at NBS under the guidance of Dr. Stephen Hsu with the close participation of Prof. Elmer Klaus who visited NBS frequently.

Dr. James Eberhardt, Mrs. Terry Levinson, and Mr. David Mello of the DOE ECUT Tribology Program have at the same time sponsored a major Tribology program at NBS. That program also benefited from the studies conducted by Mr. Gates, Mr. Yellets, and Mr. Deckman. These students, while not working on sponsored projects directly, enabled NBS to explore some high risk, high pay off projects parallel to ECUT projects. When appropriate, the students were supported by ECUT for some time. To this, we gratefully acknowledge the generous support of DOE ECUT, without whose support many ideas would not be explored.

Stephen M. Hsu  
Chief, Ceramics Division



## ABSTRACT

This report describes a systematic study that has been conducted to develop methods for measuring the tribological properties of ceramic materials under concentrated contacts. Step-loading four-ball and ball-on-three-flat wear tests were developed to provide friction and wear characteristics of ceramic/lubricant combinations under various lubrication conditions. These measurement techniques now enable one to study the effect of different materials processing parameters, material microstructures, and different lubricants on the friction and wear performance of ceramics.

Water was found to react with alumina in a wearing contact to produce lubricous products. A combination of x-ray diffraction and thermogravimetric analysis techniques were used to investigate the kinetics of alumina-water reactions. These experiments determined that transition (gamma) alumina reacts with water at  $\approx 200^{\circ}\text{C}$  to form aluminum oxide hydroxide (boehmite -  $\text{AlO}(\text{OH})$ ), while reactions at  $\approx 100^{\circ}\text{C}$  produce aluminum trihydroxide (bayerite -  $\text{Al}(\text{OH})_3$ ). A mechanism for lubrication of alumina with water is proposed whereby stresses in the contact junction cause a phase transformation from alpha to gamma alumina. The gamma alumina subsequently reacts with water to form a lubricous, layer lattice, hydroxide.



# CONTENTS

	Page
FOREWORD . . . . .	iii
ABSTRACT . . . . .	v
LIST OF TABLES . . . . .	xi
LIST OF FIGURES . . . . .	xiii

## Chapter

I.	INTRODUCTION AND SCOPE	1
II.	CERAMIC WEAR TEST METHODOLOGIES: BACKGROUND AND LITERATURE SURVEY	
	A. Basic Types of Tribological Studies . . . . .	5
	B. Current Efforts in Fundamental Ceramic Tribological Studies . . . . .	8
	C. Key Differences Between Ceramics and Metals . . . . .	12
	D. Approach to Evaluation of Ceramic Wear Used in This Report . . . . .	18
III.	EXPERIMENTAL APPARATUS AND OPERATING PROCEDURES	
	A. Wear Tester Selection . . . . .	19
	B. Specimen Material Selection . . . . .	25
	C. Lubricant Selection . . . . .	25
	D. Specimen Characterization Methods . . . . .	27
	E. Friction and Wear Measurement . . . . .	38
	F. Specimen Preparation . . . . .	40
	G. Operating Procedure Descriptions . . . . .	42
IV.	RESULTS AND DISCUSSION	
	A. Constant Condition Four-Ball Wear Testing Study	
	1. Base Conditions . . . . .	45
	2. Explanation of Severity Differences Between Steel and Ceramic Tests Conducted at the Same Operating Conditions . . . . .	46
	3. Four-Ball Constant Condition Test: Effect of Test Duration . . . . .	50
	4. Four-Ball Constant Condition Test: Effect of Load . . . . .	55
	B. Wear Test Severity Overlay . . . . .	61
	C. Analysis of Wear Scars . . . . .	64
	D. Four-Ball Constant Condition Test: Effect of Batch to Batch Variations in Specimen Material . . . . .	78

E.	Step-Loading Four-Ball Wear Testing Study	
1.	Base Conditions . . . . .	81
2.	Step-Loading Test: Effect of Speed . . . . .	86
3.	Step-Loading Test: Effect of Specimen Material . . . . .	86
F.	Ball-on-Three-Flat Testing . . . . .	89
1.	Comparison of Results to Four-Ball Tests . . . . .	89
2.	Ball-on-Three-Flat Test: Interpretation of Friction Data . . . . .	93
3.	Ball-on-Three-Flat Test: Effect of Specimen Material . . . . .	96
G.	Summary . . . . .	99
V.	ALUMINA/WATER TRIBOSYSTEM: INTRODUCTION AND LITERATURE SURVEY	
A.	Preliminary Explanation of Lubrication Mechanisms for Alumina With Water . . . . .	100
B.	Structures and Nomenclature of Aluminum Oxides and Hydroxides . . . . .	103
C.	Approach . . . . .	112
VI.	ALUMINA/WATER TRIBOSYSTEM: EXPERIMENTAL APPARATUS AND OPERATING PROCEDURES	
A.	Test Approaches . . . . .	113
1.	Static Kinetic Tests . . . . .	114
2.	Powder Friction Tests . . . . .	119
3.	Dynamic Wear Tests . . . . .	119
B.	Reference Powders . . . . .	120
C.	Analytical Techniques . . . . .	129
1.	Thermogravimetric Analysis (TGA) . . . . .	131
2.	Differential Scanning Calorimetry (DSC) . . . . .	141
3.	X-Ray Powder Diffraction (XRPD) . . . . .	141
4.	Fourier Transform Infrared (FTIR) Analysis . . . . .	144
5.	Scanning Electron Microscopy (SEM) . . . . .	145
VII.	ALUMINA/WATER TRIBOSYSTEM: RESULTS AND DISCUSSION	
A.	Kinetic Experiments on Powders . . . . .	146
B.	Powder Friction Tests . . . . .	158
C.	Wear Debris Analysis . . . . .	162
VIII.	SUMMARY AND CONCLUSIONS . . . . .	175
IX.	RECOMMENDATIONS FOR FUTURE WORK . . . . .	179
	REFERENCES . . . . .	180
	APPENDIX A - Selected Bulk Properties of Cer 006 and Cer 021 Alumina . . . . .	184



APPENDIX B - Coefficient of Friction Calculation for the Four-Ball Apparatus . . . . .	185
APPENDIX C - Equivalent Wear Scar Diameter Concept . . . . .	187
APPENDIX D - Specimen Cleaning Procedure . . . . .	190
APPENDIX E - Pressure-Temperature Relationship for the Alumina/Water Bomb Reactor . . . . .	192
APPENDIX F - X-Ray Powder Diffraction Patterns for Reference Powders AL1 through AL6 . . . . .	195
APPENDIX G - Interplaner Spacings, 2 Thetas, and Relative Line Intensities for X-Ray Powder Diffraction Patterns of Alumina's, Aluminum Oxide Hydroxides and Aluminum Trihydroxides . . . . .	201
APPENDIX H - An Estimate of the Hertzian Contact Diameter, Mean Pressure, and Maximum Pressure for 52100 Steel, and Alumina Specimens, in the Four-Ball Apparatus . . . . .	205
APPENDIX I - Derivation of a Pseudo First Order Dependence for the Gamma Alumina/Water Reaction at 194°C . . . . .	210
APPENDIX J - Mean Pressure Test Severity Plot for Wear Scar Diameter vs Load (psi) . . . . .	213
APPENDIX K - Mean Pressure Test Severity Plot for Wear Scar Diameter vs Load (MPa) . . . . .	214

NOTE: Certain commercial equipment, instruments, or materials are identified in this report to adequately specify the experimental procedure. Such identification does not imply recommendation or endorsement by the National Bureau of Standards, nor does it imply that the materials or equipment identified are necessarily the best available for the purpose.



## LIST OF TABLES

Table	Title	Page
1	Wear Test Design Philosophies	6
2	ASTM Wear Test Methods Applicable to Ceramic Materials	11
3	Comparison of Physical and Mechanical Properties of Selected Metals and Ceramics	14
4	Typical Properties of Dense High Alumina Ceramics	26
5	Summary of Selected Characterization Data on the Alumina Ceramics Used in This Study	34
6	Nomenclature for Hydroxides of Aluminum	104
7	Analytical Techniques Utilized in the Investigation of Alumina/Water Reactions	129
8	Thermogravimetric Analysis of Reference Powders	138
9	Kinetic Data for Reaction of Gamma Alumina (AL <sub>2</sub> ) and Water at 194°C	154
10	Summary Friction Data for Alumina Based Powders in Water	171



# LIST OF FIGURES

<u>Figure</u>	<u>Title</u>	<u>Page</u>
1	Stress-Strain Relationship for Typical Metals and Ceramics	16
2	Four-Ball Contact Geometry	20
3	NBS Modified Four-Ball Apparatus Design	22
4	Ball-on-Three-Flat Wear Test Contact Geometry	24
5	SEM Photomicrograph of Fracture Surface of Cer 004 Alumina - 2000X	29
6	SEM Photomicrograph of Fracture Surface of Cer 005 Alumina - 1000X	29
7	SEM Photomicrograph of Fracture Surface of Cer 006 Alumina - 1500X	30
8	SEM Photomicrograph of Fracture Surface of Cer 021 Alumina - 1000X	30
9	SEM Photomicrograph of Polished Surface of Cer 004 Alumina - 500X	32
10	SEM Photomicrograph of Polished Surface of Cer 005 Alumina - 500X	32
11	SEM Photomicrograph of Polished Surface of Cer 006 Alumina - 500X	33
12	SEM Photomicrograph of Polished Surface of Cer 021 Alumina - 500X	33
13	SEM Photomicrograph of Polished/Etched Surface of Cer 004 Alumina - 5000X	36
14	SEM Photomicrograph of Polished/Etched Surface of Cer 005 Alumina - 5000X	36
15	SEM Photomicrograph of Polished/Etched Surface of Cer 006 Alumina - 5000X	37
16	SEM Photomicrograph of Polished/Etched Surface of Cer 021 Alumina - 5000X	37

17	Comparison of Applicable Ranges for Optical and Weight Loss Wear Measurement Techniques	41
18	Comparison of Hertzian Contact Pressure for 52100 Steel versus Alumina	49
19	Typical Wear Regimes for a Wear Test	51
20	Wear-in Behavior of Alumina under Unlubricated and Paraffin Oil Lubricated Conditions	53
21	Friction Behavior of Alumina under Unlubricated and Paraffin Oil Lubricated Conditions	54
22	Change in Friction Behavior with Time for Unlubricated Alumina Tests at Different Loads	56
23	Comparison of Friction Behavior with Time for Unlubricated Alumina Tests with and without Heating Pretreatment	58
24	Comparison of Wear as a Function of Load for Unlubricated, Paraffin Oil Lubricated, and Water Lubricated Alumina Constant Condition Tests	60
25	Comparison of Coefficient of Friction as a Function of Load for Unlubricated, Paraffin Oil Lubricated, and Water Lubricated Alumina Constant Condition Tests	63
26	Low Magnification SEM Photograph of a Wear Scar from an Unlubricated Alumina Test	65
27	High Magnification SEM Photomicrograph of Lower Specimen Wear Scar from an Unlubricated Alumina Wear Test	65
28	SEM Photomicrograph of Wear Debris from Unlubricated Wear Test - 1000X	66
29	SEM Photomicrograph of Wear Debris from Unlubricated Wear Test - 10,000X	66
30	Low Magnification SEM Photograph of a Wear Scar from a Water Lubricated Alumina Test	68
31	High Magnification SEM Photomicrograph of Lower Specimen Wear Scar from a Water Lubricated Alumina Wear Test	68
32	SEM Photomicrograph of Upper Specimen Wear Track Water Lubricated Run 2748R - 25X	69



33	SEM Photomicrograph of Upper Specimen Wear Track Water Lubricated Run 2748R - 100X	69
34	SEM Photomicrograph of Upper Specimen Wear Track Water Lubricated Run 2748R - 500X	71
35	SEM Photomicrograph of Upper Specimen Wear Track Water Lubricated Run 2748R - 1000X	71
36	SEM Photomicrograph of Upper Specimen Wear Track Water Lubricated Run 2748R - 5000X	72
37	SEM Photomicrograph of Lower Specimen Wear Scar Water Lubricated Run 2748R - 50X	72
38	SEM Photomicrograph of Wear Debris from Water Lubricated Wear Test - 1000X	73
39	SEM Photomicrograph of Wear Debris from Water Lubricated Wear Test - 5000X	73
40	Low Magnification SEM Photograph of a Wear Scar from a Paraffin Oil Lubricated Alumina Test	75
41	High Magnification SEM Photomicrograph of Lower Specimen Wear Scar from a Paraffin Oil Lubricated Alumina Wear Test	75
42	SEM Analysis of Wear Debris from Paraffin Oil Lubricated Wear Test - 1000X	76
43	SEM Analysis of Wear Debris from Paraffin Oil Lubricated Wear Test - 10,000X	76
44	Comparison of Wear as a Function of Load for Different Batches of Alumina under Paraffin Oil Lubricated Conditions (Constant Condition Tests)	78
45	Comparison of Wear as a Function of Load for Different Batches of Alumina under Water Lubricated Conditions (Constant Condition Tests)	79
46	Wear as a Function of Load for Unlubricated Alumina Step-Loading Four-Ball Tests	81
47	Wear as a Function of Load for Water Lubricated Alumina Step-Loading Four-Ball Tests	82
48	Wear as a Function of Load for Paraffin Oil Lubricated Alumina Step-Loading Four-Ball Tests	84

49	Effect of Speed on Step-Loading Four-Ball Wear Test Results	86
50	Comparison of Wear Behavior as a Function of Load for Paraffin Oil Lubricated Step-Loading Four-Ball Tests on Silicon Nitride, Silicon Carbide, and Alumina	87
51	Comparison of Ball-on-Three-Flat and Four-Ball Wear Results for Paraffin Oil Lubricated Alumina	90
52	Friction Traces for Paraffin Oil Lubricated Ball-on-Three-Flat (BTF) Test 2727 R	93
53	Coefficient of Friction Values versus Load for Paraffin Oil Lubricated BTF Test 2727 R	94
54	Comparison of Wear Results for NBS Produced Alumina versus Commercial Alumina (Paraffin Oil Lubricated BTF Tests)	96
55	Comparison of Friction Traces for NBS Alumina versus Commercial Alumina	97
56	Structure of $\text{Al}(\text{OH})_3$	106
57	Layer Stacking Sequence for Gibbsite and Bayerite	107
58	Phase Diagram for $\text{Al}_2\text{O}_3$ - $\text{H}_2\text{O}$ System	109
59	Decomposition Sequences for Aluminum Hydroxides	110
60	High Pressure Bomb Reactor Design	114
61	Temperature-Pressure Relationship for Bomb Reactor	115
62	Temperature Inside Bomb versus Time during Heating	117
63	1000X Secondary Emission SEM Photograph of Powder AL1	122
64	10,000X Secondary Emission SEM Photograph of Powder AL1	122
65	1000X Secondary Emission SEM Photograph of Powder AL2	123
66	10,000X Secondary Emission SEM Photograph of Powder AL2	123
67	1000X Secondary Emission SEM Photograph of Powder AL3	124

68	10,000X Secondary Emission SEM Photograph of Powder AL3	124
69	1000X Secondary Emission SEM Photograph of Powder AL4	125
70	10,000X Secondary Emission SEM Photograph of Powder AL4	125
71	1000X Secondary Emission SEM Photograph of Powder AL5	126
72	10,000X Secondary Emission SEM Photograph of Powder AL5	126
73	1000X Secondary Emission SEM Photograph of Powder AL6	127
74	10,000X Secondary Emission SEM Photograph of Powder AL6	127
75	Isothermal TGA of Powder AL3 (Boehmite)	132
76	Temperature Scan TGA of Powder AL3 (Boehmite)	133
77	Temperature Scan TGA of Powder AL1 (Boehmite)	135
78	Temperature Scan TGA of Powder AL2 (Gamma Alumina)	136
79	Temperature Scan TGA of Powder AL6 (Gibbsite)	137
80	X-Ray Powder Diffraction Apparatus and Sample Spectrum	141
81	Temperature Scan TGA of Reaction Product of Gamma Alumina/Water at 100°C for 24 Hours	146
82	Temperature Scan TGA of Reaction Product of Gamma Alumina/Water at 194°C for $\approx$ 1 Hour	147
83	Temperature Scan TGA of "Gel" Phase of Reaction Product of Gamma Alumina/Water at 194°C for $\approx$ 1 Hour	149
84	Temperature Scan TGA of "White" Phase of Reaction Product of Gamma Alumina/Water at 194°C for $\approx$ 1 Hour	150
85	Temperature Scan TGA of Reaction Product of Gamma Alumina/Water at 194°C for 31 Minutes	151

86	Temperature Scan TGA of Reaction Product of Gamma Alumina/Water at 194°C for 59 Minutes	152
87	Temperature Scan TGA of Reaction Product of Gamma Alumina/Water at 194°C for 119 Minutes	153
88	Pseudo First Order Data Plot for Gamma Alumina/Water Reaction at 194°C	156
89	Friction Traces for Powder Tests at 5 kg Load	158
90	Friction Traces for Powder Tests at 2 kg Load	159
91	Comparison of Final Coefficient of Friction Values for Different Alumina Powders at 2 and 5 kg Load	160
92	X-Ray Powder Diffraction Spectrum for Wear Debris from Water Lubricated Alumina Test	162
93	Temperature Scan TGA of Wear Debris from Water Lubricated Alumina Test	164
94	FTIR Spectrum of Wear Debris from Water Lubricated Alumina Test	166
95	Model for the Alumina/Water Tribosystem	167
96	Effect of Various Alumina Based Powders on Friction for Water Lubricated Alumina	172
97	Lubricating Effect of Boehmite Powder for Water Lubricated Alumina	174

## Chapter I

## INTRODUCTION AND SCOPE

Ceramic or ceramic-like materials have been used in tribological applications for thousands of years. A typical example is the thresholds used in Assyrian villages 6000-7000 years ago during the stone age.<sup>1</sup> Stone sockets were used as pivot points for wooden poles providing a means of opening and closing the "door."

These early crude uses of ceramics eventually led to more sophisticated applications better designed to take advantage of the unique properties ceramics have to offer. Watches, for example, have small crystals of diamond or sapphire ("Jewels") which are used as pivot points for the inner workings. The low friction and wear associated with these materials allows for many years of trouble free operation. Still today, manufacturers of fine watches advertise the number of jewels in the movement as a badge of quality.

More recently, advances in ceramic materials have produced new structural or advanced ceramics. Current technology, being forced to higher and higher performance from ever dwindling resources, has placed greater demands on new materials. The result is a tremendous increase in research in strong high temperature materials capable of functioning in environments not suitable for conventional metals. This research has been mainly centered on studies involving high temperature "superalloys," powder metallurgy, and advanced

ceramics.<sup>2-6</sup> The superalloy and powder metallurgy suffer from the drawback that they require certain rare "strategic" materials (cobalt, chromium, tungsten, tantalum, nickel) which must be imported and thus place the United States in a dependent role. Ceramic raw materials on the other hand are commonly available from domestic suppliers. Silicon and aluminum, two of the most abundant elements in the earth's crust, are common in many important structural ceramics.

Advanced ceramic materials therefore have several attractive features which make them ideal candidates for high technology applications. Their low thermal conductivity gives them insulating properties which allow better thermodynamic efficiency for designs such as low heat rejection engines. Their high temperature strength and corrosion resistance allows them to operate under conditions unsuitable for metals. Their high hardness would seem to make them good candidates for low wear under the commonly held belief that wear rate is inversely proportional to hardness.<sup>7</sup> In addition, they can be made from non-strategic raw materials.

Much of the screening work on advanced ceramics has focused on the evaluation of candidate materials based on chemical and mechanical property data.<sup>8</sup> Testing is then conducted by fabricating actual ceramic parts and evaluating their performance.<sup>9-11</sup> The result is often an expensive trial and error approach which contributes little or no fundamental understanding of the tribological behavior of ceramic materials. What is needed to complete the picture is a



simple, inexpensive, repeatable system for evaluating the tribological behavior of advanced ceramic materials and gaining a better understanding of fundamental processes or mechanisms which govern their behavior.

The objective of this study is to gain an understanding of the wear test methodology that might be employed to evaluate the tribological properties of ceramic materials. The scope of this study is limited to structural or advanced ceramics under high contact stress conditions. Lubricants are limited to paraffin oil, water, and no lubricant to represent the three most common basic forms of lubrication of hydrocarbon-based fluids, water-based fluids, and unlubricated conditions.

This report is organized in the following manner. First, a background and literature survey is presented to familiarize the reader with the present status of ceramic tribology. The wear testing approach used in this report is also presented in the context of previous research efforts. Second, the experimental apparatus and operating procedures are described. Third, experimental results are presented with interpretation and discussion. Initially, alumina is used as a representative ceramic for most of the exploratory phase of this work. Later, silicon carbide and silicon nitride ceramics are evaluated using the fully developed methodology.

Interesting results for water-lubricated alumina prompted an in-depth study of the possible lubrication mechanism for this system. This is presented in the latter part of this report under the alumina/water tribosystem headings and includes additional information on a literature survey, experimental apparatus and operating procedures, and results and discussion.

## Chapter II

### CERAMIC WEAR TEST METHODOLOGIES: BACKGROUND AND LITERATURE SURVEY

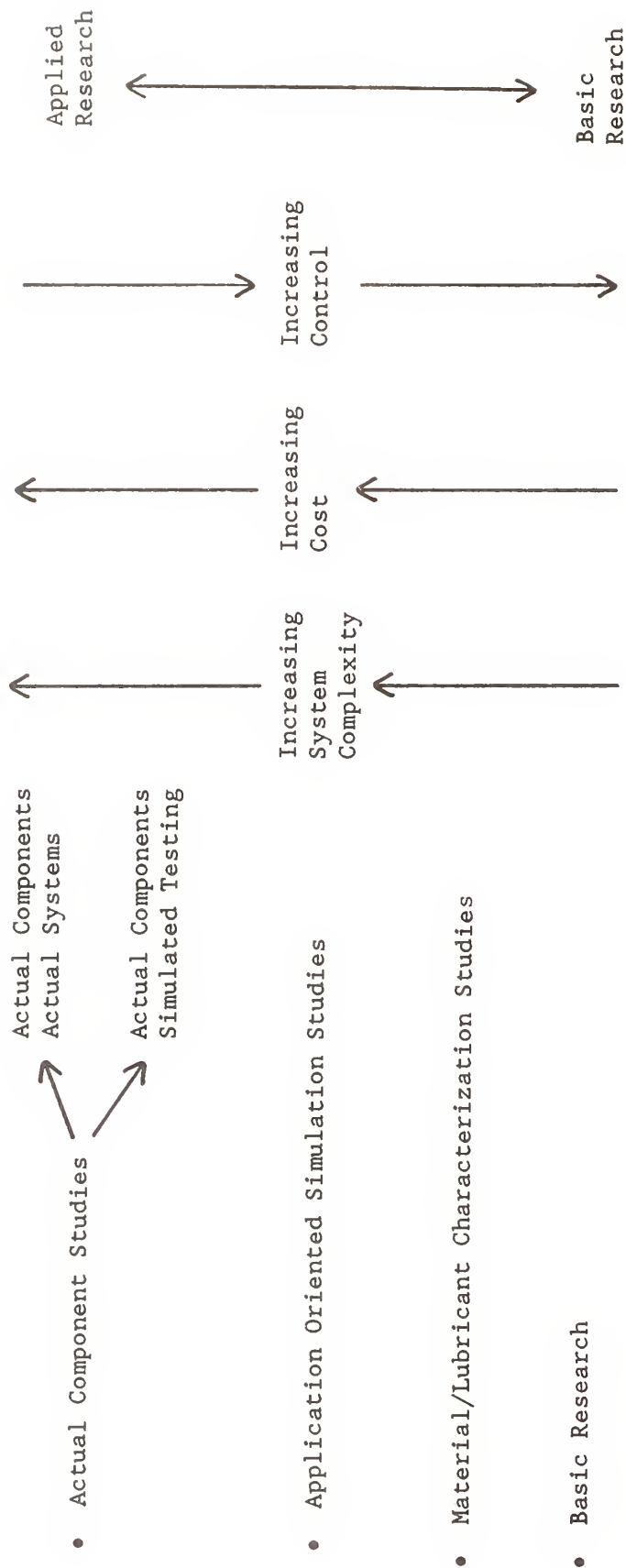
#### A. Basic Types of Tribological Studies

There are four basic wear test design philosophies that are currently used in tribological testing. These can be classified as: actual component studies; application oriented simulation studies; material/lubricant characterization studies; and basic research. These wear test design philosophies are listed in table 1 with additional information on relative complexity, cost, and control.

Actual component studies can either involve a full scale working piece of equipment with the appropriate components made of the selected materials, or a test rig constructed to utilize the components in the exact same way they would be used in service. An example of the different approaches can be found in the use of ceramic piston liners and rings in an adiabatic diesel engine. The actual system approach would consist of fabricating piston liners and piston rings and running them in the actual engine. The actual component test rig approach would use the same components; however, they would be placed on a simulation test rig that duplicates the primary conditions (motions, loads, temperatures, etc.) but with better control. There is usually some sacrifice of simulation in going to a test rig (such as no combustion products or no thermal cycling) but

Table 1

## Wear Test Design Philosophies



this is a tradeoff for better control. Examples of this approach, used for adiabatic diesel engines and gas turbines, are given in references.<sup>12-13</sup>

Application-oriented simulation studies consist of using the same materials as needed but not the actual components. Using the piston ring and liner example, an apparatus that produces a reciprocating line contact at appropriate speeds and loads would be used. This wear test approach usually results in an increase in test control but, again, by sacrificing some simulation aspects. Examples of this approach, used for engine, tool, bearing, and grinding applications are found in references.<sup>14-17</sup>

The material/lubricant characterization approach consists of running friction and wear tests at a variety of conditions using the actual material. This results in an understanding of the tribological behavior of the material under selected severities (speed, load, temperature, etc.). It may also be possible to gain an understanding of the wear mechanisms for the material at different severities (i.e., a wear map). The material thus characterized can be evaluated for a particular end application. If, for example, it is found that a particular ceramic material has a transition to a very high wear rate above 6.9 MPa (1000 psi) and 800°C for slow speed sliding, the material would be unsuitable for an application where pressures and temperatures exceed these limits. Examples of studies using the

material/lubricant characterization approach are given in references.<sup>18-20</sup>

The basic research approach focuses on understanding a fundamental processes and mechanisms. These experiments are usually highly controlled and often simplify a system to a select set of test conditions. In many cases, very specialized equipment is required therefore this is not always the least expensive approach. In some cases, the distinction between some of these design philosophies is not clear and they overlap. It is possible, for example, to conduct a study incorporating philosophies from material/lubricant characterization studies and basic research.

The material/lubricant characterization approach was the one selected for this study. Besides the factor of cost (and budget), this approach offers the attractive features of reduced complexity and enhanced control to gain a better fundamental understanding of the tribological characteristics of ceramic materials.

#### B. Current Efforts in Fundamental Ceramic Tribological Studies

There have been numerous attempts to define the fundamental tribological properties of certain ceramic materials using bench wear tests. In general these studies can be divided into two groups: single crystal ceramic studies and polycrystalline ceramic studies.



Single crystal studies are usually undertaken to study the anisotropy of the tribological properties<sup>18</sup> although some studies use single crystals merely as a source of pure material. Usually single speeds and loads are used but many authors will select a few speeds or loads, and note an apparent change in mechanism or wear rate for different conditions.

Polycrystalline ceramic studies<sup>19</sup> are simpler in some ways because the orientation becomes randomized and does not have to be controlled during a test. In other ways they are more complex because the additional variable of a second phase (grain boundaries) must be considered. Frequently it is the grain boundaries that are the weakest link in the structure of the polycrystalline ceramic. An understanding of the tribological behavior of a single crystal ceramic therefore does not necessarily endow an understanding of the tribological behavior of polycrystalline forms of the same material. Some authors use both single crystal and polycrystalline studies<sup>20</sup> to gain a complete understanding of the fundamental tribological behavior of the single crystals and its relationship to the behavior of polycrystalline materials.

The studies cited above represent attempts to understand the tribological properties of ceramics from a variety of viewpoints, and a wide range of conditions. Different wear test equipment is used because there is no standard method or piece of equipment designed to study the sliding friction and wear properties of ceramics. A

compilation of ASTM wear test methods conducted by Blau in late 1985<sup>21</sup> revealed only six test methods applicable to ceramics (table 2). Five of these methods do not pertain to sliding wear and the sixth (G77) is originally designed for metals. The scope section of this method (G77) indicates that any materials can be used (plastics, ceramics); however, representative precision data are given only for metals. In addition, one of the specimens in method G77 is a 2-inch diameter ring with an inner taper. Dimensional tolerances are very tight ( $\pm 0.025$  mm (0.001 in) for all dimensions,  $\pm 5$  minutes for the taper angle) with a surface roughness of approximately  $0.2 \mu\text{m}$  RMS. These factors would make these specimens quite expensive to fabricate using ceramics. In addition, post-test analyses (SEM for example) would be hindered by the large size of the specimen.

More recently, new efforts are being made to develop international standard test methods for ceramics under the guidance of the Versailles Advanced Materials and Standards (VAMAS) project.<sup>22</sup> The ceramic wear test method development phase of the project centers on comparison of wear and friction measurements using a pin on disc (or ball on disc) tribometer. Many participants (including NBS) from seven countries are participating in this study. An initial dry (unlubricated) testing round robin offered promising results; however, several procedural problems with sample cleaning, handling, and test environment were encountered. Only a single speed and load is currently being used in this study. In addition, the nature of the

Table 2

## ASTM Wear Test Methods Applicable to Ceramic Materials

ASTM Test #	Applications	Materials	Comments or Apparatus
C448	Porcelain Enamel	Ceramics	NBS Lapping Machine
C501	Tile	Ceramics	Taber Abraser
C704	Refractory Brick	Ceramics	Room Temperature Jet Erosion
G32	Cavitation	Metals Ceramics Plastics	Vibration in Liquid Bath
G76	Erosion	Metals Ceramics Plastics	Particles Against Flat
G77	Sliding Wear	Metals Ceramics Plastics	Block on Ring

Source: Blau (21)

effort (International, round robin) makes for slow progress in method development.

### C. Key Differences between Ceramics and Metals

There are fundamental differences in the nature of interatomic bonding between atoms in ceramics, and metals, that lead to differences in chemical and physical properties. These differences in turn lead to mechanistic differences in wear and friction.

Interatomic bonding in ceramic solids consists of a combination of ionic, covalent, van der Waals, and hydrogen bonds, with ionic and covalent bonding being the most important.<sup>23</sup> Covalent bonds are very strong bonds formed when electrons are shared between atoms. The resulting short bond lengths (1.54 Å for C-C bond in diamond) produce some of the strongest bonds known. Ionic bonds result when complete transfer of electrons takes place between atoms producing charged ions. The coulombic attraction between the charged ions (for example  $\text{Na}^+$  and  $\text{Cl}^-$ ) produce relatively strong bonds with moderate bond lengths (2.8 Å for Na - Cl bond in halite). In both of these bond types, electrons are localized to specific atoms or shared between pairs of atoms. Van der Waals and hydrogen bonds are relatively weak bonds. Van der Waals bonds arise from dipole forces between atoms. Hydrogen bonds arise from the interaction of the slightly electropositive H atom and an electronegative atom (O or F for example). Even though these atoms are bound to other atoms, there may

be enough residual electropositive and electronegative nature to set up this weak interaction. Both of these weak bonds can be found between layers of layered ceramic structures. For example, Van der Waals bonding takes place between layers in graphite. Bond lengths are characteristically large (3.4 Å for the C-C bond between layers in graphite).

Metals are held together through metallic bonding. These bonds are the result of attractive forces (Coulombic) between positive metallic atoms and a sea of free negative electrons. The result is relatively strong bond strength and bond lengths similar to ionic bonds;<sup>24</sup> however, these bonds are not as directional as ionic or covalent bonds. This may result in an improved ability to yield to relieve a stress.

The difference in the nature of the bonding between metals and ceramics results in differences in their properties. The electron mobility in metals for example allows them to have higher thermal and electrical conductivity. Thermal conductivity is usually lower for ceramics because conduction occurs mainly through phonon (thermal vibration) transfer. In metals, both phonon transfer and electron transport usually allow much higher thermal conductivity. (An exception is diamond which is the best conductor known, perhaps due to the very short bond length which may make phonon transfer very efficient.) A comparison of typical physical and thermal properties for selected ceramics and metals is given in table 3.

Table 3  
Comparison of Physical and Mechanical Properties of Selected Metals and Ceramics

Property	Units	Ceramics <sup>(1)</sup>						Metals <sup>(2)</sup>				
		Material →	Al <sub>2</sub> O <sub>3</sub>	α-SiC	Si <sub>3</sub> N <sub>4</sub>	PSZ	SiALON	Carbon Steel	Iron	Aluminum Alloy	Brass (Naval)	Magnesium Alloy
		Manuf. →	Coors	Carbor-undum	GTE	Nilsen	Lucas					
	Ident. →	AD995	Hexaloy	SNW1000	TS	Syalon 101		Cookson 1020	Wrought	3003	464	AZ91A
Density	g/cm <sup>3</sup>	3.9	3.1	3.3	5.8	3.24		7.86	7.70	2.73	8.41	1.81
Thermal Conductivity	w/m K	35.6	126	27	1.8	21.3		51.9	60.3	159	117	53.4
Heat Capacity	J/kg K	880	2803	810	400	620		448	460	962	377	1025
Thermal Expansion Coefficient	10 <sup>-6</sup> /K	7.1	4.0	2.3	10.1	3.04		12.1	11.4	23.2	19.8	26.1
Electrical Resistivity	Ω-cm	>10 <sup>14</sup>	0.2-300	>10 <sup>14</sup>	>10 <sup>11</sup>	10 <sup>8</sup>		10 <sup>-5</sup>	10 <sup>-5</sup>	10 <sup>-6</sup>	10 <sup>-5</sup>	10 <sup>-5</sup>
Hardness Knoop	GPa	14.7	27.4	12.7	10.0	91(HRA)		---	---	---	---	---
Brinnell	#	---	---	---	---	---		130	100	40	90	67
Elastic Modulus	GPa	372	410	276	205	288		207	200	69.0	103	44.8
Tensile Strength	MPa	262	---	---	---	450		448	331	152	386	228
Compressive Strength	MPa	2620	---	---	1850	>3500		---	---	---	---	---
Flexural Strength	MPa	379	550	665	690	---		---	---	---	---	---
Yield Strength	MPa	---	---	---	---	---		262	207	145	152	152
Elongation %	%	---	---	---	---	---		30	30	16	40	3
Fracture Toughness	MPa√m	---	4.6	4.5	9.5	7.7		---	---	---	---	---
Maximum Service Temp. (Air)	°C	1750	1650	-1200	950	1400		---	---	---	---	---
Melting Point	°C	2015	-2700	-1900	---	---		1516	1510	644	885	596

--- indicates data not available.  
(1)Source: Compiled from company literature.  
(2)Source: Perry (25).

In general, ceramics have lower densities, thermal conductivity, thermal expansion, and electrical resistivity than metals. They also have higher hardness and elastic modulus than metals, and tend to retain their strengths to higher temperatures. Collecting data for a comparison of this nature is very difficult for a variety of factors. Ceramics and metals behave differently; therefore, different properties are measured and highlighted. Tensile strength, for example, is often not reported for ceramics because ceramics are inherently weak in tension. Often, there is an order of magnitude difference between compressive strength and tensile strength. Metals on the other hand have tensile strengths much closer to their compressive strengths ( $\approx$  factor of 2 or 3). The different behavior for metals versus ceramics is also apparent when comparing their stress strain relationships (fig. 1). This relationship is used to determine the response of a material to applied stress. The initial straight line portion of the figure is the elastic response. From the slope, the elastic modulus can be calculated (large slope - high modulus). At some point, the material behavior changes. For many ceramics, failure occurs as brittle fracture. This failure point defines the tensile strength of the material. For metals, the material usually yields plastically before failing completely (usually by necking - ductile failure). Thus, for metals, yield strength and elongation are measured in addition to tensile strength.

In some cases, ceramic properties are so different from metals, separate techniques are used to measure them. This makes comparison



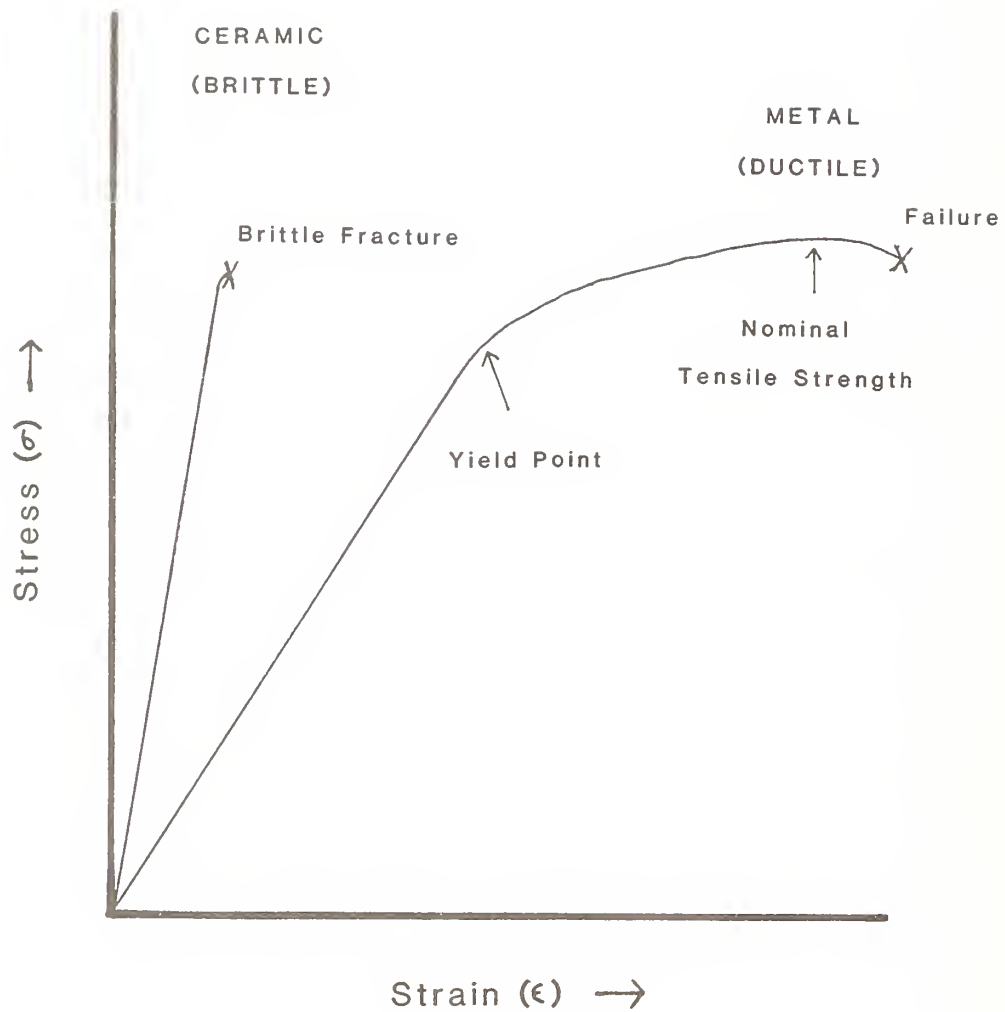


Figure 1. Stress-Strain Relationship for Typical Metals and Ceramics

of properties very difficult. Metals are relatively soft, therefore hardness is reported as Brinell number or Rockwell number. These values are usually based on indentation with a hard ball. Hardness measurements for ceramics, on the other hand, require diamond indentation techniques (Knoop or Vickers), which do not have a direct conversion to the metal hardness values.

Another difference between metals and ceramics is the nature of their processing. Metals are usually formed from a melt and cooled to form the desired structure. Ceramics are usually sintered from a powder. There may be a fundamental weakness introduced by this technique which causes an inherent brittleness. The mere process of sintering may cause impurities to collect in specific sites within grain boundaries, for example, thus weakening the entire structure. This behavior of impurities concentrating in phase boundaries has been observed for metal systems and is actually used to purify them in the technique known as zone refining.

The difference in the nature of the bonding also affects the mechanisms by which these materials function tribologically. For metal systems, one of the primary mechanisms of wear is through adhesion. This is the result of micro welding of asperities and subsequent removal of these welds from the parent material resulting in many small "adhesive wear" particles. In ceramics, it appears that the nature of the bonding does not allow adhesion (micro welding) to take place easily between asperities. The dominant form of surface

degradation may instead be due to locally high stresses resulting in microfracture.<sup>26</sup> In developing a methodology for wear testing of ceramics therefore it is important to be aware of differences in the nature of the bonding of the atoms, unique properties, and potential mechanistic differences for ceramic materials.

#### D. Approach to Evaluation of Ceramic Wear Used in This Report

The following approach to evaluating the wear of ceramic materials was used base on an understanding of the literature and the nature of ceramic materials. A tester was selected which allowed good control of important test variables for a wide range of test severities. A representative ceramic material was selected for a parametric study of the effect of different test parameters on friction and wear. A wide range of test severities were encompassed in an effort to ensure that a bias of expected performance (based on metals) was not limiting the study. Finally, a cycle of testing/data analysis/interpretation was used to evolve into a more efficient and informative test method as the study progressed.

### Chapter III

#### EXPERIMENTAL APPARATUS AND OPERATING PROCEDURES

##### A. Wear Tester Selection

There are a wide variety of wear test devices available for measuring the tribological properties of material lubricant combinations. The Catalog of Friction and Wear Test Devices<sup>27</sup> published by the American Society of Lubrication Engineers contains a detailed description of 234 different tribometers. Each apparatus has particular strengths and weaknesses, however, given the requirements of a ceramic material tribometer in the particular lubrication regime we wished to study, a logical wear test device selection can be made. The general requirements for the tribometer are: high contact stresses to ensure that we are operating in the boundary lubrication regime; good control of operating parameters of speed, load, temperature, duration, atmosphere; high sensitivity of wear and friction measurements; and fairly small specimens that can be easily fabricated. The four-ball wear test geometry was selected as the best apparatus to combine these features.

The four-ball wear test apparatus used in this study is an NBS modification of a standard four-ball wear tester. Modifications were made in order to enhance the load and temperature capabilities, and repeatability of the standard device. The basic specimen configuration (fig. 2) consists of a tetrahedral arrangement of four

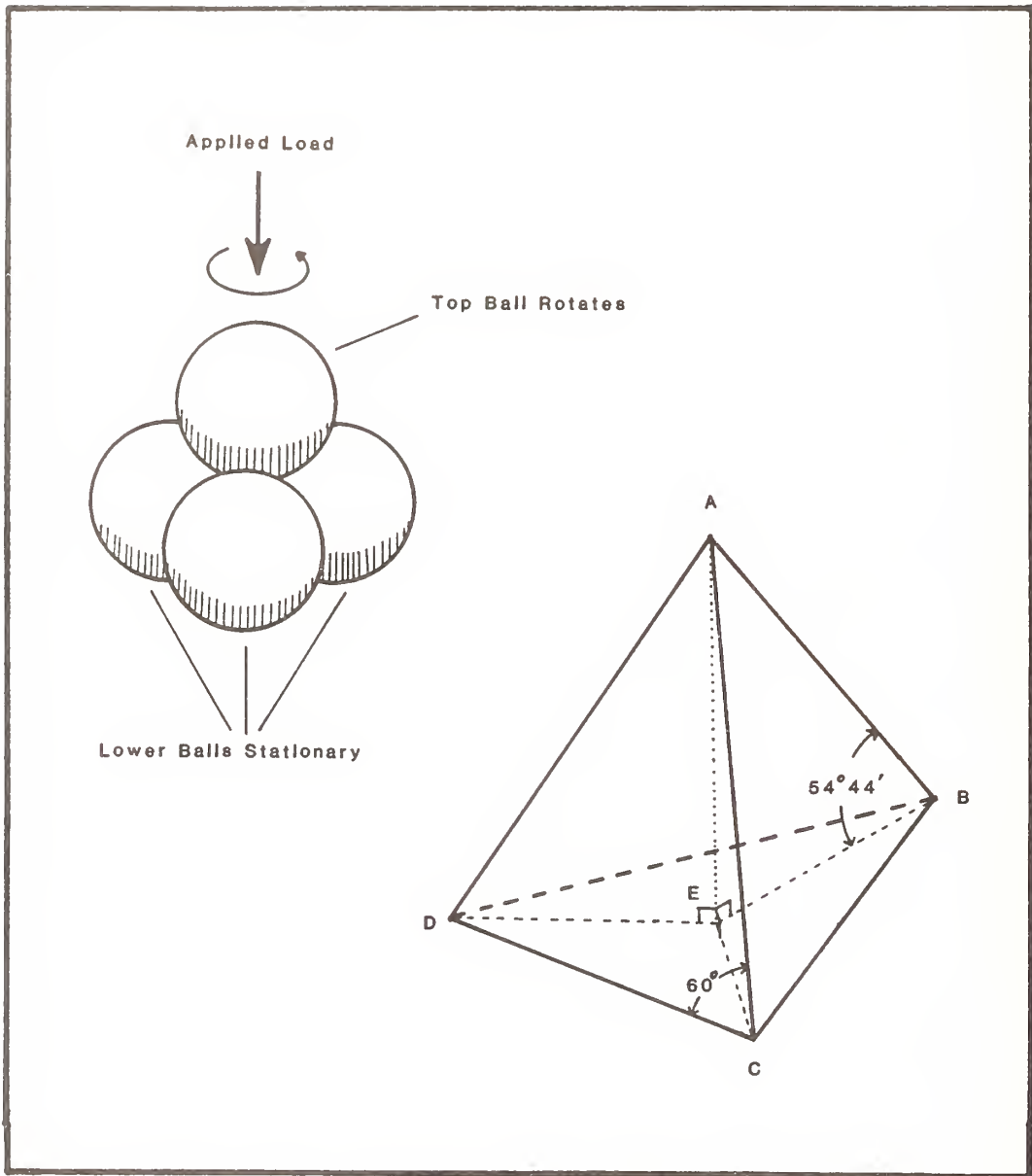


Figure 2. Four-Ball Contact Geometry

half-inch diameter spheres. The three lower balls forming the base of the pyramid are locked in place in a test cup. A fourth ball held in a chuck, is nested on top of the three balls and provides three point contacts. The upper ball rotates to provide a sliding motion between the surfaces. An axial force is provided to adjust the loading between the upper and lower specimens. A diagram of the overall NBS four-ball assembly is shown in figure 3. The entire set of specimens can be immersed in a lubricant and atmosphere control is obtained by feeding the desired gases into the test chamber using flowmeters equipped with needle valves. The specimen cup rests on a heating block that is capable of providing temperatures up to 540°C. The entire test cup/heater assembly rests on a frictionless air bearing which serves to thermally isolate the assembly from the loading piston, and allows for a high degree of sensitivity in friction measurement. Friction produced in the contact points produces a torque in the test cup assembly. This torque is measured, as a force from a lever arm extending out of the assembly, using an electronic force transducer. The force transducer sends an electric voltage which is proportional to the applied force to a strip chart recorder. Thus friction can be continuously monitored during a wear test.

The four-ball tribometer satisfies all of the original ceramic tribometer requirements. The three point contacts coupled with the load capability provide test severities normally associated with boundary lubrication. Good control of speed, load, temperature, duration, and atmosphere are easily accommodated. Wear and friction

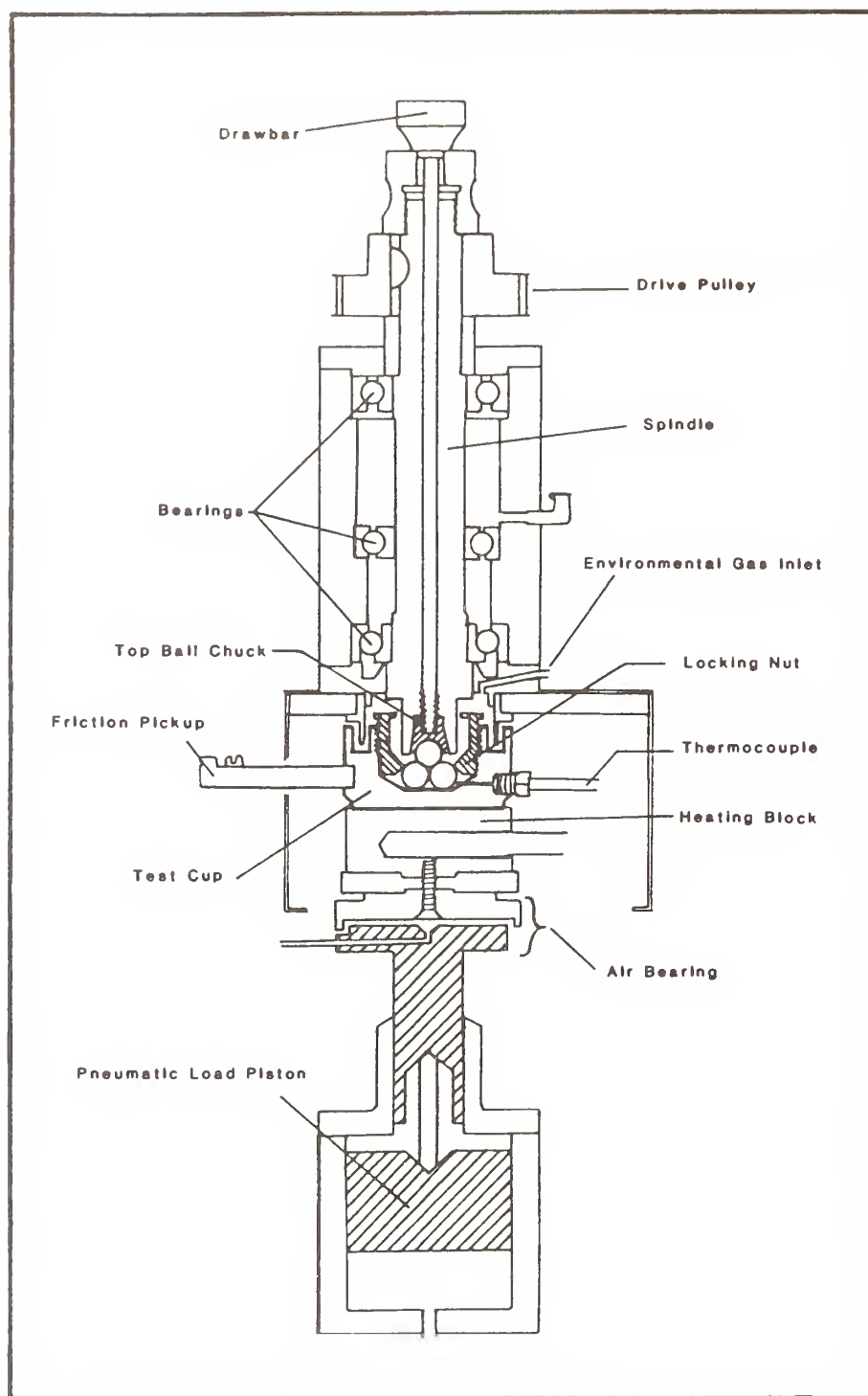


Figure 3. NBS Modified Four-Ball Apparatus Design



measurements are easy to obtain and sensitive enough for our purposes. Half-inch diameter spheres are available in many ceramic materials. In addition, the nature of the four-ball contact geometry with frictionless air bearing allows the specimens to be largely self-aligning. This reduces the alignment problem common with wear test devices, and allows for a high degree of sensitivity and repeatability.

A second configuration is possible with this apparatus by replacing the three lower balls with 6.35 mm diameter (0.25 in), 1.59 mm thick (0.0625 in) disc specimens ("flats") as shown in figure 4. This produces three point contacts between the upper ball and the lower "flats" at exactly the same points as for the four-ball contacts. The main difference between the two configurations is that the four-ball test produces convex-convex surface contacts whereas the ball-on-three-flat test produces convex-flat surface contacts. In addition, the size and geometry of the flats provides a more thermally conductive pathway between the wear contact and the metal test cup. The ramifications of these differences will be discussed in a later section.

The ball-on-three-flat geometry allows for testing of materials not easily obtainable in ball form. Flats can be fabricated most easily by cutting thin sections from 1/4-inch diameter rod stock which is easily available, or by diamond core drilling of a 1/16-inch

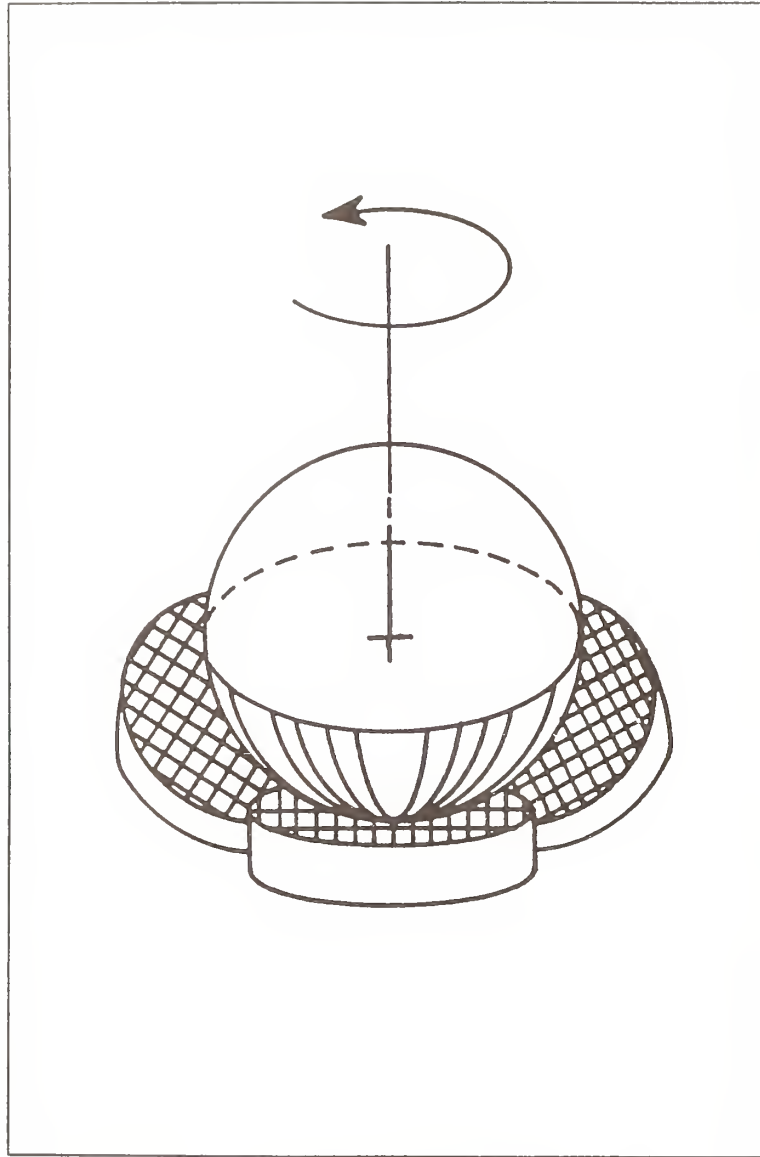


Figure 4. Ball-on-Three-Flat Wear Test Contact Geometry

thick sheet of material. The combination of diamond core drilling and sectioning allows flats to be fabricated from materials of almost any shape.

#### B. Specimen Material Selection

A single representative ceramic material was selected for initial test method development work. This material was selected based on the following criteria: Polycrystalline ceramic; mechanical, thermal, and chemical properties typical of ceramic materials; and available with good uniformity at relatively low cost. Based on these requirements, polycrystalline aluminum oxide (alumina -  $\text{Al}_2\text{O}_3$ ) specimens were selected for preliminary testing. Alumina possesses mechanical, thermal, and chemical properties fairly typical of ceramic materials and is easily obtained in ball and flat form with good uniformity at low cost. A listing of the approximate properties of this alumina material is given in table 4.

#### C. Lubricant Selection

Three different lubricant environments were selected for initial studies. Dry tests (no lubricant) were conducted in an effort to establish a baseline for unlubricated friction and wear. A purified paraffin oil was selected as a typical unformulated hydrocarbon (nonpolar) lubricant of low viscosity (125/135 SUS). Tests were also conducted using deionized water (polar) as a lubricant. The water not

Table 4  
Typical Properties of Dense High Alumina\* Ceramics

Property	Units	Conditions	Approximate Values
Density	g/cm <sup>3</sup>		3.8-4.0
Young's Modulus	GPa		330-390
Hardness	#	ASTM E18-67 Rockwell 45N	78-90
Compressive Strength	MPa	25°C 1000°C	2000-3800 480-1930
Tensile Strength	MPa	25°C 1000°C	200-310 100-220
Flexural Strength	MPa	25°C 1000°C	275-550 170-410
Thermal Expansion Coefficient	10 <sup>-6</sup> /°C	25-200°C 25-1000°C	5.3-6.8 7.4-8.6
Thermal Conductivity	W/cm °C	25°C	0.2-0.33
Specific Heat	J/g °C	25-100°C	0.75-0.88

Source: Condensed from Ceramic Source 1986, Vol. I, p. 334-335.

\*Approximately 99% Alumina.

only served as a polar medium but also serves as a baseline for possible usefulness of water based lubricants for ceramics.

#### D. Specimen Characterization Methods

A comprehensive review of the literature regarding tribology of ceramics conducted with Jeff Yellets,<sup>28</sup> revealed a lack of adequate specimen characterization in most cases. It is thought that detailed pre and post-test characterizations can enhance the possibilities for correct mechanistic interpretation of the data. I have therefore tried to accurately characterize the materials used in this program.

In the course of this study, three separate batches of alumina ball specimens were obtained (Cer 004, Cer 005, Cer 021). Later tests were also conducted on flat alumina specimens obtained from rod stock (Cer 006). Selected bulk properties of some of these specimens are given in Appendix A.

Specimens were characterized using profilometry, fractography, and ceramography. Profilometry is a technique which determines the surface roughness of a sample. A diamond stylus is carefully drawn over the surface of a sample. The stylus moves in response to the microscopic contours of the sample as it is drawn over the surface. This movement is amplified electronically and the electronic signals are processed in such a way that a number representing the measured roughness of the surface is obtained. Those wishing a more detailed

description of profilometry and its interpretation are referred to reference 29. Ball specimens were obtained with a high degree of uniformity of  $12.7 \text{ mm} \pm 0.000635 \text{ mm}$  ( $0.5 \text{ in} \pm 0.000025 \text{ in}$ ) and a highly polished surface finish of  $0.038 \text{ } \mu\text{m AA}$  ( $1.5 \text{ } \mu\text{in}$ ). Flat specimens were approximately  $1.59 \text{ mm}$  ( $0.0625 \text{ in}$ ) thick with a surface finish of approximately  $0.04 \text{ } \mu\text{m}$  ( $1.6 \text{ } \mu\text{in}$ ).

Fractography entails producing a fracture surface on a specimen and observing the shapes and sizes of grains that become exposed. Fracture surfaces were produced on ball specimens by cutting a notch 75% of the way through the ball with a diamond saw, then cleaving the ball in half with a wedge. The rod stock was notched and cleaved in a similar fashion. Once in the fractured state, specimens were mounted on SEM studs, covered with thin conductive coatings ( $\approx 20 \text{ nm}$ ) of gold/palladium and analyzed in the SEM.

The scale marker on each of the SEM photomicrographs is interpreted as follows. The left mark is the calibration mark. Its length represents a unit length on the photograph which depends on the number of dashes which follow the calibration mark. One dash signifies the calibration mark is  $1 \text{ } \mu\text{m}$  long. Two dashes signifies the calibration mark is  $10 \text{ } \mu\text{m}$  long.

Fracture surfaces from the four different alumina batches were analyzed in the SEM resulting in the photomicrographs shown in figures 5-8. A wide crystallite size distribution is seen for all four



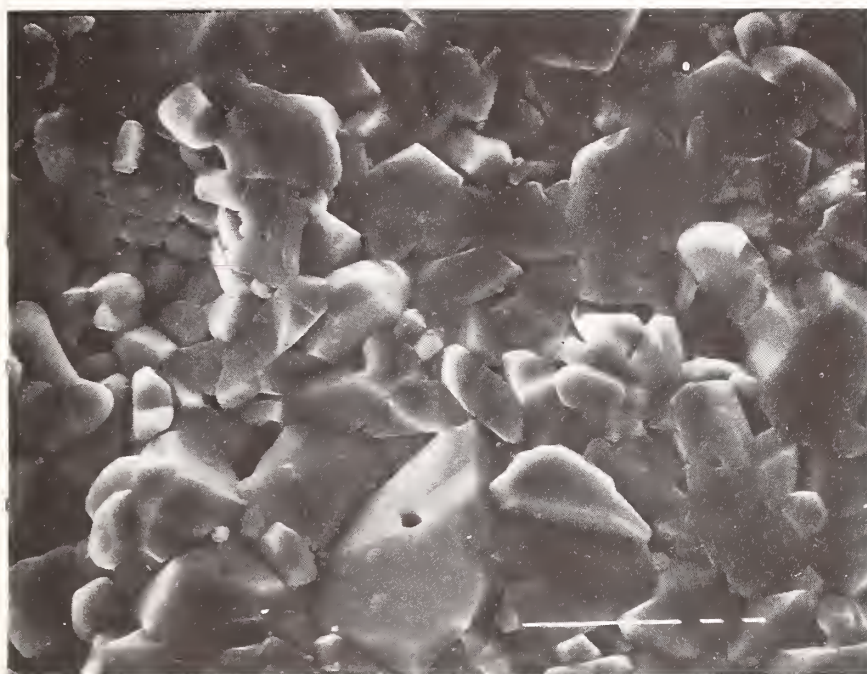


Figure 5. SEM Photomicrograph of Fracture Surface of Cer 004 Alumina - 2000X



Figure 6. SEM Photomicrograph of Fracture Surface of Cer 005 Alumina - 1000X



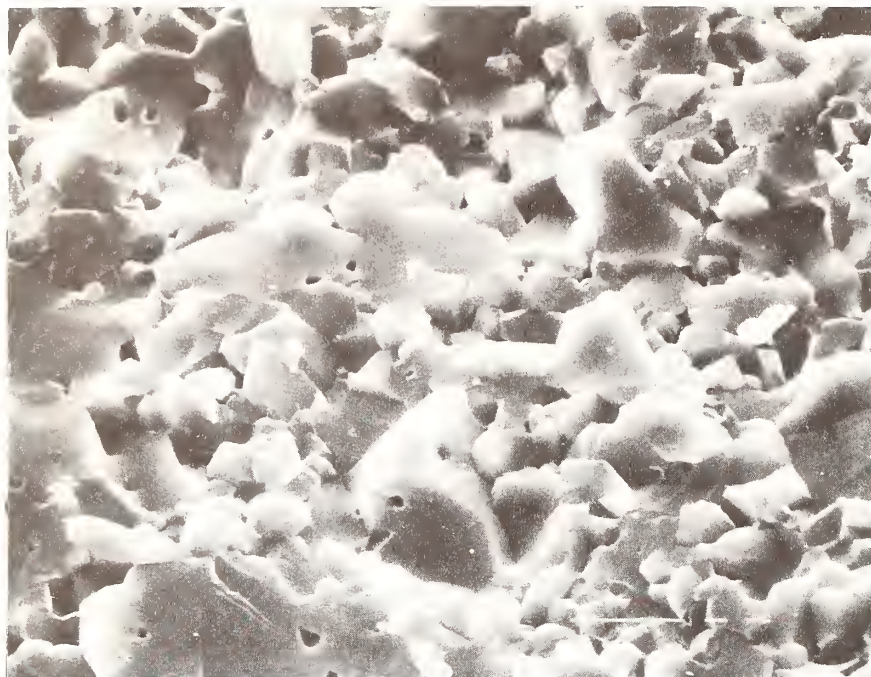


Figure 7. SEM Photomicrograph of Fracture Surface of Cer 006  
Alumina - 1500X

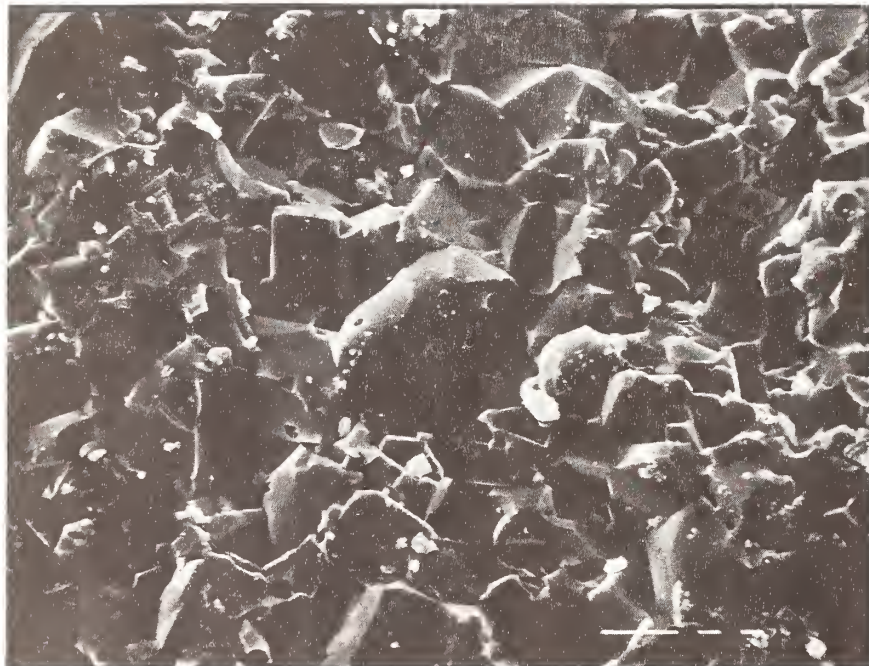


Figure 8. SEM Photomicrograph of Fracture Surface of Cer 021  
Alumina - 1000X

samples with a range of approximately 1 to 20  $\mu\text{m}$ . Grains appear to be approximately equiaxial, and small ( $\approx 1 \mu\text{m}$ ) pores can be seen within some of the crystallites.

Ceramography consists of cutting a section through a specimen and polishing the cut surface with successively finer diamond polishing compounds to reveal microstructural detail. Optical microscopy and SEM are the most frequent analysis tools. In many cases chemical or thermal etching is used to highlight the microstructure.

SEM photomicrographs of the polished surfaces (figs. 9-12) reveal the porosity of the surface. Samples Cer 005 and Cer 021 both appear to have a similar porosity. Both large ( $\approx 20 \mu\text{m}$ ) and small ( $1\text{-}5 \mu\text{m}$ ) pores are observed. Sample Cer 004 also shows approximately the same bimodal distribution of pore size. Sample Cer 004 however appears to have more of the smaller pores than Cer 005 and Cer 021. Sample Cer 006 appears to have a single small pore size distribution with pores ranging from 0.5 to 8  $\mu\text{m}$ . In addition, the number of pores is much higher than that observed for any of the other samples. The SEM observations of the pores seems to agree quite well with the calculated porosity for the different samples presented in table 5.

Polished samples were thermally etched at 1450°C for 5-10 minutes to reveal the grain boundaries. This technique, suggested in a phone conversation with a researcher at Adolph Coors Company,<sup>30</sup> was claimed to introduce no cracking or grain growth within their high alumina

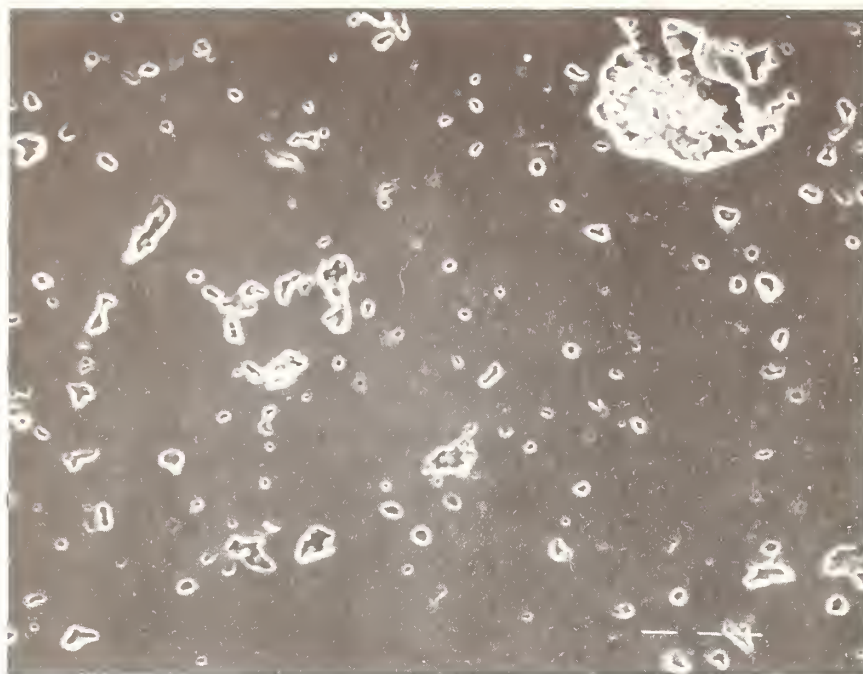


Figure 9. SEM Photomicrograph of Polished Surface of Cer 004 Alumina - 500X

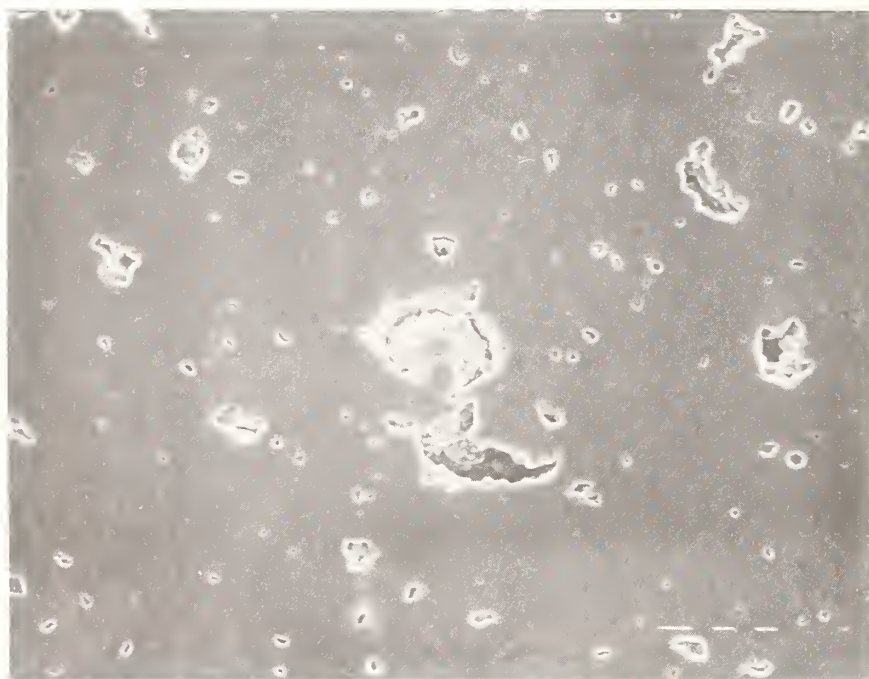


Figure 10. SEM Photomicrograph of Polished Surface of Cer 005 Alumina - 500X





Figure 11. SEM Photomicrograph of Polished Surface of Cer 006 Alumina - 500X

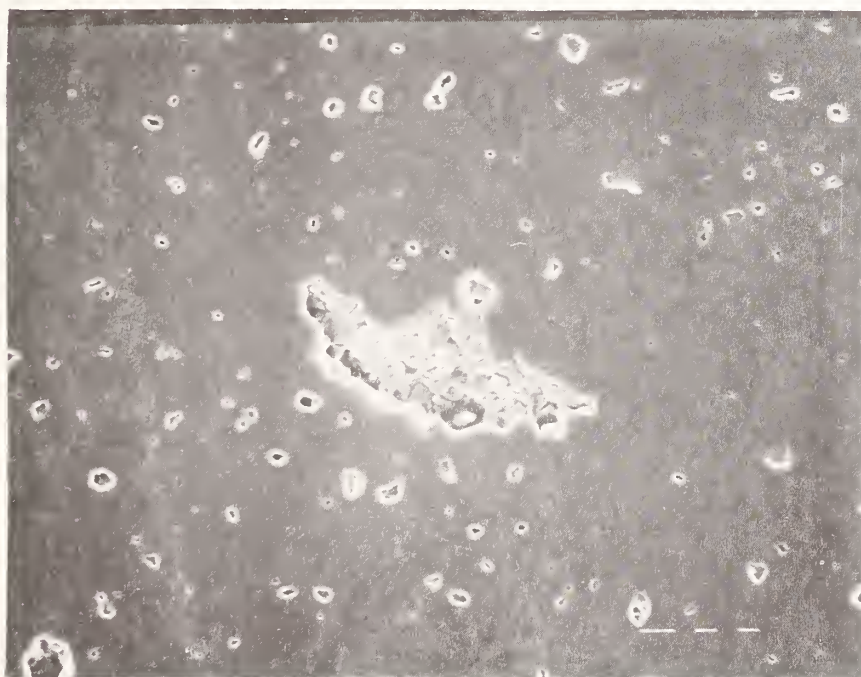


Figure 12. SEM Photomicrograph of Polished Surface of Cer 021 Alumina - 500X

Table 5

Summary of Selected Characterization Data on the  
Alumina Ceramics Used in This Study

Sample	Approximate Crystallite Size Observed			
	Fracture Surfaces	Polished/ Etched Surfaces	% Theoretical Density <sup>(1)</sup>	Porosity <sup>(2)</sup>
Cer 004	1-10 $\mu\text{m}$	0.5-10 $\mu\text{m}$	96.4	3.6
Cer 005	1-20 $\mu\text{m}$	0.5-15 $\mu\text{m}$	97.8	2.2
Cer 006	1-10 $\mu\text{m}$	0.5-10 $\mu\text{m}$	96.2	3.8
Cer 021	3-15 $\mu\text{m}$	1-10 $\mu\text{m}$	98.5	1.5

<sup>(1)</sup> Measured via mass and volume calculations except for Cer 006 which was supplied by the supplier literature.

<sup>(2)</sup> 100% - theoretical density.

samples. SEM photomicrographs of these surfaces show the individual crystallites defined by their grain boundaries (figs. 13-16). For these particular photomicrographs, regions were selected away from larger pores in order to examine the cross sectional grain boundary pattern. In all the photographs, a wide distribution of grain sizes is observed. Both intracrystalline and intercrystalline pores are observed. (Some of these intercrystalline pores may be due to pullout of parts of grains during the polishing process.) Cer 004 has individual crystallites ranging from approximately 0.5 to 10  $\mu\text{m}$ . Cer 005 has crystallites ranging from approximately 0.5 to 15  $\mu\text{m}$ ; Cer 006 from 0.5 to 10  $\mu\text{m}$ ; and Cer 021 from 1 to 10  $\mu\text{m}$ . The tracks observed going through the crystallites are residual polishing marks. SEM photomicrograph observations from the polished-etched, and fractured samples are summarized in table 5. The crystallite size information from the fracture and polished/etched samples seem to give similar information, and indicate subtle differences in microstructure for the different batches of alumina. Samples Cer 005 and Cer 021 appear to be slightly coarser grained than the other two samples. They also appear to be slight more dense. This agrees well with our understanding of the sintering process where during the high temperatures encountered, grain growth occurs, resulting in larger grains<sup>31</sup> (and lower final porosity).



Figure 13. SEM Photomicrograph of Polished/Etched Surface of Cer 004 Alumina - 5000X

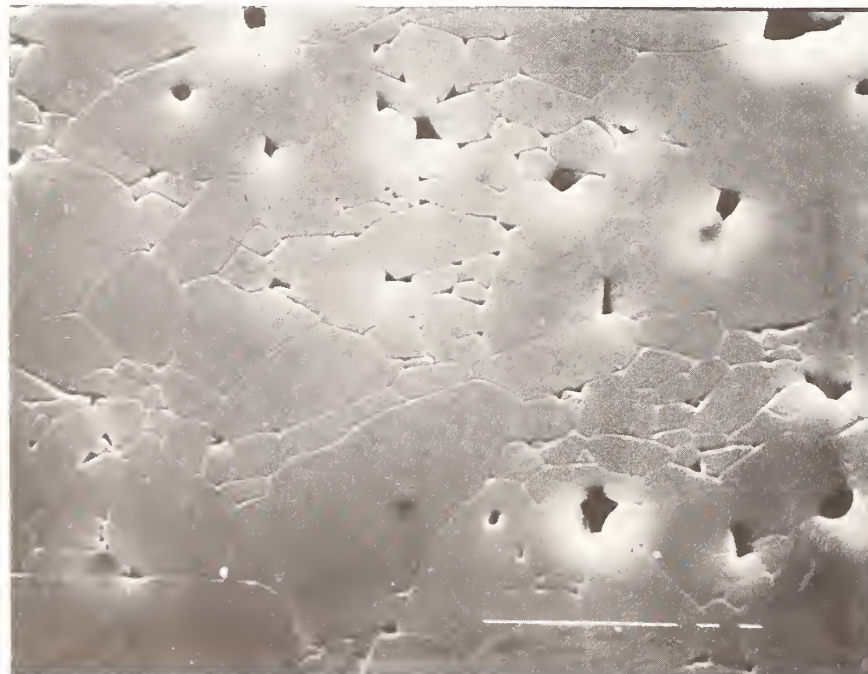


Figure 14. SEM Photomicrograph of Polished/Etched Surface of Cer 005 Alumina - 5000X



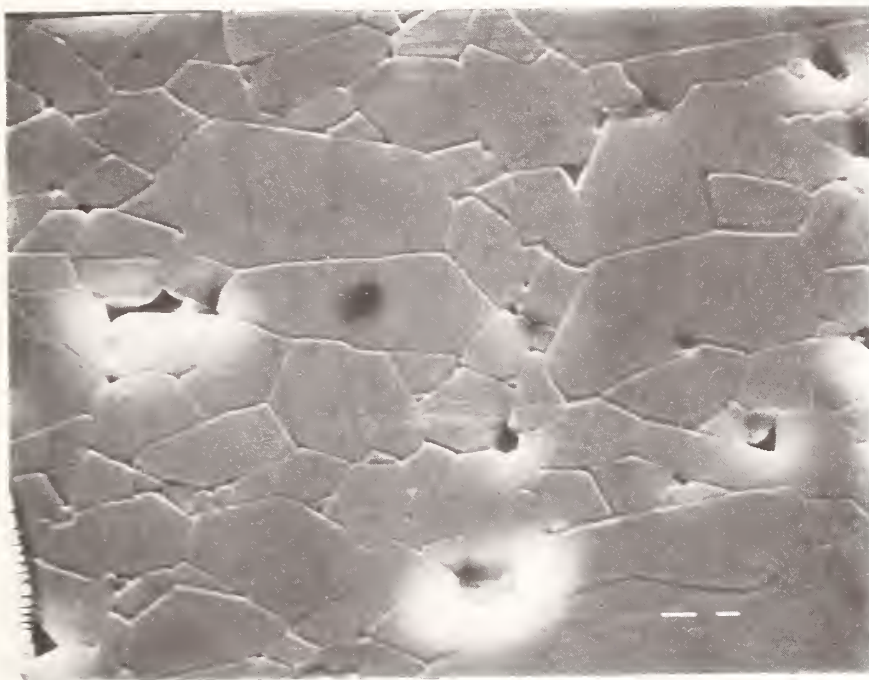


Figure 15. SEM Photomicrograph of Polished/Etched Surface of Cer 006 Alumina - 5000X

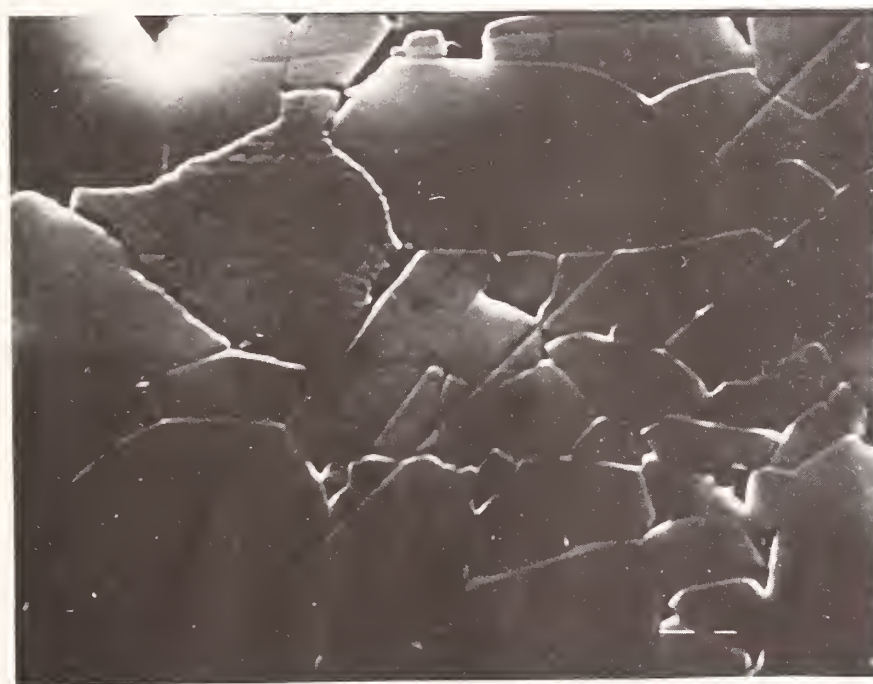


Figure 16. SEM Photomicrograph of Polished/Etched Surface of Cer 021 Alumina - 5000X

### E. Friction and Wear Measurement

As mentioned previously, friction is continuously recorded during a test via an electronic force transducer. The paper output of the strip chart gives a history of friction throughout the test. Coefficient of friction can be calculated for any test where both the friction and applied load are known, given the equation derived in Appendix B.

$$\mu = \frac{0.02339 \text{ } f}{L}$$

where  $f$  = measured friction force in grams,

$L$  = applied 4 ball machine load in  $\text{kg}_f$ , and

$\mu$  = coefficient of friction.

Wear can be measured in a variety of ways; however, for the purposes of our tests two principal methods were used: weight loss and wear scar diameter. The weight loss method requires careful weighing of specimens before and after a test using a semimicrobalance with a repeatability of  $\pm 0.03$  mg for a single measurement. This method works quite well for tests in which wear is fairly severe resulting in substantial weight loss; however, it is not adequate for tests with low wear. In addition, this method has the advantage that both upper and lower wear is measured and therefore the degree of asymmetric wear can be observed.

The second technique for wear measurement, the wear scar diameter measurement, consists of locating and measuring the scar under an optical microscope fitted with a graduated reticle eyepiece. The wear scar is usually oriented under the objective lens such that the direction of sliding is horizontal (i.e., from left to right). Both horizontal (left to right) and vertical (top to bottom) wear scar measurements are recorded for each scar. The geometric average of the two measurements  $[ab]^{1/2}$  on each scar are calculated and the arithmetic average of the three scar values is taken as the diameter (or equivalent diameter) of the wear scar. The equivalent diameter, based on geometric value, was used because it was felt that this was a more accurate representation of wear for our testing where elliptically shaped wear scars were the rule rather than the exception. Derivation of the equivalent diameter concept for a wear scar is given in Appendix C. This technique also has the advantage that if the wear scar is circular, the arithmetic average and geometric average of the two measurements are the same. Therefore, taking the geometric average merely extends the accuracy of wear scar measurement representation to the elliptically shaped wear scar regime.

Optical wear scar measurement has an advantage over weight loss measurement in its ability to accurately reflect very low levels of wear. The optical technique is capable of measuring as little as 0.1 mm diameter wear scars (although locating these wear scars is often a tedious search). This would represent a weight loss of approximately

0.015  $\mu\text{g}$  of material (in the case of alumina), which is far less than we can accurately weigh. Figure 17 compares the two wear measurement methods used in terms of their useful ranges. In general optical wear scar measurement is accurate in the range of 0.1 mm to 5.0 mm. The lower limit is imposed from the resolution of the microscope measurement system and increasing difficulty in locating these size scars. The upper limit is due to the fact that very large wear scars tend to be highly irregular in shape (approaching teardrop shapes) and the wear scar diameter fails to accurately reflect wear in a meaningful way. Weight loss measurements are accurate from approximately 0.8 mm wear scar diameters and above. The lower limit is imposed by the accuracy and repeatability of weight loss measurement. This is caused by a combination of factors including balance sensitivity but is mostly due to the repeatability of sample cleaning and handling procedures.

#### F. Specimen Preparation

Ball specimens were received in a finished state and required only solvent cleaning prior to testing. Flat specimens 6.35 mm (0.25 in) in diameter and 1.59 mm (0.0625 in) thick were cut (oversized in thickness) from rod stock using a slow speed, low deformation, diamond saw. They were polished using 240 grit then 11-14  $\mu\text{m}$  bonded diamond abrasives followed by a series of successively smaller grain size diamond polishing pastes of 6, 3, and 1 micron.

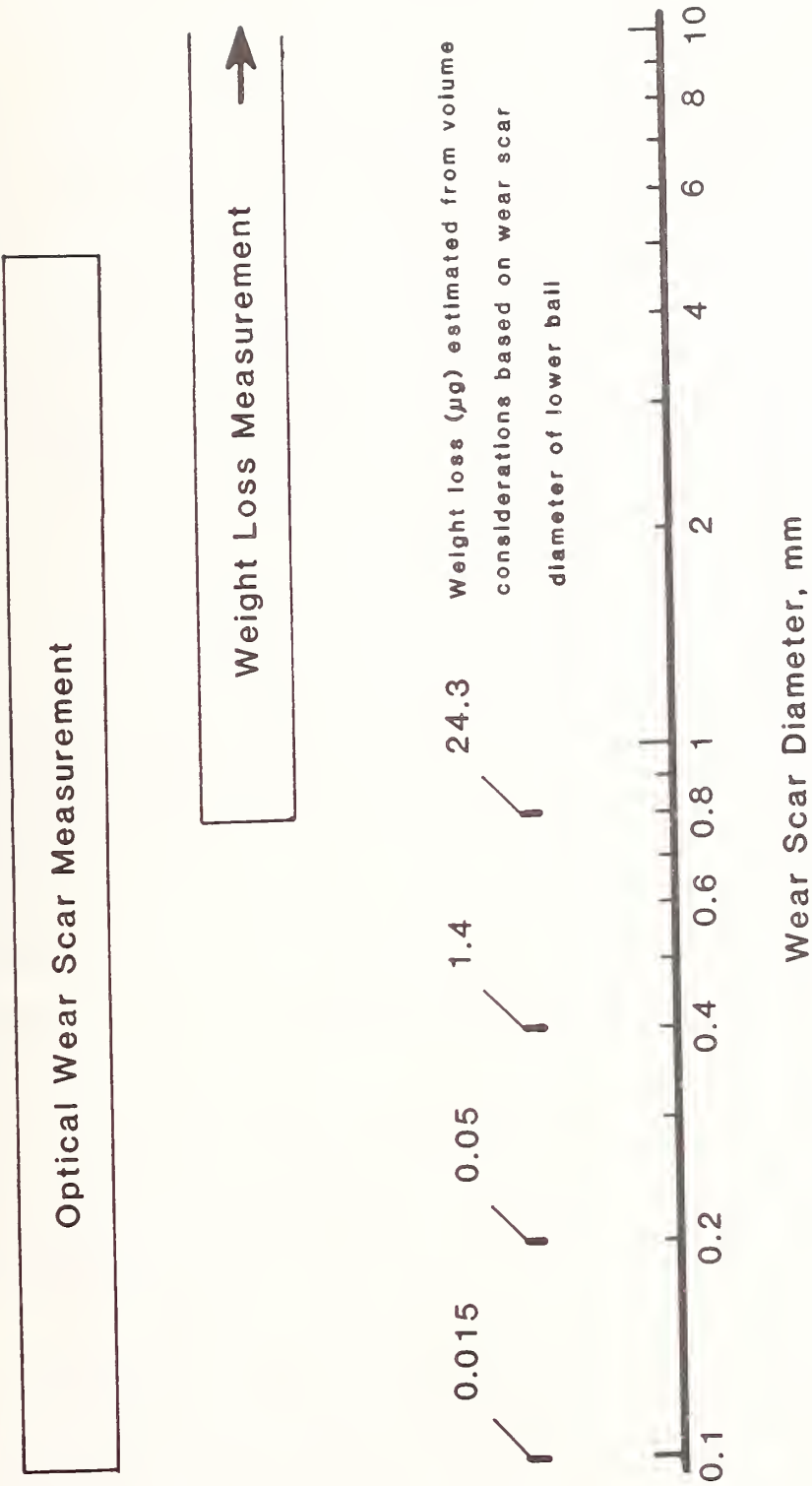


Figure 17. Comparison of Applicable Ranges for Optical and Weight Loss Measurement Techniques

This resulted in specimens of desired thickness with a surface roughness of approximately  $0.04\text{ }\mu\text{m}$  ( $1.6\text{ }\mu\text{in}$ ) AA.

Just prior to testing, the specimens were cleaned in a series of solvents to remove residual cutting and polishing oils, fingerprint oils, and a variety of other possible contaminants. The complete cleaning procedure, described in more detail in Appendix D consisted of a series of ultrasonically agitated rinses in hexane/toluene (9:1), hexane, and acetone, followed by drying in a stream of nitrogen gas. This produced a clean surface which gave adequate repeatability for most of the tests. In the special case of dry tests, it was found that trace impurities in the acetone (probably water) remained on the surface and reduced friction and wear for very low load tests. This effect was corrected by heating the test cup under argon atmosphere to  $110^{\circ}\text{C}$  for 10 minutes to drive off the water then cooling it back down before commencing the test.

#### G. Operating Procedure Descriptions

Two operating procedures were used for this study; one for constant condition tests (CCT's) and one for step-loading tests (SLT's). In addition, the procedures are slightly different depending on whether four-ball (FB) or ball-on-three-flat (BTF) wear tests are being conducted. For constant condition four-ball tests the specimens and test parts that come in contact with the specimens or the lubricants are cleaned with solvents. After drying with nitrogen gas,



the three lower specimens are positioned in the test cup and secured in place with a locking ring. The upper rotating ball is pressed into the ball chuck, and the ball-chuck assembly is secured onto the end of the spindle. Ten milliliters of lubricant are placed in the lower specimen holder and the assembly placed on the heater/air bearing. The air bearing valve is adjusted to give lift to the air bearing and the load is adjusted to zero to just support the weight of the entire heater/air bearing, test cup assembly. This assembly is carefully slid upwards until the upper and lower specimens just contact each other.

The friction force measuring chain is connected to the specimen cup and the test cup is then balanced such that no force is exerted on the electronic force transducer. This balancing step is necessary to ensure the accuracy of the friction measurement at low loads. If the test is being conducted at temperatures above ambient, the heater and temperature controller are engaged. The timer is set to the desired time, the load is applied, and the test commences when the desired test temperature is reached. At the end of the test, the upper specimen stops rotating, the load is removed, and the test cup and upper specimen assemblies are removed and disassembled for post test specimen analysis.

Step-loading tests are conducted in a similar fashion except that after a test segment is conducted at a particular load, the lower specimen assembly is removed from the heater/air bearing. The



lubricant is removed and the surfaces of the wear scar gently wiped with a cotton swab moistened with hexane if a hydrocarbon lubricant was used. The scars are then measured with the lower specimens still locked in place, using an optical microscope. New lubricant is added to the test cup, the assembly is put back on the heater/air bearing and balanced. The new load is applied and the next segment of the test is conducted. This cycle continues until the desired maximum load is completed.

The procedures for ball-on-three-flat tests are similar to the four-ball tests except only one and a half milliliters of lubricant are required. In order to ensure re-alignment of the specimens for the step-loading ball-on-three-flat tests, double sided adhesive tape is used to prevent the lower specimens from moving during handling for wear scar measurements. The tape is applied as a thin (0.075 mm) backing to the specimens and secures them to the bottom of the holder recesses.

## Chapter IV

## RESULTS AND DISCUSSION

A. Constant Condition Four-Ball Wear Testing Study1. Base Conditions

Ceramic wear test parametric studies were conducted by selecting a set of base conditions and adjusting each parameter individually and noting the effect. The initial base set of conditions selected were:

Speed:	600 rpm (23 cm/s)
Load:	20 kg
Temperature:	Ambient (21°C)
Duration:	10 minutes
Lubricant:	10 ml Purified Paraffin Oil, Water, or unlubricated (dry)
Atmosphere:	0.25 l/min dry Air
Material:	Alumina Ceramic Cer 004

These values of speed and load represent conditions intermediate to the capabilities of the equipment (speed range: 0.6 - 10,000 rpm; load range: 0.5 - 300 kg) that are well into the boundary lubrication regime. These conditions produced wear scars of 3.16 mm for the dry case, 1.70 mm for the paraffin oil lubricated case, and 1.01 mm for the water lubricated case. Thus a ranking of wear for these conditions is: Dry > Paraffin Oil lubricated > Water lubricated.

Coefficient of friction values for these tests produce a different ranking however: Dry (0.64) > Water lubricated (0.29) > Paraffin Oil lubricated (0.12). As a point of reference, these values can be compared to results obtained for paraffin oil lubricated tests using 52100 steel specimens: Wear Scar = 0.34 mm, Coefficient of Friction = 0.085. At first it seems that the steel is far superior to the alumina under the same test severity however it will be shown that the same applied wear test conditions lead to different actual test severities when ceramic specimens are used.

## 2. Explanation of Severity Differences Between Steel and Ceramic Tests Conducted at the Same Operating Conditions

Tests run on different materials (ceramics vs metals) on the four-ball wear test under identical machine test conditions (speed, applied load, temperature) actually run under different test severity. This is because severity is also a function of material parameters and ceramics have very different properties than metals. More specifically, the severity is different for conditions of actual load (pressure) experienced by the surface in contact, and also for conditions of temperature.

In the case of pressure in the contact, we must look at the geometry of the contact and how it is influenced by material parameters. As shown before, the general geometry of the four-ball contacts provide a distribution of force based on the applied load of

$N = 0.408 L$ , where  $L$  is the applied load in kilograms, and  $N$  is the normal load on the surface of a single ball in kilograms. This is entirely based on geometry, and material parameters play no part. Material parameters do play a part in how this normal load is applied to the surface. The general contact geometry for a single contact is convex surface on convex surface. As a load is applied, these surfaces press together deforming and providing a contact surface (disc) which carries the load. The diameter of this disc is a function of the applied load, the radii of the contacting surfaces, and two material properties: Poisson's ratio and Young's modulus. This relationship is described in the Hertz equation given in Appendix H; however, in general, the diameter increases with decreasing Young's modulus and Poisson's ratio. Poisson's ratio is the ratio of the thickness decrease to the length increase (per unit width and length) when a material is extended in tension.

$$\nu = \frac{\Delta d/d}{\Delta \ell/\ell}$$

where  $\nu$  = Poisson's ratio. Young's modulus is the proportionality constant between stress (normal tensile) and strain in Hooke's law

$$\sigma = E\epsilon$$

where  $\sigma$  is the normal stress,  $E$  is Young's modulus, and  $\epsilon$  is the normal strain. The basic result of these material parameters on the Hertz contact diameter is that harder materials deform less under

stress and produce higher contact pressures. A graph of calculated maximum contact pressures (from Appendix H) for alumina and 52100 steel are given in figure 18. They show that assuming elastic contact, the maximum contact pressures for alumina are 50% higher than steel given the same applied load. The pressure provided by steel at twenty kilogram load is experienced by alumina at a bit less than six kilograms. These calculations should not be taken too literally in the sense that the assumption that alumina will behave elastically at 40 kg (750 kpsia) is not realistic. (The compressive strength of alumina at room temperature is approximately 300 kpsia.) However, this example serves as a caution that the contact severities for alumina are higher because of its material properties.

The second severity parameter that may be different for different material is temperature. During a wear test, friction in the contact junction generates heat and raises the local temperature. This heat dissipates into the lubricant and specimens and eventually an equilibrium is established between rate of heat generation and dissipation. The result is a steady state local temperature higher than the ambient temperature of the test. Materials with lower thermal conductivity do not allow heat to dissipate as rapidly and give higher local temperatures. The difference in thermal conductivity and thermal diffusivity between ceramics and metals provide higher local contact temperatures for ceramics under the same test conditions. A recent study by Munro<sup>32</sup> which modeled the temperature distribution within test specimens of the four-ball wear

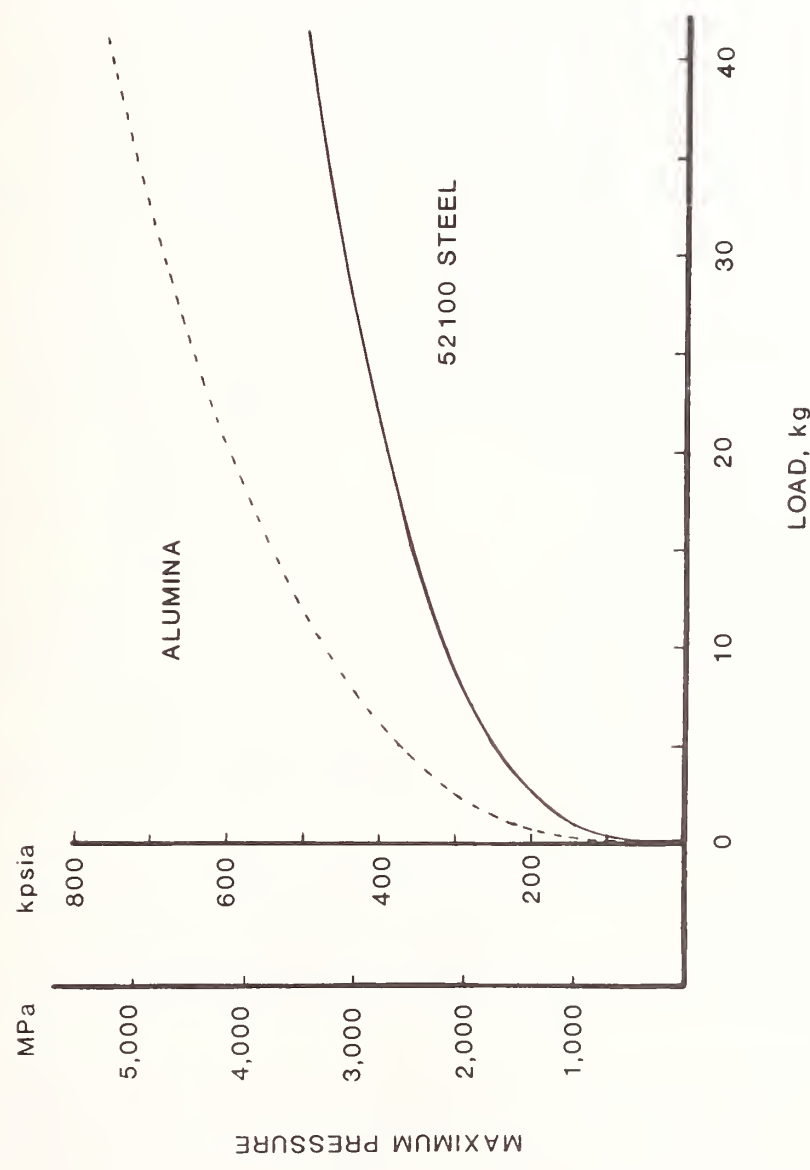


Figure 18. Comparison of Hertzian Contact Pressure for 52100 Steel versus Alumina

test predicted very different temperatures for alumina specimens versus 52100 steel specimens. Under conditions of 500 rpm, 40 kg load, and coefficient of friction of 0.075 (lubricated) temperatures of  $\approx 160^{\circ}\text{C}$  were predicted for the contact junction using steel specimens. Temperatures of  $\approx 400^{\circ}\text{C}$  were predicted for alumina - a difference of  $240^{\circ}\text{C}$ . In addition, thermal gradients in the alumina were much sharper. The absolute values for the temperatures obtained in his study are of course a function of the conditions he selected (friction coefficient, convective heat loss values, etc.). The conclusion he reached, that thermal conductivity of test specimens has a profound effect on contact temperatures, is still valid. Thus higher temperature results in a higher thermal severity for alumina specimens run under the exact same applied test conditions as 52100 steel.

These two examples of contact pressure and temperature differences between alumina and steel specimens illustrate the need to understand the actual contact severity conditions, not just the applied test conditions. Therefore, data interpretation should take these factors into account.

### 3. Four-Ball Constant Condition Test: Effect of Test Duration

In general, a wear test can be composed of three different wear regimes as shown in figure 19. Initially, very high wear rates (Part I) are observed as the surfaces wear-in to adjust to the test

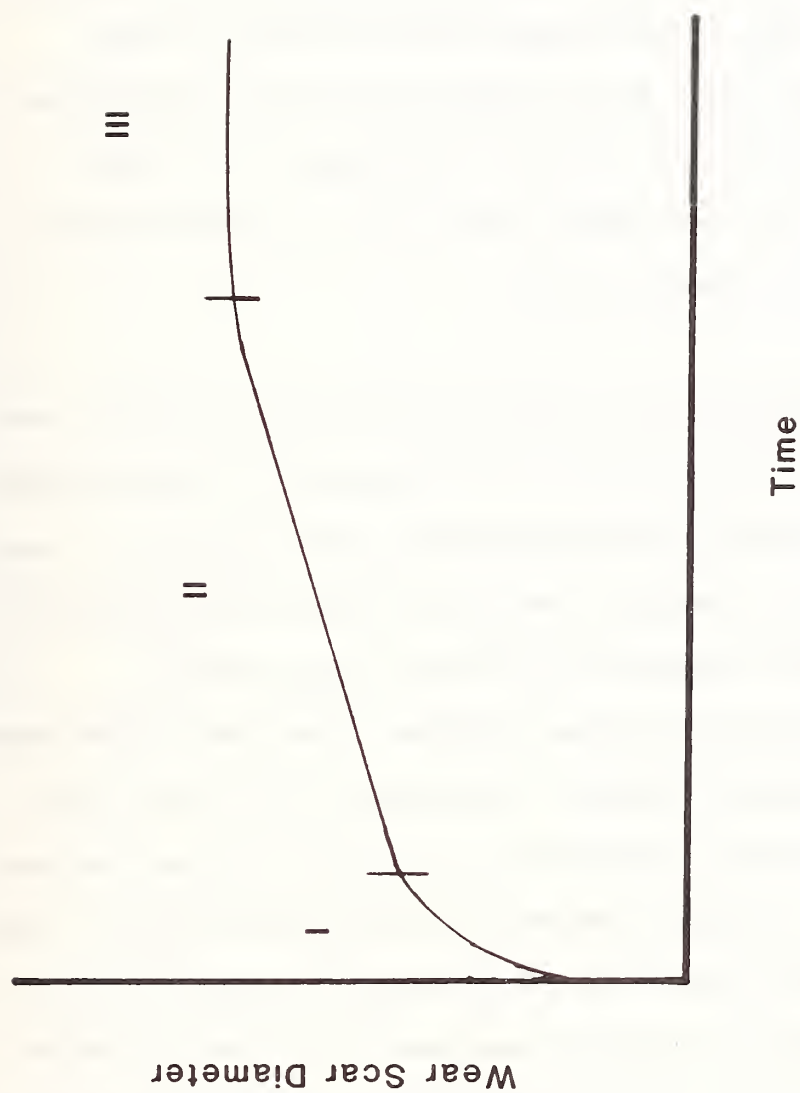


Figure 19. Typical Wear Regimes for a Wear Test



conditions. This wear-in phase of a test is usually fairly severe and can be very unpredictable especially with regard to friction.<sup>33</sup> Reproducibility of test results in this regime are usually poor. Eventually, a condition can be reached in which wear rates are relatively constant with time. This is the steady state wear regime (Part II). Eventually, a third regime may be reached in which essentially no wear occurs as the surfaces are so well worn in that hydrodynamic lubrication can separate the surfaces. It is also possible to switch to a new steady state wear rate (either lower or higher) at any point during the test.

Tests were conducted using alumina under unlubricated (dry) and paraffin oil lubricated conditions to see the effect of test duration on wear. This was done to ensure that later tests would be run long enough to allow them to progress beyond the severe wear-in regime of the test. Tests were conducted at 600 rpm, 20 kg, ambient temperature, using Cer 004 alumina specimens. Wear results from these tests (fig. 20) indicate different wear behavior for the two cases. Paraffin oil starts with a moderate wear scar of 1.17 mm at 1 minute and increases in a nonlinear fashion up to 10 minutes duration. After ten minutes, the wear rate (slope of line) drops to near zero. The dry tests also start at a moderate wear scar of 1.40 mm at 1 minute. However, the wear rate is more rapid than the paraffin oil lubricated case. After ten minutes, the wear rate drops considerably to a much lower value. The accompanying final coefficient of friction data for these tests (fig. 21) show a tremendous difference between the two

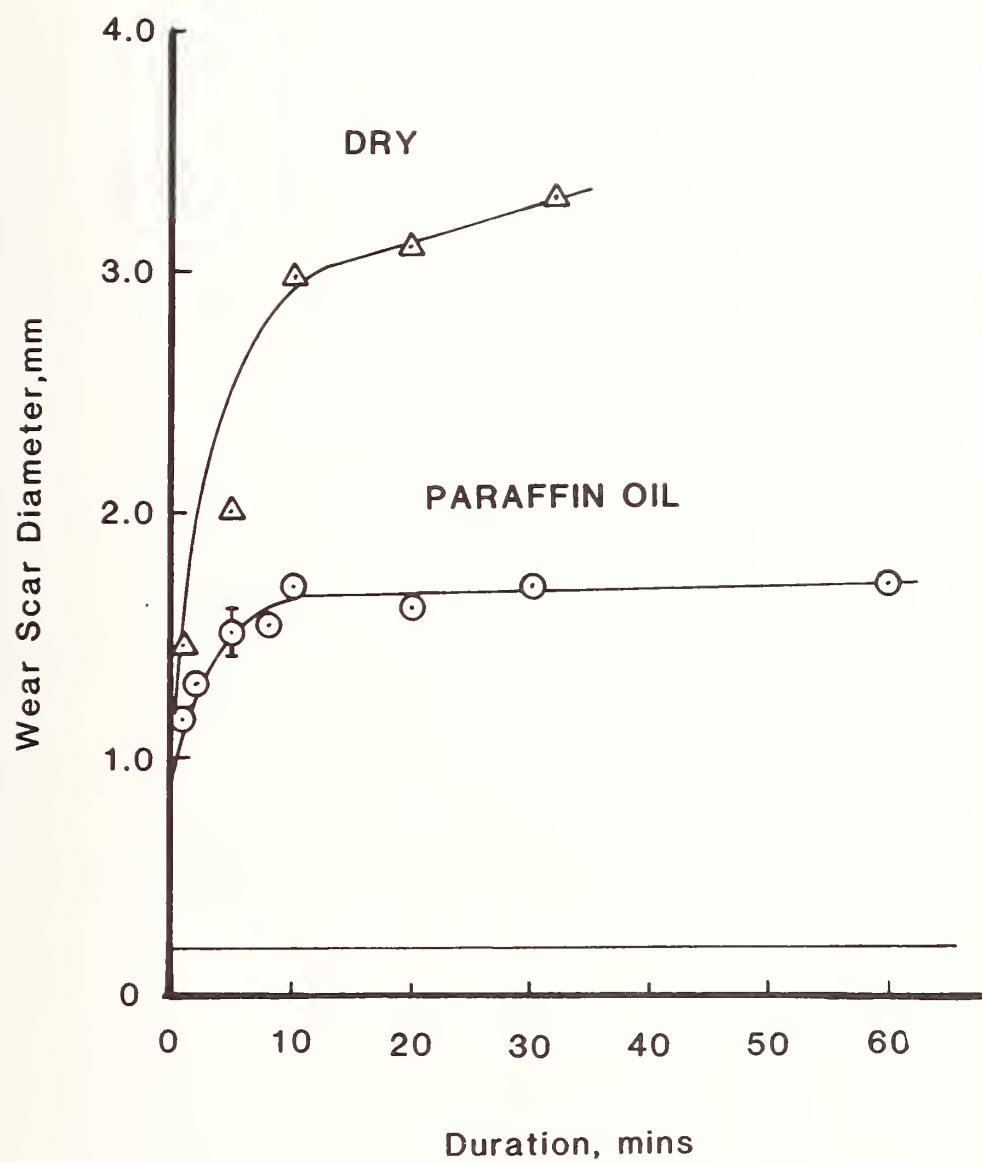


Figure 20. Wear-in Behavior of Alumina under Unlubricated and Paraffin Oil Lubricated Conditions

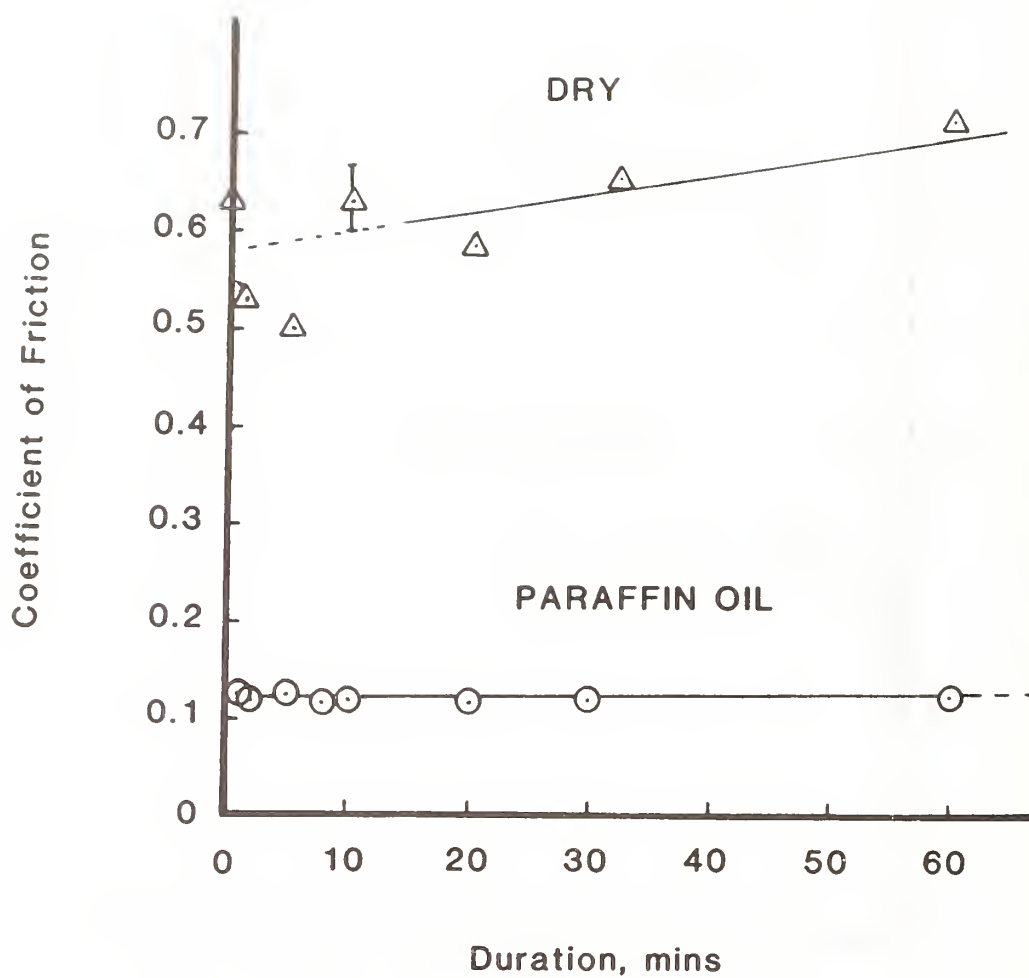


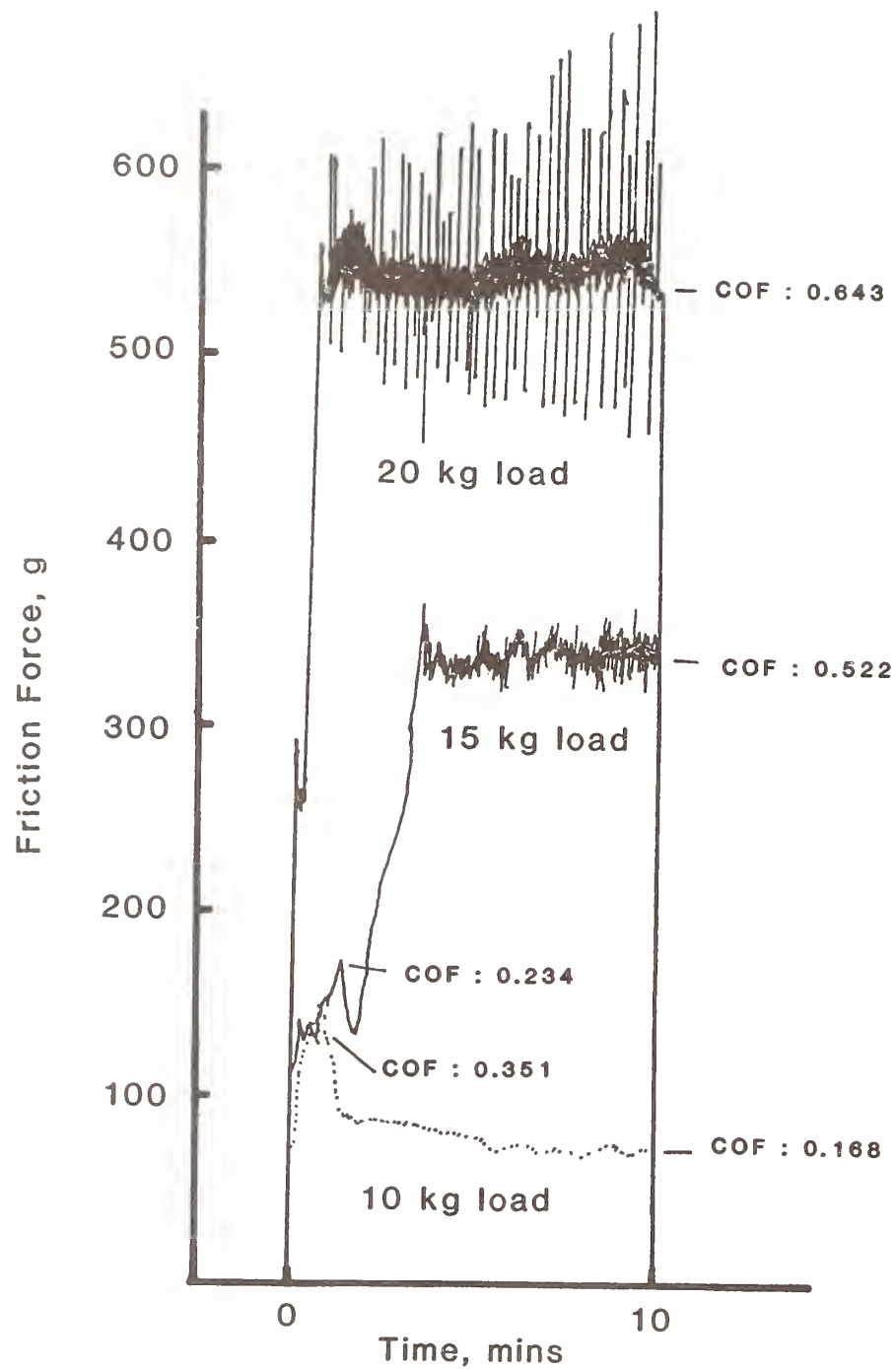
Figure 21. Friction Behavior of Alumina under Unlubricated and Paraffin Oil Lubricated Conditions

cases. The paraffin oil lubricated tests all have very low coefficient of friction values (0.123) even for the high wear rate wear-in regime. Repeatability of the friction measurement is good ( $\pm 0.009$ ). The unlubricated tests have a much poorer repeatability ( $\pm 0.035$ ). They also show a distinctly higher level of friction ( $\mu = 0.64$ ) than for the paraffin oil lubricated case. In addition there appears to be a slight rise in coefficient of friction with time. Based on the results of these tests, a duration of ten minutes was selected for subsequent tests. This duration allows the test to complete the more severe wear-in phase of the test thus increasing the repeatability. Tests longer than ten minutes only serve to lengthen the time required for each test and do not appear to give any additional information or better repeatability. This is especially true for the paraffin oil lubricated case which has a very low wear rate after ten minutes.

#### 4. Four-Ball Constant Condition Test: Effect of Load

Once the proper duration was selected, the next step was to see the effect of load on wear and friction. Constant condition tests were conducted at various loads and friction and wear values at the end of the test were recorded.

Dry tests at different loads showed unusual friction behavior. A comparison of friction traces from test at three different loads is shown in figure 22. Loads of 20 kg or greater display the functional



Conditions : 600 rpm, 0.25 l/min dry air, 10 min duration, alumina specimens

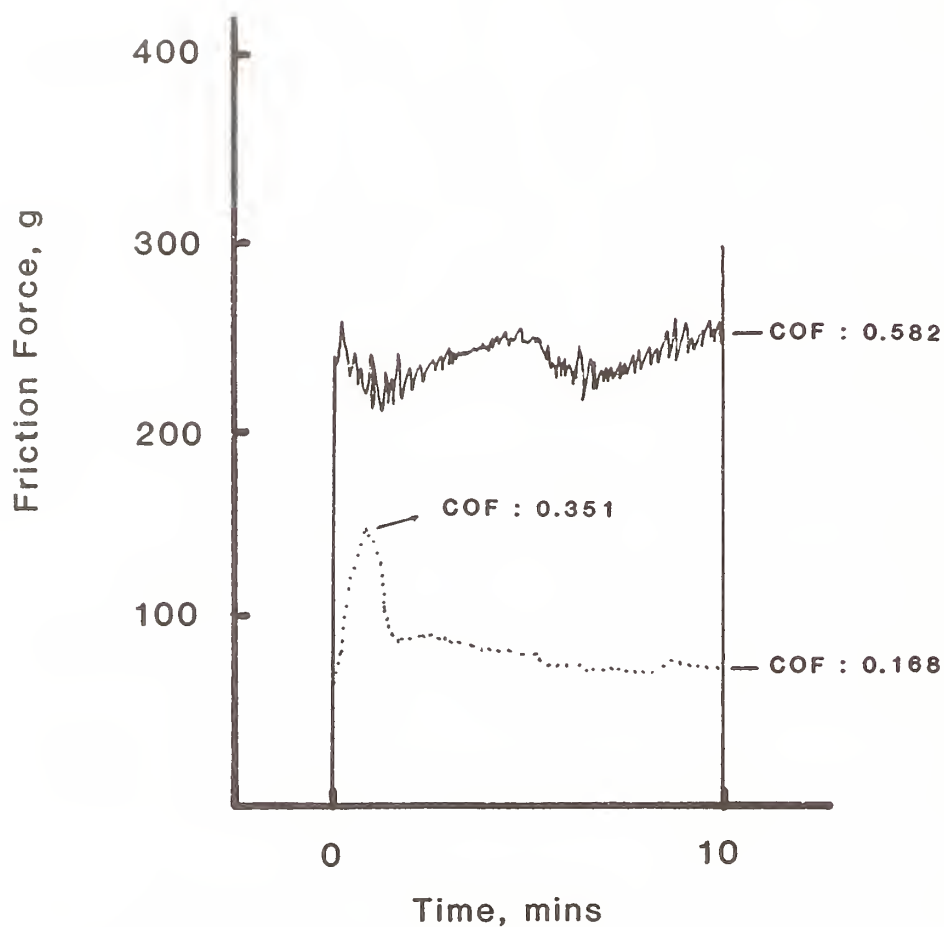
Figure 22. Change in Friction Behavior with Time for Unlubricated Alumina Tests at Different Loads

behavior shown in the upper friction trace. The coefficient of friction is very high (0.65) from the very beginning of the test to the very end. The friction trace is very rough and spiky, indicating the severity of the wear process. These tests were also accompanied by a combination of grinding and squeaking sounds from the test cup. A test conducted at 15 kg starts out with a low coefficient of friction (0.234) but during the course of the test, jumps to a higher level of friction ( $\mu = 0.522$ ). There appeared to be something protecting the surface during the initial stages of the test that produced low friction. A test at low load (10 kg) produced a low level of friction which continued until the end of the test ( $\mu = 0.168$ ). The difference between the three tests was the severity of the load. This has a direct bearing on the temperature in the contact junction during a test since the temperature is proportional to load.<sup>34</sup> This data therefore suggests that a surface contaminant was present on the surface of the specimens after the cleaning procedure. It may have been some kind of hydrocarbon impurity left over from the cleaning solvents, hydrocarbons from the air in the lab, or water from the solvents or lab atmosphere. These contaminants were able to protect the surface during the low temperature low load tests. At high loads, temperatures generated by friction are sufficient to remove the contaminant from the surface, increasing the friction level. This hypothesis was checked by repeating the ten kilogram test with a procedural modification (fig. 23). In this test, just prior to testing, the test cup was heated to 150°C for ten minutes under a flow of argon. The specimens were then cooled (still under a flow of



Upper Trace : Specimens heated to remove contaminants

Lower Trace : No pre-heat treatment



Conditions : 600 rpm, 10 kg, 0.25 l/min dry air,  
10 min duration, alumina specimens

Figure 23. Comparison of Friction Behavior with Time for Unlubricated Alumina Tests with and without Heating Pretreatment

argon) until they reached room temperature. The test was then started and run under dry air and the friction recorded. As can be seen in figure 23, the coefficient of friction immediately rose to a level of 0.58 and stayed there throughout the test, indicating complete removal of the contaminant by the heating procedure.

The friction and wear behavior of alumina was determined for several loads under unlubricated, water lubricated, and paraffin oil lubricated conditions. No unlubricated runs were conducted at loads less than ten kilograms due to an instability of the wear test apparatus under these conditions. Attempts to conduct tests at two and five kilograms resulted in severe excessive vibration of the entire test cup assembly. Apparently the vibration induced by wear at these loads coupled with the inherent stiffness and mass of the test assembly set up a resonant frequency response. Attempts to mitigate this problem by adjusting the stiffness and mass of the test assembly met with very limited success. This instability was not observed for the lubricated runs at any load, nor for any of the unlubricated runs at higher loads.

Wear results for the unlubricated and lubricated tests are given in figure 24. This data is plotted as log wear scar diameter versus log load as is the usual procedure for four ball testing. This convention is followed for several reasons. 1) Scales are compressed and allow concise plotting of a wide range of data. 2) The relationship between Hertzian wear scar diameter and load is a

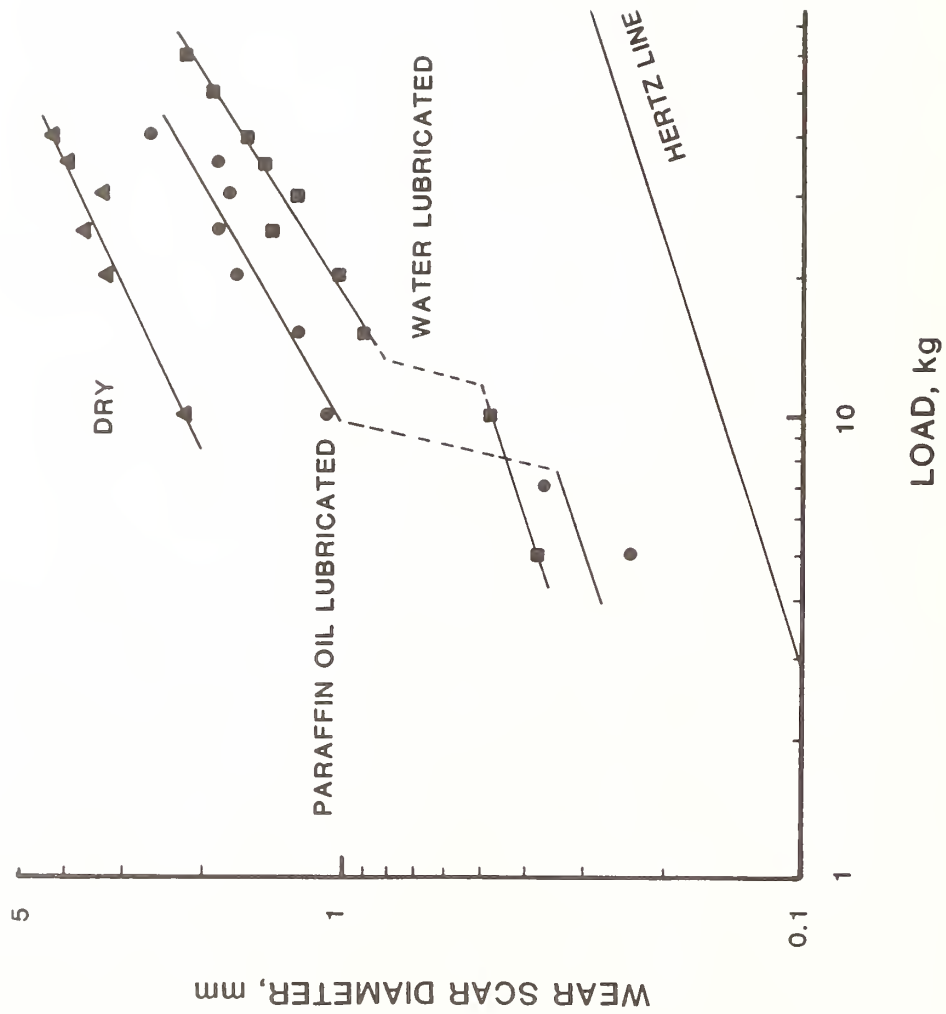


Figure 24. Comparison of Wear as a Function of Load for Unlubricated, Paraffin Oil Lubricated, and Water-Lubricated Alumina Constant Condition Tests

straight line of slope  $1/3$  when plotted log/log (Appendix H). This serves as a good reference point for the data since the Hertzian wear scar diameter represents a minimum wear value at the specified load.

3) Data plotted in this fashion tend to fall on straight lines.

#### B. Wear Test Severity Overlay

During the course of this study it was found that a new method of describing the relative severity of a test was needed. This was because comparisons of data (wear scar diameter) were being made at different loads. One solution was to define the severity at the end of a test by the mean pressure produced in the contact junction. The mean pressure is merely the normal force at the contact divided by the area of the wear scar. This offers an easy method for comparing test results since a lubricant/material combination which can sustain a load of 50,000 psi would be better than one that causes more wear and produces a larger wear scar such that the mean pressure drops to 10,000 psi. The relationship between wear scar diameter, load, and pressure is such that a plot of log wear scar diameter versus load will yield straight lines of constant mean pressure. An overlay (transparency) can therefore be easily fabricated to determine the mean pressure for a given load and wear scar size. Two test severity figures are included in Appendix J and K of this report (J is in psi, K is in MPa). Transparencies can be made from these figures and used as overlays to estimate mean pressures for any of the log wear scar diameter vs log load plots. The sizes of all log/log plots of wear

scar diameter versus load have been standardized to allow easy determination of mean pressures of the different phases of each test using the overlays.

Figure 24 shows a large difference in wear between the three different cases. The corresponding coefficient of friction levels at the ends of these tests is given in figure 25. The unlubricated alumina tests show the highest level of friction and wear throughout the load range investigated. Mean pressure was approximately 10.3 MPa (1,500 psi) throughout the load range showing that unlubricated, the specimens can only support very low contact pressures. The water lubricated tests show the second highest level of friction through most of the load range however wear is lower than the paraffin oil lubricated case for all but the lowest (5-7 kg) loads. Mean pressures for the water case are approximately 207 MPa (30,000 psi) for the low load region and 83 MPa (12,000 psi) for the high load region after the wear transition. The paraffin oil lubricated tests show the lowest level of friction for all except the 40 kg test. Paraffin oil has the lowest wear at low loads but intermediate wear at higher loads. Mean pressures for paraffin oil lubricated tests are approximately 345 MPa (50,000 psi) for the low load region and 48 MPa (7,000 psi) for the high load region after the wear transition. Both lubricated tests appear to have transitions in their wear behavior at low loads of 8 kg for paraffin oil and 11 kg for water lubricated tests. There appears to be a fair amount of scatter in the wear behavior but straight lines seem to represent the wear trends quite well. Interestingly enough

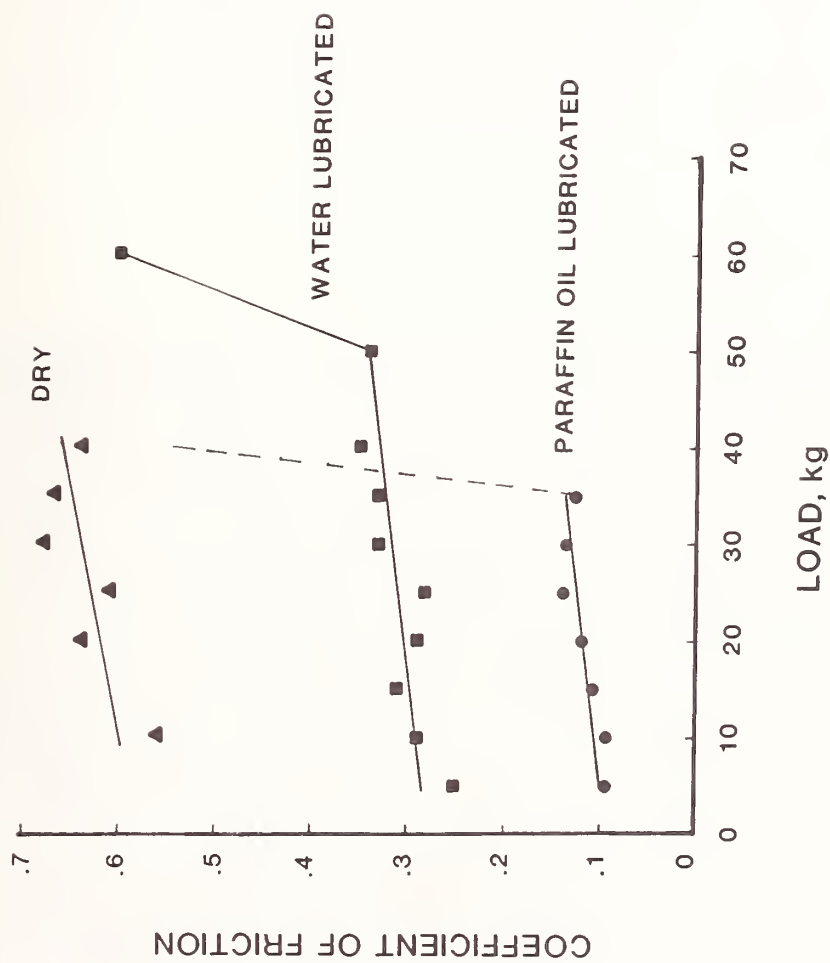


Figure 25. Comparison of Coefficient of Friction as a Function of Load for Unlubricated, Paraffin Oil Lubricated, and Water-Lubricated Alumina Constant Condition Tests



the coefficient of friction values fail to give any indication of the wear transition. All three cases tend toward higher coefficient of friction values at higher loads. This may be due to a higher surface plasticity at higher temperatures (at higher loads). Both lubricated cases show large friction transitions at very high loads (60 kg for water; 40 kg for paraffin oil). This may be due to complete failure of the lubricant at these loads. This is substantiated by the observation that the friction levels appear to be approaching that of the unlubricated tests.

### C. Analysis of Wear Scars

Scanning electron micrographs of the wear scars and wear debris produced from unlubricated, water lubricated, and paraffin oil lubricated tests are presented in figures 26-43. The unlubricated tests (figs. 26 and 27) show interesting morphology. The lower specimen wear scar is teardrop shaped because of a large amount of wear on the upper (rotating) ball. The lower magnification photograph shows a relatively uniform distribution of small areas of apparent plastic flow of material. Higher magnification (fig. 27) confirms the apparent smearing of material along with evidence of large amounts of very fine (submicron) debris littering the surface. Analysis of the wear debris (figs. 28 and 29) confirms the very small size ( $0.2\ \mu\text{m}$ ) of the debris. A separate particle size and shape analysis of wear debris from the unlubricated test indicated that most of the wear

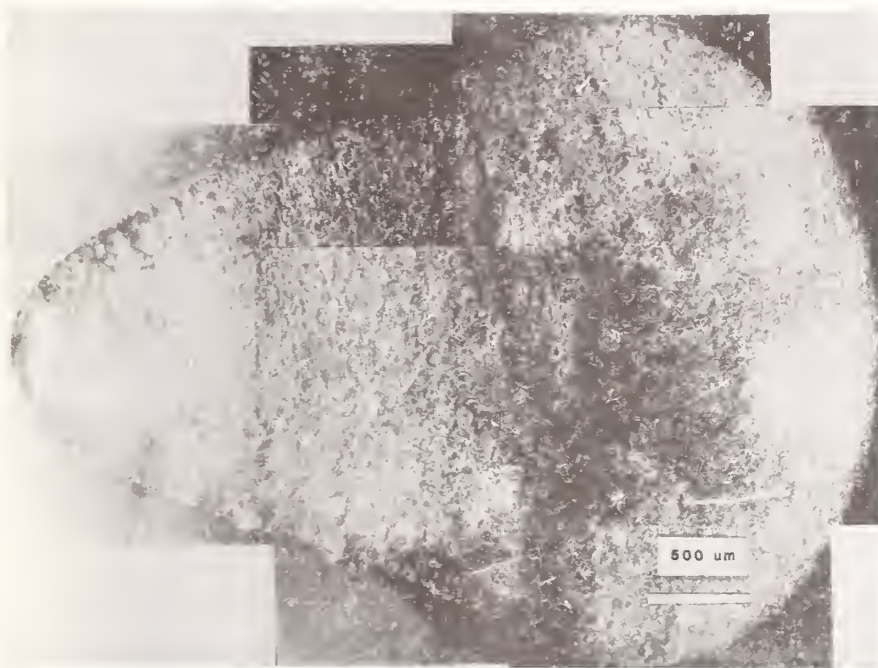


Figure 26. Low Magnification SEM Photograph of a Wear Scar from an Unlubricated Alumina Test

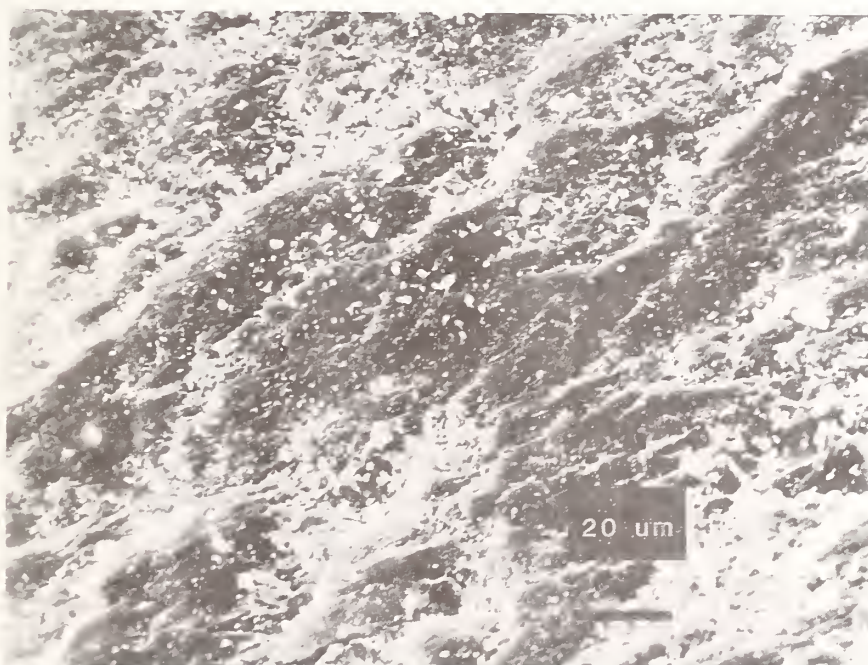


Figure 27. High Magnification SEM Photomicrograph of Lower Specimen Wear Scar from an Unlubricated Alumina Wear Test

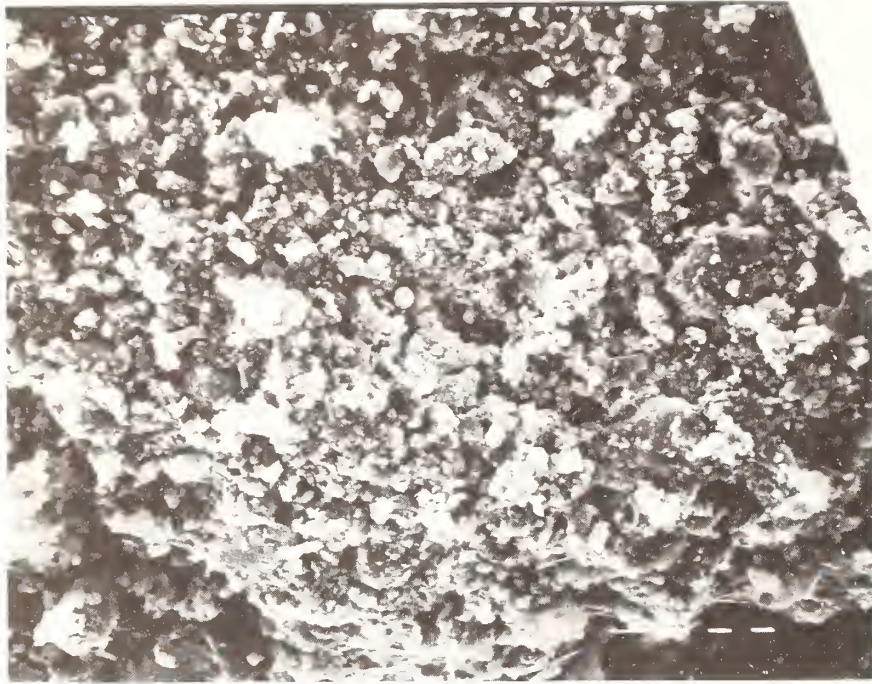


Figure 28. SEM Photomicrograph of Wear Debris from Unlubricated Wear Test - 1000X

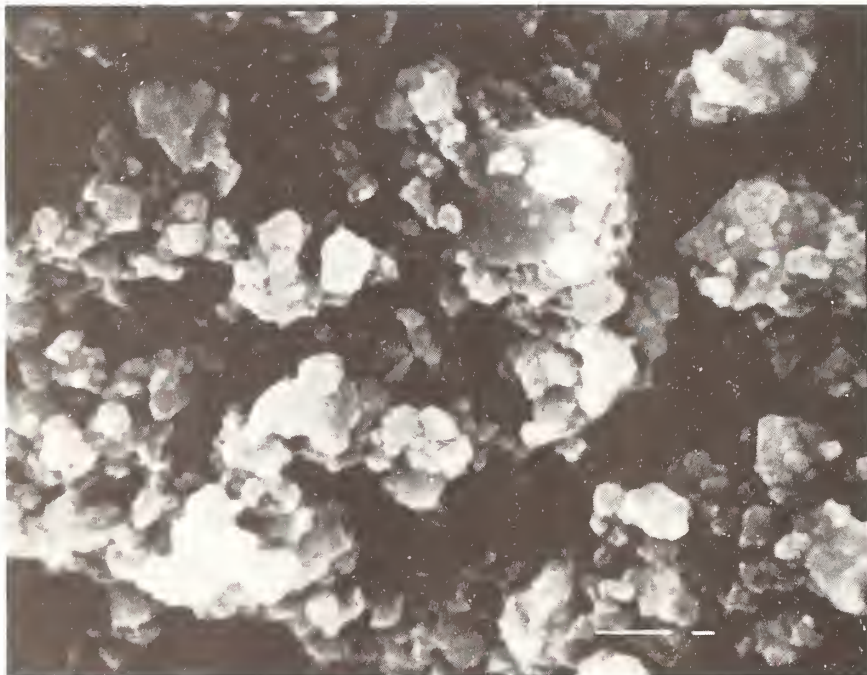


Figure 29. SEM Photomicrograph of Wear Debris from Unlubricated Wear Test - 10,000X



particles were equiaxial and less than  $0.1\text{ }\mu\text{m}$ .<sup>35</sup> Given the size of the debris, and the fact that the original material was composed of 1-20  $\mu\text{m}$  sized grains, these photomicrographs indicate large amounts of intragranular breakdown of material. This is probably due to a combination of plastic deformation and abrasion. The apparent plasticity seen is unusual for a brittle materials such as alumina at room temperature and suggests high temperatures are generated from frictional heating during the test.

Wear scars from water-lubricated alumina wear tests show a very different behavior. Low magnification (fig. 30) indicates two distinct regions within the wear scar. It appears that half of the wear scar is covered with a film. The other half is relatively smooth and contains much of the surface character (porosity, etc.) of the original polished surface. Higher magnification photomicrographs (fig. 31) of the surface shows some compacted debris filling in some of the smaller pits (pores?) of the worn surface. A second, longer duration test confirmed the presence of a "film" and provided a more detailed look at its structure. Low magnification photomicrographs of the wear track of the worn upper ball (fig. 32) clearly show the presence of a "film". The upper wear track in figure 32 seems to be made up of a smear of compacted material. The curved line apparent in the middle of the picture is the impression of the lower specimen wear scar left in the track at the end of the test as the specimens stopped sliding. Direction of sliding of the ball on the track is right to left. A higher magnification shot of this region (fig. 33) shows



Figure 30. Low Magnification SEM Photograph of a Wear Scar from a Water-Lubricated Alumina Test

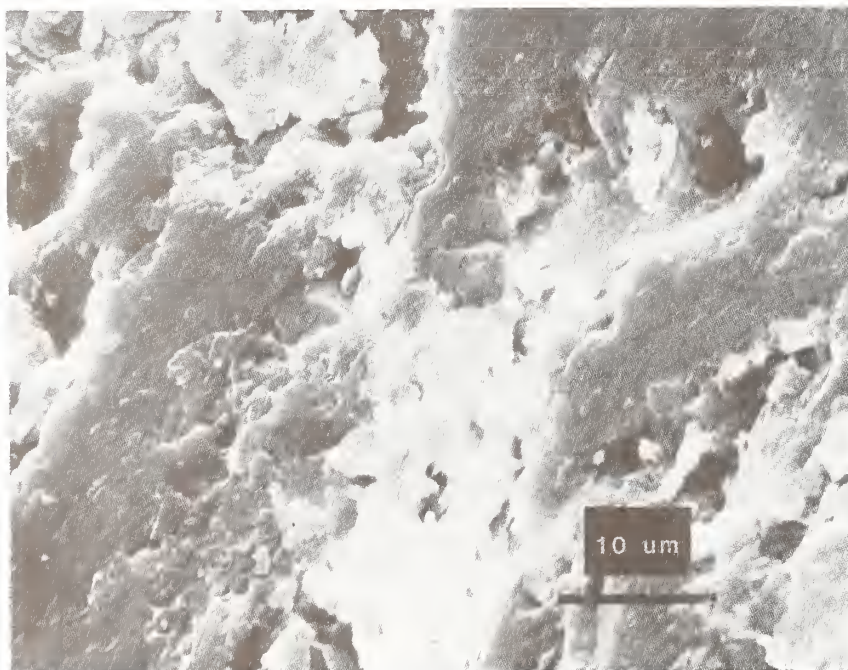


Figure 31. High Magnification SEM Photomicrograph of Lower Specimen Wear Scar from a Water-Lubricated Alumina Wear Test

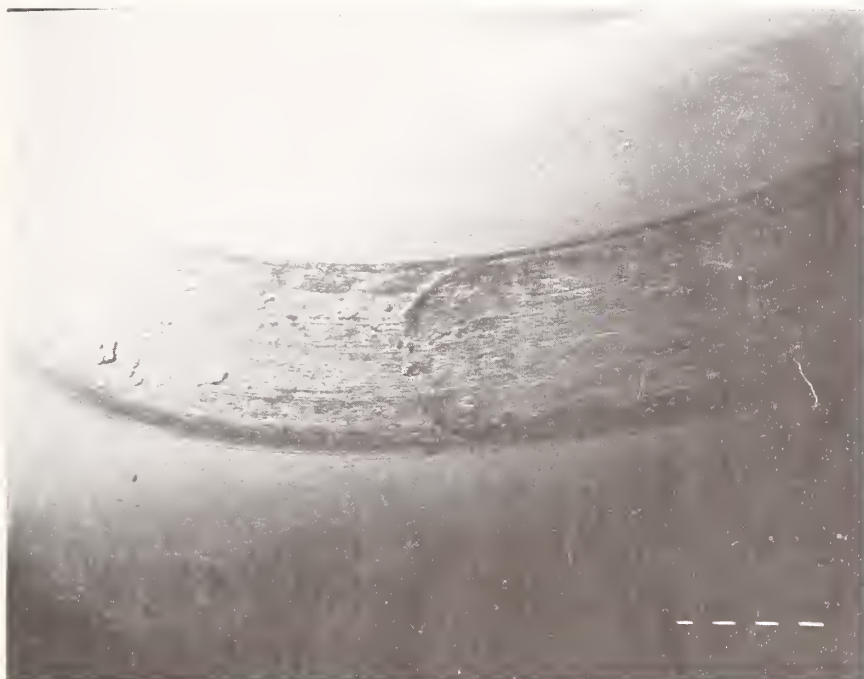


Figure 32. SEM Photomicrograph of Upper Specimen Wear Track  
Water-Lubricated Run 2748R - 25X

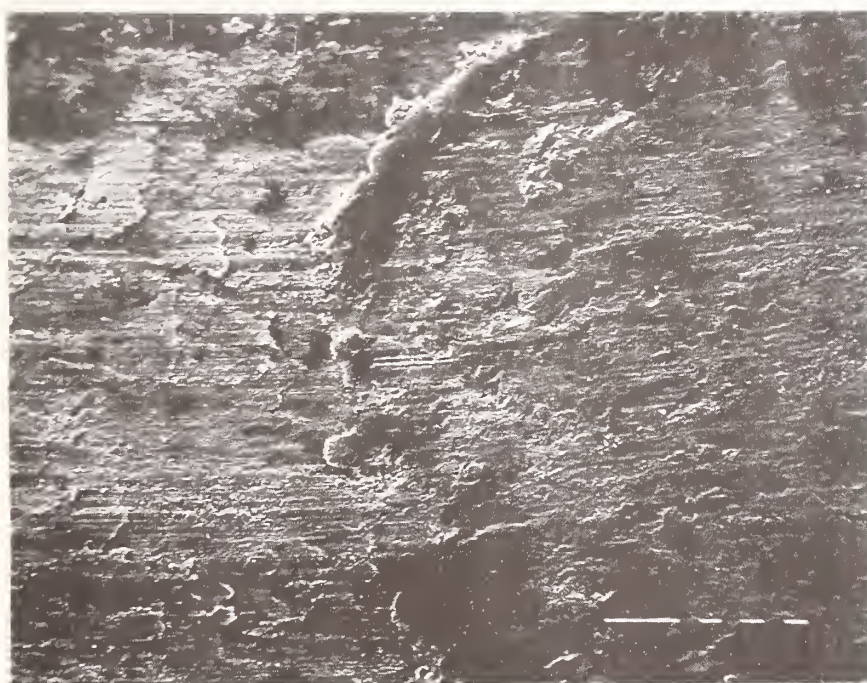


Figure 33. SEM Photomicrograph of Upper Specimen Wear Track  
Water-Lubricated Run 2748R - 100X



thin smears of compacted material forming platelets which eventually merge to form a fairly uniform film. The buildup outlining the contact between the wear track and the lower ball indicates a small pileup of material being pushed in front of the wear scar, evidence of the fairly ductile nature of the film. At higher magnifications (fig. 34), the plate-like, smeared, nature of the film becomes apparent. It appears that it is composed of small particles which smear into a very smooth surface when adequate stress is applied (fig. 35). The particles which make up this film are very small (fig. 36) and are on the order of  $0.1\text{ }\mu\text{m}$  or less. They appear to exhibit some cohesive properties (they hold together when smearing); however, it appears that these forces are fairly weak as evidenced by the cracks and fissures seen in the film platelet of figure 36. Photomicrographs of the lower wear scar from the same test confirm that the film is present on both surfaces (fig. 37). The film was observed to be of the same nature as the film for the upper wear track. Regions were found where the film was very granular, and other regions were found where the grains were compacted into a very smooth film. After the wear tests were conducted, samples of the used lubricant (water) were filtered ( $0.2\text{ }\mu\text{m}$  pore Nylon) and analyzed under the SEM. Two types of wear debris were found as seen in figures 38 and 39. Very small particles (most  $<0.1\text{ }\mu\text{m}$ ) were abundant. Several large "flakes" or platelets were relatively common. The high magnification slot at 5000X (fig. 39) indicates that the platelet is composed of very small particles (edge of flake) with a very smooth surface and a large number of small particles adhering to the surface.

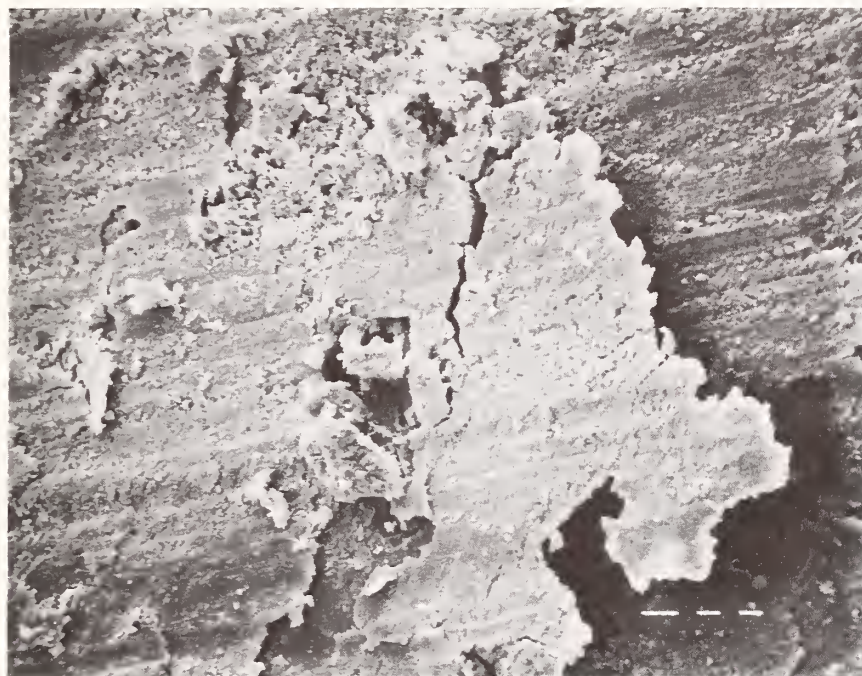


Figure 34. SEM Photomicrograph of Upper Specimen Wear Track  
Water-Lubricated Run 2748R - 500X

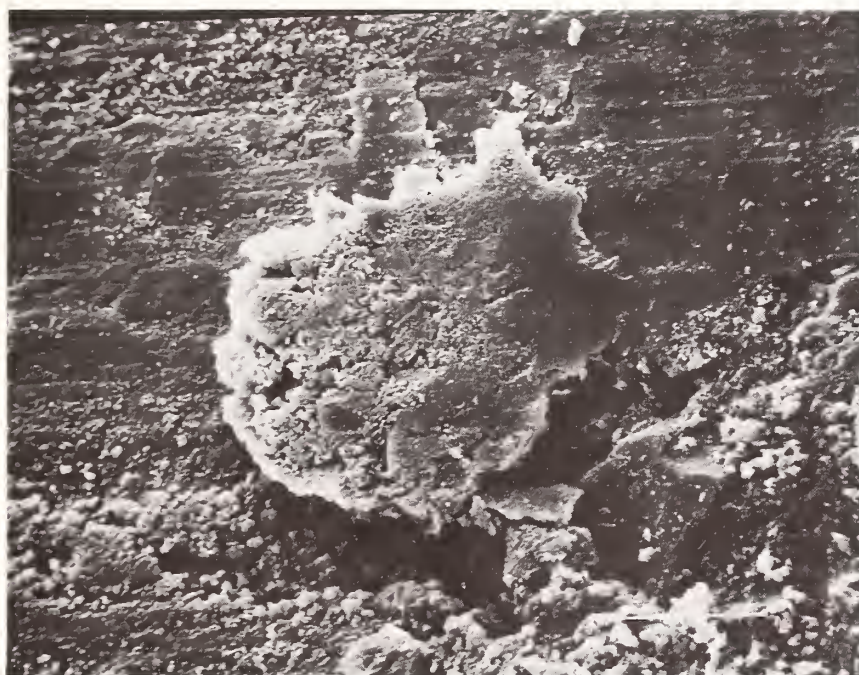


Figure 35. SEM Photomicrograph of Upper Specimen Wear Track  
Water-Lubricated Run 2748R - 1000X





Figure 36. SEM Photomicrograph of Upper Specimen Wear Track  
Water-Lubricated Run 2748R - 5000X

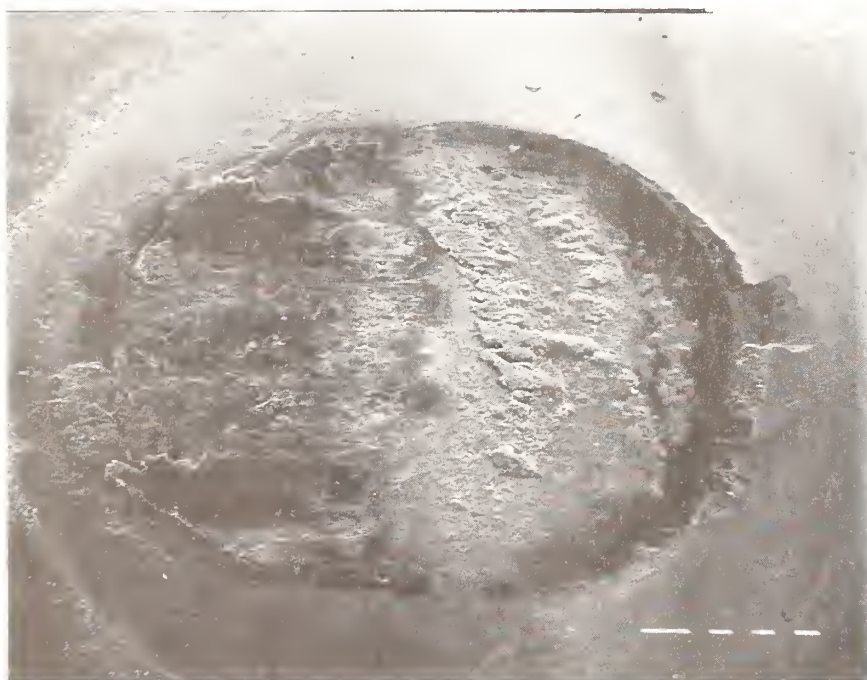


Figure 37. SEM Photomicrograph of Lower Specimen Wear Scar  
Water-Lubricated Run 2748R - 50X

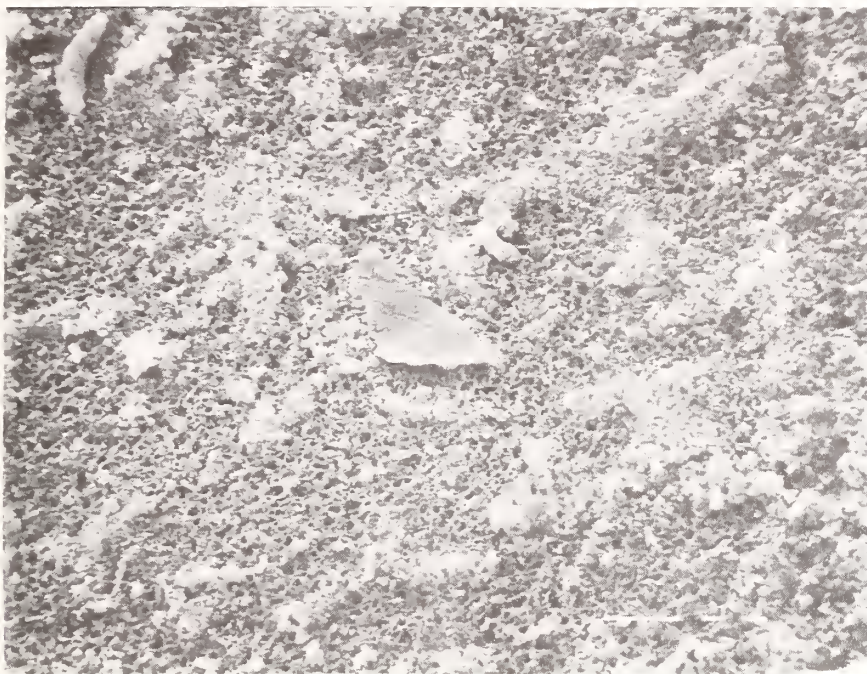


Figure 38. SEM Photomicrograph of Wear Debris from Water-Lubricated Wear Test - 1000X

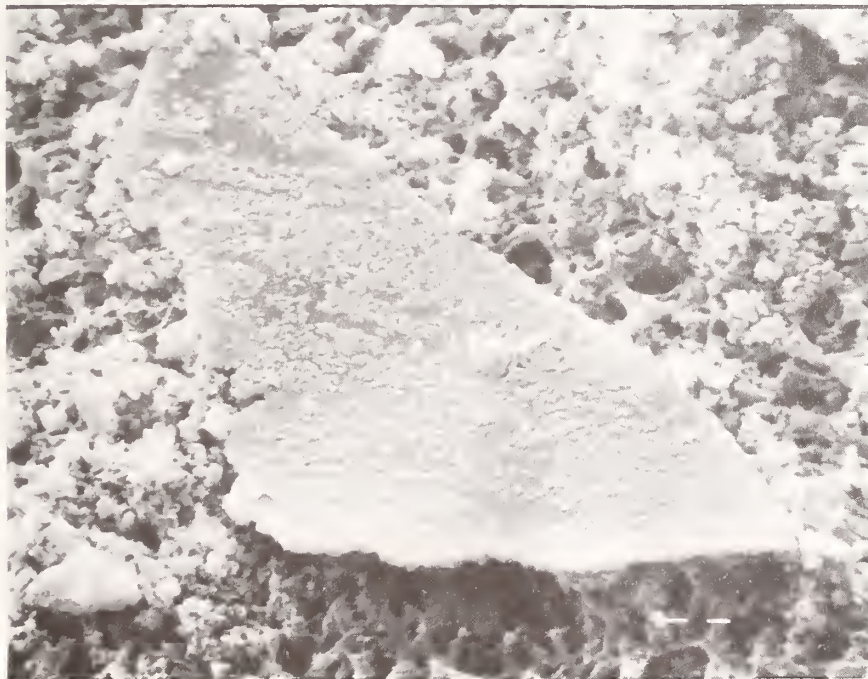


Figure 39. SEM Photomicrograph of Wear Debris from Water-Lubricated Wear Test - 5000X



The small particles appear to have been placed on the surface after it was formed. Whether they "grew" there or were attracted by some cohesive force between the particles and the platelet is not known.

Wear scars produced from paraffin oil lubricated alumina tests display a third wear scar character. At low magnification, figure 40 shows an enhanced isotropic roughness within the wear scar. No film is apparent. Higher magnification (fig. 41) reveals distinct pits in the surface. The sharp planes of the pits are facets of individual grains and indicate that grain pullout has occurred. There is no evidence of plasticity perhaps because of reduced temperatures in the contact junction. These lower temperatures could be due to surface cooling by the lubricant or reduced heat generation because of the low level of friction for these tests (coefficient of friction = 0.1, see fig. 25). Analysis of the wear debris (figs. 42 and 43) indicate the presence of large ( $10\text{ }\mu\text{m}$ ) particles produced by pullout of individual grains (intragranular fracture) as well as smaller particles ( $0.1\text{-}2\text{ }\mu\text{m}$ ) which must have been formed from intragranular fracture of the parent material.

The intragranular fracture may have occurred by gradual wearing of the exposed surfaces of the grains as well as crushing of grains or parts of grains that were pulled out of the original polycrystalline matrix. Free wear debris in the contact junction may also contribute to considerable abrasive (three body) polishing of the surface. The

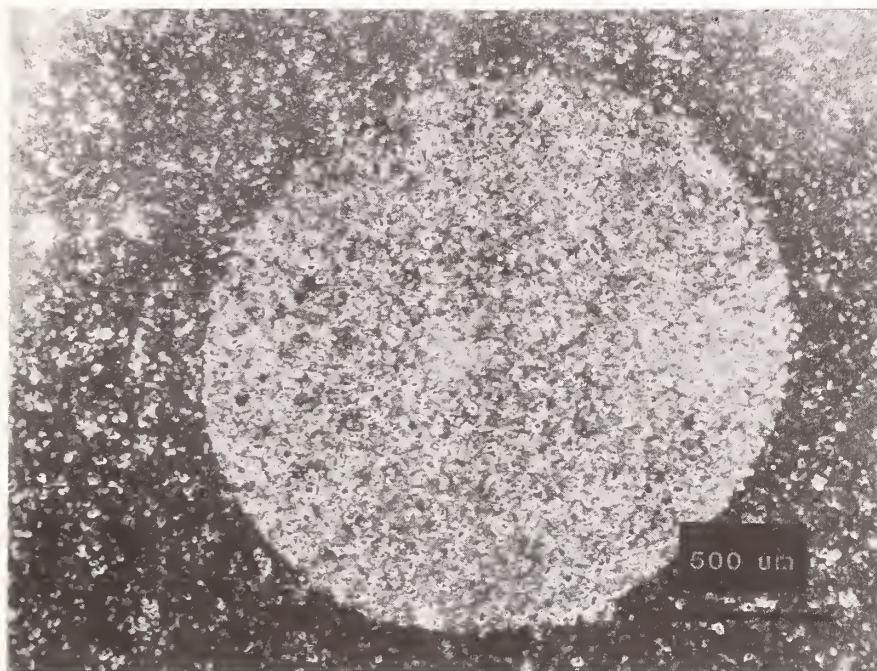


Figure 40. Low Magnification SEM Photograph of a Wear Scar from a Paraffin Oil Lubricated Alumina Test

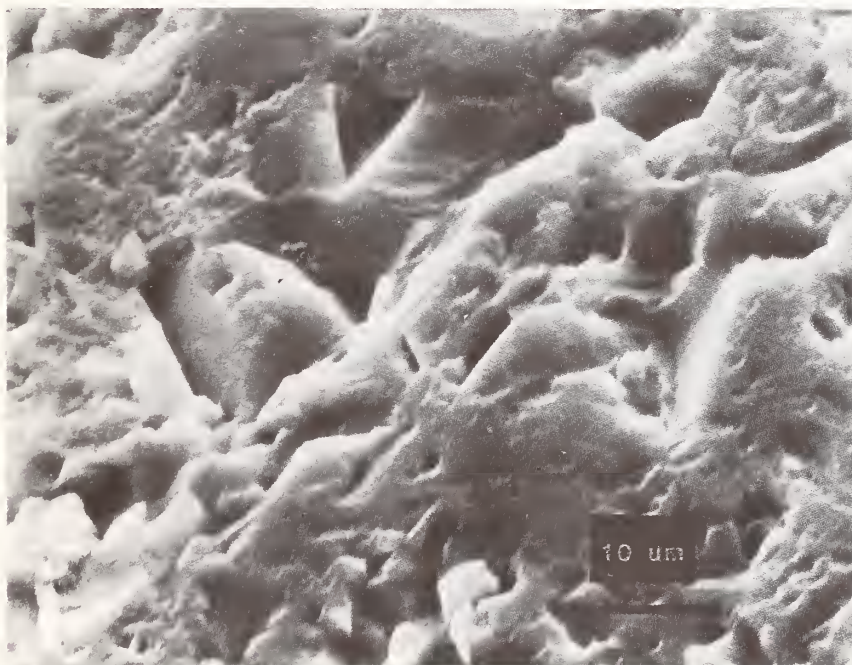


Figure 41. High Magnification SEM Photomicrograph of Lower Specimen Wear Scar from a Paraffin Oil Lubricated Alumina Wear Test



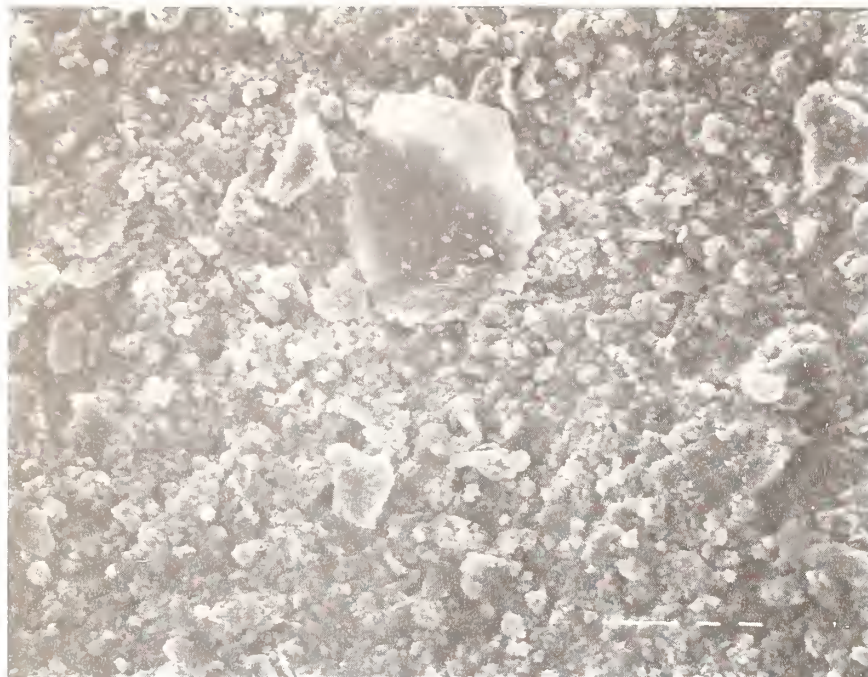


Figure 42. SEM Analysis of Wear Debris from Paraffin Oil Lubricated Wear Test - 1000X



Figure 43. SEM Analysis of Wear Debris from Paraffin Oil Lubricated Wear Test - 10,000X

surface and wear debris morphology support all three of these wear mechanisms.

Some researchers suggest that adhesion may play an important role in the friction and wear of ceramics. Buckley and Miyoshi<sup>36</sup> for example suggest adhesion plays a critical role in the alumina/alumina contact. Their experiments, conducted using sapphire under ultrahigh vacuum, suggested that the adhesion between the surfaces was 1) orientation dependent (anisotropic) and 2) extremely surface chemistry conditions which they attributed to water vapor. Their experiments with olive oil suggested hydrocarbons may have a similar effect on reducing adhesion and would help to explain the reduce friction observed in the four-ball results presented in this report.

Summarizing the results of the wear analysis: Dry wear appears to produce very small particles of debris and some evidence of flow of material is observed. Water lubrication results in the formation of a surface film which protects the surface and reduces friction and wear. Paraffin oil lubrication produces wear through a combination of intragranular fracture (perhaps through those body abrasion) and grain pullout.

D. Four-Ball Constant Condition Tests: Effect of Batch to Batch  
Variations in Specimen Material

The purpose of wear testing is to determine the tribological properties of the selected material/lubricant combination. The preliminary testing was conducted using early batches of alumina balls with the bulk of the testing on Cer 004 alumina. A new batch of alumina (Cer 005) was also tested using constant condition tests and plotted as wear scar diameter versus load for both water and paraffin oil lubricated conditions. Both aluminas were high purity and low porosity. Wear data from these tests (figs. 44 and 45) show distinct behavior for the two batches of alumina under both lubricating conditions. Under water-lubrication (fig. 44) Cer 005 shows slightly lower wear at low loads (mean pressure = 310 MPa (45,000 psia) vs 200 MPa (24,000 psia) for Cer 004) and slightly higher wear at higher loads (mean pressure = 48.3 MPa (7000 psia) vs 82.7 MPa (12,000 psia) for Cer 004) with a lower transition load from low to high wear (7.5 kg vs 11 kg). Under paraffin oil lubrication (fig. 45) a similar behavior is seen: lower wear is observed for low loads (mean pressure = 621 MPa (90,000 psia) vs 349 MPa (50,000 psia) for Cer 004), wear rates at higher loads are similar (mean pressure = 48.3 MPa (7000 psia), and the transition load is lower (3.5 kg vs 8.5 kg). Strict interpretation of the reason for the wear difference in the two materials cannot be made without an extensive examination of the materials both before and after the tests. This data indicates, however, that this wear test method is quite sensitive

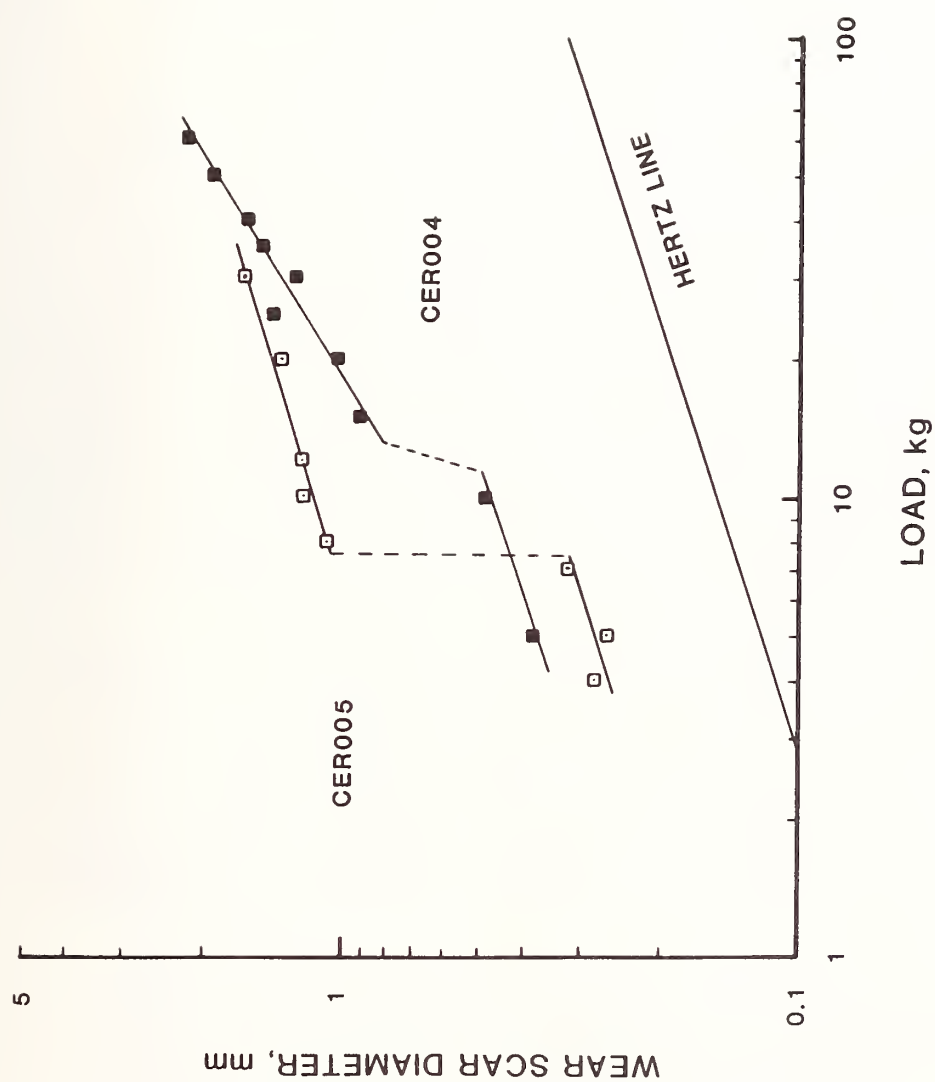


Figure 44. Comparison of Wear as a Function of Load for Different Batches of Alumina under Water-Lubricated Conditions (Constant Condition Tests)

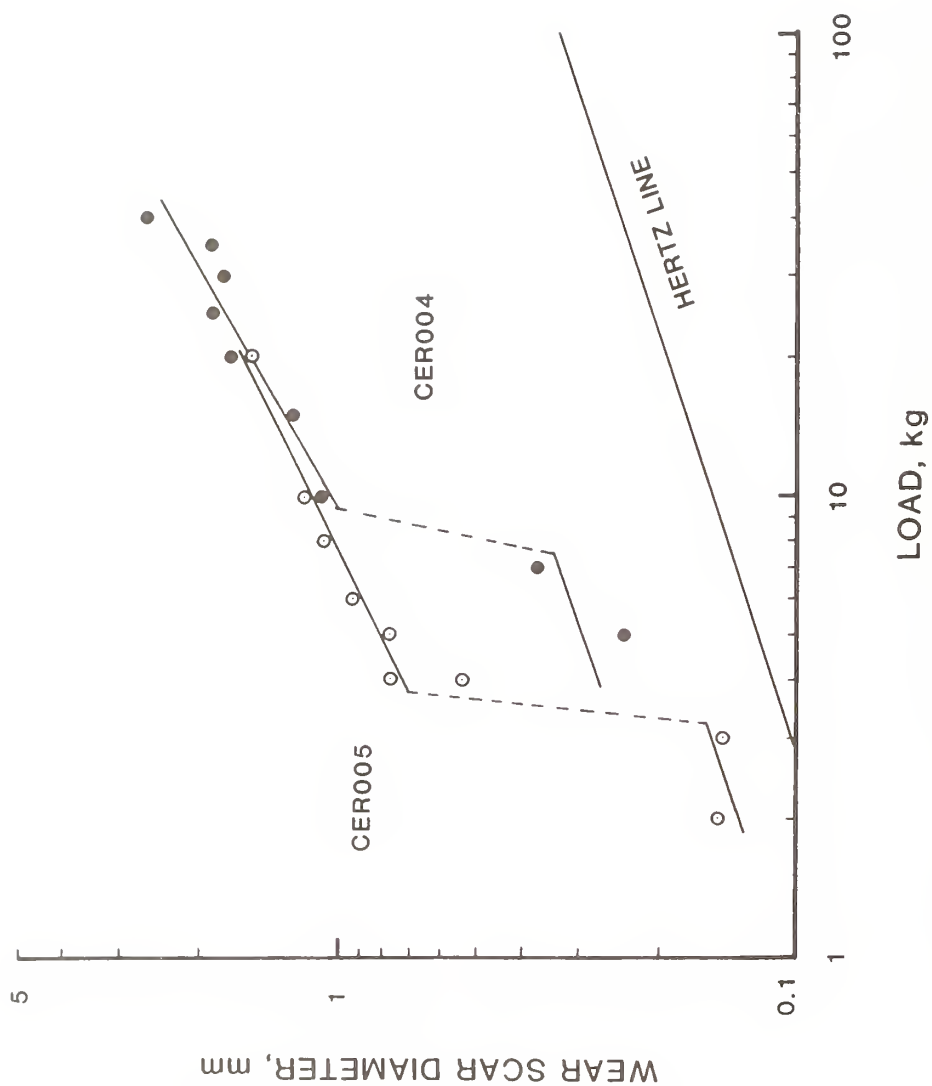


Figure 45. Comparison of Wear as a Function of Load for Different Batches of Alumina under Paraffin Oil Lubricated Conditions (Constant Condition Tests)

to small variations in materials as seen batch to batch. This high sensitivity also suggests that it may be possible to study the effect of processing variables on wear results. This would prove extremely valuable to optimizing ceramic materials for tribological applications.

#### E. Step-Loading Four-Ball Wear Testing Study

##### 1. Base Conditions

Constant condition test results plotted as wear scar diameter versus load give valuable information of the tribological properties of ceramic materials. Unfortunately, it may take ten or more tests to adequately describe the material behavior. This is both time consuming and potentially expensive. As a result, a step-loading procedure was developed to derive the same information but using a single test. This procedure was described in the experimental section of this report.

Two unlubricated step-loading tests are shown in figure 46 for Cer 005. The repeatability of the test is good and the data are identical to the data obtained using constant condition tests. Mean pressures of approximately 8.3 MPa (1,200 psi) are obtained.

Water-lubricated step-loading tests (fig. 47) also show good repeatability for low and high load wear conditions, and also for the transition load. When compared to the constant condition test

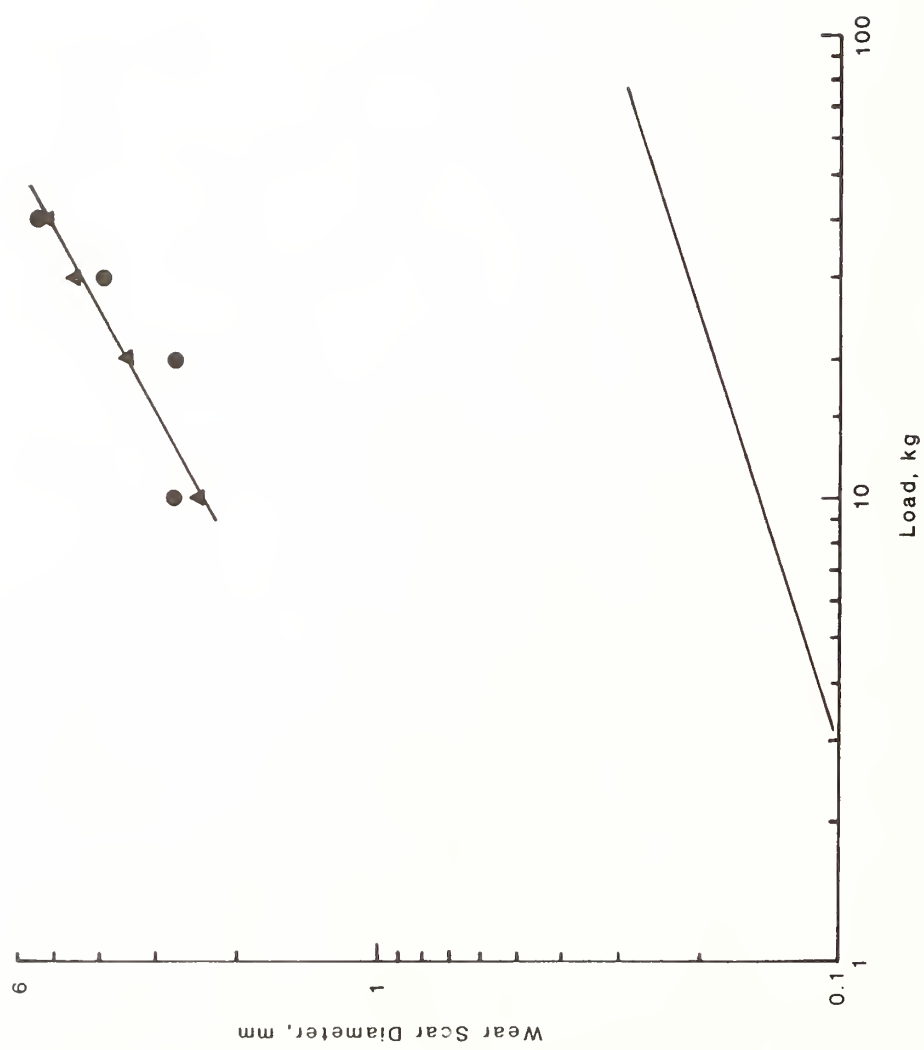


Figure 46. Wear as a Function of Load for Unlubricated Alumina Step-Loading Four-Ball Tests



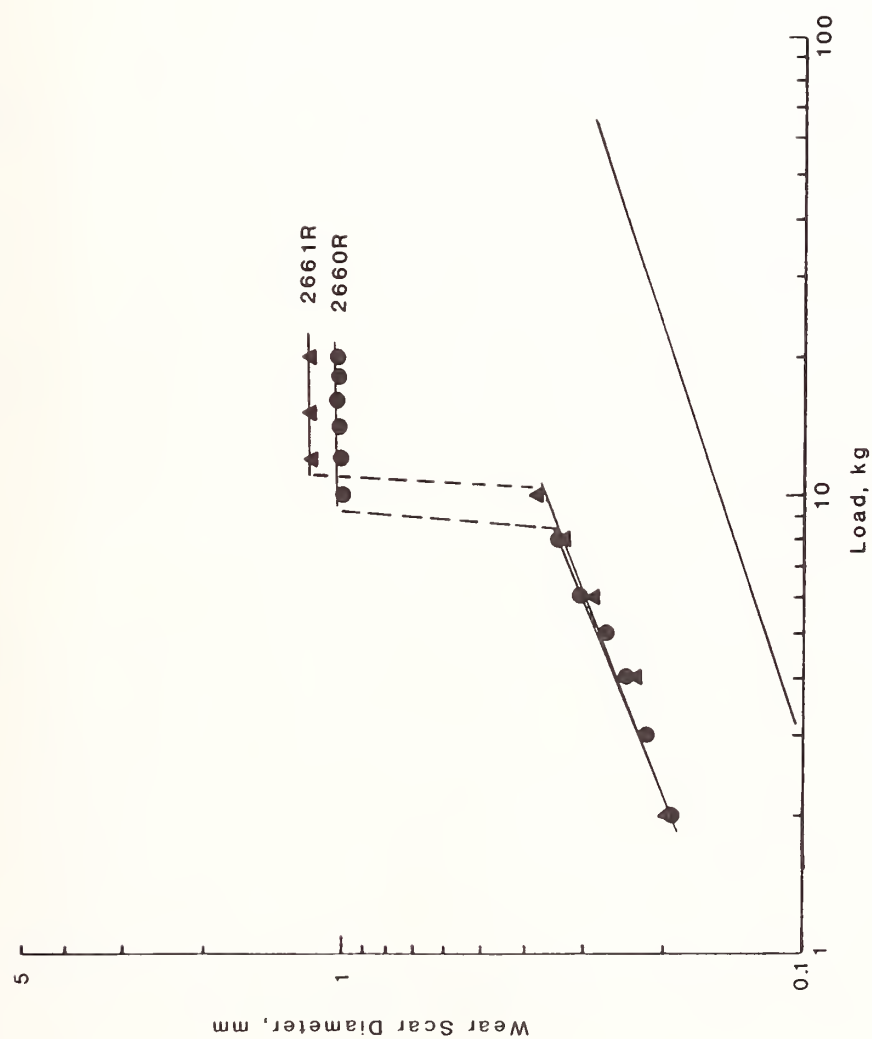


Figure 47. Wear as a Function of Load for Water-Lubricated Alumina Step-Loading Four-Ball Tests

results, the step-loading tests produce slightly higher low load mean pressures of 345 MPa (50,000 psi). The transition load is slightly higher and the high load wear has much flatter response to load variation. The mean pressure after the wear transition is 41 MPa (6,000 psi). The difference between step-loading and constant condition test results is due, I believe, to the higher severity at the beginning of the constant condition tests at each load (virgin surfaces).

Paraffin oil lubricated step-loading tests also show good repeatability, especially for low load conditions, and transition load values (fig. 48). The upper, high wear region shows slightly poorer repeatability. Compared to the constant condition tests, the low wear regime has a slightly higher mean pressure of 483 MPa (70,000 psi), the transition load is slightly higher, and the high wear region has a mean pressure of 41 MPa (6,000 psi) except for the high load level portion of run 2659 R. These minor differences can be attributed to the severity differences at the beginning of each load. For the constant condition tests, the surfaces are unworn at the beginning and stresses are very high. All but the initial load in the step-loading tests start on a pre-worn scar. At large wear scars, the increase in load may not be sufficient to cause a significant severity increase in the test and a flat wear versus load plot may be observed. Besides these minor differences, the step-loading gives essentially the same information as the constant condition test but in one test.

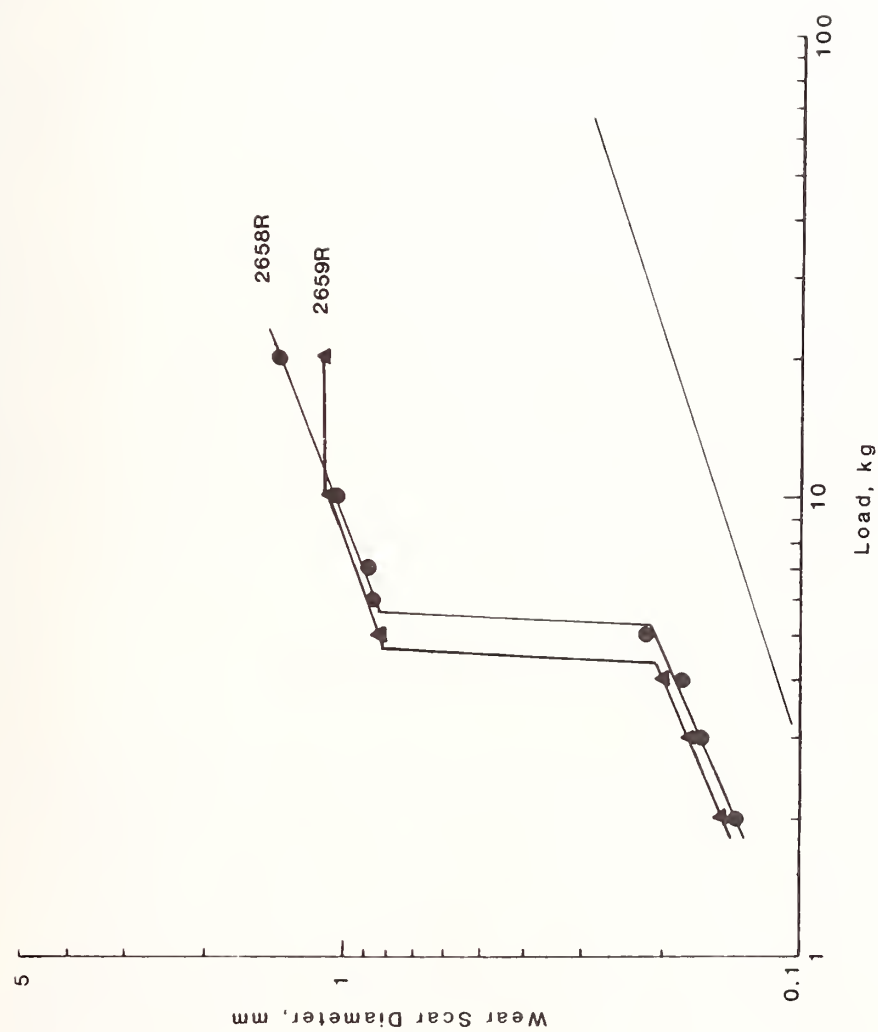


Figure 48. Wear as a Function of Load for Paraffin Oil Lubricated Alumina Step-Loading Four-Ball Tests

## 2. Step-Loading Test: Effect of Speed

A study was made of the effect of speed on step-loading wear results. Tests at 1000, 200, and 10 rpm, shown in figure 49, indicate an effect on both the low and high wear levels and also the wear transition load. The differences in low and high wear levels (both location and slope) are attributable to wear-in effects. At high speed (1000 rpm) the wear-in has progressed to the steady state or low wear regime and the plot of wear scar versus load results in lines roughly parallel to the lines of constant pressure. At lower speeds (200 rpm), the specimens slide only 20% of the distance of the 1000 rpm test, steady state wear rates may not be achieved and the plot produces lines with slopes greater than the lines of constant pressure indicating continued wear-in. At still lower speeds (10 rpm) even less wear-in is achieved and the plots produce lines with still steeper slopes. The differences in transition loads may be due to a dynamic rate phenomenon of temperature or possibly hydrodynamics.

## 3. Step-Loading Test: Effect of Specimen Material

Three different ceramic materials were evaluated using the step-loading four-ball test. Data from tests run on alumina (Cer 005), silicon carbide (Cer 020), and silicon nitride (Cer 016), under paraffin oil lubrication, are shown in figure 50. These materials show markedly different behavior in this test. Alumina shows moderate

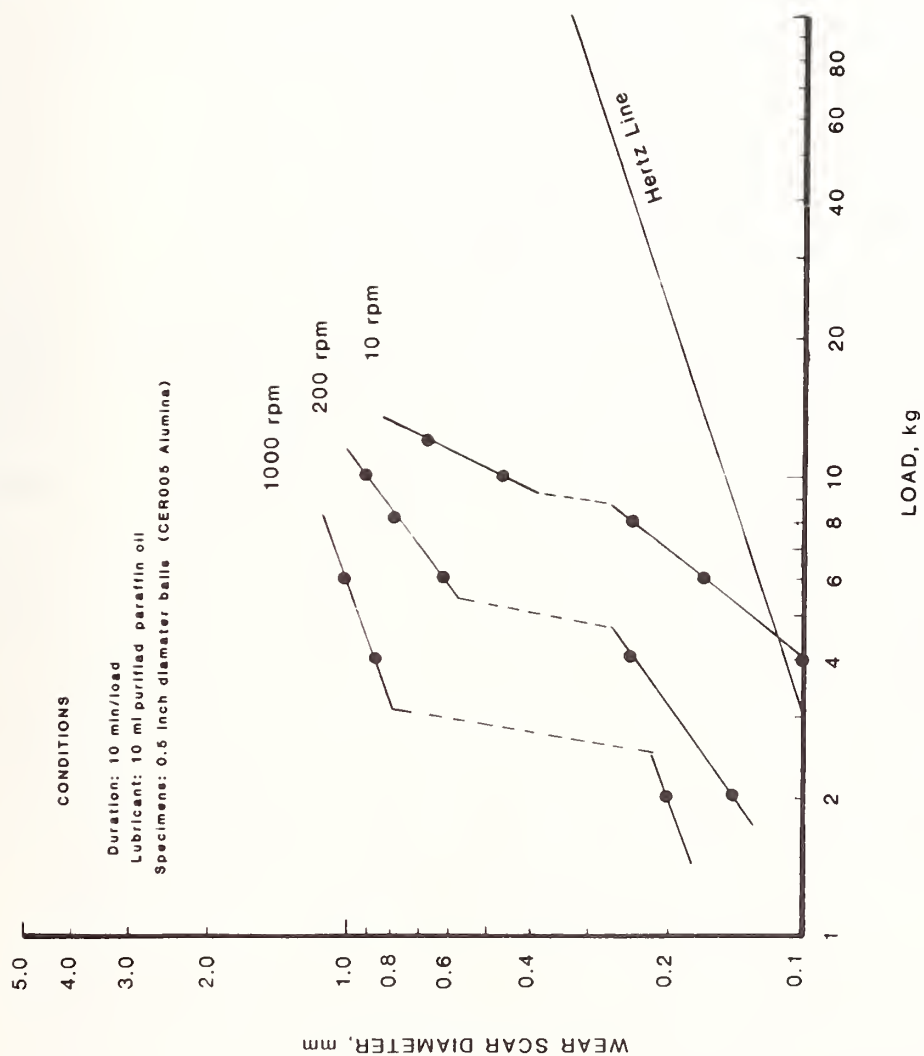


Figure 49. Effect of Speed on Step-Loading Four-Ball Wear Test Results

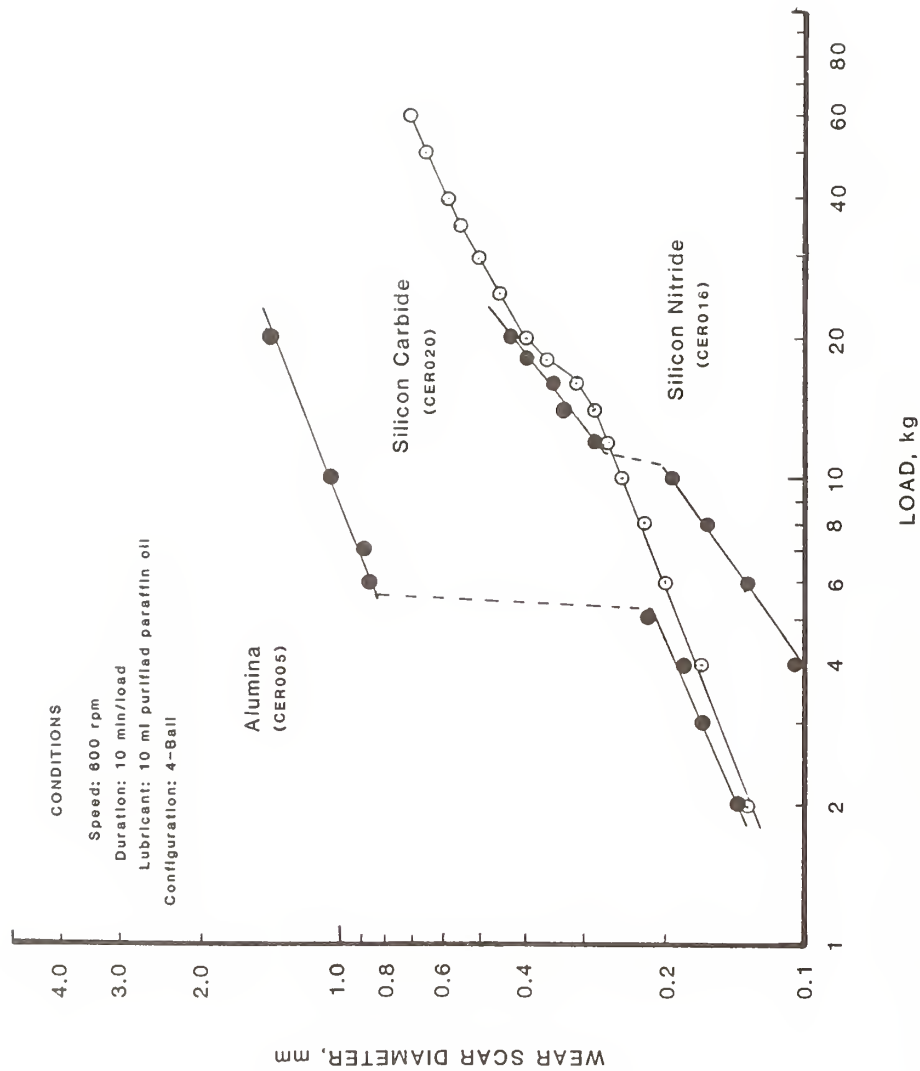


Figure 50. Comparison of Wear Behavior as a Function of Load for Paraffin Oil Lubricated Step-Loading Four-Ball Tests on Silicon Nitride, Silicon Carbide, and Alumina

levels of wear at low load (mean pressure = 483 Mpa or 70,000 psi), a transition at 5.5 kg, and a relatively high level of wear above 5.5 kg (mean pressure = 48 MPa or 7,000 psi). Silicon carbide also exhibits moderate levels of wear at low load (690 MPa or 100,000 psi), however this moderate level of wear continues up to at least 60 kilograms load. A slight transition is seen at 19 kg but wear is still only moderate above this load. Silicon nitride shows very low wear at low loads (mean pressure is 1,380 MPa or 200,000 psi) a small wear transition is seen at 11 kg however wear increases only to a moderate level up through at least 20 kg (mean pressure is 620 MPa or 90,000 psi).

#### F. Ball-on-Three-Flat Testing

Step-loading four-ball tests suffer from the drawback that four balls are required for a test. Some ceramic materials are not readily available in ball form however it is still desirable to understand their tribological properties. Therefore, a modified technique was developed to allow testing of ceramic materials not available in ball form. The small discs used in this ball-on-three-flat (BTF) test are easily fabricated from readily available rod stock.

##### 1. Comparison of Results to Four-Ball Tests

A ball-on-three-flat test was conducted on a sample of alumina to see if results were similar to four-ball tests. The data, presented



in figure 51, indicate some similarity of results at low loads, but differences are seen in both the transition load (13 kg in BTF vs 5 kg in FB) and high load wear values. The four-ball tests give low load mean pressures of 552 MPa (80,000 psi), and mean pressures of only 48 MPa (7000 psi) are observed after the wear transition. The ball-on-three-flat test has slightly higher mean pressures before the wear transition of 690 MPa (100,000 psi). After the wear transition the mean pressure drops to approximately 20.7 MPa (3,000 psi) which is the same low wear pressure as was observed for the dry sliding four-ball case. These differences may be due to several factors. 1) The difference in severity between the convex on convex contact of the four-ball test and the convex on flat contact of the ball-on-three-flat test. 2) The difference in material (the four-ball test ran Cer 005 on Cer 005 while the BTF test ran Cer 021 on Cer 006). 3) The much smaller thermal resistance of material in the case of the BTF test, resulting in lower operating temperatures in the contact junction.

I believe that the second two reasons may best explain the results. While it is true that the calculated hertzian contact pressure for a four-ball contact is 50% higher than the same load using ball-on-three-flat, this is based on an initial condition (no wear). Each load increment (except the first) for the step-loading test however starts on a pre-worn wear scar, therefore, the significance of the geometric differences between the two tests would be reduced.

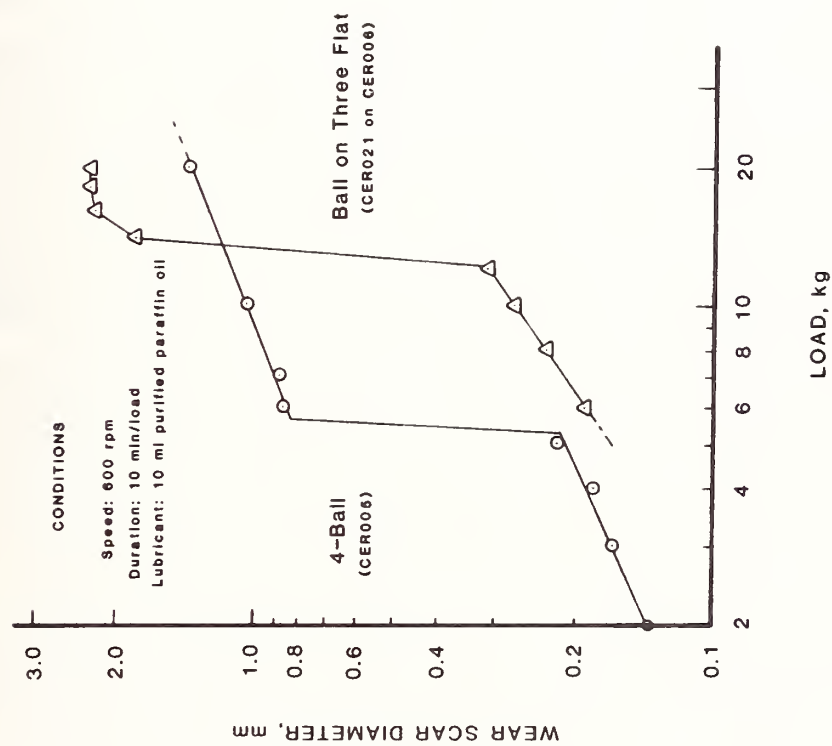


Figure 51. Comparison of Ball-on-Three-Flat and Four-Ball Wear Results for Paraffin Oil Lubricated Alumina

The difference in materials probably plays the strongest role in the differences in wear behavior between the four-ball and BTF tests. Cer 006 is a 99.8% pure alumina while Cer 021 is a 99.5% pure alumina. The purity of Cer 005 is not known exactly but is in the 99+% range. We have already seen that these tests are sensitive enough to detect wear performance differences among different batches of the same material. The small compositional and structural differences between Cer 006, Cer 021, and Cer 005 may therefore be enough to give different wear results.

Temperature may also play an important role in this test. During a test, an equilibrium is established between rate of heat generation (friction) and dissipation (conduction through specimens and fluid). This resulting equilibrium establishes the contact junction temperature for a load. In the case of the four-ball test heat must be conducted through a 1/2" diameter low thermal conductivity ceramic ball. In addition, there is only a small point contact between the ball and the metal test cup. Resistance to heat flow is therefore very high and high contact junction temperatures would be expected. The ball-on-three-flat test, on the other hand, has a very small amount (only 1/16 in) of material between the contact and the metal test cup. In addition, the contact between the ceramic specimen and test cup is over a large area (the entire back and sides of the specimen). Heat transfer is enhanced, and therefore a different, lower equilibrium temperature is obtained under the same conditions of load and friction.

## 2. Ball-on-Three-Flat Test: Interpretation of Friction Data

A small study was performed in order to determine how more useful friction information could be gained from these ball-on-three-flat (and also step-loading and constant condition) tests. Friction traces from run 2727 R (fig. 52) were used to calculate coefficient of friction values during each load increment. In addition to final "steady state" coefficient of friction, values were calculated for initial steady state, lower "steady" level, upper "steady" level, and highest value for the seizure recovery spike of one was observed. These values were plotted as coefficient of friction versus load in figure 53. At low loads, friction is very steady with very little difference between initial, final, high, and low values of friction. As the load increases, variation in friction tends to increase, with initial friction values starting low and final friction values being high. Finally at 14 kg a spike occurs in the friction trace with a coefficient of friction approximating the unlubricated case. The high friction spikes coincide with the wear transition. The 16 kg load run also contains a spike. Wear takes a corresponding increase at this load and large variations in "steady" state friction are seen for these two loads. The 18 and 20 kg loads do not have any spikes and the wear is correspondingly low as seen by the small slope of the wear scar vs load line in figure 51. Variations in "steady" state friction are also very small.

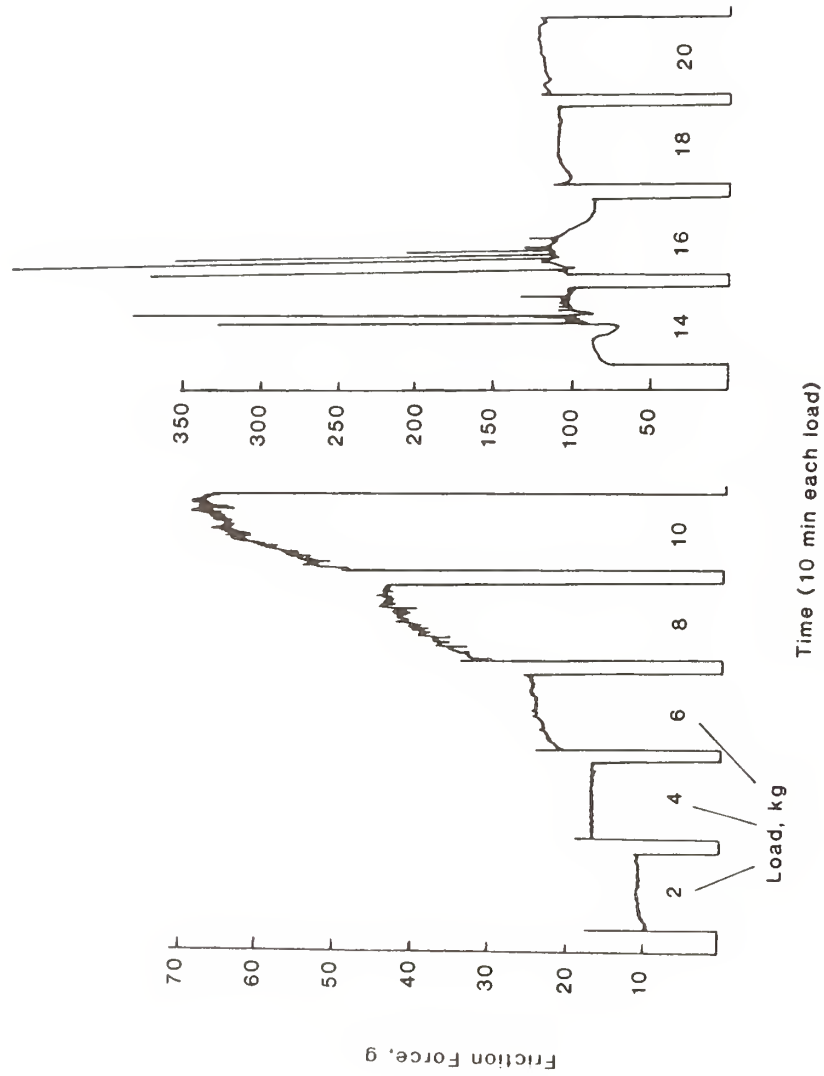


Figure 52. Friction Traces for Paraffin Oil Lubricated Ball-on-Three-Flat (BTF) Test 2727 R

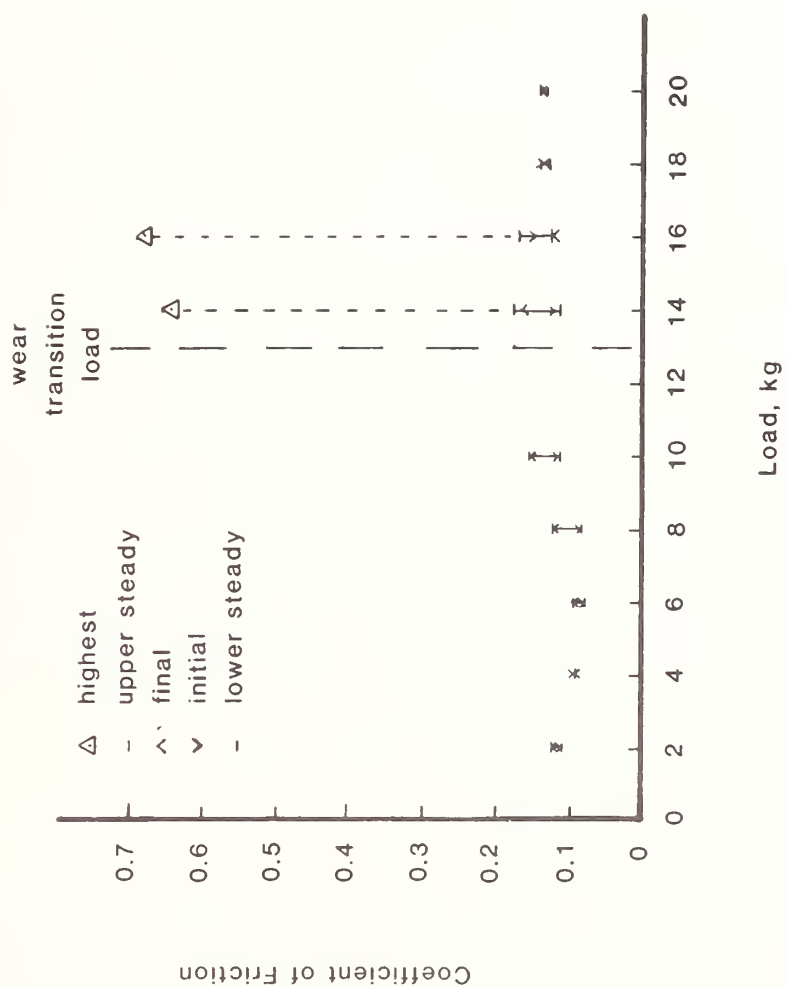


Figure 53. Coefficient of Friction Values versus Load for Paraffin Oil Lubricated BTF Test 2727 R



These results indicate the need for more than just the final friction value for some tests. In this test, if only the final coefficient of friction values were plotted, a relatively straight line would be seen. There would be no hint of anything other than normal wear behavior. The increasing variation of friction with increasing load seem to give some indication that the test is approaching a transition. The friction spikes correlate well with the high wear regions of the test during and after the wear transition and give evidence of the severe nature of the transition during this test.

### 3. Ball-on-Three-Flat Test: Effect of Specimen Material

A paraffin oil lubricated ball-on-three-flat test was conducted on a set of alumina specimens produced at NBS. This was done to see if we could use the test to evaluate materials produced under controlled processing conditions, and thus determine the effect of processing variables on wear performance. The NBS alumina (fig. 54) showed a very different behavior than the commercial grade alumina. At low loads, the commercial alumina showed relatively low wear while the NBS alumina had moderate wear. At higher loads, the commercial alumina showed a transition to high wear while the NBS alumina still exhibited only moderate wear. The mean pressure for the NBS alumina was constant at 207 MPa (30,000 psi) throughout the load range. In addition, the friction traces show evidence of sharp friction transitions for many of the loads (fig. 55) indicating possible micro wear transitions within each load. The NBS alumina may be

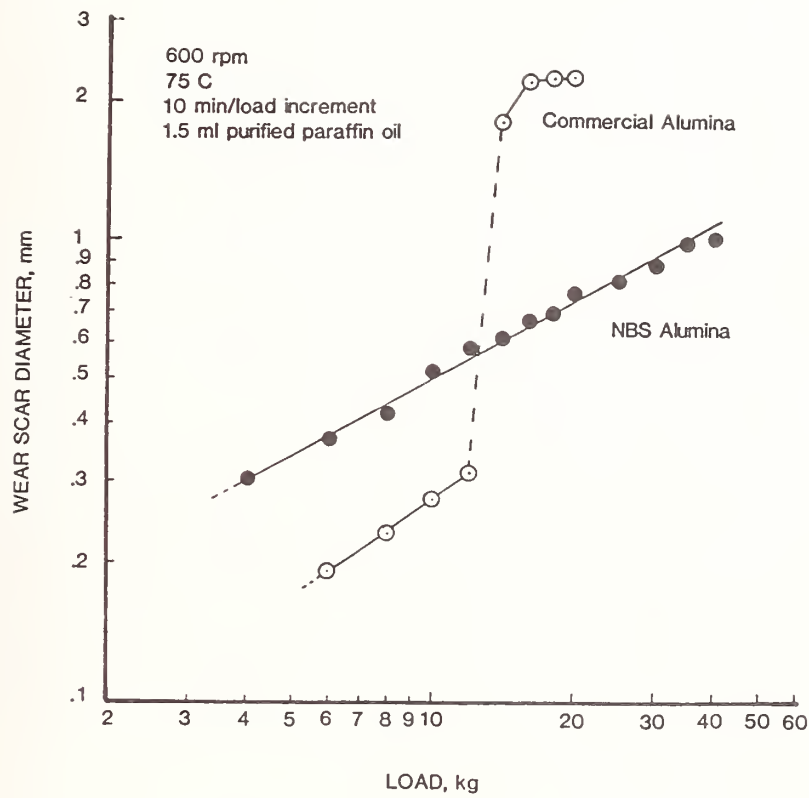


Figure 54. Comparison of Wear Results for NBS Produced Alumina versus Commercial Alumina (Paraffin Oil Lubricated BTF Tests)

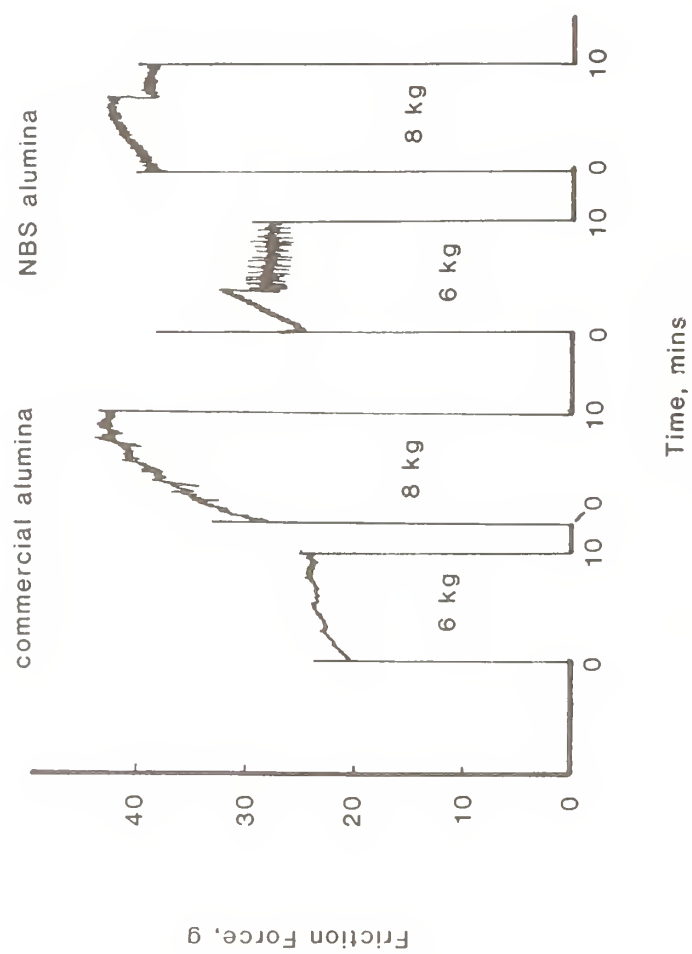


Figure 55. Comparison of Friction Traces for NBS Alumina versus Commercial Alumina

sacrificially wearing at a moderate rate in order to avoid the transition to high wear seen in the commercial product.

#### G. Summary

Three wear tests method for ceramic materials have been developed and described: four-ball constant condition tests, four-ball step-loading tests, and ball-on-three-flat (step-loading) tests. Plots of wear scar diameter versus load results in valuable information on relative wear performance. This is enhanced by the use of a test severity overlay which quickly provides the severity (mean pressure) present during the test. In many cases friction data can also be obtained that leads to a better understanding of the underlying tribological processes. These techniques are very sensitive to compositional and structural differences in ceramic materials and will provide a means of studying the underlying relationship between structure and tribological performance.

## Chapter V

## ALUMINA/WATER TRIBOSYSTEM: INTRODUCTION AND LITERATURE SURVEY

A. Preliminary Explanation of Lubrication Mechanisms for  
Alumina With Water

During the development of a wear test method for ceramic materials, it was found that water dramatically reduces the friction and wear of alumina sliding on alumina over that of the unlubricated case. Friction is reduced by 50-60%. Wear is reduced by 99% (as measured by mass loss data) at high loads of 25-40 kg and even more at lower loads before the wear transition. In an attempt to try to understand the possible mechanisms by which water would lubricate alumina, several possibilities were examined.

i) Fluid film provides some hydrodynamic lift reducing contact between the surfaces and reducing friction and wear.

ii) Water acts as a coolant and serves to reduce temperatures in the contact zone.

iii) Double layer effects or Rehbinder effects between the surface and water which alter the near surface material behavior.

iv) Chemical reactions between water and alumina which produce lubricous products.

Reduction of friction and wear through hydrodynamic lubrication is a common and useful lubrication technique. The models used to

describe hydrodynamic lubrication are derived from the Reynolds equation and in general simplify to the relationship that pressure (which supports the load) is proportional to surface velocity and viscosity.<sup>37</sup> This lubrication regime is usually found however under conditions of relatively high sliding speed, low load, and viscous fluids. The step loading test is run under conditions of relatively low sliding speed, moderate to high loads, and water is not very viscous. One would expect therefore that hydrodynamic lubrication would not play a critical role. Despite this, some researchers have claimed that hydrodynamic lubrication is possible with water at slow sliding speed with ceramics.<sup>38</sup> Their experiment, conducted using silicon nitride lubricated with water at low to moderate loads and low speed (6.5 cm/s), indicated very low coefficient of friction levels of less than 0.002. It was claimed that chemical reaction between water and the ceramic serves to chemically polish the surface to ultrasMOOTH dimensions and thus allow for hydrodynamic lubrication. Our testing however does not give as polished a surface. In addition, coefficient of friction levels are not near the very low levels ( $<0.01$ ) usually associated with this type of lubrication. Therefore, this explanation does not adequately explain the friction and wear behavior we have observed with water and alumina.

Water does indeed provide a large degree of cooling, however, if cooling were the sole explanation for the beneficial effects of water, then other lubricants which are not as good a coolant would provide



less benefit. This is not the case, as paraffin oil gives lower friction and wear than water at low loads.

Double layer effects or Rehbinder effects between surfaces and fluids have gained some popularity as a way of explaining changes in wear of materials under different environments. There appears to be some correlation between wear, zeta potential, and material properties such as hardness.<sup>39</sup> Much of the work however shows changes in wear rate by factors of two or four not the two order of magnitude that are observed in this study. This explanation therefore would not appear to be the predominant mechanism for reduction of friction and wear of alumina by water.

At first, chemical reactions between water and alumina seems a far-fetched possibility for lubrication. After all, aluminum oxide already exists in its highest oxide state and is considered very inert. Under the unusual conditions of stress and temperature that exist in a tribological contact however chemical reaction may be possible. SEM photographs of the wear scar indicated a film was present in the wear scar and appeared to cover half of the wear scar. These films were not present in either dry or paraffin oil lubricated wear scars. The other key observation that indicated that chemical reactions may play a role in lubrication is the fact that the hydrates or hydroxides of alumina are layer lattice structures. That is, they are arranged in layers with strong bonding among the atoms in the

layer and weaker bonding between layers. These weaker bonds are easily sheared which would serve to reduce friction and wear.

Layer lattice (or lamellar) compounds have been used as solid lubricants for many years.<sup>40</sup> The most popular compounds, graphite, and molybdenum disulfide, have been used for many different lubricant applications including automotive lubricants. When stressed, the weak bonds between the layers of atoms break and the layers slide easily over one another. Because the bonds are weak, it does not take much energy to break them; hence friction is very low.

It is the hypothesis of this report therefore that the unique environment in a water lubricated contact junction produce reaction products which are lubricous and reduce friction and wear. This is not to say that the other factors described of hydrodynamics, cooling, and double layer forces do not play a role in helping to reduce friction and wear but that the chemical reaction to form lubricous products is the dominant mechanism for lubrication in these tests.

#### B. Structures and Nomenclature of Aluminum Oxides and Hydroxides

There are many different forms of aluminum oxides and hydroxides therefore a brief explanation of structures and nomenclature is in order. Anyone desiring a more comprehensive explanation of the structure or properties of these compounds are referred to references

41-44. The Alcoa paper on Oxides and Hydroxides of Aluminum by Wefers and Bell<sup>41</sup> gives the best introduction to this area.

Aluminum oxide ( $\text{Al}_2\text{O}_3$ ) exists in many forms. The most common form is alpha ( $\alpha$ ) alumina (corundum) which is hexagonal. Other forms of  $\text{Al}_2\text{O}_3$  occur less frequently: gamma (tetragonal); delta (orthobombic, tetragonal); eta (cubic spinal); theta (monoclinic); chi (cubic, hexagonal); kappa (hexagonal); and iota (orthorhombic). In some cases (chi alumina for example) two crystal systems are listed. This indicates a disagreement in indexing the x-ray powder diffraction data by different authors and shows the difficulty and controversy surrounding some of these transition aluminas (all aluminas except alpha).

There is less controversy surrounding the existence and structure of the aluminum hydroxides. table 6 lists the most common forms of these compounds and gives some of the more common nomenclature presently used by different researchers. I have chosen to refer to the compounds as hydroxides instead of hydrates and use the symposium names to further identify the form. This selection was made because the crystal structures are not true hydrates. The water molecule actually breaks an H-O bond to form separate H and OH groups which become an integral part of the structure. Therefore the term hydrate for compounds such as gibbsite is actually a misnomer.

Table 6

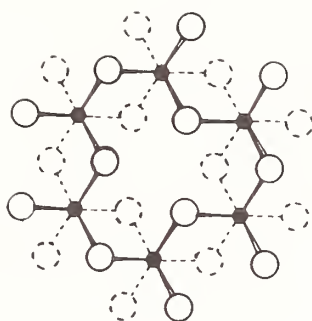
## Nomenclature for Hydroxides of Aluminum

Chemical Name	Chemical Formula	Nomenclature System	
		Symposium	Alcoa
Aluminum Oxide Hydroxides or (Alumina Monohydrate)	$\text{AlO}(\text{OH})$ or $(\text{Al}_2\text{O}_3 \cdot 3\text{H}_2\text{O})$	Boehmite  Diaspore	Alpha Alumina Monohydrate  Beta Alumina Monohydrate
Aluminum Trihydroxides or (Alumina Trihydrate)	$\text{Al}(\text{OH})_3$ or $(\text{Al}_2\text{O}_3 \cdot 3\text{H}_2\text{O})$	Gibbsite or Hydrargillite  Bayerite  Nordstrandite	Alpha Alumina Trihydrate  Beta Alumina Trihydrate

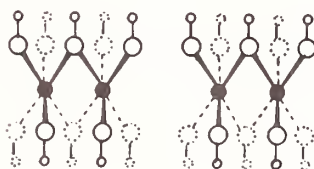
Source: Wefers and Bell (41), p. 8.

Gibbsite, bayerite, nordstrandite, and boehmite are layered structures with relatively weak bonding between the layers. All three trihydroxides have identical structures within each layer and differ only in the stacking of the layers. Each layer consists of layers of atoms of the sequence hydrogen, oxygen, aluminum, oxygen, hydrogen (fig. 56). Aluminum atoms are octahedrally coordinated to six different oxygen atoms while each oxygen atom is bonded to two aluminum and one hydrogen atoms. The stacking sequence for OH ions for gibbsite (monoclinic) is AB•BA•AB•BA (fig. 57). This superposition of layers combined with the hexagonal arrangement of Al ions within the layers leads to channels through the lattice parallel to the C axis. Bayerite (monoclinic) is arranged in layers of OH sequence AB•AB•AB•AB. This is because the OH ions do not lie directly above each other as they do for gibbsite. Instead, the OH ions of the second layer lie in the depressions between the OH groups formed by the first layer. Nordstrandite (triclinic) is described in reference 41 as having the AB•AB sequence of bayerite with the OH ions of adjacent double layers located opposite each other leading to the stacking sequence AB•AB•BA•BA.<sup>44</sup> This shows the lattice of nordstrandite to be a combination of the lattices seen for both bayerite and gibbsite. Boehmite (orthorhombic) is also described as having a layered structure although the layers are very different from the layers seen for the trihydroxides. Diaspore (orthorhombic) has more of a three dimensional structure. Wefers and Bell<sup>41</sup> give approximate Moh's hardness values for the aluminum oxides and hydroxides which show that the layer structures have much lower

Top View



Side View



≡ bond coming out of page

— bond in plane of page

--- bond going into page

● aluminum

○ oxygen

○ hydrogen

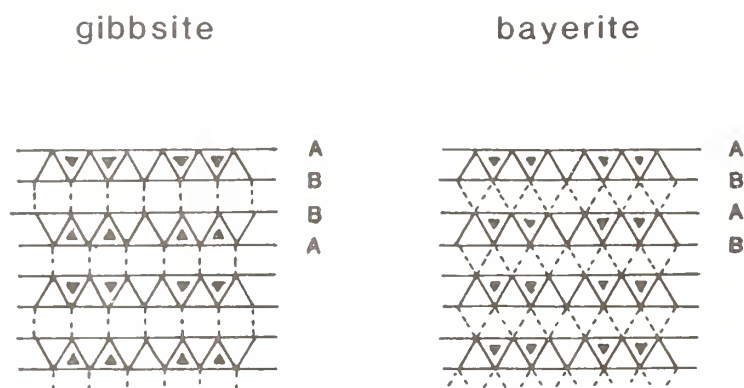
Solid, filled atoms are in the plane of the page.

Solid, unfilled atoms are above the plane of the page.

Dashed atoms are below the plane of the page.

Figure 56. Structure of  $\text{Al}(\text{OH})_3$



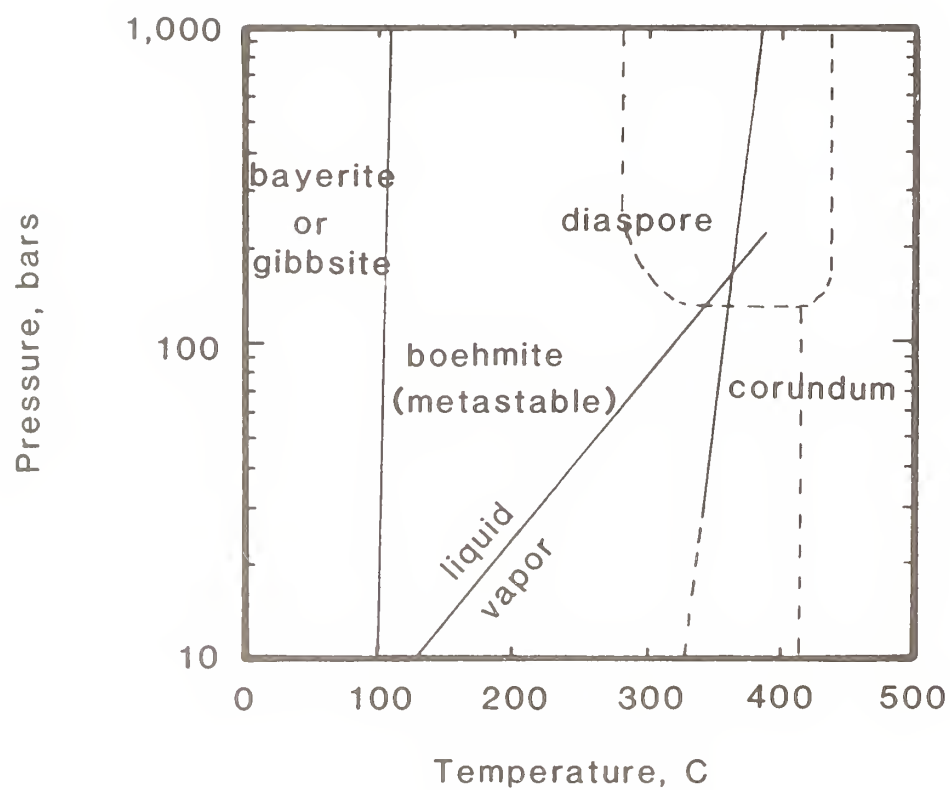


Source: Wefers and Bell (40) p19

Figure 57. Layer Stacking Sequence for Gibbsite and Bayerite

hardness. For example, gibbsite is 2.5 to 3.5 on the Moh's scale; boehmite is 3.5 to 4; diaspore is 6 1/2 to 7; and  $\alpha$   $\text{Al}_2\text{O}_3$  is 9.

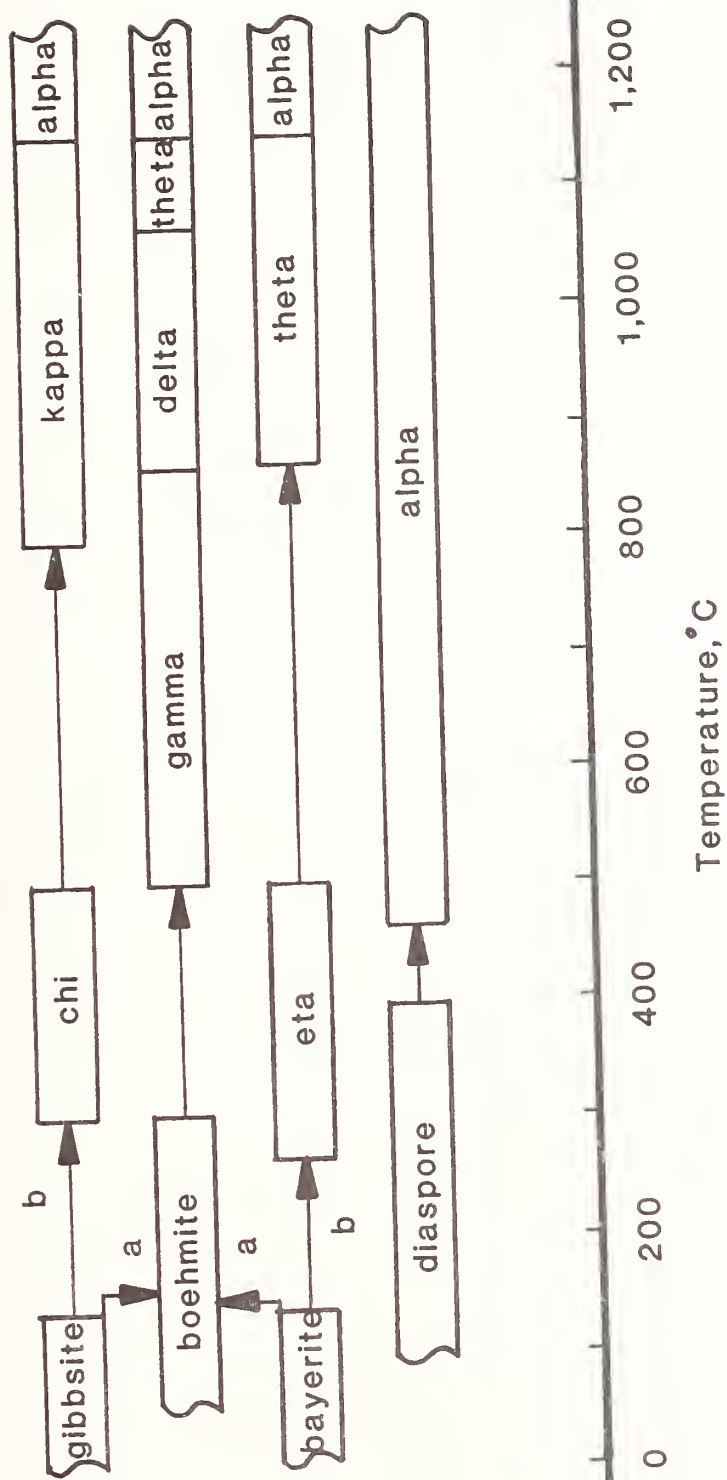
Two additional pieces of information are useful in interpreting the relationship between the different forms of alumina and alumina hydroxides. A phase diagram of the alumina water system (fig. 58) shows the relationship between several phases. Low temperature (up to 100°C) seems to favor the trihydroxide. Between 100°C and 330°C boehmite is formed. At highest temperatures alpha alumina is favored. In addition, there are indications that higher pressures may favor diaspore over boehmite. It is important to note on looking at this phase diagram that it has been defined under conditions where pressure is isotropic. In the case of a wearing surface, anisotropic shear forces are applied. Therefore, this phase diagram should not be taken as a literal representation of phases present at various temperatures and pressures in a contact junction. It does, however, indicate that low temperatures favor trihydroxides, intermediate temperatures favor monohydroxides, and high temperatures favor alpha alumina. The second useful item of information is the decomposition sequence for the aluminum hydroxides from reference 41. The decomposition sequence is useful because it gives an indication of possible reaction pathways for formation of aluminum hydroxides assuming some reversibility for the decomposition reaction. Figure 59 shows pathways for decomposition of different aluminum hydroxides. Trihydroxides are present at low temperatures. Depending on conditions of environment, pressure, and temperature, they decompose to form either transition



Source: Misra (43) p26

Figure 58. Phase Diagram for  $\text{Al}_2\text{O}_3$  -  $\text{H}_2\text{O}$  System

Path a favored by high pressure, moisture, large particle size, fast heating rate



Source: Wefers and Bell (40) p43

Figure 59. Decomposition Sequences for Aluminum Hydroxides

aluminas (path b) or boehmite (path a). Boehmite apparently decomposes in a complex pathway through the transition aluminas of gamma, delta and theta until it finally becomes alpha alumina. This suggests, therefore, that it may be possible to form lubricous layer structure alumina hydroxides from alpha alumina /and water, if the decomposition reactions are reversible.

### C. Approach

The objective of this part of the study is to determine whether tribochemical reactions take place between water and alumina to form lubricous compounds which reduce friction and wear. This is being done using three different techniques. Firstly, kinetic experiments were conducted using water and alumina powders to determine the kinetics for these reactions. Secondly, wear tests were conducted using aluminum hydroxide powders to determine whether they possessed any lubricating capabilities. Finally, extensive analysis of the wear scar surface and debris were performed in order to directly observe evidence for the formation of these compounds in tribological contacts.

## Chapter VI

## ALUMINA/WATER TRIBOSYSTEM: EXPERIMENTAL

## APPARATUS AND OPERATING PROCEDURES

A. Test Approaches

Several different approaches were used to investigate the hypothesis that alumina-water reaction products are formed in the tribocontact.

- o Static Kinetic Tests
- o Powder Friction Tests
- o Dynamic Wear Tests

The first approach consisted of trying to react alumina powder with water and analyze the reaction products. This was termed the static kinetic approach and attempted to show feasibility of alumina-water chemical reactions. The second approach involved running wear tests with different powders in the contact to determine their effect on friction. The third and most direct approach involved trying to find evidence of the product in the wear scar and wear debris. The first and second approaches were essentially a backup to the more direct (but more difficult) analysis of wear products. If it was not possible to find direct evidence of reaction products perhaps it could be inferred through kinetics and performance data.



## 1. Static Kinetic Tests

Static kinetic tests were conducted using the modified high pressure micro-oxidation bombs shown in figure 60 and described in detail by King.<sup>45</sup> The samples of alumina (0.5 g) and water (25 ml) are placed in a pyrex liner with a loose fitting pyrex cap. This is placed in a cylindrical steel bomb fitted with removable top with a pressure gage and valve. The top is secured to the cylinder with six bolts and pressure is maintained through use of a high temperature O-ring seal. At the beginning of a test, the bomb is insulated at the top and placed into an aluminum block heater containing a molten metal heat transfer fluid. The test is run for a certain length of time then terminated using water bath cooling. The contents of the pyrex reaction tubes are then removed and the water and powder phases separated using a centrifuge. The resulting powder-water slurry is dried using a watch glass. The powder is carefully ground using an agate mortar and pestle, and saved for analysis. Several key features allowed the test to be conducted in a repeatable and controlled manner. One is the use of water as a reactant. The vapor pressure-temperature relationship of liquid water in equilibrium with saturated vapor is very well documented (steam tables). The pressure-temperature relationship of air in the closed bomb can also be estimated using the ideal gas law. The combination of these two pressure-temperature relationships allow us to estimate the temperature in the reactor given the pressure. This relationship is derived in Appendix E and plotted in figure 61. A second key

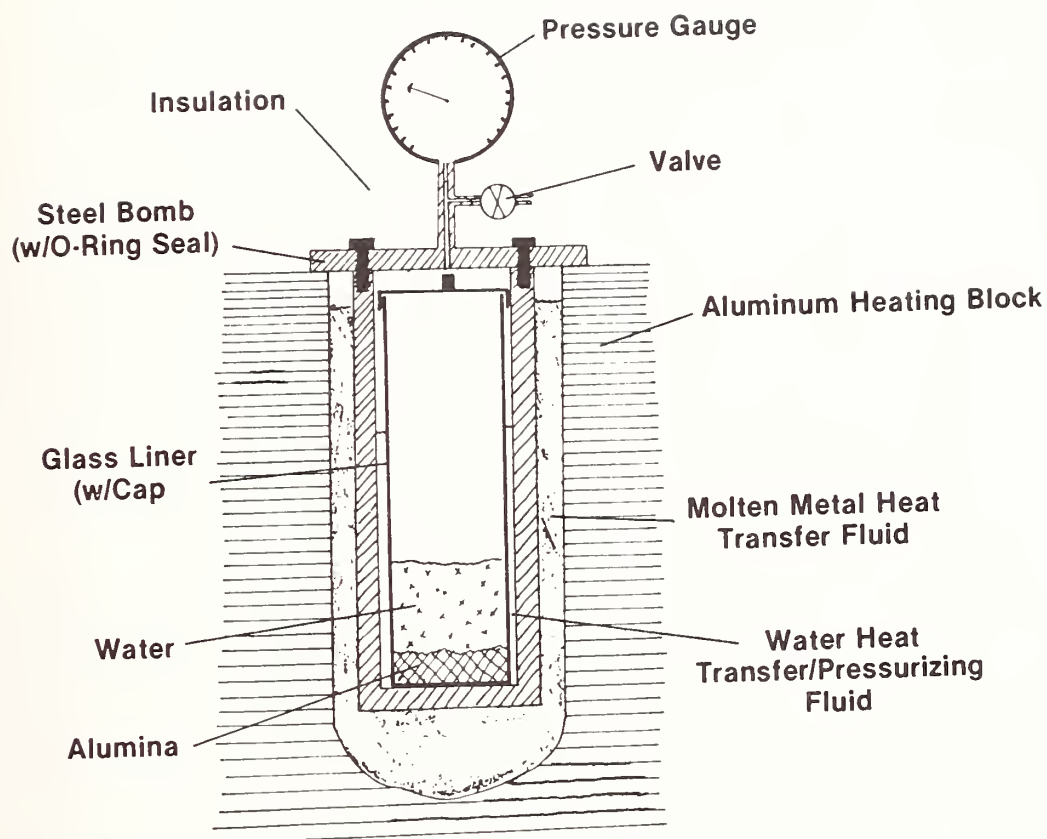


Figure 60. High Pressure Bomb Reactor Design

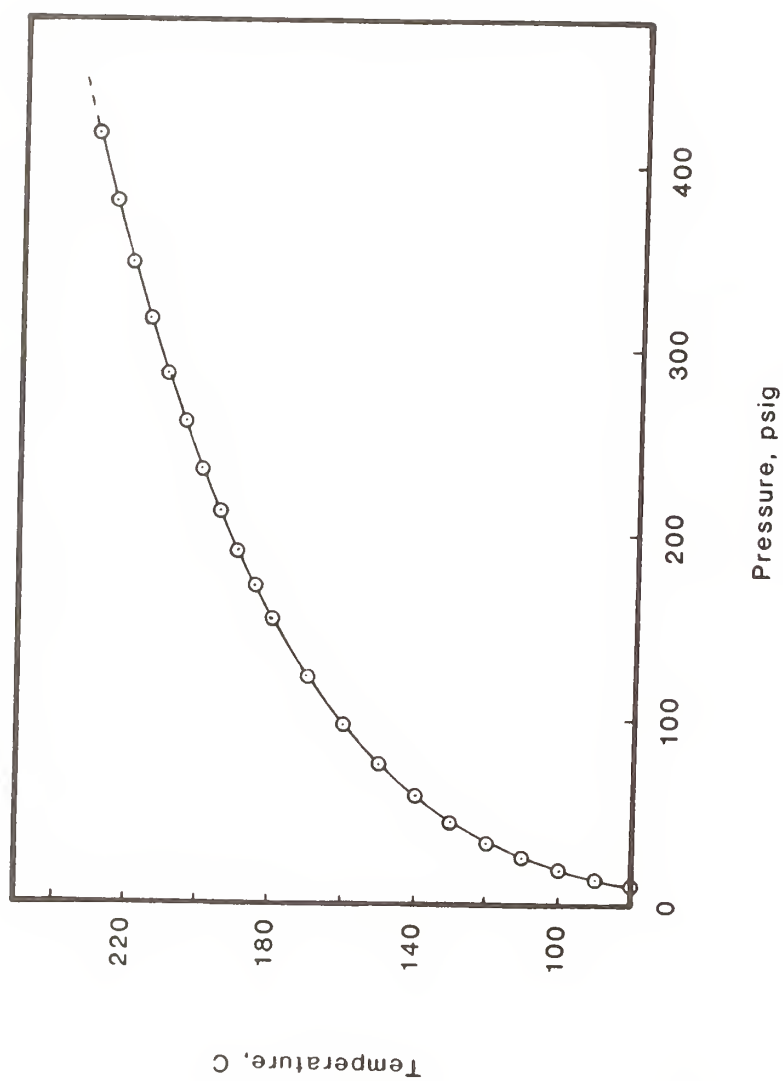


Figure 61. Temperature-Pressure Relationship for Bomb Reactor

feature is the use of water heat transfer/pressurizing fluid between the pyrex reaction vessel and the metal bomb casing. If this fluid is not present, heat transfer between the steel bomb and the glass liner tends to be much slower. In addition, boiling of the water reactant during the rapid heatup resulted in splattering of alumina on the walls of the pyrex liner and sometimes completely out of the liner. The water heat transfer/pressurizing fluid heats up faster than the water inside the pyrex liner and boils. As it boils, it pressurizes the system and reduces boiling of fluid inside the liner. Thus the boiling and splattering of alumina on the inside walls of the pyrex liner is greatly reduced.

It was estimated that less than one milliliter of liquid water would be required to produce enough saturated water vapor at 200°C to fill the bomb. The fifteen milliliters of water used as the heat transfer/pressurizing fluid is therefore more than sufficient to ensure both liquid and vapor are present at the reaction temperature. Half a gram of alumina is used as a reactant. Using reaction stoichiometry, it was estimated that approximately a quarter of a gram of water would be required to form the trihydroxide (tri-hydrate) reaction product from all of the initial alumina. By using 25 ml of water reactant, the water is present in large (100X) excess.

An experiment was conducted to determine the length of time necessary to heat the bomb to the desired temperature (fig. 62). The temperature rises quite rapidly and within five minutes has

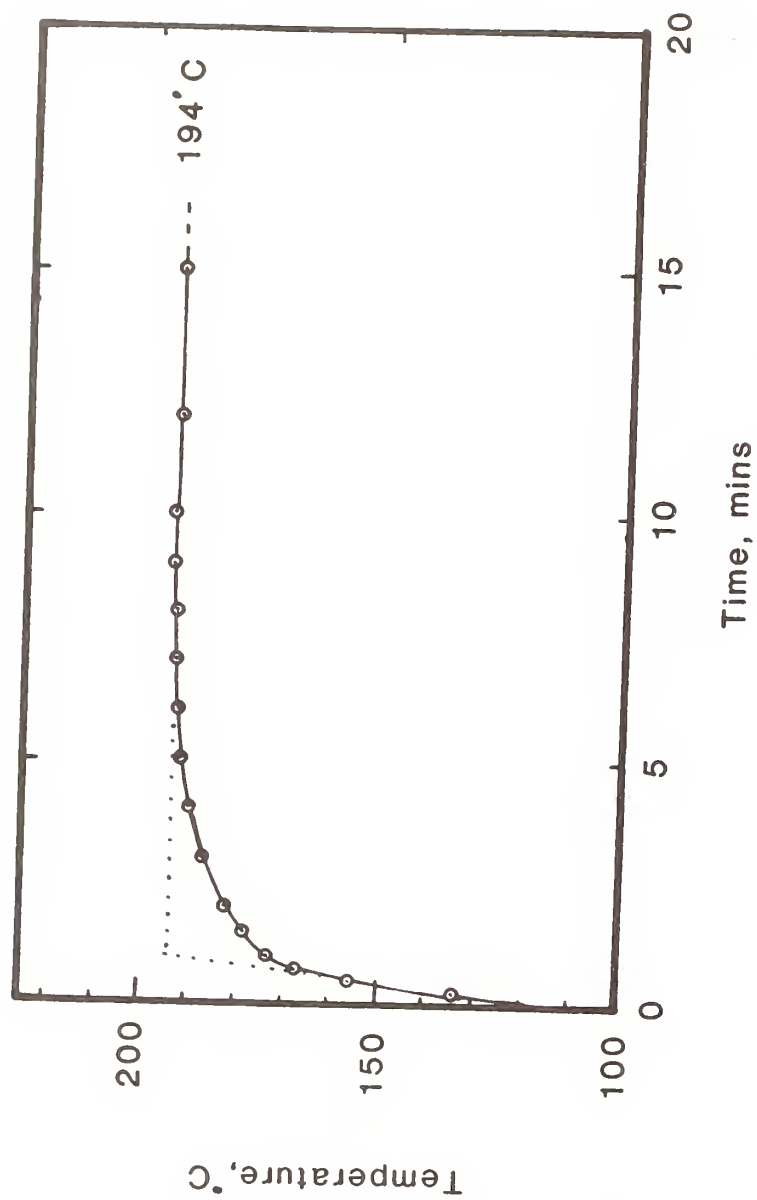


Figure 62. Temperature Inside Bomb versus Time during Heating

reached within two degrees of the final equilibrium temperature (194°C). The intersection of the initial and final slopes are used to determine the initial starting point for the reaction. This falls at approximately one minute. At one minute, the temperature is 173°C or 21°C below the final temperature. Reaction rates at this temperature are approximately 1/4 the final rates and should not have a significant contribution to the total reaction process. Therefore, one minute is subtracted from all measured reaction times to give actual reaction times used for kinetic data analysis.

## 2. Powder Friction Tests

Powder friction tests were conducted using ball-on-three-flat tests. First a dry test was conducted to provide a wear scar. Enough dry powder was put into the test cup to completely immerse the lower wear test specimens ( $\approx 1$  ml) and the friction test was conducted for one minute. The powder was then completely removed and a second, different powder was used. This was continued until each powder had been run at least twice. In addition, two different loads (2 kg and 5 kg) were used.

## 3. Dynamic Wear Tests

Ball-on-three-flat dynamic wear tests were used to generate wear debris. Once generated, this debris was recovered using a ten milliliter syringe to remove the water/suspended debris. Several



rinses of water were used to ensure recovery of as much debris as possible. The mixture was centrifuged for ten minutes using a high speed (13,000 g) centrifuge and the water was carefully withdrawn. The resultant powder water mixture was dried on a watchglass overnight, ground carefully to a fine powder using an agate mortar and pestle, and analyzed. Only very small amounts (1-2 mg) of material could be recovered which tended to compound the analytical problems. Preliminary tests produced powders that were reddish-orange in color instead of white. Atomic absorption analysis indicated traces of iron contaminant therefore an electroplated gold coating was applied to all steel parts in contact with the specimens or lubricant (chuck, lower specimen cup, spindle end, and threaded end of chuck retaining rod) to eliminate this problem.

#### B. Reference Powders

Six reference powders were obtained and used in the course of this study. They were used in the powder friction tests and also to develop the analytical tests necessary to identify and quantify the materials produced in static kinetic tests and dynamic wear tests. The powders and the arbitrary identification numbers assigned to them are:

AL1: Boehmite ( $\text{Al}_2\text{O}_3 \cdot \text{H}_2\text{O}$  or  $\text{AlOOH}$ ) [UC-1]

AL2: Gamma Alumina ( $\gamma\text{-Al}_2\text{O}_3$ ) [UC-2]

AL3: Boehmite ( $\text{Al}_2\text{O}_3 \cdot \text{H}_2\text{O}$  or  $\text{AlOOH}$ ) [UC-3]

AL4: Alpha Alumina ( $\alpha$ -Al<sub>2</sub>O<sub>3</sub>) (spray dried)

AL5: Alpha Alumina ( $\alpha$ -Al<sub>2</sub>O<sub>3</sub>) [UC-9]

AL6: Gibbsite (Al<sub>2</sub>O<sub>3</sub> • 3H<sub>2</sub>O or Al(OH)<sub>3</sub>)

The numbers and letters in the square brackets are an NBS designation to identify the particular batch of powder that was produced. These six samples represent four of the most common forms of alumina and alumina hydrates (or hydroxides), and were available in sufficient purity and quantity to make them useful for analytical procedure development.

Samples of the powders were prepared for SEM analysis by sprinkling powder on a stub painted with a thin coating of silver conducting paint. After drying, the excess powder was removed and the samples coated with a thin conductive coating of gold/palladium. 1,000X and 10,000X magnification photographs best illustrated the size and morphology of the powders.

Sample AL1 (boehmite) (figs. 63 and 64) consists of irregularly shaped particles in a wide size range of 0.1 to 10  $\mu$ m.

Sample AL2 (gamma alumina) (figs. 65 and 66) contains particles which appear to be agglomerates. Particles appear to be in the 1-10  $\mu$ m range but are themselves composed of very small particles less than 0.1  $\mu$ m in size.

Sample AL3 (boehmite) (figs. 67 and 68) has an entirely different particle morphology although it is supposed to be the same basic material as sample AL1. It appears to have been produced using a spray drying process which tends to produce spherical particles. These particles are mainly in the range of 5-20  $\mu\text{m}$  in diameter. Under higher magnification (10,000X) the material does seem to have a "waxy" appearance similar to sample AL1.

Sample AL4 (alpha alumina) (figs. 69 and 70) is a spray dried sample. The spherical particles are 1-15  $\mu\text{m}$  in diameter. Under higher magnification (10,000X) the particles appear porous, and are composed of fused microparticles approximately 0.1  $\mu\text{m}$  in size.

Sample AL5 (alpha alumina) (figs. 71 and 72) consists of irregularly shaped particles of varying shapes and sizes. Characterization of the shapes and size range is difficult due to the wide variety available however most particles appear to be "chips" approximately 20  $\mu\text{m}$  by 20  $\mu\text{m}$  by 3  $\mu\text{m}$  thick. Upon closer inspection at high magnification, the chips are composed of fused microparticles approximately 0.1  $\mu\text{m}$  in size. These microparticles appear to be very similar in size and morphology to the microparticles observed for powder AL4.

Sample AL6 (gibbsite) (figs. 73 and 74) appears to be composed of large polycrystalline agglomerates approximately 30  $\mu\text{m}$  in diameter. Higher magnification reveals cleavage planes and crystalline character

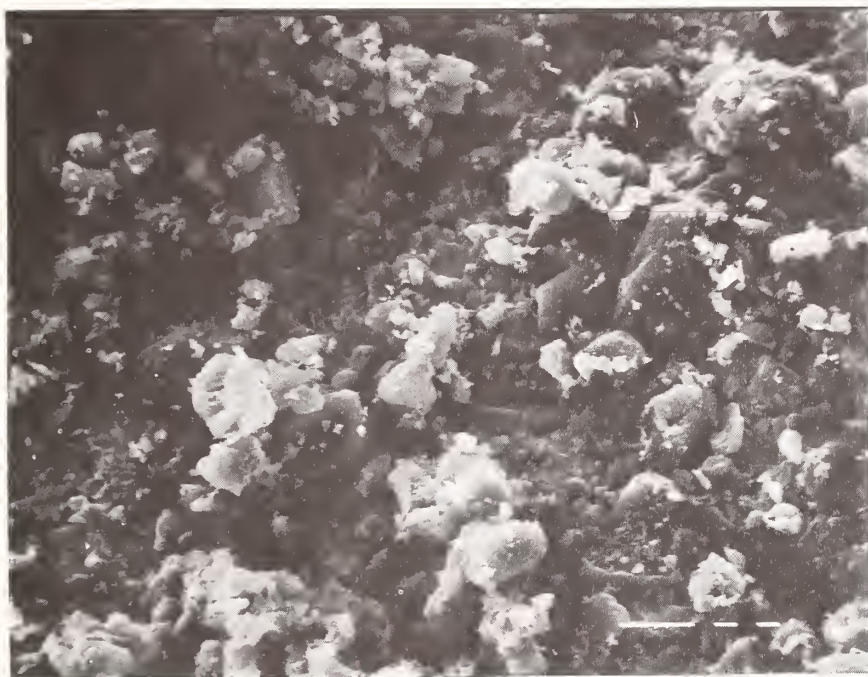


Figure 63. 1000X Secondary Emission SEM Photograph of Powder AL1



Figure 64. 10,000X Secondary Emission SEM Photograph of Powder AL1



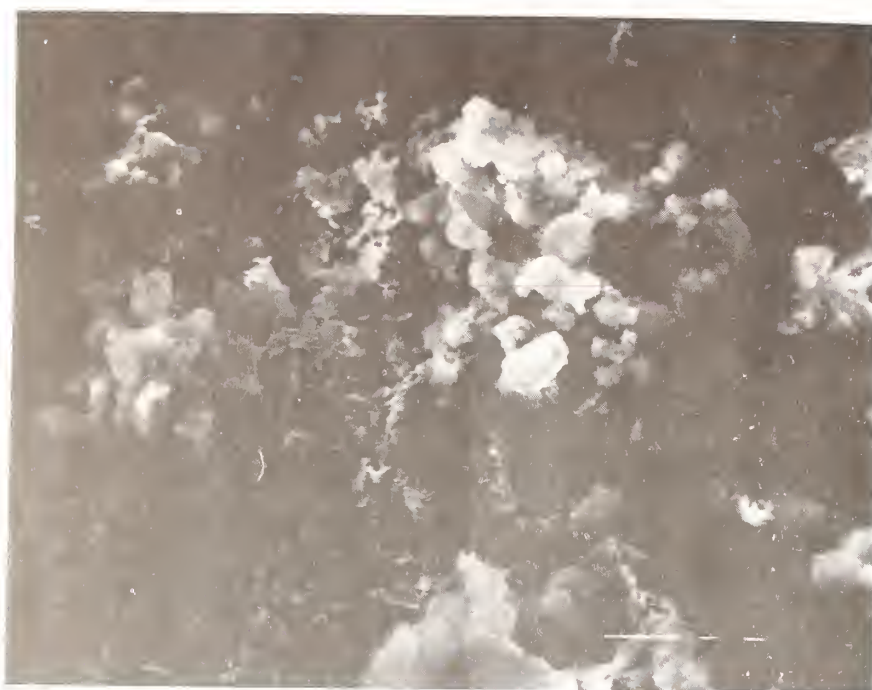


Figure 65. 1000X Secondary Emission SEM Photograph of Powder AL2



Figure 66. 10,000X Secondary Emission SEM Photograph of Powder AL2

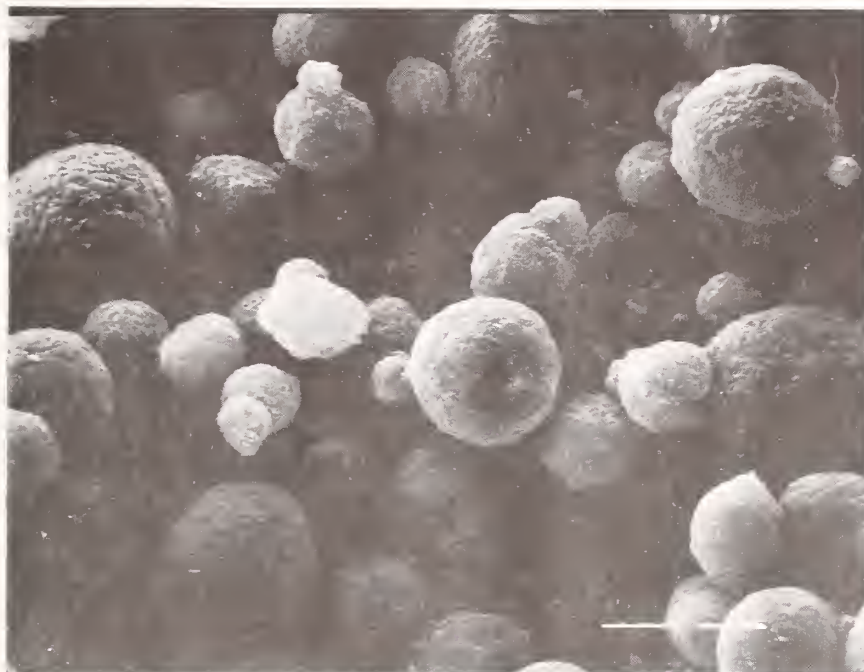


Figure 67. 1000X Secondary Emission SEM Photograph of Powder AL3



Figure 68. 10,000X Secondary Emission SEM Photograph of Powder AL3



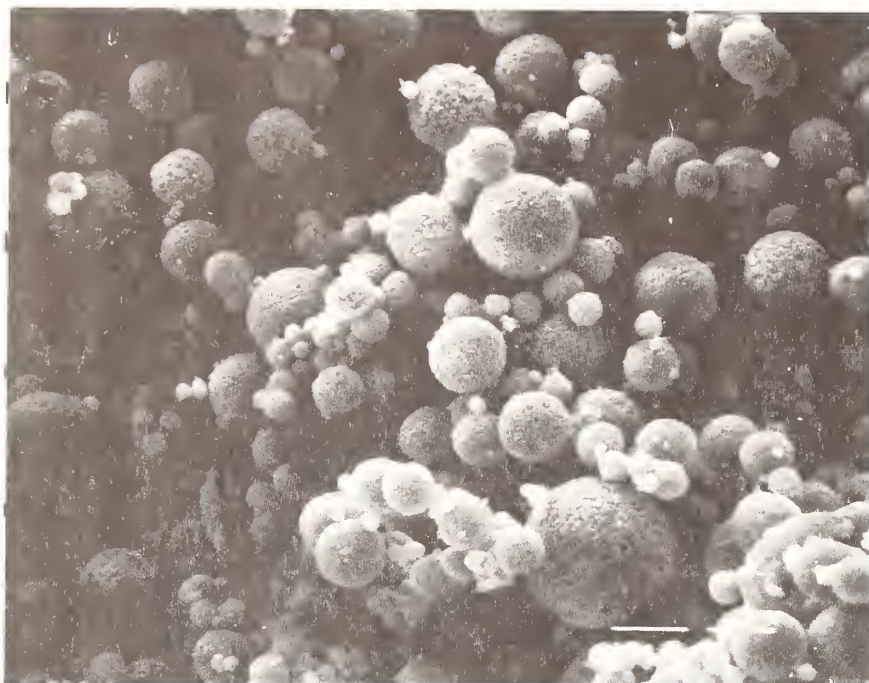


Figure 69. 1000X Secondary Emission SEM Photograph of Powder AL4

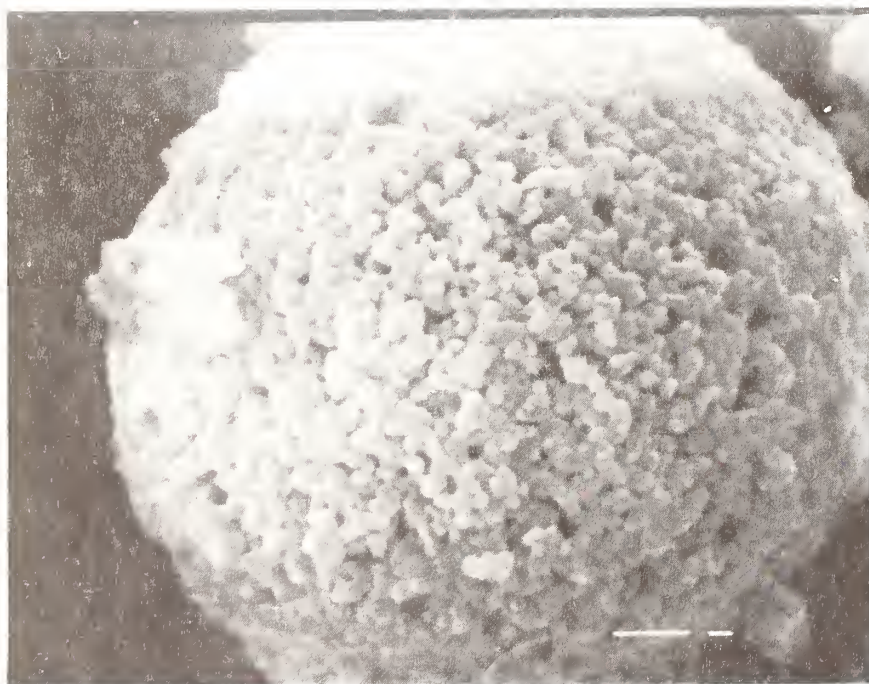


Figure 70. 10,000X Secondary Emission SEM Photograph of Powder AL4

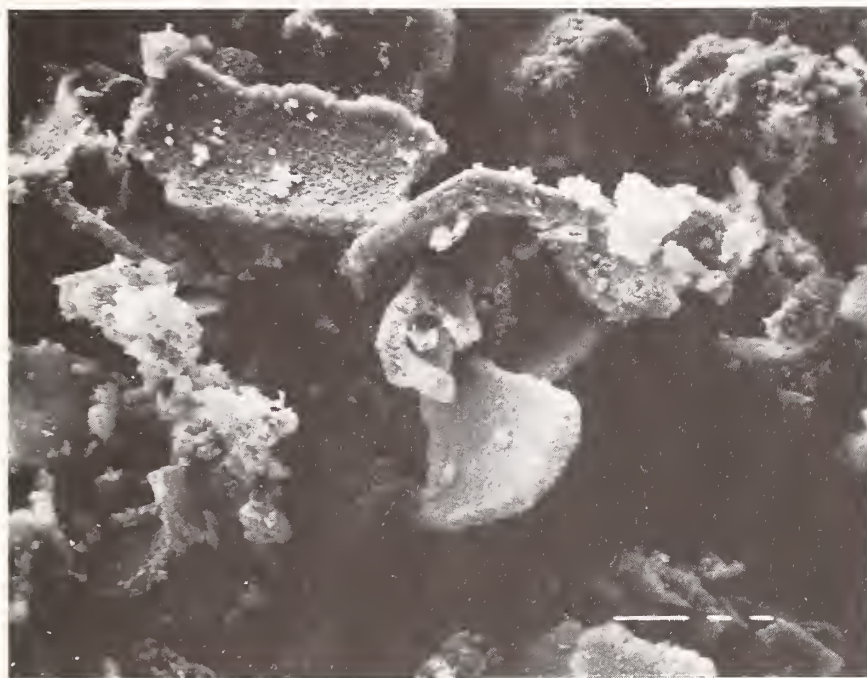


Figure 71. 1000X Secondary Emission SEM Photograph of Powder AL5

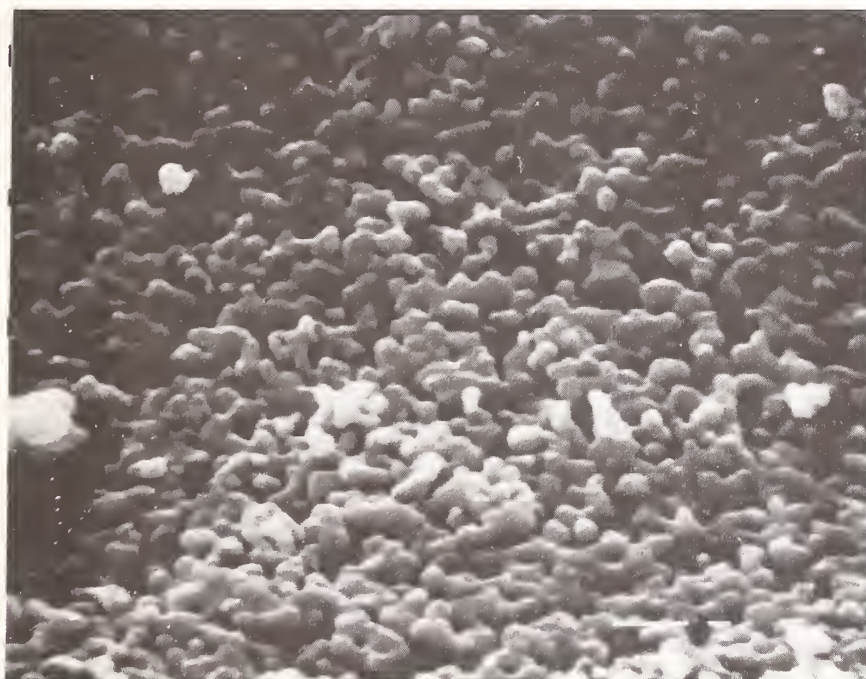


Figure 72. 10,000X Secondary Emission SEM Photograph of Powder AL5



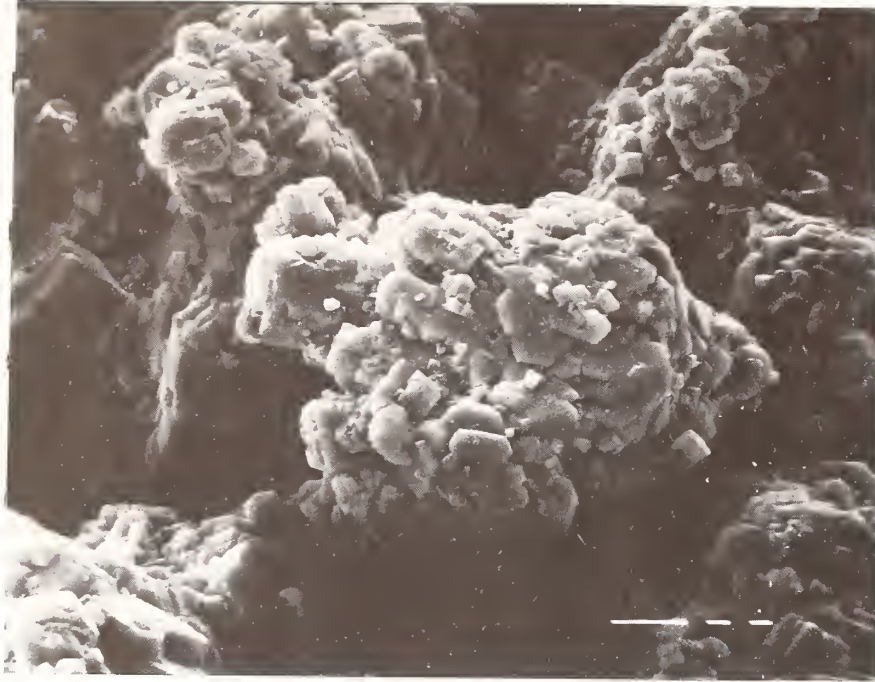


Figure 73. 1000X Secondary Emission SEM Photograph of Powder AL6



Figure 74. 10,000X Secondary Emission SEM Photograph of Powder AL6

consistent with the crystal system of gibbsite (monoclinic -001 cleavage).

X-ray powder diffraction (XRPD) patterns were run of all six samples in order to confirm their structure. These spectra are given in Appendix F. Samples AL4, AL5, and AL6 all gave very sharp XRPD peaks and indicated that they were indeed relatively pure samples of alpha alumina and gibbsite. The other samples gave very diffuse peaks that made identification more difficult. Samples AL1 and AL3 were confirmed to be boehmite even though the peaks obtained were quite diffuse. It is believed that the diffuse peaks are due to very small crystallite size for the samples. Sample AL2 also gave very diffuse peaks. Comparison of the peaks to reference data suggest that the sample may actually be delta alumina, or possibly a mixture of gamma and delta alumina. Because of the similarity of these two deformed polymorphs of alumina (both tetragonal) and the difficulty in distinguishing between them, I have maintained the title of "gamma" alumina for this sample but note that delta alumina may also be present.

### C. Analytical Techniques

Several analytical techniques were used to study aluminas, alumina hydroxides, alumina oxide hydroxides, wear scars, and wear debris. The techniques and the samples they analyzed are given in table 7. All of the techniques had some qualitative aspects, that

Table 7

Analytical Techniques Utilized in the Investigation of  
Alumina/Water Reactions

Technique	Acronym	Samples Analyzed	Qualitative	Quantitative
Thermogravimetric Analysis	TGA	Powders, Wear Debris	Semi	Yes
Differential Scanning Calorimetry	DSC	Powders, Wear Debris	Semi	Yes
X-Ray Powder Diffraction	XRPD	Powders, Wear Debris	Yes	No
Fourier Transform Infrared	FTIR	Powders, Wear Debris, Wear Scars	Semi	No
Scanning Electron Microscopy	SEM	Powders, Wear Debris, Wear Scars	Semi	No

they could sometimes distinguish between different samples because of some aspect of their performance. X-ray powder diffraction is especially useful as a qualitative analysis technique because, given an adequate sample, it can distinguish between a wide variety of materials. The key is that in many cases if a sample is not present in sufficient quantity, purity, or large enough crystallite size, it cannot be characterized using XRPD. Two of the techniques are also quantitative if it is known what the sample is. Therefore by using the combination of qualitative and quantitative techniques described here, it may be possible to adequately characterize the necessary materials.

#### 1. Thermogravimetric Analysis (TGA)

This technique essentially consists of a microbalance in tandem with a furnace. A sample is heated on a gold pan in the presence of a stream of oxygen and the weight loss from reaction/decomposition of the material is monitored. The particular unit used for this study was a Perkin Elmer TGS-2 equipped with a data analysis computer.

The analysis technique used was adapted from the procedure of Carel and Cabbiness<sup>46</sup> with minor modifications. Basically the procedure consists of heating a sample under a stream of oxygen (40 ml/minute) and observing the accompanying weight loss. The analysis is divided into two parts. The first part consists of heating a sample (usually  $\approx 10$  mg) in a gold pan to 110°C and holding the



temperatures constant for 45 minutes and recording weight loss (as % of the original weight). This is termed the isothermal phase of the analysis and determines the amount of free water associated with the sample. A typical isothermal analysis represented by a sample of boehmite is shown in figure 75. The % weight due to free water can be read directly from the graph by measuring the point at which the curve levels off.

The second part of the analysis consists of increasing the temperature from 110°C to 910°C at a rate of 10°C/min and observing the percentage weight change. This is termed the temperature scan analysis. A representative temperature scan analysis is given in figure 76 for boehmite and shows what information can be obtained with this technique. The weight loss curve shows the relationship between weight of the remaining sample and temperature. The decrease in weight at approximately 300°C is due to water loss from the decomposition of boehmite.



Knowing the stoichiometry of the reaction, we can then back-calculate the amount of original material present.

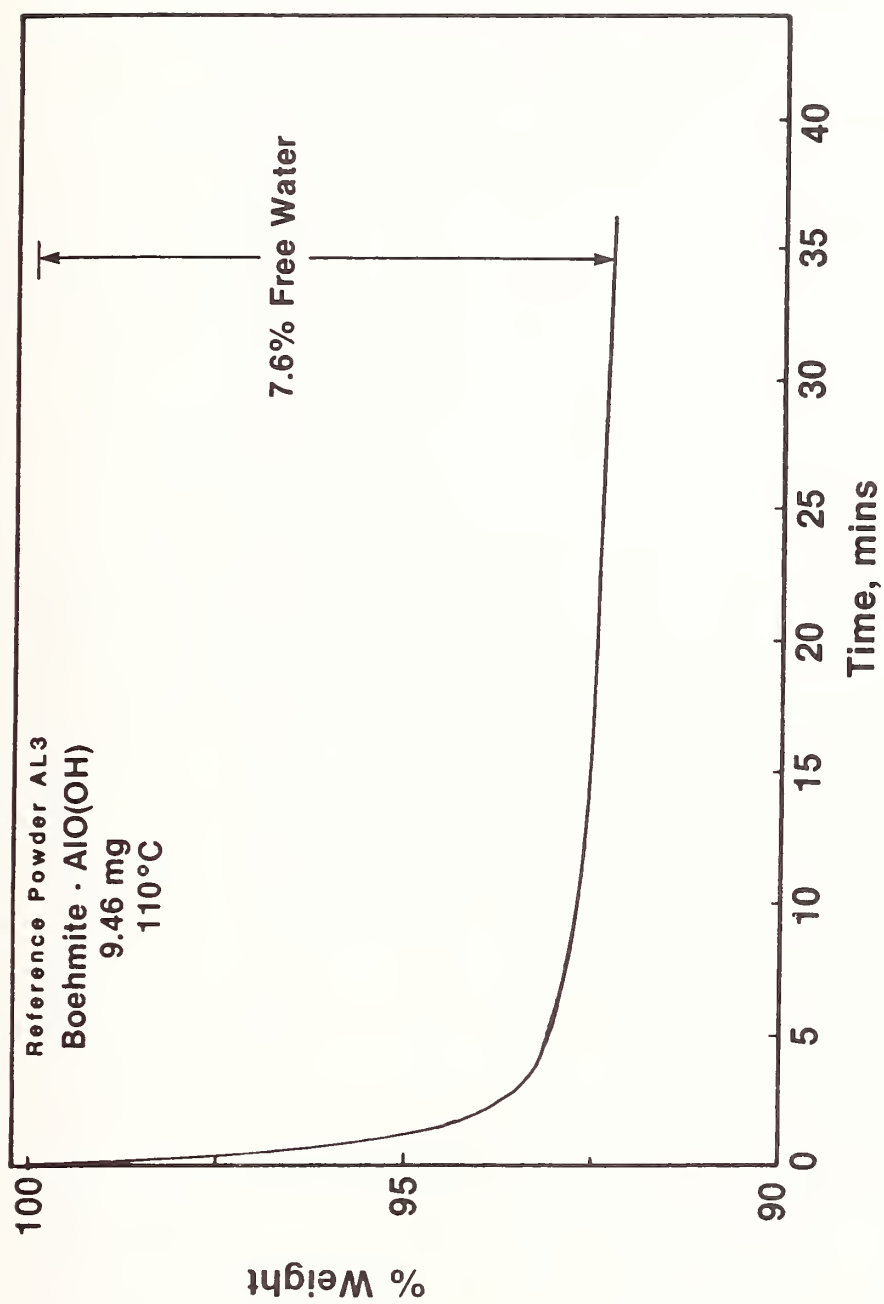


Figure 75. Isothermal TGA of Powder AL3 (Boehmite)

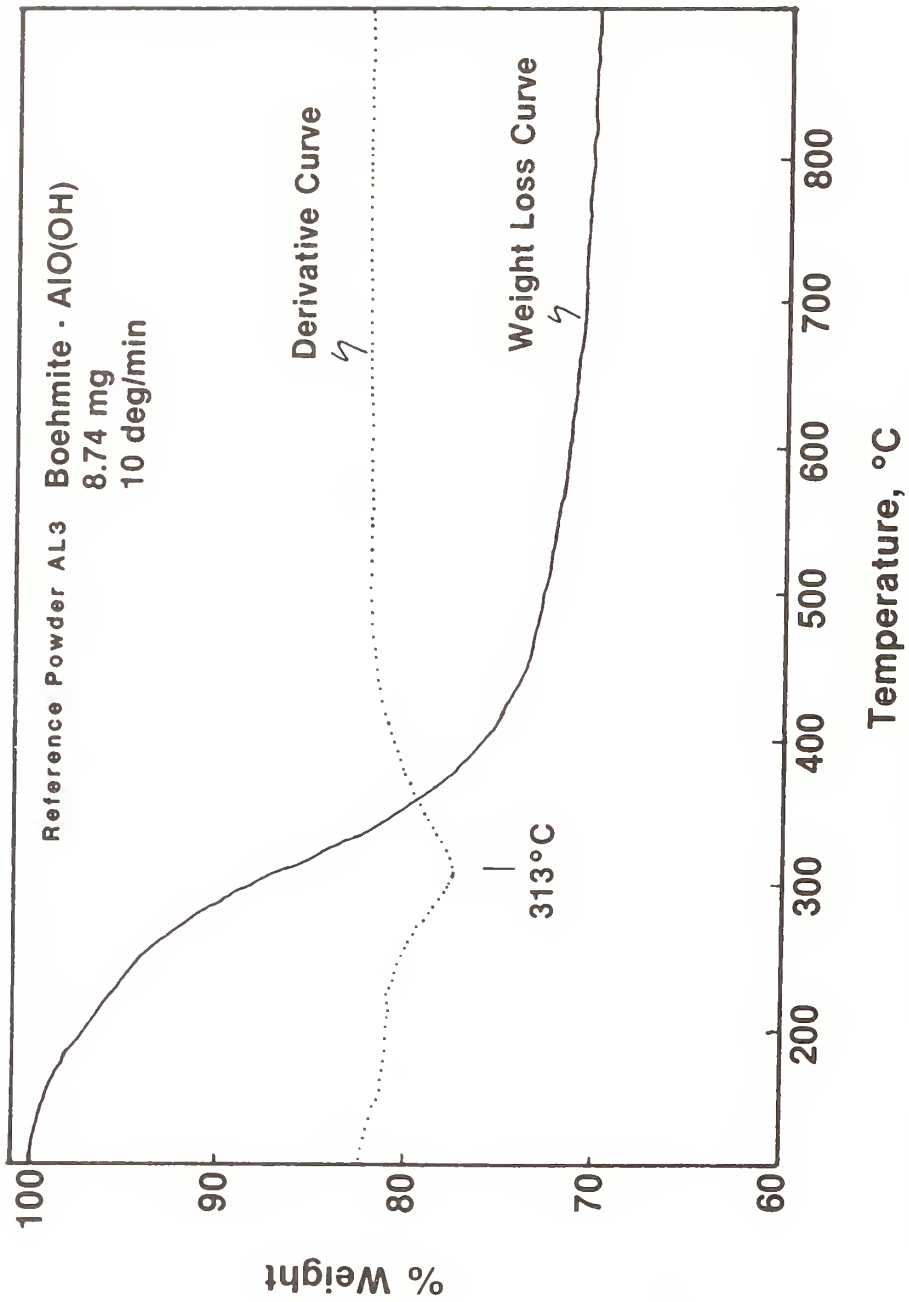


Figure 76. Temperature Scan TGA of Powder AL3 (Boehmite)

A derivative curve can be superimposed on the weight loss curve to allow for a more accurate determination of the maximum rate of weight loss. These maxima (actually minima in the derivative curve) were then used as representative of characteristic decomposition temperatures of the different aluminum hydroxide phases. For mixtures of different hydroxide phases, it is possible to separate the weight loss contribution from individual phases using areas from the derivative curves (as demonstrated by Carel and Cabiness); however, this was not necessary for samples encountered in this study.

Temperature scan analyses for some of the other reference powders are displayed in figures 77-79 and summary data are tabulated in table 8. Boehmite (sample AL3) (fig. 76) consisted of one main peak at 313°C with another minor peak at lower temperature. This lower temperature weight loss may be due to more strongly adsorbed (chemisorbed?) water being driven from the surface of the powder. The other boehmite sample AL1 (fig. 77) showed a derivative peak at 399°C and a slightly larger chemisorbed water peak than AL3. At this point it is not clear why the two samples have such different maximas (perhaps it is due to the different particle size and morphology) but this observation shows that some variations in decomposition temperature can be expected. The total % weight loss results for the two boehmite samples (28.3% and 24.6%) are higher than the theoretical % weight loss of 15.0% for pure boehmite. This is due to the presence of chemisorbed water and possibly small amounts of other hydroxide phases. The gamma alumina sample (AL2) (fig. 78) shows a gradual

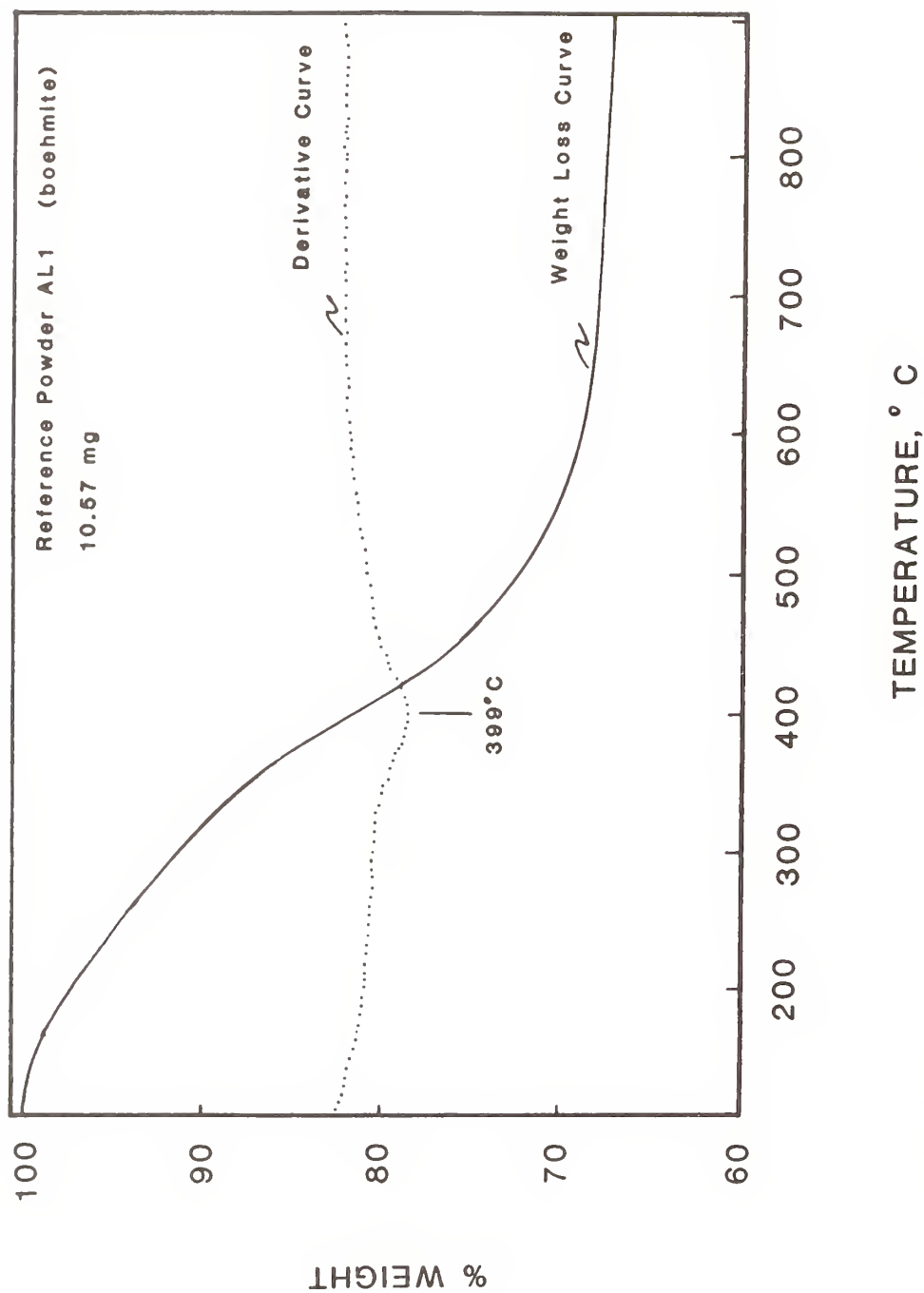


Figure 77. Temperature Scan TGA of Powder AL1 (Boehmite)

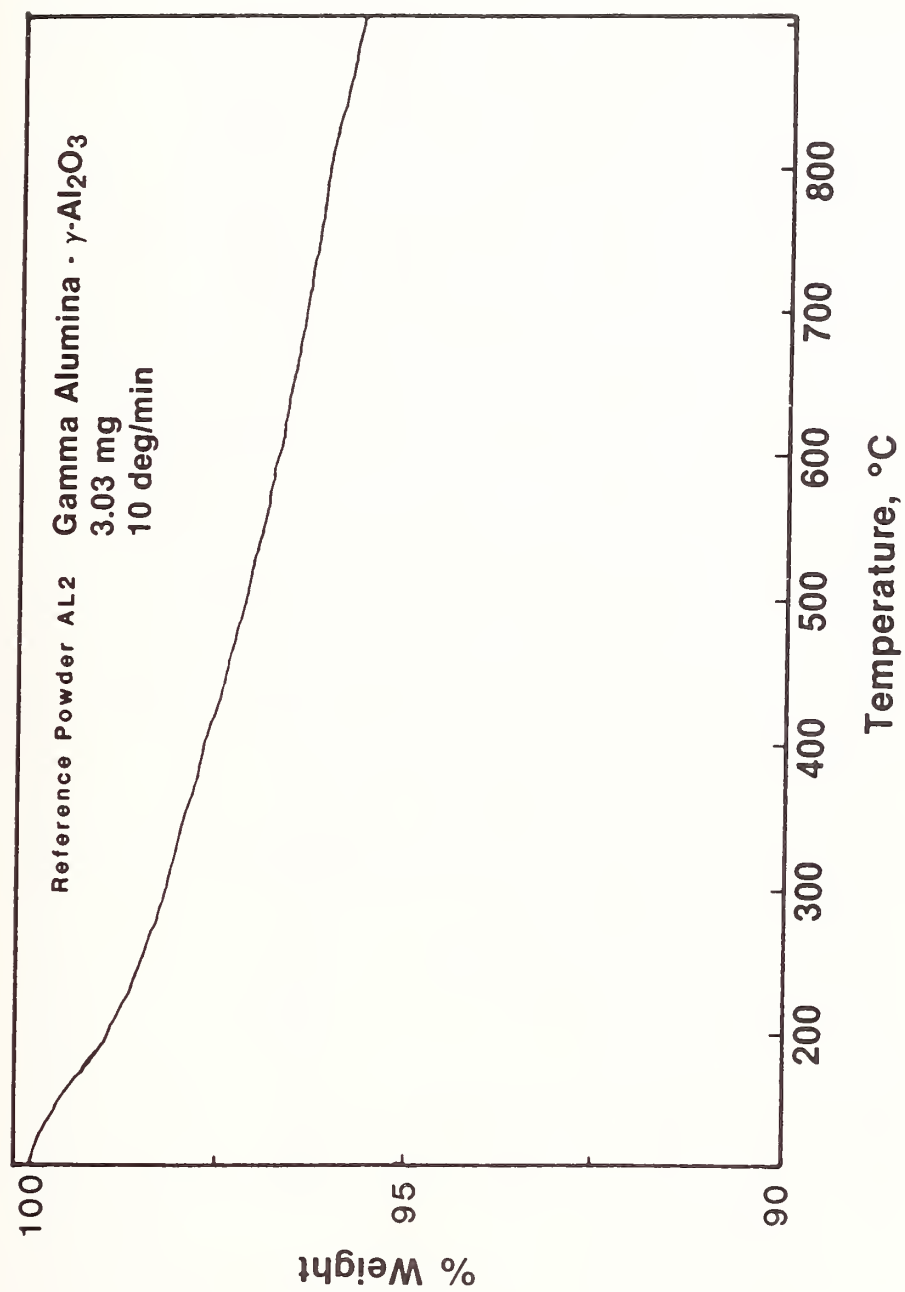


Figure 78. Temperature Scan TGA of Powder AL2 (Gamma Alumina)



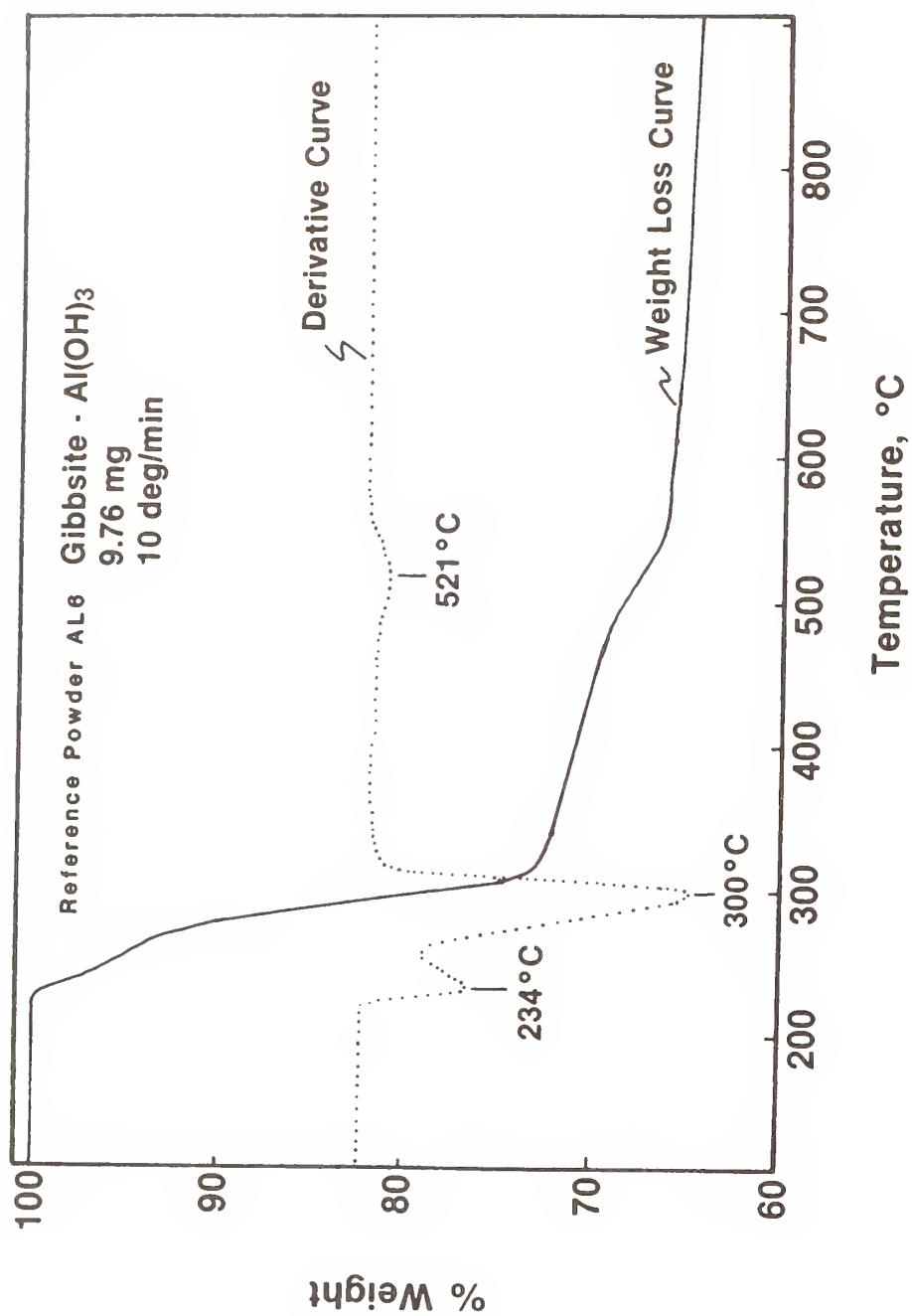


Figure 79. Temperature Scan TGA of Powder AL6 (Gibbsite)

Table 8

## TGA Analysis of Reference Powders

Reference Powder #	Sample Name	Free Water (%)	Total Decomp. Weight Loss (%)	Theor. Decomp. Weight Loss (%)	Temperature of Derivative Peaks		
					#1	#2	#3
AL1	Boehmite	5.9	28.3	15.02	399		
AL2	$\gamma$ Alumina	2.3	4.0				
AL3	Boehmite	7.6	24.6	15.02	313		
AL4	$\alpha$ Alumina	0.2	1.6	0			
AL5	$\alpha$ Alumina	0	0	0			
AL6	Gibbsite	0	34.8	34.64	234	300	521
		0	34.9	34.64	237	306	530
		0	34.9	34.64	235	299	525

weight loss over the duration of the temperature scan analysis. This is due to water in the structure which helps to stabilize the deformed structure of gamma alumina. The bound water content in gamma alumina reference powder AL2 was determined to be only 4.0%. Gibbsite (AL6) (fig. 79) gave a very distinct temperature scan TGA curve, with the derivative curve indicating three distinct decomposition peaks. The smaller peaks at 234 and 521°C could be due to minor impurities of other phases or they could be indicating that multiple decomposition reactions are taking place in this sample. For example, some of the gibbsite may transform to the monohydrate at 234°C via the reaction



The main complete decomposition of gibbsite may occur at 300°C as



and finally, at 521°C the monohydrate that was formed at 234°C can decompose



This hypothesis is also in agreement with the multiple reaction pathways presented by Wefer and Bell in figure 59. It is thought that a pressure buildup inside the particles of gibbsite due to release of water and diffusion limitations favors the formation of monohydrate.<sup>46</sup>

Total percentage weight loss for the gibbsite sample (AL6) of 34.8 - 34.9% agrees very well with the theoretical weight loss of pure trihydrate of 34.64% (table 8). Comparison of the three separate temperature scan runs indicates a good repeatability for both weight loss measurement and characteristic decomposition temperature peaks. Samples of alpha alumina (AL4 and AL5) showed little or no weight loss for both isothermal and temperature scan TGA analyses.

## 2. Differential Scanning Calorimetry (DSC)

This technique gives information similar to the TGA technique in that decomposition temperatures can be defined. Quantification is possible if the heat of reaction is known. DSC analysis of gibbsite produced the same three peaks as the TGA analysis at approximately the same temperatures. Since no new information was gained by this technique, it was not used for further work.

## 3. X-Ray Powder Diffraction (XRPD)

This analytical technique consists of distributing a powder sample on a surface in a random orientation and determining the angles at which x-rays are diffracted (fig. 80). The angles and relative intensity of the diffracted x-rays are characteristic of particular crystalline materials. Only small amounts of material (0.5 g) are required, and the technique is completely nondestructive as long as x-ray energies are not sufficient to disturb your sample.

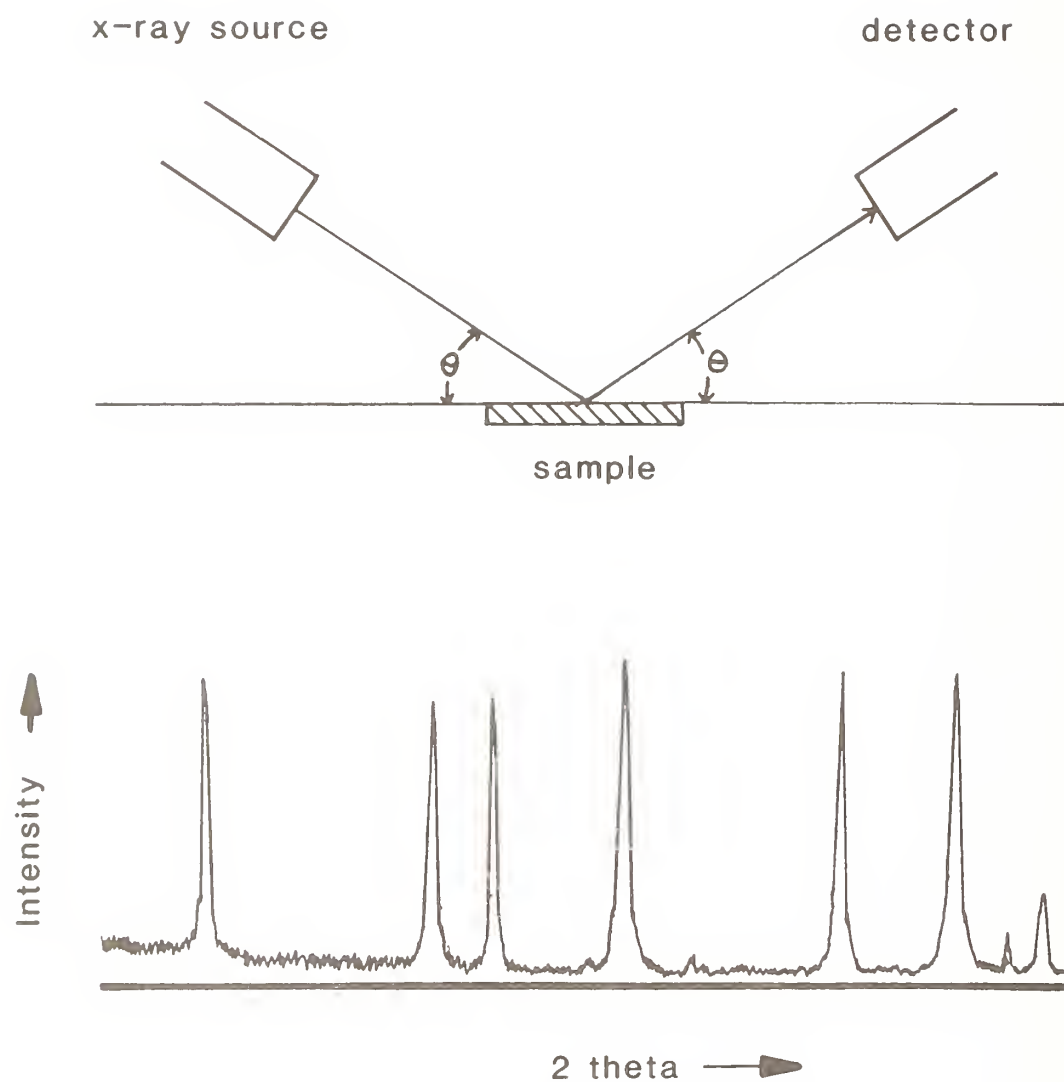


Figure 80. X-Ray Powder Diffraction Apparatus and Sample Spectrum

Identification of powders from their power diffraction data are made by comparing the peak locations ( $2\theta$ 's) and relative intensities ( $I/I$ ) of the unknown to similar data on known materials. This is best accomplished by consulting the Joint Committee on Powder Diffraction Standards (JCPDS) data base. This very valuable reference data is a compilation of thousands of XRPD analyses on known compounds performed by researchers around the world over approximately the past thirty-five years. Data are reported as d-spacing (in Angstroms) and relative intensity ( $I/I$ ) for each of the peaks on the x-ray powder diffraction spectra. D-spacings are related to  $2\theta$  (the actual angle usually measured for each analysis) through the Bragg equation

$$\lambda = 2d \sin \theta$$

where  $\lambda$  = wavelength of incident x-ray

$d$  = d spacing in angstroms

$\theta$  = incident angle in degrees

In the case of my analyses,  $\text{CuK}_{\alpha 1}$ , radiation was used with a wavelength of 1.54051 Å which reduced the equation to

$$d \sin \theta = 0.770255$$



which describes the relationship between  $\theta$  and d spacing for the apparatus used. In actual practice values of  $2\theta$  are used to describe the angles of peaks.

A search of the JCPDS data files produced a list of over 25 different reference data files pertaining to alumina and aluminum hydroxides. Twelve of these data files were selected for referencing. The rest of the files were rejected for a variety of reasons ranging from inability of the original author to index the d spacings to a particular crystal system, to insufficient number or quality of peaks. Thus only the best quality data was used. A compilation of all of the JCPDS file data are given in Appendix G along with d spacings, calculated  $2\theta$ 's, and relative peak intensities. Comparison of the unknown peak  $2\theta$ 's and relative intensities with the JCPDS data permitted identification of the unknown material.

#### 4. Fourier Transform Infrared (FTIR) Analysis

FTIR is a specialized infrared analytical technique that can detect the presence of characteristic functional groups in a sample. In infrared spectrometry, infrared light is passed through or reflected from a sample and the intensity of the light transmitted is measured as a function of its frequency. The nature of the chemical bonding in a sample allows it to absorb certain frequencies of infrared radiation characteristic of the bond. By noting which frequencies in the infrared spectrum are being absorbed by the sample,

certain conclusions can be made regarding the chemical bonds in that sample. Fourier transform is merely a specialized technique for taking and storing the infrared spectral data. Instead of storing the data as intensity versus frequency, the spectra is broken down into constituent fourier series and the more concise fourier transformed data is stored.

FTIR data was collected in three different samples using two different techniques.

Focused reflectance within wear scar - microscope  $\approx$  0.25 mm spot size

Focused reflectance outside wear scar in debris - microscope  $\approx$  0.25 mm spot size

Diffuse reflectance on powders - 1.0 mm spot size.

##### 5. Scanning Electron Microscopy (SEM)

Scanning electron microscopy was performed on an ISI Super IIIA SEM. Most samples were coated with approximately a 20 nm conductive coating of gold/palladium, and analyzed in the microscope at 12 keV accelerating voltage.

## Chapter VII

## ALUMINA/WATER TRIBOSYSTEM: RESULTS AND DISCUSSION

A. Kinetic Experiments on Powders

Initial kinetic experiments were conducted on alpha alumina and gamma alumina to determine their reactivity with water at different temperatures. Low temperature experiments were conducted at approximately 100°C in a covered beaker on a hot plate. Higher temperature experiments were conducted in the bomb at approximately 200°C.

Alpha alumina was unreactive at low temperatures even for times as long as 24 hours. Gamma alumina on the other hand appeared to react. The TGA curve for the reaction product (fig. 81) shows a distinct single decomposition peak at 272°C. X-ray powder diffraction of the reaction product indicated bayerite was present. This is consistent with the observation by Wefers and Bell<sup>41</sup> that bayerite decomposes to a disordered eta alumina at 230-350°C.

Higher temperature bomb reactions determined that alpha alumina was unreactive with water at 200°C for 3 hours. Gamma alumina however was reactive and forced a whitish looking precipitate quite different from the gelatenous looking gamma alumina water mixture. TGA analysis of the homogeneous reaction product gave a small single peak at approximately 570°C (fig. 82). The solid remaining after reaction

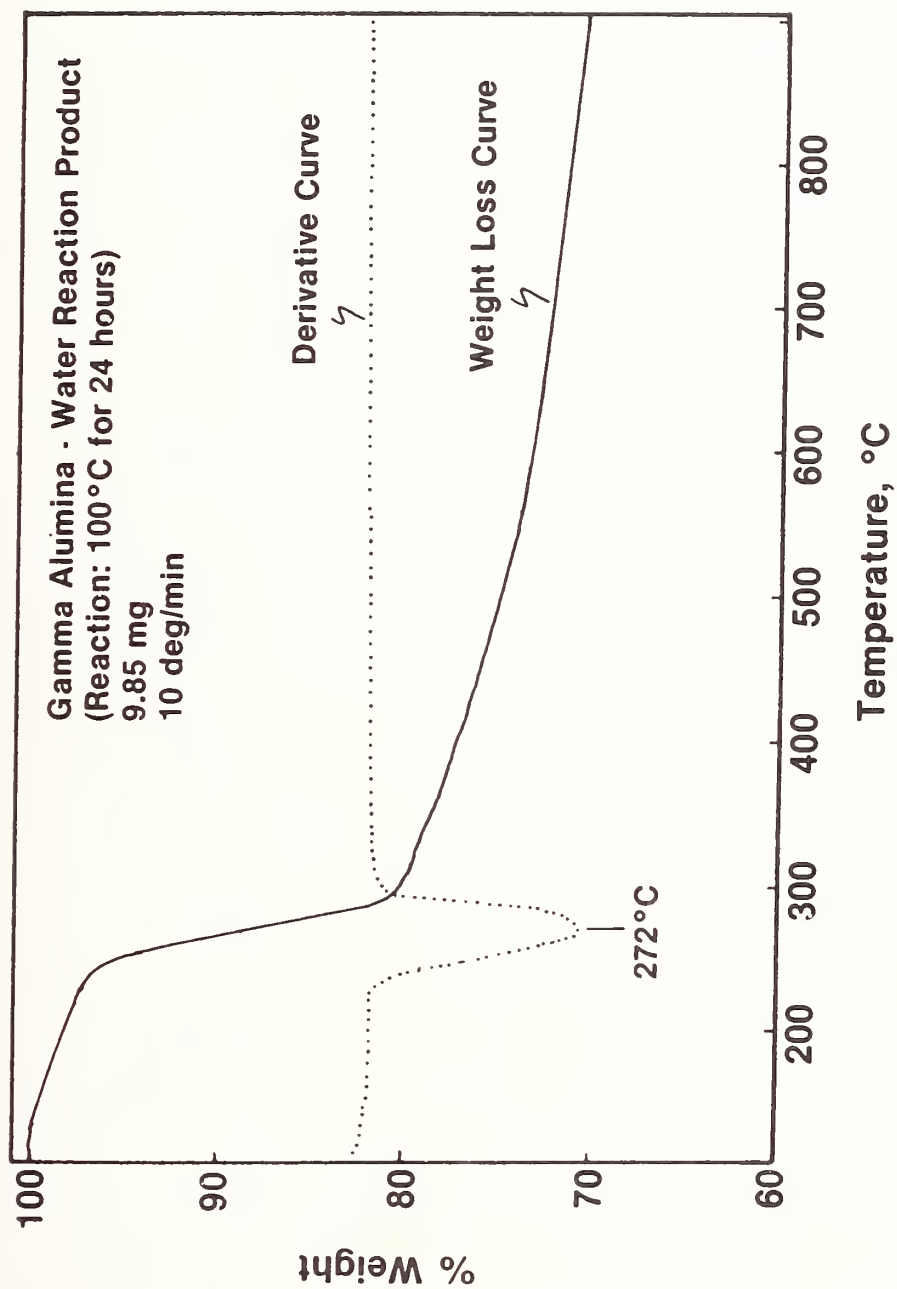


Figure 81. Temperature Scan TGA of Reaction Product of Gamma Alumina/Water at 100°C for 24 Hours

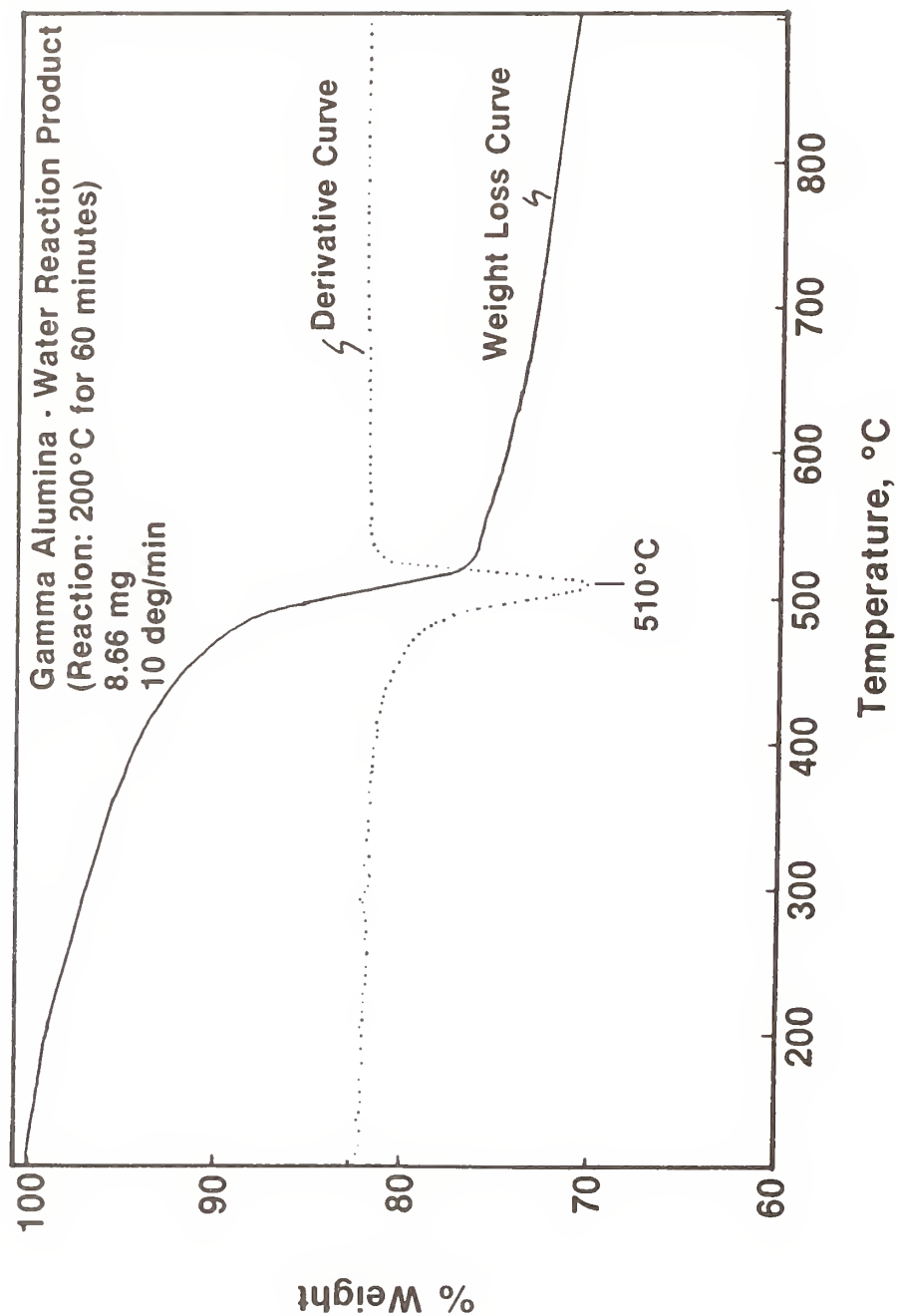


Figure 82. Temperature Scan TGA of Reaction Product of Gamma Alumina/Water at 194°C for ~1 Hour

was also separated into two phases. The "gel" phase (fig. 83) gave a TGA curve that looked like unreacted gamma alumina while the "white" phase (fig. 84) gave a single distinct peak at 520°C. X-ray powder diffraction patterns from the two samples confirmed that the "gel" phase was gamma alumina and determined that the "white" phase was boehmite. This data is in good agreement with the phase diagram information in that low temperatures favor production of the trihydroxide (bayerite) while higher temperatures favor production of the monohydroxide (boehmite).

TGA was successfully used to qualitatively show that reactions between water and gamma alumina were possible. The next set of experiments were conducted to see if TGA could be quantitative and allow an understanding of the kinetics of these reactions. Three bombs were charged with gamma alumina and water and placed in the heating block at the same time and heated to 194°C. The bombs were removed at different times and quickly cooled, resulting in reaction times of 31, 59, and 119 minutes. TGA analysis of the reaction products (figs. 85-87) produced weight loss curves which could be quantitatively analyzed. By knowing the weight loss due to water from the decomposition of boehmite, the percentage boehmite (and then the fractional conversion) in the reaction product could be calculated (table 9). Quantitative information is derived from the TGA temperature scan runs in the following manner. First, straight lines are drawn parallel to the weight loss curves before and after the decomposition point. These lines tend to be roughly parallel to one



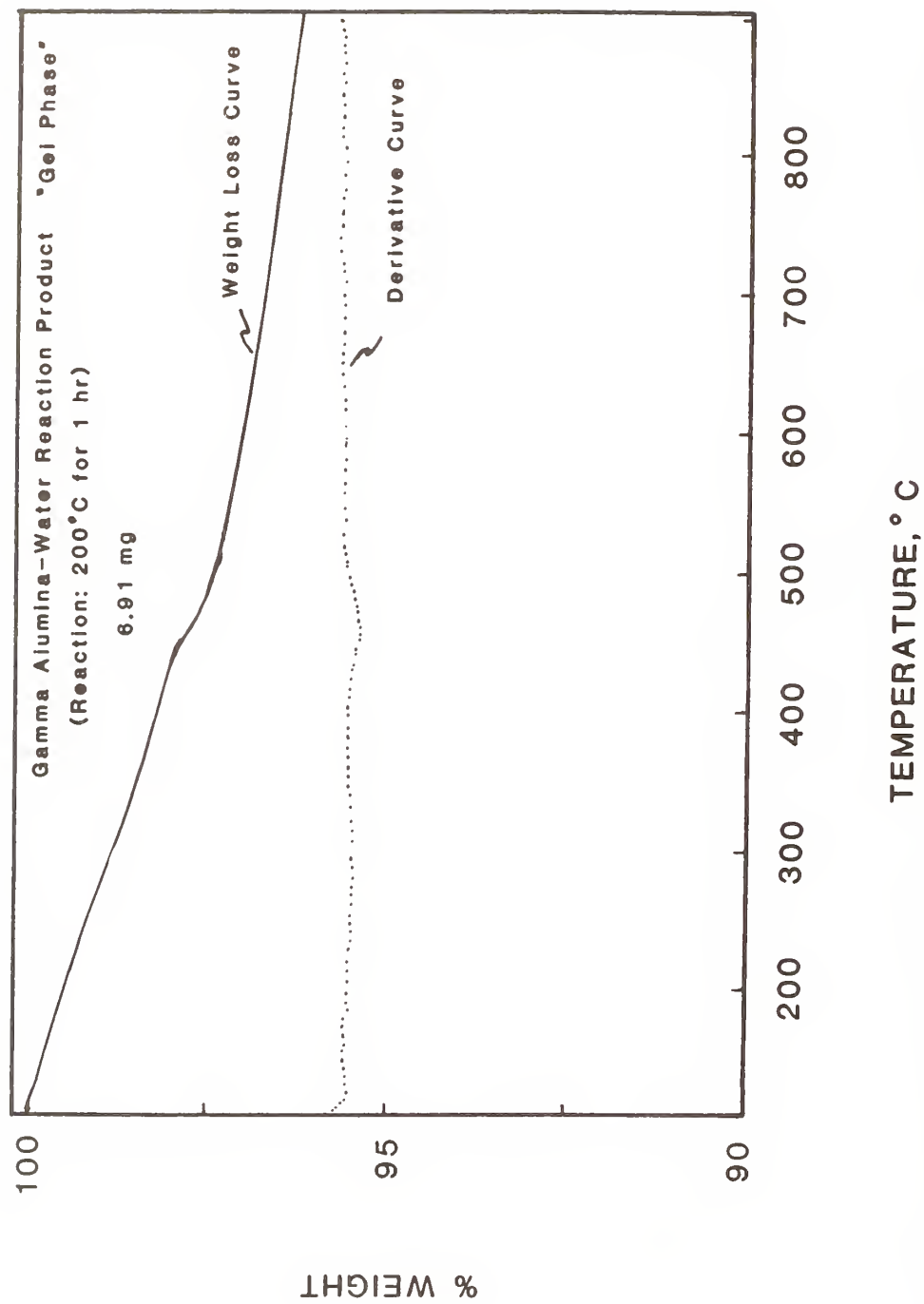


Figure 83. Temperature Scan TGA of "Gel" Phase of Reaction Product of Gamma Alumina/Water at 194°C for ~ 1 Hour

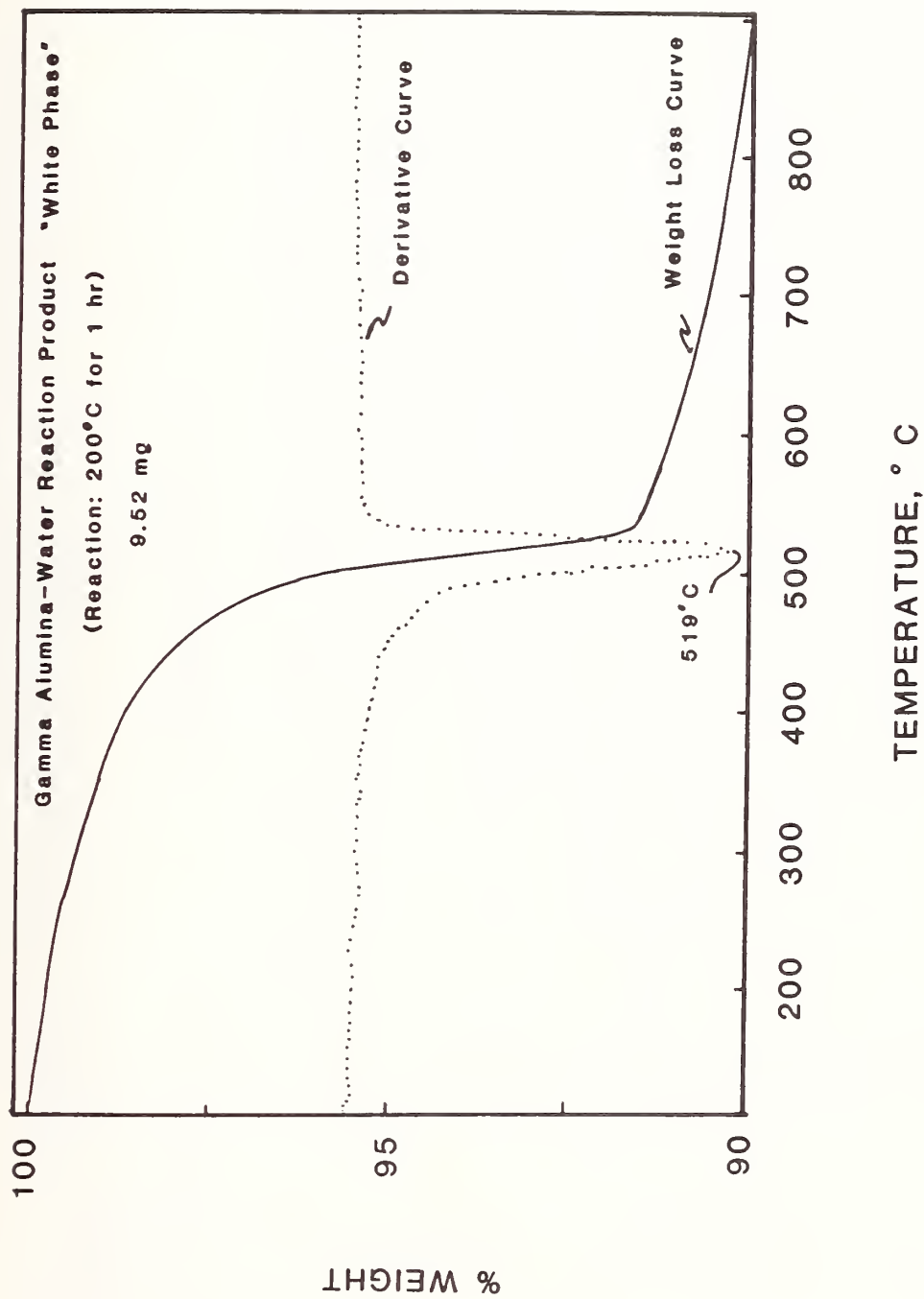


Figure 84. Temperature Scan TGA of "White" Phase of Reaction Product of Gamma Alumina/Water at 194°C for ~ 1 Hour

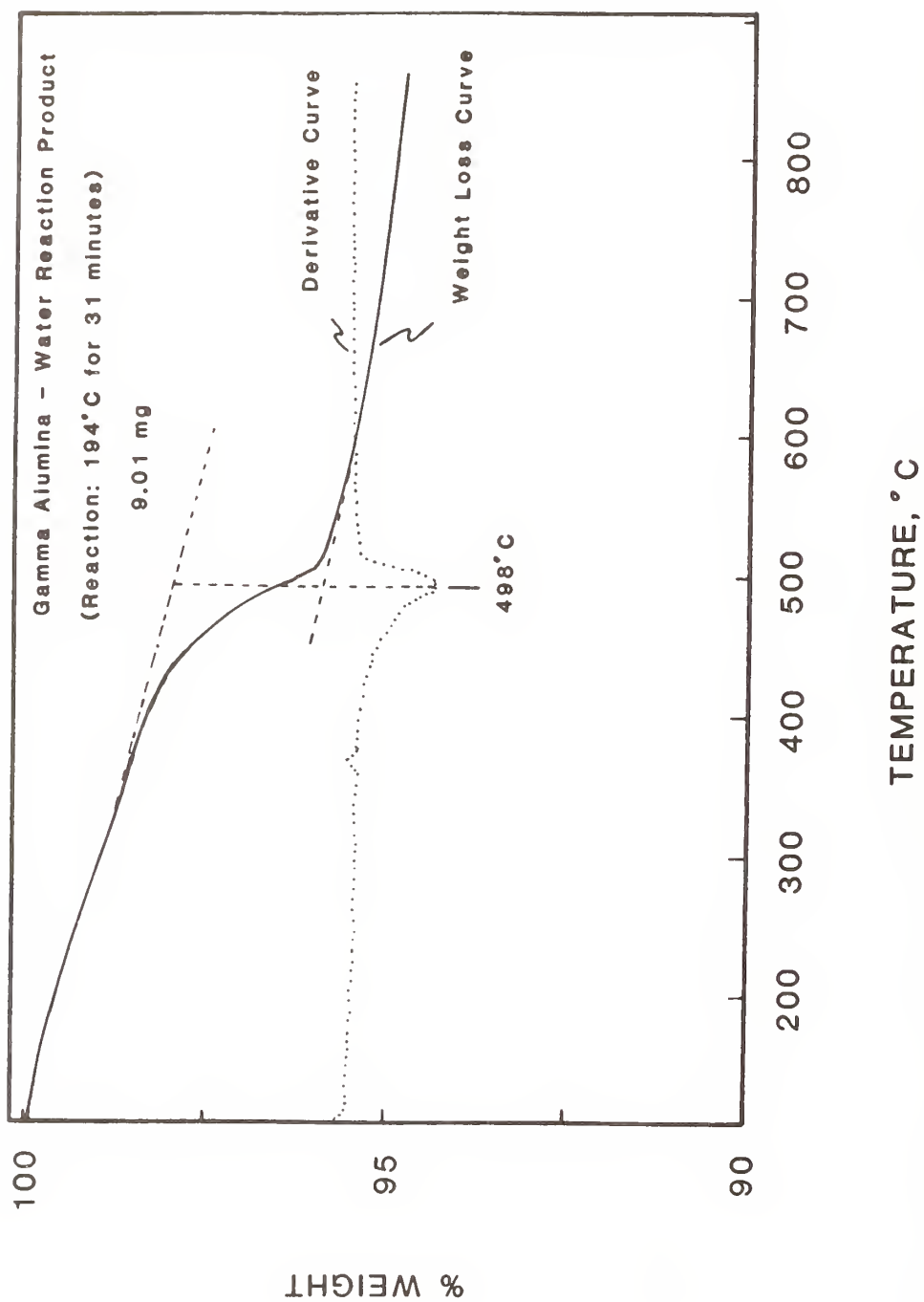


Figure 85. Temperature Scan TGA of Reaction Product of Gamma Alumina/Water at 194°C for 31 Minutes

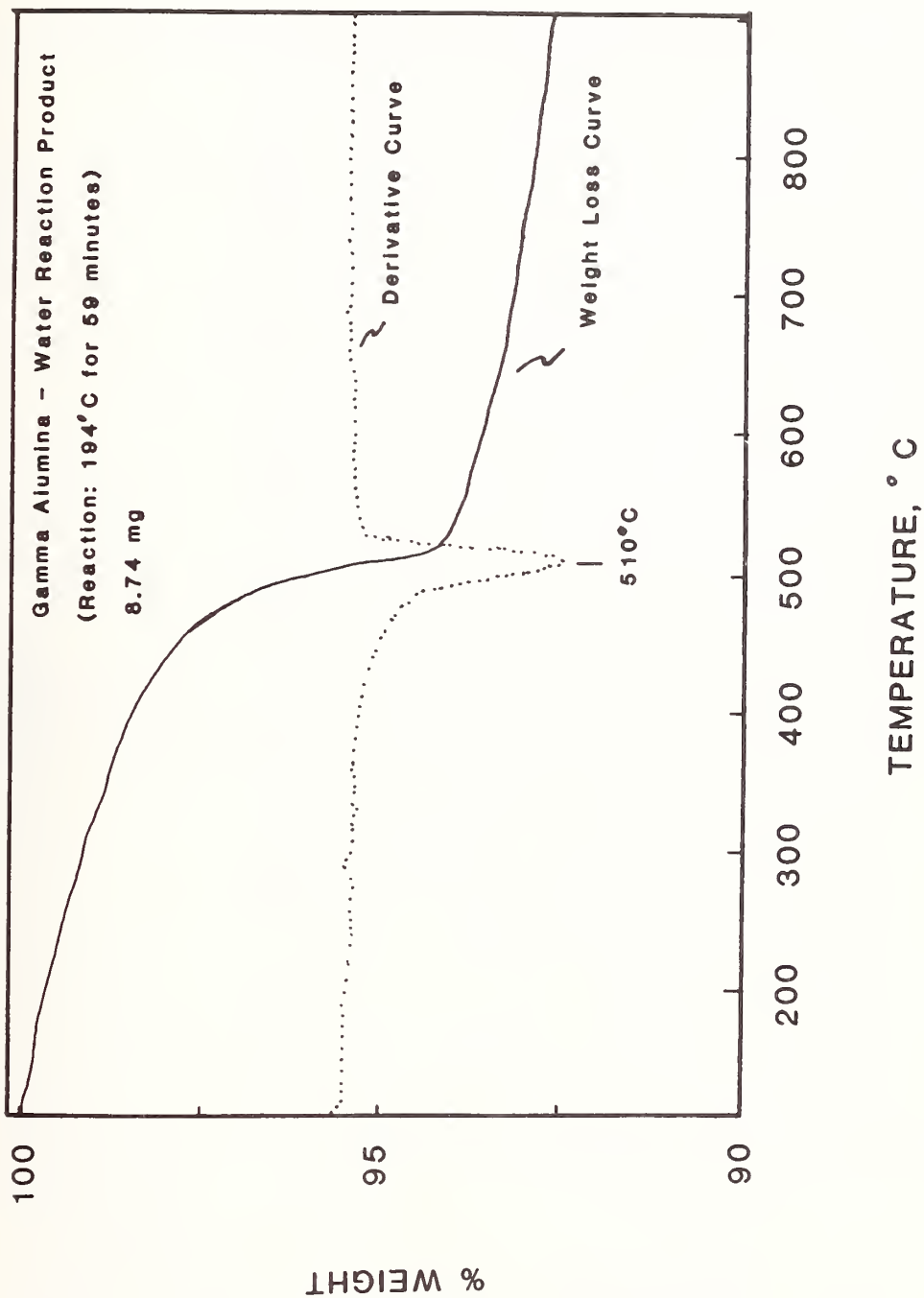


Figure 86. Temperature Scan TGA of Reaction Product of Gamma Alumina/Water at 194°C for 59 Minutes

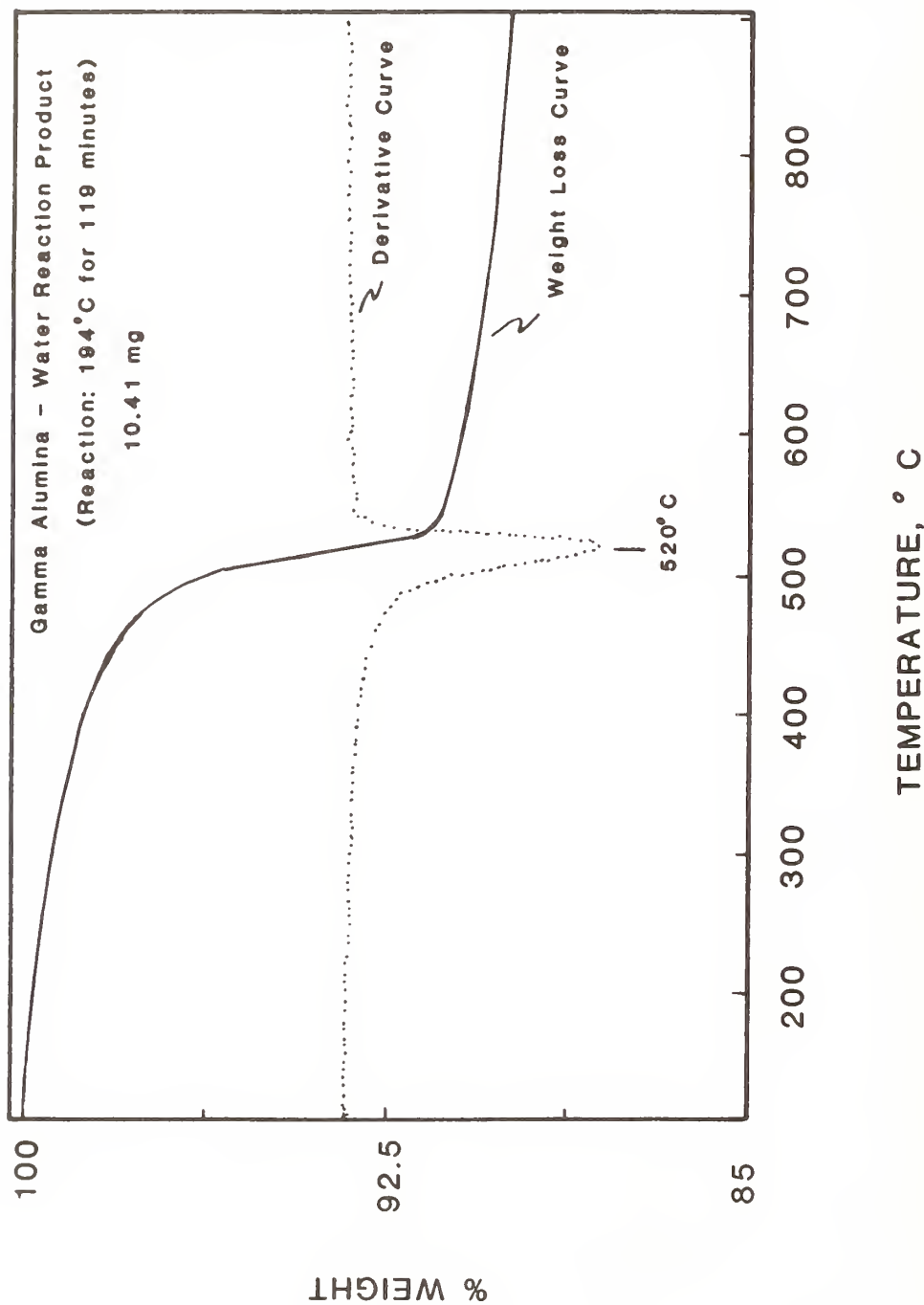


Figure 87. Temperature Scan TGA of Reaction Product of Gamma Alumina/Water at 194°C for 119 Minutes

Table 9

Kinetic Data for Reaction of Gamma Alumina (AL2) and Water at 194°C

Reaction Time (min)	Water Weight Loss during Decomposition (y%)	Fractional Conversion (f)	$\ln(1-f)$
0	0	0	0
31	2.05	0.136	-0.146
59	4.12	0.274	-0.320
119	6.82	0.454	-0.605

$y_{\text{theoretical}}^* = 15.02$  for boehmite

$f = y/y_{\text{theoretical}}^*$



another. This serves to eliminate the bias from the residual gamma alumina in the sample which exhibits a continuous weight loss with temperature (as seen in figure 83). Next, a vertical line is drawn at the minimum of the derivative curve. Finally, the length of the vertical line between the parallel lines is measured the % weight loss is obtained by comparing the length of this line to the vertical scale.

Once the rate data was obtained, a predictive model was sought to describe the data. Using the simplest approach of assuming a homogeneous system and mass action kinetics the equation for a first order dependence was derived (Appendix I). The data (table 9) was plotted (fig. 88) and seems to fit the model quite well. Other simple orders were tried (0 order, 2nd order) but the data did not fit as well. The rate constant for this reaction, determined from the slope of the line, was  $5.1 \times 10^{-3} \text{ min}^{-1}$ .

The combination of tools of x-ray powder diffraction and TGA offer a powerful technique for investigating the kinetics of these systems. X-ray powder diffraction determines the structure of the product. From this, the stoichiometry of the reaction can be obtained. By knowing stoichiometry of the reaction, TGA can be used to quantify the products and provide rate data. Ultimately, the kinetics of the system can be understood.

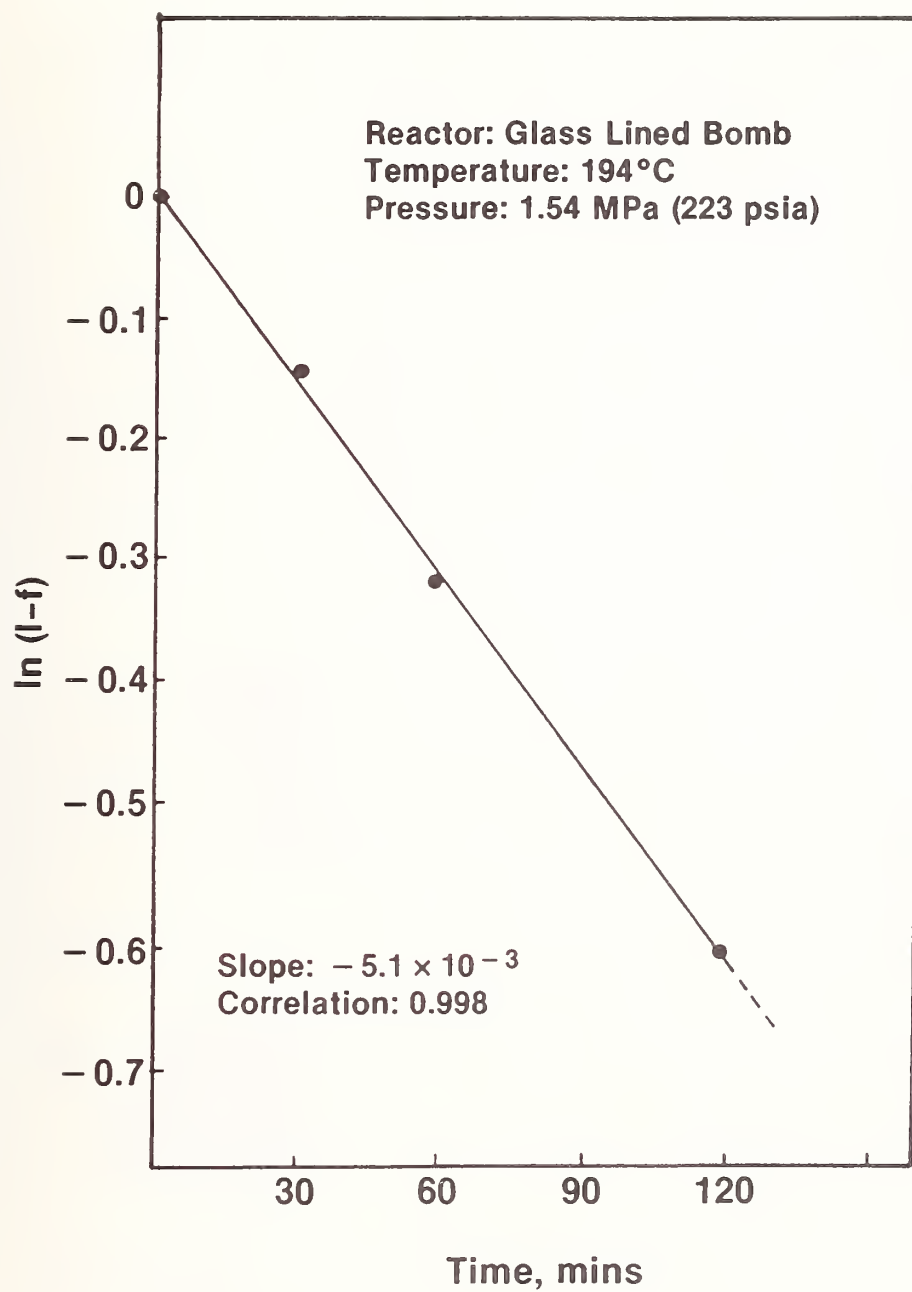


Figure 88. Pseudo First Order Data Plot for Gamma Alumina/  
Water Reaction at 194°C

## B. Powder Friction Tests

The kinetic experiments with powders demonstrated the feasibility of forming reaction products in the contact junction however it does not demonstrate that these products have any lubricating qualities. Therefore, a series of dry wear tests were conducted using the reference powders to see if these powders modified friction. Five kilogram load tests (fig. 89) indicate both different friction levels and different friction variability among the three main classification of powders. Alpha alumina powder gives the highest level of friction and greatest degree of variability. Large spikes of both high and low friction show up regularly. Boehmite gives a slightly lower coefficient of friction and less variability. Gibbsite gives a much lower friction coefficient and a noticeably smoother friction trace. Test at 2 kg load (fig. 90) produce the same coefficient of friction ranking with a few differences in the traces. The alpha alumina friction trace for example shows a bit less variability than was seen in the 5 kg load test. A comparison of the final coefficient of friction values for the six tests (fig. 91) shows good agreement among the rankings with alpha alumina producing the highest friction, boehmite offering a modest decrease in friction, and gibbsite producing a large ( $\approx 40\%$ ) decrease in friction. This data demonstrates the solid lubricating ability of the hydroxides of alumina, especially the trihydroxides.

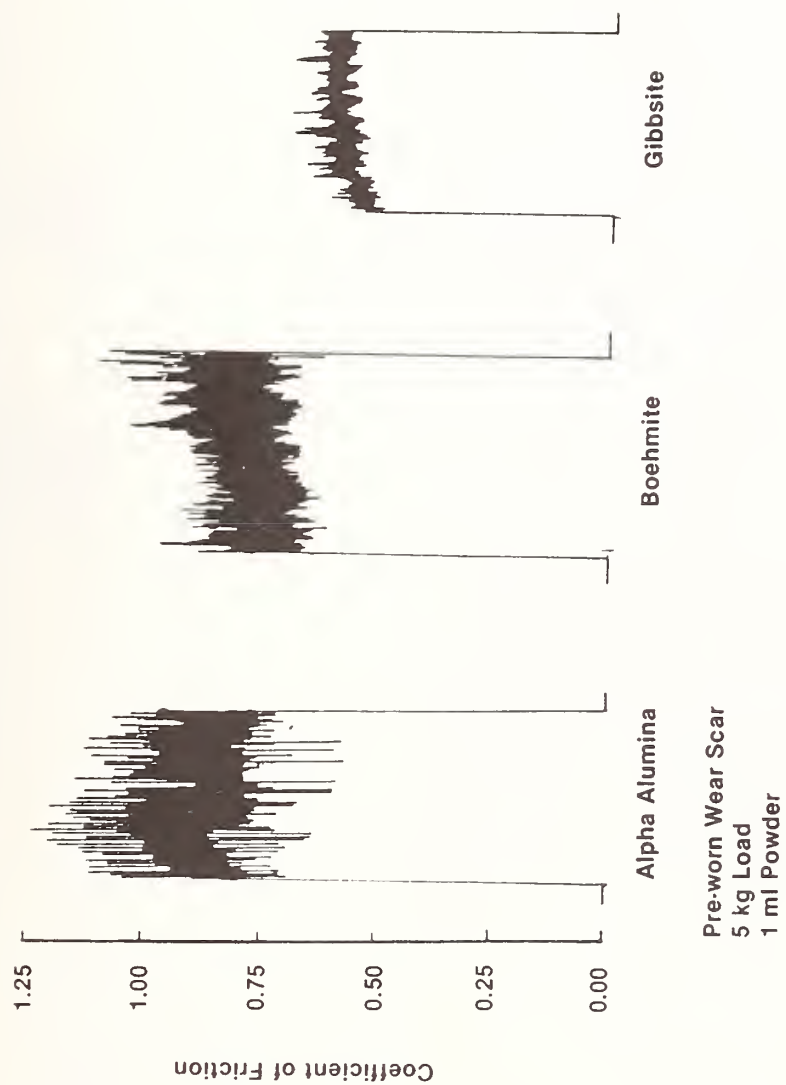


Figure 89. Friction Traces for Powder Tests at 5 kg Load

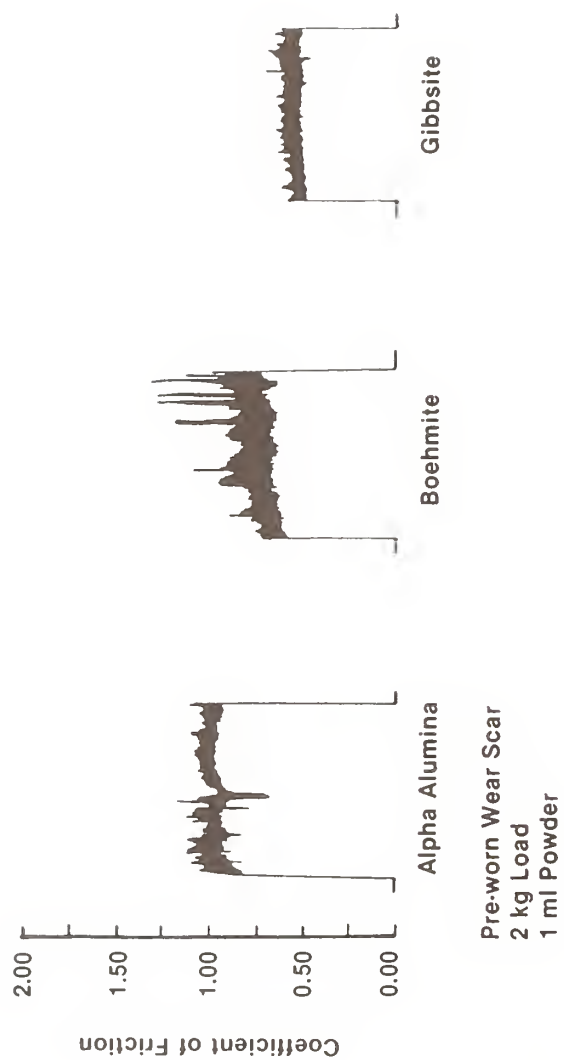


Figure 90. Friction Traces for Powder Tests at 2 kg Load

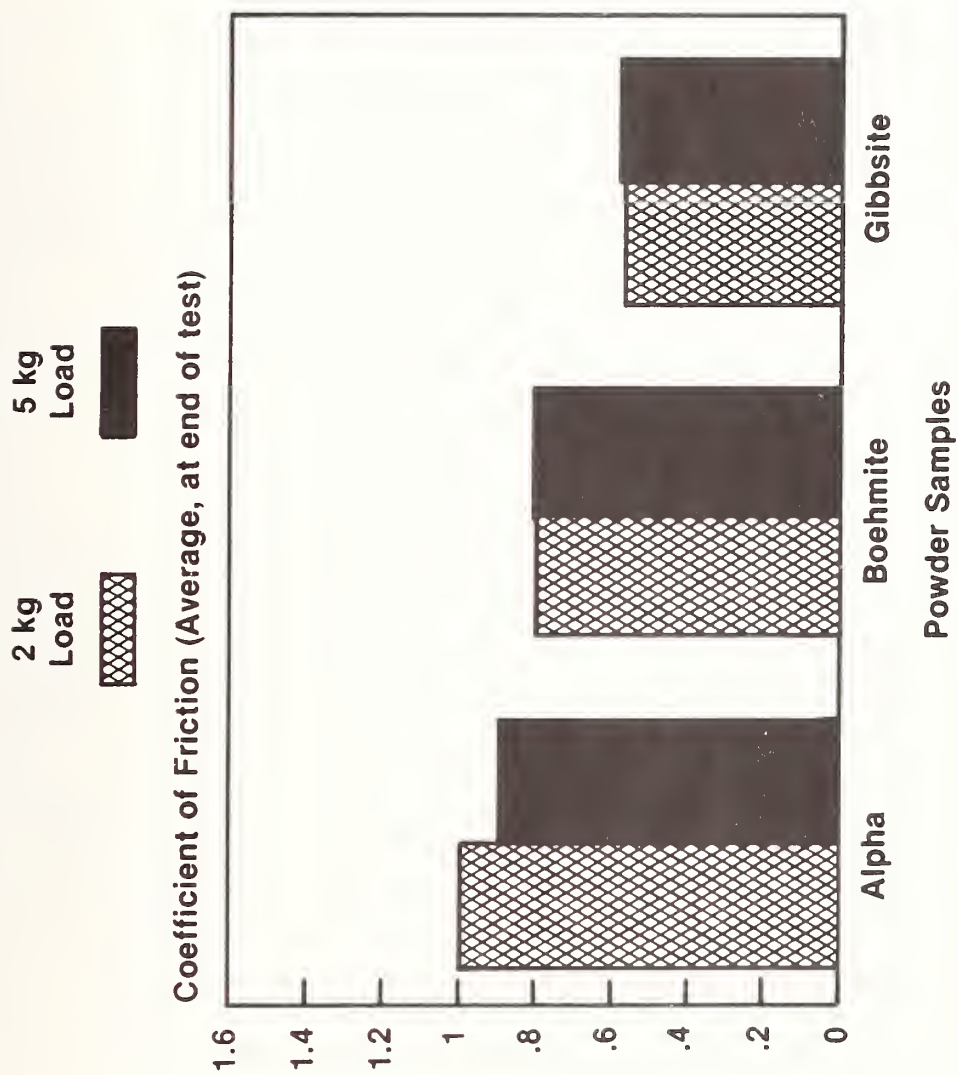


Figure 91. Comparison of Final Coefficient of Friction Values for Different Alumina Powders at 2 and 5 kg Load



### C. Wear Debris Analysis

Analysis of the wear debris and wear scar was very difficult due to the very small amount of material produced. This approach, however, offered the best opportunity for direct evidence for the hypothesis that water and alumina react to form lubricous products.

X-ray powder diffraction patterns were gathered using a computer operated diffractometer, and a thin smear of powder on an oriented quartz slide. The thin smear was used because there was insufficient powder (by a factor of 20) to perform a normal powder diffraction pattern. The computer control and data analysis was necessary to allow for very long analysis times. This enhanced the signal to noise ratio and gave the best opportunity for peak identification. A forty-eight hour run of the region from 10 to 70 degrees (45 minutes/degree) indicated three components (fig. 92). The peak identification shows the three components as alpha alumina ( $\alpha$ ), a contaminant on the quartz slide (c), and bayerite (b). The bayerite peaks were very small and represent the two strongest x-ray powder diffraction peaks for this material indicating that bayerite is only present in small amounts. Additional runs were performed at very slow scan speeds of 450 minutes/degree to enhance the detail in this region. These runs, shown as enlargements in the figure, indicate definite small peaks are present.

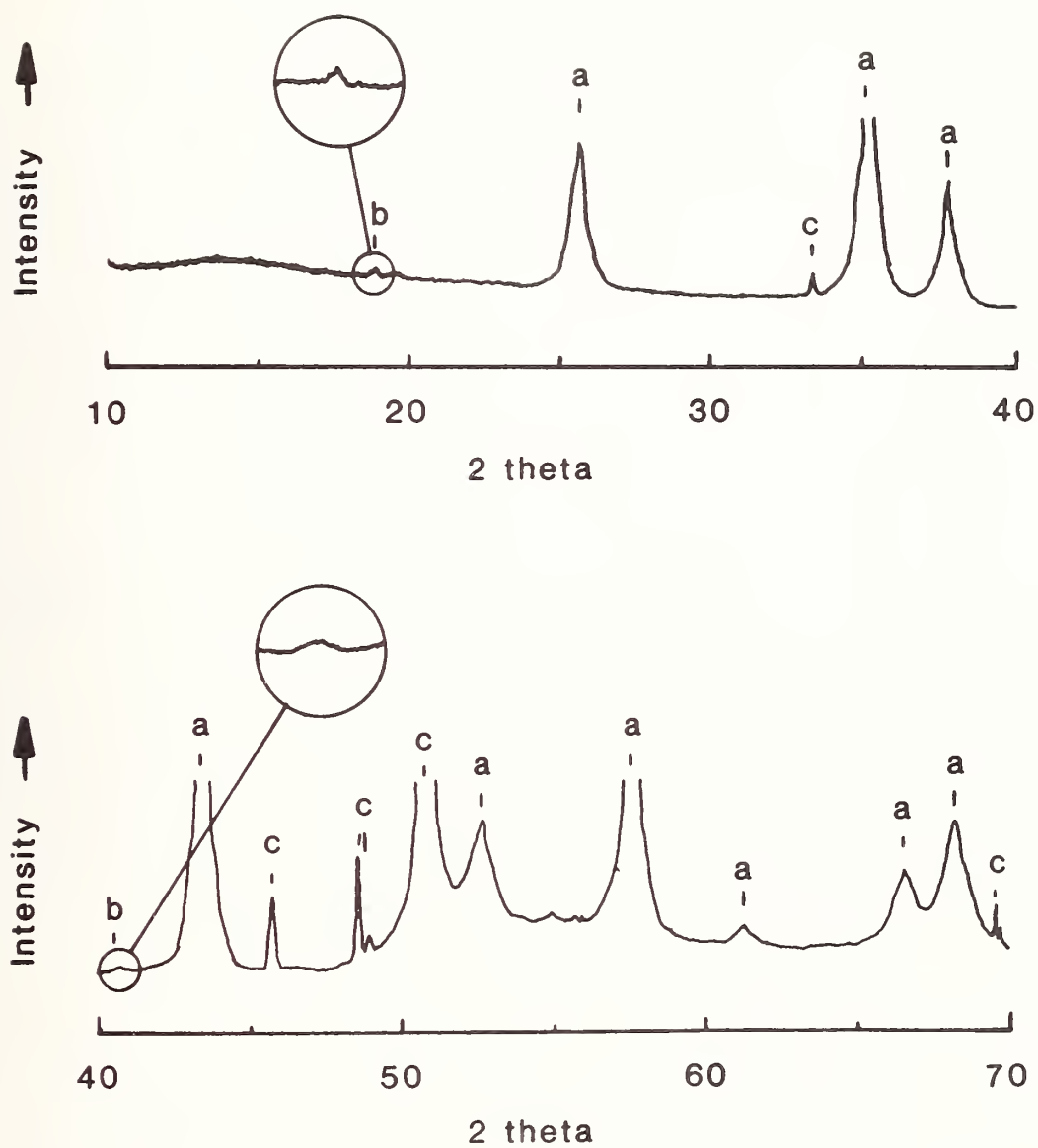


Figure 92. X-Ray Powder Diffraction Spectrum for Wear Debris from Water-Lubricated Alumina Test

TGA analysis of wear debris from a water-lubricated wear test is shown in figure 93. Three general peaks can be seen. A broad peak is seen with a minimum at 263°C. A second small peak as seen at 325°C. A very sharp peak is observed at 249°C. The location of the sharp peak is close to the location of the peak seen for the bayerite reaction product from the kinetic tests. The difference between the TGA peaks is that the wear debris bayerite peak is much sharper and the minimum is at a lower temperature (249°C vs 272°C). I believe that the wear debris and kinetic test reaction products are the same material and that the differences in TGA results are attributable to the smaller particle size for the wear debris produced bayerite. Bayerite particles produced in the wearing contact would tend to be very small because of the high shear stresses in the contact junction. The particles produced in the kinetic tests were fairly coarse grained. During the course of a TGA run, the temperature is increased. At the decomposition temperature of bayerite, water is lost and weight loss occurs. Weight loss can only occur if water is allowed to diffuse through the crystal lattice and escape into the atmosphere. In the case of the wear debris, particles are small, diffusion distances are small, and weight loss is rapid resulting in a sharp peak. In the case of the kinetic experiments, the large particles inhibit the diffusion of water and broaden and delay the minimum of the peak. The difference in minimum is only 23°C which corresponds to a delay of only 138 seconds. Diffusion limitations could easily account for this difference.

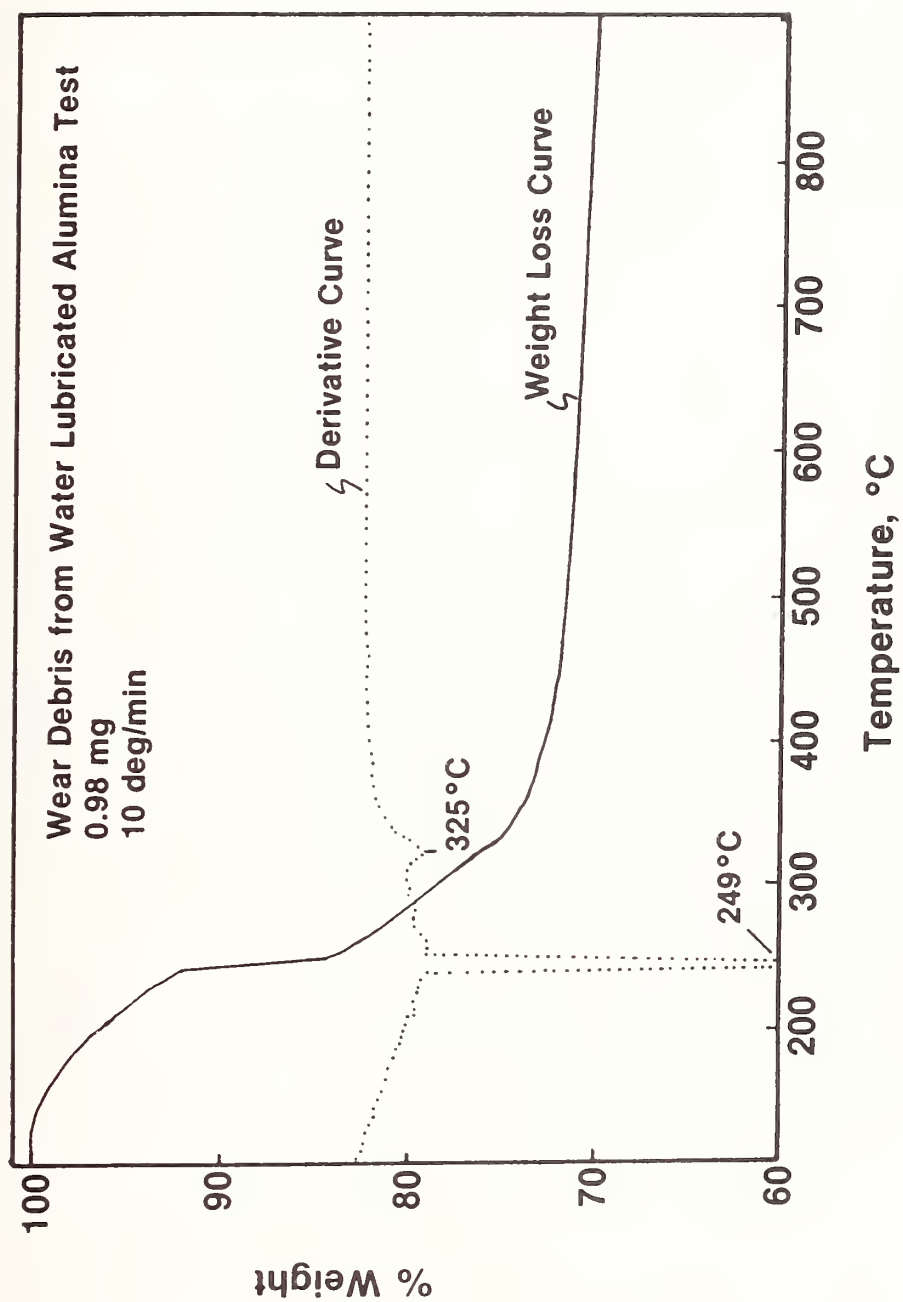


Figure 93. Temperature Scan TGA of Wear Debris from Water-Lubricated Alumina Test

Fourier transform infrared spectroscopy was used to find evidence of hydroxides in the wear debris and wear scar. Analysis of the wear scar itself did not give a clear indication of a hydroxide peak probably because the layer was too thin. Analysis of some of the debris piled outside the wear scar however (fig. 94) showed definite presence of OH.

The three analysis techniques applied all indicate the presence of a reaction product between water and alpha alumina in the contact junction. The x-ray powder diffraction and TGA experiments indicate that the product is bayerite aluminum trihydroxide ( $\text{Al}(\text{OH})_3$ ). Since the kinetic work indicated that alpha alumina is nonreactive with water but gamma alumina is, something must take place in the contact junction to produce gamma alumina (or perhaps another reactive transition alumina). This missing part is supplied by the research performed by Hines, Bradt, and Biggers.<sup>48</sup> Their finding was that when alpha alumina is subjected to abrasion in an unlubricated wear test, particles of delta alumina (a deformed alumina, very difficult to distinguish from gamma alumina) were produced. This observation complements the findings in this study and supplies the missing link in the chain of events. The following sequence of events (see figure 95) therefore seems to be necessary for production of lubricous wear products:

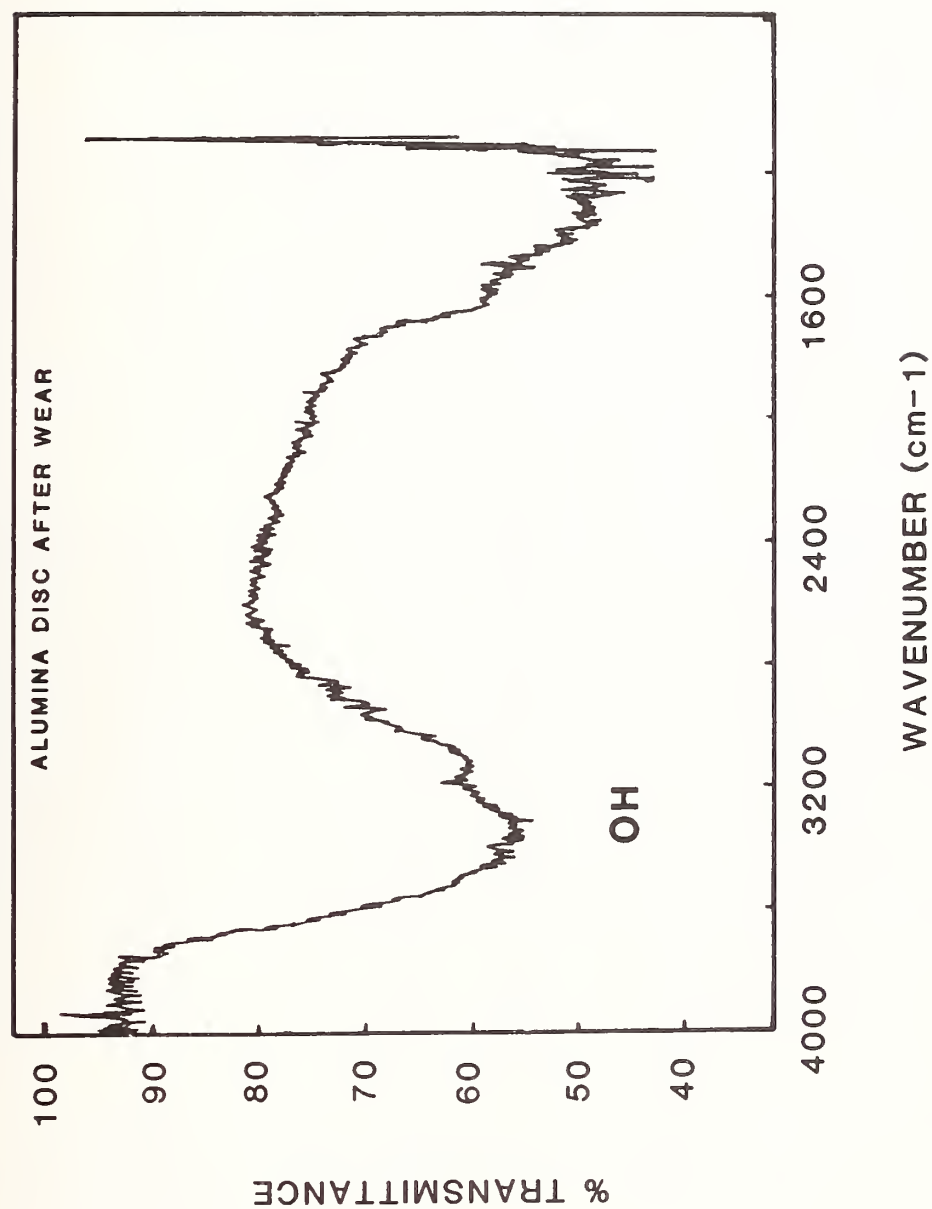


Figure 94. FTIR Spectrum of Wear Debris from Water-Lubricated Alumina Test



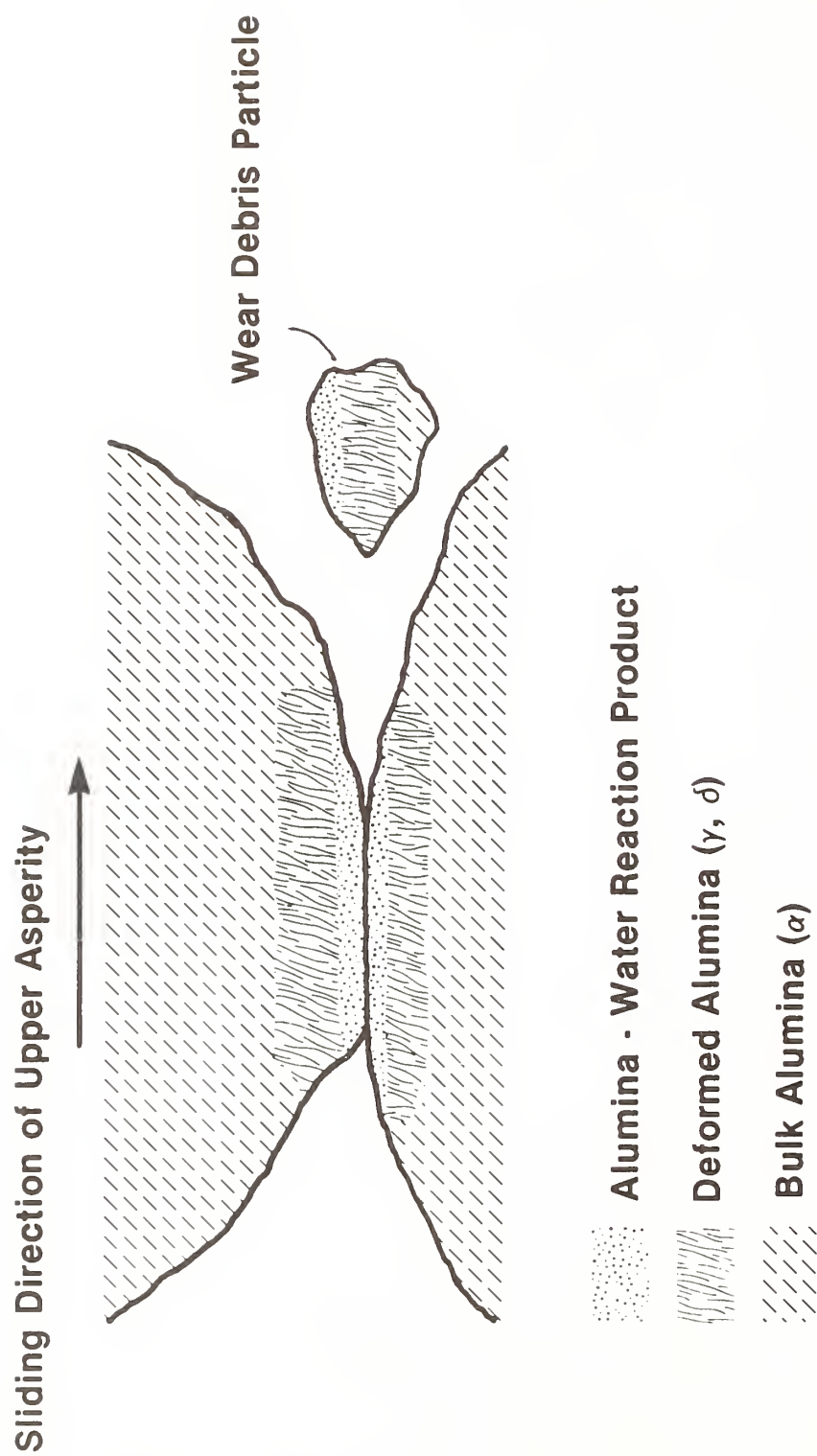


Figure 95. Model for the Alumina/Water Tribosystem

- 1) High pressure, temperature, and shear stresses in the contact junction produce a deformed alumina such as the gamma phase transition alumina.
- 2) High temperature high pressure reaction between water and the transition alumina produce an aluminum hydroxide. The exact form depends on the conditions.
- 3) The aluminum hydroxide (in our case trihydroxide-bayerite was observed), being a layer lattice structure, acts as a solid lubricant and reduces friction and wear.

The model depicts a large chunk of material being removed from the surface of the asperity, consisting of all three phases of material. In actuality, I believe that two types of wear debris would dominate. Where temperatures and stresses are optimum, very small particles of easily sheared hydroxide particles will be produced. At locations where stresses are too high and temperatures are too high (or too low), larger particles of debris (mostly alpha alumina) will be produced.

A series of tests was conducted to observe the relative "solid lubricating" ability of several alumina-based powders. First, a set of alumina ball-on-three-flat specimens were run at 600 rpm and 10 kg load for 2 minutes to provide a wear scar on the specimens. This was done to reduce the contact pressure and allow the surfaces to conform.

Subsequent tests were conducted under the same conditions of speed, load, and duration using 1.5 ml of deionized water lubricant with approximately 2% (w) powder in suspension. Coefficient of friction values were taken as the steady state values obtained during the test. These values were then ratioed to the coefficient of friction obtained using deionized water alone to give a measure of the effect of the powders on friction relative to the base case (water lubricated). The results of these tests are given in table 10.

Samples of alpha and gamma alumina powders in water increase friction approximately 9 percent. This slight increase may be due to the three-body "abrasive" contribution expected for non-lubricating solids. The boehmite sample gave a 24 percent reduction in friction indicating its potential as a solid lubricant. The gibbsite and bayerite samples produced slight increases in friction of 13 and 7 percent, respectively. The lack of friction reduction from the trihydroxides gibbsite and bayerite was disappointing. These powders however had large ( $> 10 \mu\text{m}$ ) crystallites that may have resulted in more of an abrasive mechanism. This is supported by the relatively rough friction traces obtained for these powders (fig. 96). Tests conducted using water and the other powders (all with smaller particles sizes) produced smooth friction traces.

An interesting effect was observed with the boehmite tests. After the initial boehmite powder test, the cup was rinsed with water and a new test was conducted on the same wear scars with pure

Table 10

## Summary Friction Data for Alumina-Based Powders in Water

Lubricant*	Coefficient of Friction $\mu$	Ratio of Friction Coefficient $\mu/\mu_{H_2O}$
Deionized Water	$0.230 \pm 0.007$	1.00
$\alpha$ (AL5)	0.250	1.09
$\gamma$ (AL2)	0.250	1.09
Boehmite (AL1)	$0.175 \pm 0.003$	0.76
Gibbsite (AL6)	0.259	1.13
Bayerite (Alcoa C-37)	0.245	1.07

\*All powders present at approximately 2% (w).

Test Conditions:      Ball-on-Three-Flat Test Configuration  
                          Alumina Specimens:    Ball - CER 021  
    Flats - CER 006  
                          Speed:    600 rpm  
                          Load:    10 kg  
                          Duration:   2 minutes

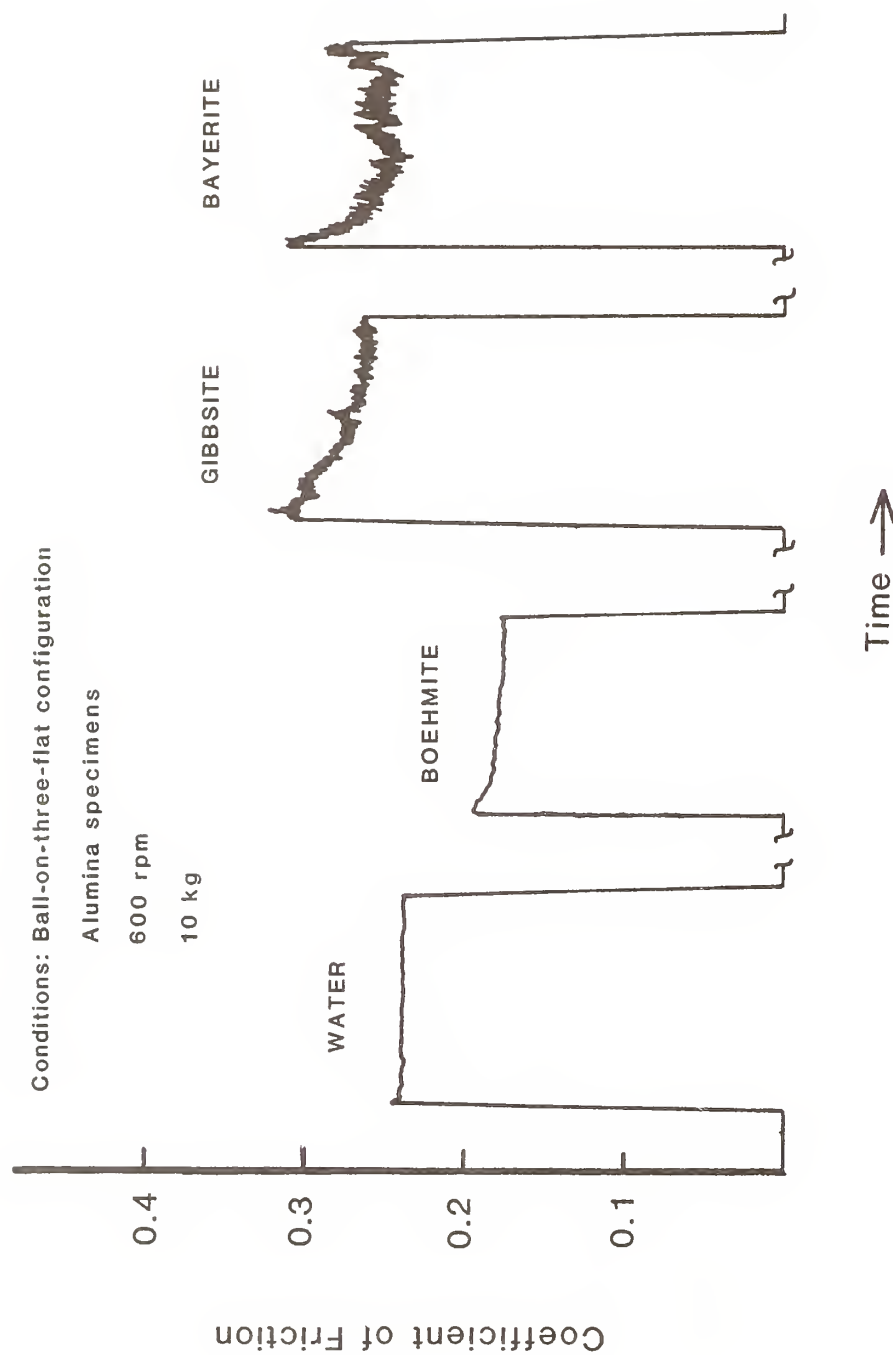


Figure 96. Effect of Various Alumina Based Powders on Friction for Water-Lubricated Alumina

deionized water. When this was done, some residual low friction was still observed providing evidence that the lubricating "film" was still present. A repeat of the rinse increased the friction slightly back to the level of friction of the original deionized water case (fig. 97). This "memory" effect indicates something about the behavior of boehmite as a lubricant. First, it does not have to be present in large quantities to work. Second, it appears to be fairly tenacious in its ability to remain in the contact region even after the circulating supply of powder has been removed. As the burnished powder in the contact is gradually worn away and the circulating water replaced, the friction gradually increases.



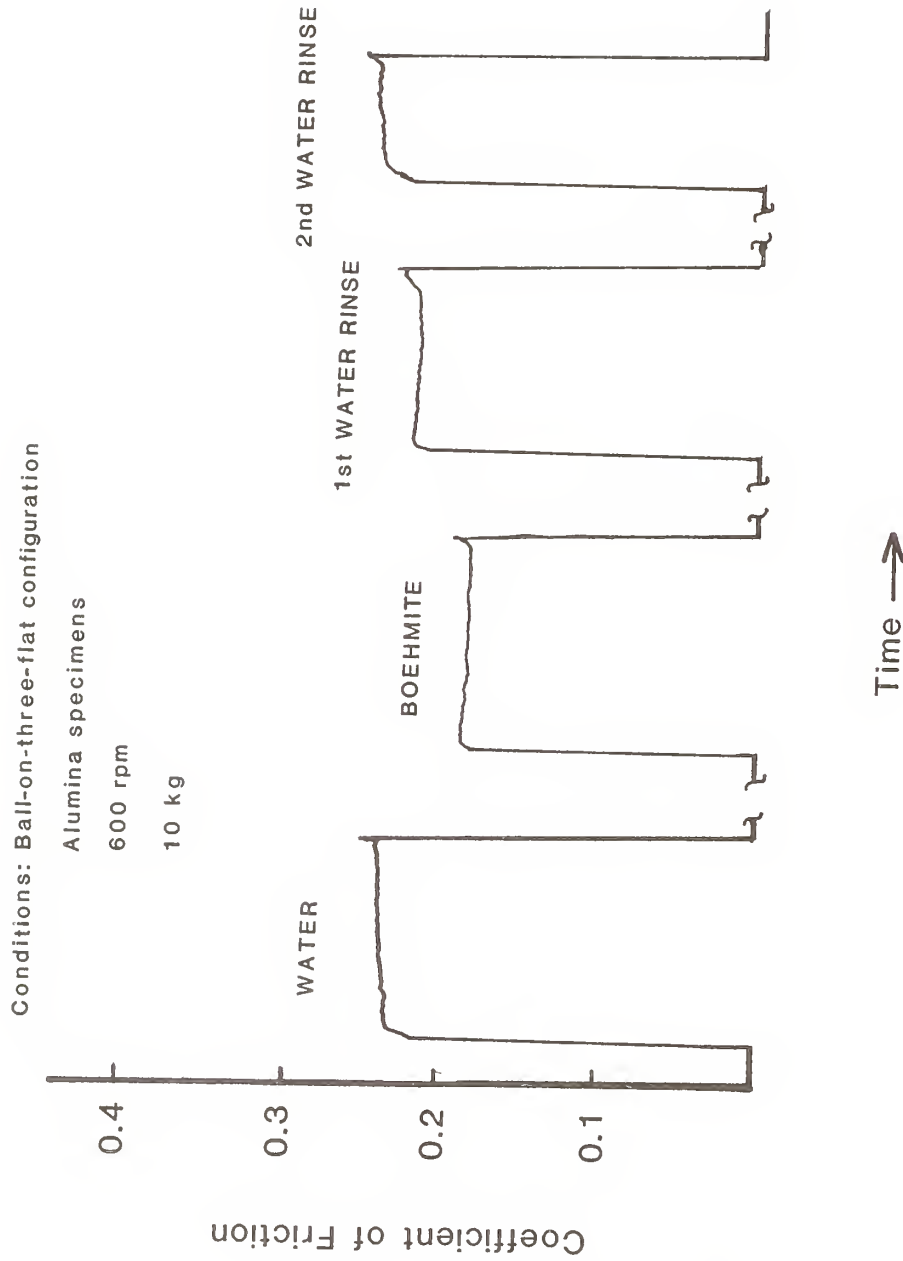


Figure 97. Lubricating Effect of Boehmite Powder for Water - Lubricated Alumina

## Chapter VIII

## SUMMARY AND CONCLUSIONS

This study has led to several valuable developments in the area of ceramic tribology. Wear test methods have been developed, new data analysis techniques have been employed, and a fundamental understanding of the nature of tribochemical reactions between water and alumina has been gained. The highlights of this study are:

- i) A step-loading four-ball wear test procedure has been developed to measure the friction and wear properties of ceramic materials under a range of test severities using a single set of specimens.
- ii) A ball-on-three-flat modification of this procedure has been developed which gives information similar to the four-ball test but allows testing of materials not available in ball form, thus expanding the utility of the test.
- iii) A test severity overlay technique was developed which allows for quick interpretation of the severity of the test in terms of mean pressure in the contact junction. This provides a significant, easy method for comparison of wear results over the entire range of load conditions.

- iv) These procedures are sensitive to minor processing and material parameters (batch to batch variations, etc.) and therefore provide an opportunity to systematically study the effects of processing and material variables on friction and wear of ceramics.
- v) Water-lubricated alumina gives much lower friction and wear than the unlubricated case over a wide range of test loads. SEM analysis revealed the presence of some sort of film which may have played a lubricating role.
- vi) Kinetic experiments using alumina powders confirmed the possibility of reactions occurring between water and gamma alumina. Aluminum oxide hydroxide - boehmite [ $\text{AlO}(\text{OH})$ ] is formed at  $194^\circ\text{C}$  and aluminum trihydroxide - bayerite [ $\text{Al}(\text{OH})_3$ ] is formed at  $\approx 100^\circ\text{C}$ . Alpha alumina was not reactive at these temperatures. Formation of aluminum oxide hydroxide (at  $194^\circ\text{C}$ ) followed a pseudo first order dependence.
- vii) Friction testing conducted on powder samples in a dry contact confirmed that aluminum oxide hydroxide (boehmite) and aluminum trihydroxide (gibbsite) have lubricating capability when compared to the parent alpha alumina. Approximate reductions of 10-20% were found for boehmite and 35-44% for gibbsite.

- viii) Friction testing conducted on powder samples in water at 2% concentration confirmed that aluminum oxide hydroxide has lubricating capability when compared to the water-lubricated case. Reduction in friction of 24% was observed.
  
- ix) Analysis of wear debris using techniques of Fourier transform infrared spectroscopy, thermogravimetric analysis, and x-ray powder diffraction indicate the presence of aluminum trihydroxide phase (bayerite) in the wear debris.

The water-lubricated alumina wear test results obtained in this report point to very interesting interactions between water and aluminum oxide in a tribocontact. A protective film is formed in the contact which is a reaction product between water and alumina. Water may also interact with these products (adsorption, etc.) to produce other desirable lubricating behavior in addition to the contribution of the easily sheared layer lattice structure (Gelatinous boehmite?). These results have potential application in at least two important areas. First, water-lubricated operations involving alumina may benefit from additions of small amounts of boehmite powder. The second application may be in the aluminum industry. Aluminum metal is very susceptible to oxidation. Fortunately, the product of oxidation forms a protective barrier to further oxidation; therefore, this

reaction is limited to the outermost surface of the metal. The outer layer is aluminum oxide and may therefore benefit from the lubrication mechanisms investigated in this report. Small amounts of boehmite added to water-based lubricants (or perhaps even oil-based lubricants) may result in reduced friction and wear.

## Chapter IX

## RECOMMENDATIONS FOR FUTURE WORK

This study has laid the groundwork for a wide variety of possible research areas in ceramic tribology and ceramic tribochemistry. The wear test methods developed during this study can be very useful in studies relating wear performance with processing parameters and material structure. They could also be used for ceramic/lubricant interaction studies to see the effect of lubricants and lubricant additives on the friction and wear behavior of ceramics. Finally, studies of tribochemical reactions between ceramics and lubricants would be of great interest. Using the case of alumina/water reactions as an example, it would be interesting to find the influence of different chemical parameters (pH, aqueous impurities, etc.) on the formation rates of aluminum trihydroxide and aluminum oxide hydroxide. These types of studies may have a tremendous impact on areas like machinability of alumina, the use of alumina inserts in machining of metals, and the compatibility of these alumina parts with water-based working fluids.

## REFERENCES

1. Dowson, D., History of Tribology, p. 16, Longman, London, 1979.
2. ASTM Standardization News - "Advanced Materials" issue, 14, No. 9, October 1986.
3. Steinberg, M.A., "Materials for Aerospace," Scientific American, October 1986, pp. 67-72.
4. Liedl, G.L., "The Science of Materials," Scientific American, October 1986, pp. 127-134.
5. Kear, B. H., "Advanced Metals," Scientific American, October 1986, pp. 159-167.
6. Bowen, H.K., "Advanced Ceramics," Scientific American, October 1986, pp. 169-176.
7. Rabinowicz, E., Friction and Wear of Materials, John Wiley & Sons, New York, 1965.
8. Larsen, D.C., Adams, J.W., Johnson, L.R., Teotia, A.P.S., and Hill, L.G., Ceramic Materials for Advanced Heat Engines, Technical and Economic Evaluation. Noyes, Park Ridge, 1985.
9. The Adiabatic Diesel Engine, SAE SP 543, Society of Automotive Engineers, Warrendale, 1983.
10. Adiabatic Engines: Worldwide Review, SAE SP 571, Society of Automotive Engineers, Warrendale, 1984.
11. Advances in Adiabatic Engines, SAE SP 610, Society of Automotive Engineers, Warrendale, 1985.
12. Shimauchi, T., Murakami, T., Nakagaki, T., Tsuga, Y., and Umeda, K., "Tribology at High Temperature for Uncooled Heat Insulated Engine," SAE Paper No. 840429, SP 571, Society of Automotive Engineers, pp. 35-45, 1984.
13. Timoney, S.G., "Engine Rig for Screening Ceramic Materials," SAE Paper No. 840433, SP 571, Society of Automotive Engineers, pp. 71-78, 1984.
14. Moorhouse, P., Mortimer, B., and Kamo, R., "Solid Lubrication Studies for Adiabatic Diesel Engines," SAE Paper No. 850508, SP 610, Society of Automotive Engineers, pp. 103-112, 1985.
15. King, A. G., "Ceramics for Cutting Metals," American Ceramic Society Bulletin, 43, No. 5, pp. 395-401, 1964.



16. Bhushan, B. and Sibley, L., "Silicon Nitride Rolling Bearings for Extreme Operating Conditions," ASLE Transactions, 25, No. 4, pp. 417-428, 1982.
17. Hines, J. E., Bradt, R. C., and Biggers, J.V., "Grain Size and Porosity Effects on the Abrasive Wear of Alumina," Wear of Materials 1977, pp. 462-467.
18. Steijn, R.P., "Friction and Wear of Single Crystals," Wear, 7, pp. 48-66, 1964.
19. Ishigaki, H., Kawaguchi, I., Iwasa, M., and Toibana, Y., "Friction and Wear of Hot Pressed Silicon Nitride and Other Ceramics," Wear of Materials 1985, pp. 13-21.
20. Miyoshi, K., Buckley, D., and Srinivasan, M., "Tribological Properties of Sintered Polycrystalline and Single-Crystal Silicon Carbide," American Ceramic Society Bulletin, 62, No. 4, pp. 494-500, 1983.
21. Blau, P.J., "Wear Testing and Standardization," ASTM Standardization News, pp. 34-36, October 1985.
22. Schwartz, L. and Steiner, B., "Versailles Project on Advanced Materials and Standards," ASTM Standardization News, pp. 40-44, October 1986.
23. Kingery, W.D., Bowen, H.K., and Uhlmann, D.R., Introduction to Ceramics, 2nd Edition, John Wiley & Sons, New York, 1976.
24. ASM Metals Reference Book, 2nd Edition, American Society for Metals, Metals Park, pp. 85-89, 1983.
25. Perry, R.H. and Chilton, C.H., Chemical Engineers Handbook, 5th Edition, McGraw Hill, New York, NY, 1973, pp. 23-38 to 23-53.
26. Fischer, T.E. and Tomizawa, H., "Interaction of Tribochemistry and Microfracture in the Friction and Wear of Silicon Nitride," Wear, 105, pp. 29-45, 1985.
27. Benzing, R., Goldblatt, I., Hopkins, V., Jamison, W., Mecklenburg, K., and Peterson, M., Friction and Wear Devices, 2nd Edition, American Society of Lubrication Engineers, Park Ridge, 1976.
28. Yellets, J.P., "The Design and Construction of a State-of-the-Art High Temperature Tribometer," M.S. Thesis, Pennsylvania State University, 1987.
29. Phone conversation with Dan Briggs, Adolph Coors Testing Laboratories (by Dennis Minor - NBS, 11/12/86).

30. Booser, E.R., (Editor), CRC Handbook of Lubrication (Theory and Practice of Tribology) Volume II, Theory and Design, Chapter 1, "The Shape of Surfaces" by J.B.P. Williamson, CRC Press, Boca Raton, pp. 3-16, 1986.
31. Kingery, W.D., Bowen, H.K., and Uhlmann, D.R., Introduction to Ceramics, 2nd Edition, John Wiley and Sons, New York, p. 469, 1976.
32. Munro, R.G., "Temperature Considerations in the Study of Surfaces Using a Four-Ball Apparatus," J. Appl. Phys., 57, 11, pp. 4950-4953, June 1, 1985.
33. Blau, P.J., "Interpretations of the Friction and Wear Break-in Behavior of Metals in Sliding Contact," Wear, 71 pp. 29-43, 1981.
34. Hsu, S.M., "The Effects of Chemical Reactions in Boundary Lubrication," Ph.D. Thesis, The Pennsylvania State University, pp. 275-280.
35. Dragoo, A., Robbins, R., and Minor, D., "Powder Characterization," Ceramics Technical Activities 1985, Institute for Materials Science and Engineering, National Bureau of Standards, U.S. Department of Commerce, NBSIR 85-3188, p. 45, 1985.
36. Buckley, D.H. and Miyoshi, K., "Fundamental Tribological Properties of Ceramics" from Proceedings of the 9th Annual Conference on Composites and Advanced Ceramic Materials, pp. 919-939, January 20-23, 1985. American Ceramic Society, Columbus, 1985.
37. Booser, E.R. (Editor), CRC Handbook of Lubrication (Theory and Practice of Tribology) Volume II: Theory and Design, CRC Press, Boca Raton, p. 71, 1984.
38. Tomizawa, H. and Fischer, T. E., "Friction and Wear of Silicon Nitride and Silicon Carbide in Water: Hydrodynamic Lubrication at Low Sliding Speed Obtained by Tribochemical Wear" ASLE Transactions 30, 1, pp. 41-46, 1987.
39. Ciftan, M. and Saibel, E., "Rebinder Effect and Wear," Wear, 56, pp. 69-80, 1979.
40. Booser, E.R. (Editor), CRC Handbook of Lubrication (Theory and Practice of Tribology) Volume II: Theory and Design, CRC Press, Boca Raton, p. 269, 1984.
41. Wefers, K. and Bell, G.M., "Oxides and Hydroxides of Aluminum," Technical Paper No. 19, Alcoa Research Laboratories, 1972.

42. Dorre, E., Hubner, H., Alumina, Processing, Properties, and Applications, Springer-Verlag, New York, 1984.
43. Gitzen, W.H., Alumina as a Ceramic Material, American Ceramic Society, Columbus, 1970.
44. Misra, C., Industrial Alumina Chemicals, ACS Monograph 184, American Chemical Society, Washington, 1986.
45. King, K.J., "Development of a Pressurized System for Oxidation Studies of Volatile Fluids," MS Thesis, The Pennsylvania State University, 1983.
46. Carel, A.B. and Cabiness, D.K., "Analysis of Alumina by Combined TG/X-Ray Diffraction," American Ceramic Society Bulletin, 64, No. 5, pp. 716-719, 1985.
47. Misra, C., Industrial Alumina Chemicals, ACS Monograph 184, American Chemical Society, Washington, 1986, p. 81.
48. Hines, J.E., Jr., Bradt, R.C., and Biggers, J.V., "Delta Alumina Formation during the Abrasive Wear of Polycrystalline Alumina," Wear of Materials 1979, pp. 540-550.

## Appendix A

Selected Bulk Properties of Cer 006 and Cer 021 Alumina<sup>(1)</sup>

Property	Units	Values		
		Conditions	Cer 006	Cer 021
Density	g/cm <sup>3</sup>		3.82	3.90
Compressive Strength	MPa (kpsi)	25°C	>2071 (>300)	2620 (380)
Flexural Strength	MPa (kpsi)	25°C 1000°C	331 (48) 193 (28)	379 (55)
Tensile Strength	MPa (kpsi)	25°C		262 (38)
Elastic Modulus	GPa (10 <sup>6</sup> psi)	25°C	345 (50)	372 (54)
Poisson's Ratio				0.22
Thermal Conductivity	W/mK	25°C 100°C 400°C 800°C	29.4 23.0	35.6 25.9 12.1 6.3
Coefficient of Linear Thermal Expansion	10 <sup>-6</sup> /°C	25-200°C 25-500°C 25-800°C 25-1000°C	6.7 7.3 7.8 8.0	7.1 7.6 8.0 8.3

<sup>(1)</sup> Product Literature for Coors AD995 (Cer 021) and AD998 (Cer 006).  
Alumina supplied by Coors Porcelain Company, Golden, Colorado.

## Appendix B

Coefficient of Friction Calculation for the  
Four-Ball Apparatus

The coefficient of friction can be calculated for the NBS modified four ball wear tester by considering the load application and friction force measurement geometries. As described before, the four-ball (or ball-on-three-flat) geometry produces a relationship between applied load (L) and normal load (N) of  $N = 0.408L$ , where L is the total applied load and N is the normal load on a single ball.

The friction force measurement system consists of an electronic force transducer which measures the force applied at the end of a lever arm (10.48 cm) due to the torque of the ball pot. The torque of the ball pot is due to the friction force in the contact junction which is on a much smaller lever arm. The actual distance between the center of rotation and the center of the area of contact (wear scar) is 0.366 cm. The ratio of the lever arms gives the force attenuation factor (10.48/0.366 or 28.63). This indicates that an actual friction force ( $F_a$ ) of 28.63  $g_f$  in the contact junctions will produce a torque which will register only 1.0  $g_f$  force (measured force or  $F_m$ ) on the electronic force transducer.

$$F_a = F_m(28.63) \quad [1]$$

The friction force due to one ball will of course be one third of the total friction force.

Coefficient of friction ( $\mu$ ) is defined as the ratio of the actual friction force to the normal force.

$$\mu = \frac{F_a}{N} \quad [2]$$

Substituting, we have for a single ball

$$\mu = \frac{F_m (28.63)}{(3) (0.408)L} = 23.39 \frac{F_m}{L} \quad [3]$$

where  $F_m$  and  $L$  are in the same units ( $\text{kg}_f$ ). In most cases, friction force is measured in grams and applied load is measured in kilograms.

Thus

$$\mu = \frac{0.02339 F_m}{L} \quad [4]$$

where  $F_m$  = measured friction force in  $\text{g}_f$

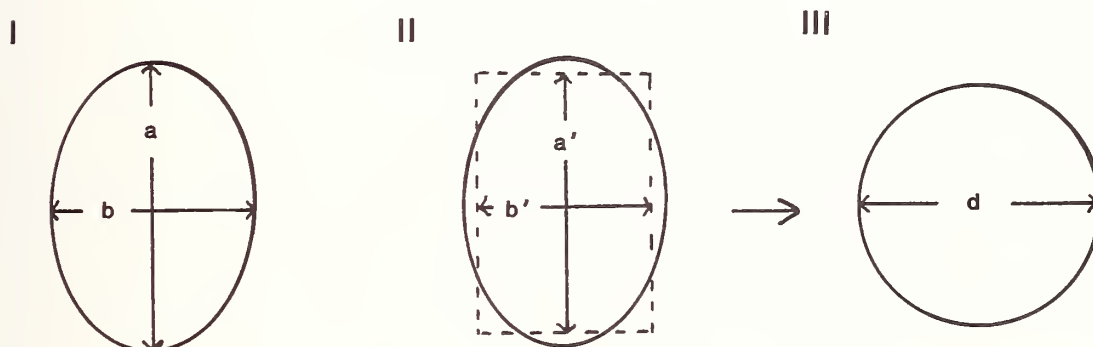
$L$  = applied load in  $\text{kg}_f$

## Appendix C

## Equivalent Wear Scar Diameter Concept

For regular uniform wear scars, the arithmetic average of the optical wear scar measurements (1 in the direction of sliding and 1 perpendicular to the direction of sliding for each of 3 lower specimens) is reported as the wear scar diameter.

For irregular wear scars the concept of equivalent wear scar diameter may be useful since it is not the length or width of the wear that is most important but instead, the load supporting area of the scar.



Using the method recommended by Hsu,<sup>(1)</sup> an imaginary rectangle can be placed over the wear scar (I) such that the area of the rectangle is equal to the area (A) of the elliptical wear scar (II). If this scar were transformed into a circle of the same area (III) it would have a diameter  $d$  - the "equivalent diameter". That is, the diameter of the circle with an equivalent area.

$$\text{II. Area} = A_{\text{rectangle}} = a'b'$$



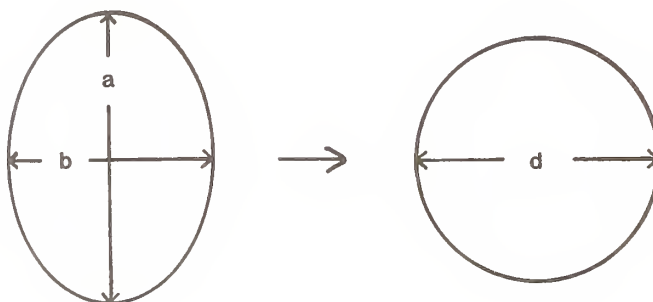
$$\text{III. Area} = A_{\text{circle}} = \pi r^2 = \pi d^2/4$$

$$A_{\text{rectangle}} = A_{\text{circle}}$$

$$\pi d^2/4 = a'b'$$

$$d = 2(a'b'/\pi)^{1/2}$$

which would be more accurate than the simple arithmetic average of  $a$  and  $b$ . Unfortunately we do not usually measure  $a'$  and  $b'$  instead we measure  $a$  and  $b$ . In addition, the placing of a rectangle of equal area over the wear scar is very subjective. There is however a method that may be employed to estimate that the area of the wear scar if it is elliptical.



The area of an ellipse with major axis  $a$  and minor axis  $b$  is  $(a/2)(b/2)\pi$ . This area can be set equal to the area of a circle:

$$A_{\text{ellipse}} = A_{\text{circle}}$$

$$\frac{a}{2} \frac{b}{2} \pi = \pi \frac{d^2}{4}$$

$$d^2 = ab$$

$$d_E = (ab)^{1/2}$$

Thus the equivalent diameter can be obtained for elliptical wear scars by taking the geometric average of the wear scar measurements.

$$d_E = (ab)^{1/2}$$

An example of values calculated for d for elliptical scars:

Major Axis	Minor Axis	Ratio Major/Minor (Aspect Ratio)	d Avg. ( $d_A$ )	d Equivalent ( $d_E$ )	$\Delta d$ ( $d_A - d_E$ )	% $\Delta d$ ( $\Delta d/d_{Avg}$ ) $\times 100$
1.0	1.0	1.0	1.0	1.0	0	0
1.1	1.0	1.1	1.05	1.049	.001	0.1
1.2	1.0	1.2	1.10	1.095	.005	0.5
1.3	1.0	1.3	1.15	1.140	.010	0.9
1.4	1.0	1.4	1.30	1.183	.017	1.4
1.5	1.0	1.5	1.25	1.225	.025	2.0
1.6	1.0	1.6	1.30	1.265	.035	2.7
1.7	1.0	1.7	1.35	1.304	0.46	3.4
1.8	1.0	1.8	1.40	1.342	.058	4.1
1.9	1.0	1.9	1.45	1.378	.072	5.0
2.0	1.0	2.0	1.50	1.414	.086	5.7

$$d_A = (a+b)/2$$

$$d_E = (ab)^{1/2}$$

(1) S.M. Hsu, Ph.D. Thesis, Department of Chemical Engineering, Pennsylvania State University, University Park, PA 1976, p. 81.

## Appendix D

### Specimen Cleaning Procedure

Thorough cleaning of wear test specimens and equipment is important in ensuring good test precision and repeatability. Therefore the following procedure was used to remove contaminants and impurities from the specimens and equipment.

- Specimens:
- 1) Immerse in a mixture of hexane\*/toluene\* (9:1) in an ultrasonic bath for sixty seconds.
  - 2) Pour off the liquid and repeat step 1) but only for ten seconds ultrasonic treatment. Pour off the liquid.
  - 3) Rinse specimens in pure hexane.
  - 4) Immerse specimens in acetone\* in an ultrasonic bath for sixty seconds.
  - 5) Pour off the liquid and repeat step 4) but only for ten seconds ultrasonic treatment. Pour off the liquid.
  - 6) Rinse with fresh acetone.
  - 7) Dry with a stream of nitrogen.\*\*

\*ACS grade solvents are used.

\*\*In some very special cases (e.g., low load unlubricated runs) even the ACS grade solvents contain enough impurities to affect the test results. In these cases, follow the acetone rinse with ultrasonic cleaning using a laboratory detergent (e.g., Micro) followed by complete rinsing with deionized water.

Equipment: Same as for specimens in the case of loose parts. In the case of fixed parts which cannot be moved or placed in an ultrasonic bath, only rinsing with the appropriate sequence of solvents is required.

## Appendix E

## Pressure Temperature Relationship for the Alumina/Water Bomb Reactor

Since there is a pressure gage attached to the bomb reactor, we may get an indirect measure of the temperature in the reactor from the total pressure. At any temperature  $T$ , the pressure in the reactor is the sum of the partial pressure of air in the reactor plus the vapor pressure of water in the reactor (-14.7 psia to correct from absolute pressure to gage pressure).

$$P_{\text{gage}} = P'_{\text{air}} + P'_{\text{H}_2\text{O}} - 14.7$$

where  $P_{\text{gage}}$  = estimated gage pressure reading for the reactor at temperature  $T$  (psig)

$P'_{\text{air}}$  = partial pressure of air in reactor at temperature  $T$  (psia)

$P'_{\text{H}_2\text{O}}$  = vapor pressure of water in reactor at temperature  $T$  (psia)

For a constant volume reactor where the air does not react, the partial pressure of air can be estimated (at low pressures) using the ideal gas law and

$$\frac{P_i}{T_i} = \frac{P_f}{T_f}$$

where i and f indicate initial and final states.

In our case,  $T_i = 21^\circ\text{C} = 294^\circ\text{K}$

$$P_i = 14.7 \text{ psia.}$$

therefore

$$P_f = \frac{P_i T_f}{T_i} = 0.0500 T_f$$

or

$$P'_{\text{air}} = 0.0500 T_f$$

where  $T_f$  is in  $^\circ\text{K}$ .

Values of  $P'_{\text{H}_2\text{O}}$  are available in the steam table under vapor pressure of water above  $100^\circ\text{C}$  (for example CRC Handbook of Chemistry and Physics 56th Ed, page D180).

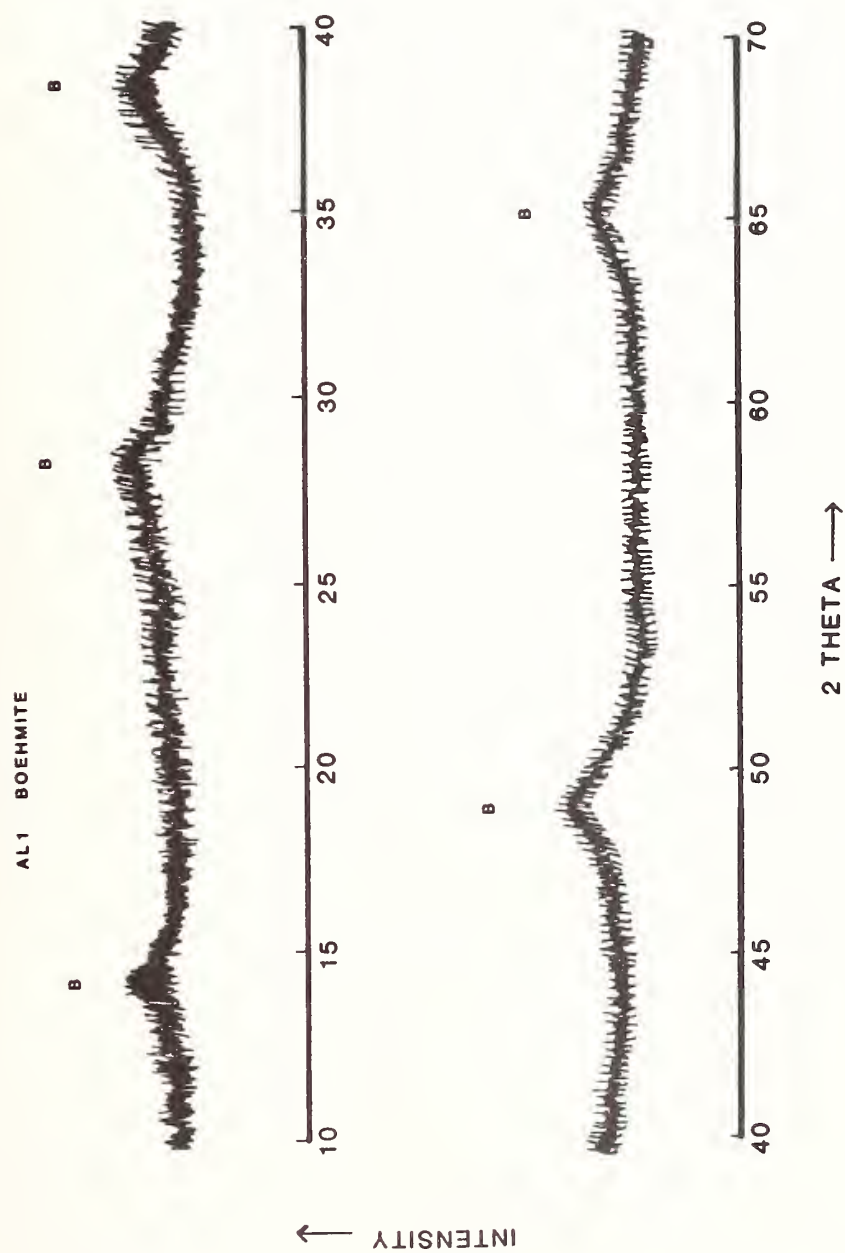
A table can therefore be constructed by selecting several temperatures, looking up the values of  $P'_{\text{H}_2\text{O}}$  at each temperature, calculating  $P'_{\text{air}}$ , and ultimately finding the value for  $P_{\text{gage}}$  at each temperature. A plot of temperature ( $^\circ\text{C}$ ) versus Pressure ( $P_{\text{gage}}$ ) can then be constructed as a calibration (figure 61). The temperature of

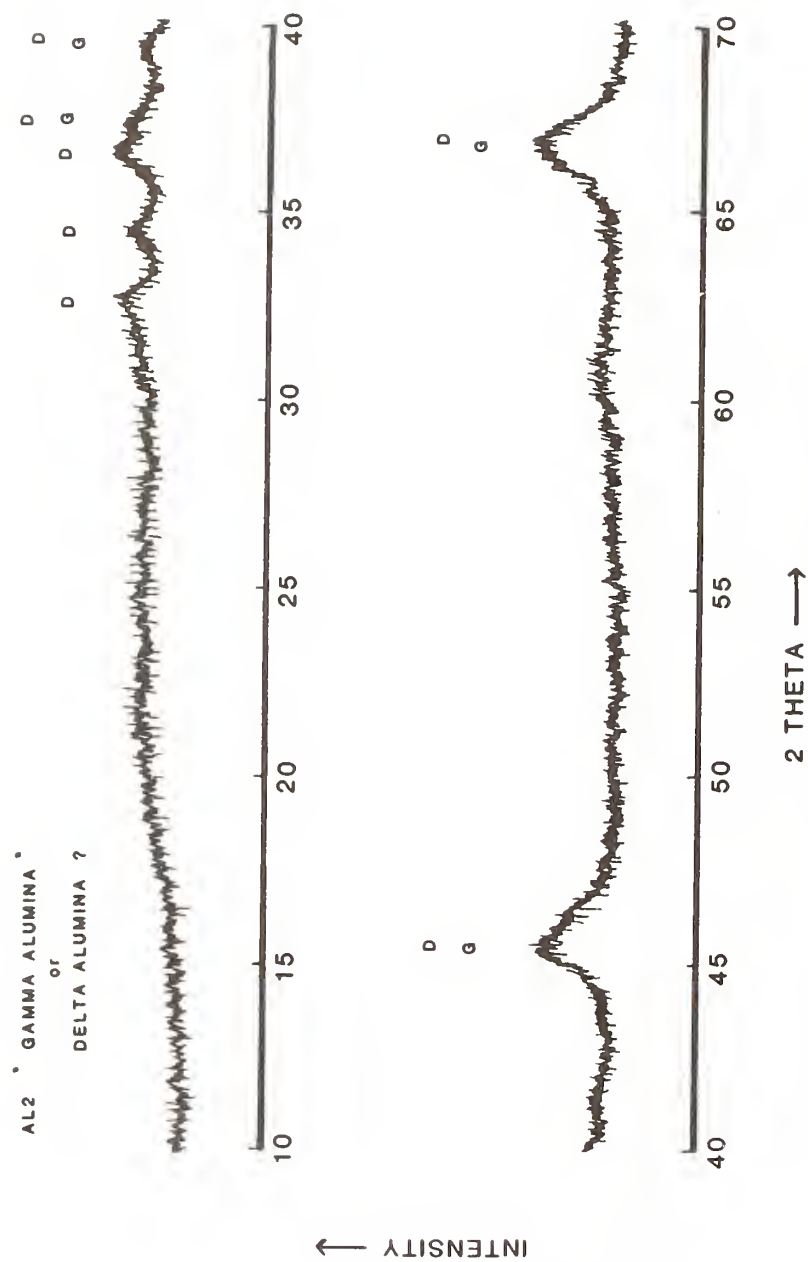
the reaction can therefore be obtained by reading the gage pressure and using the calibration chart (figure 61).

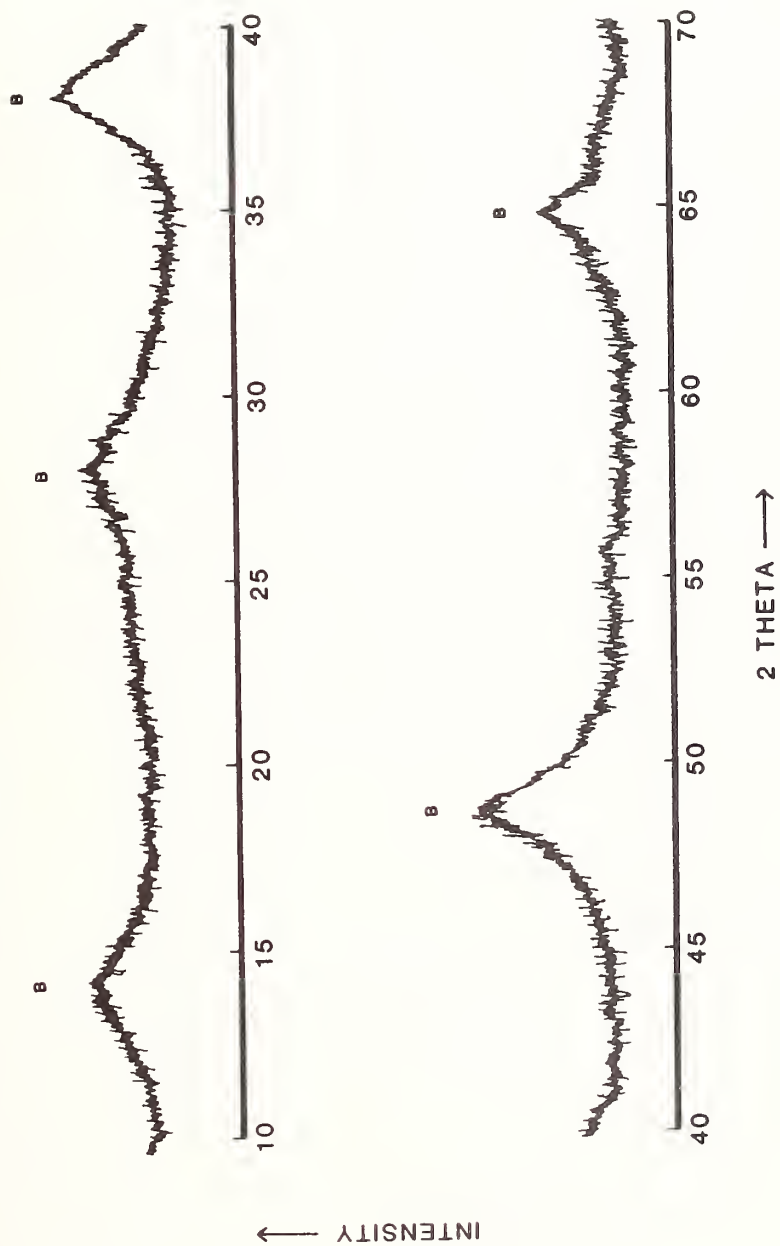


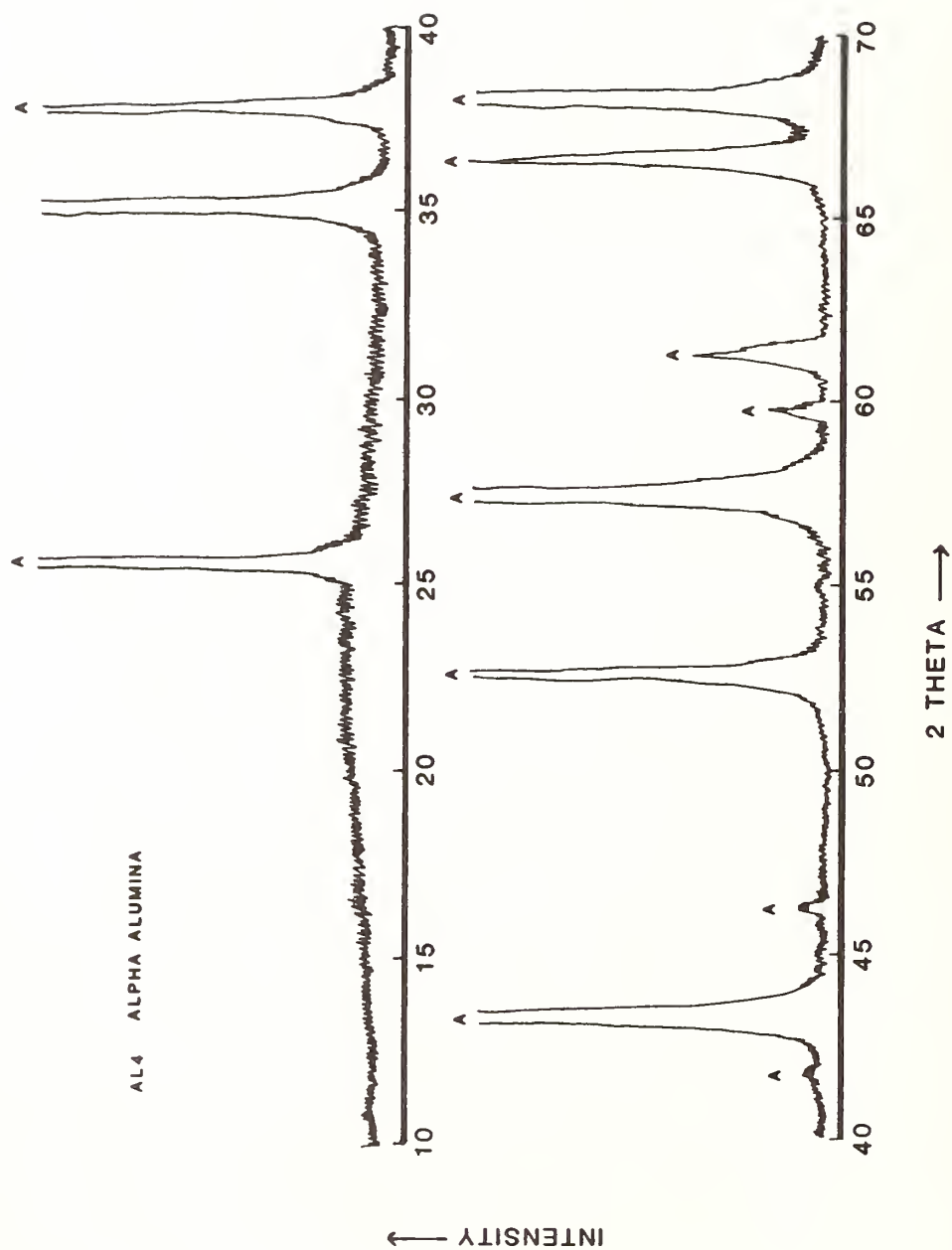
## Appendix F

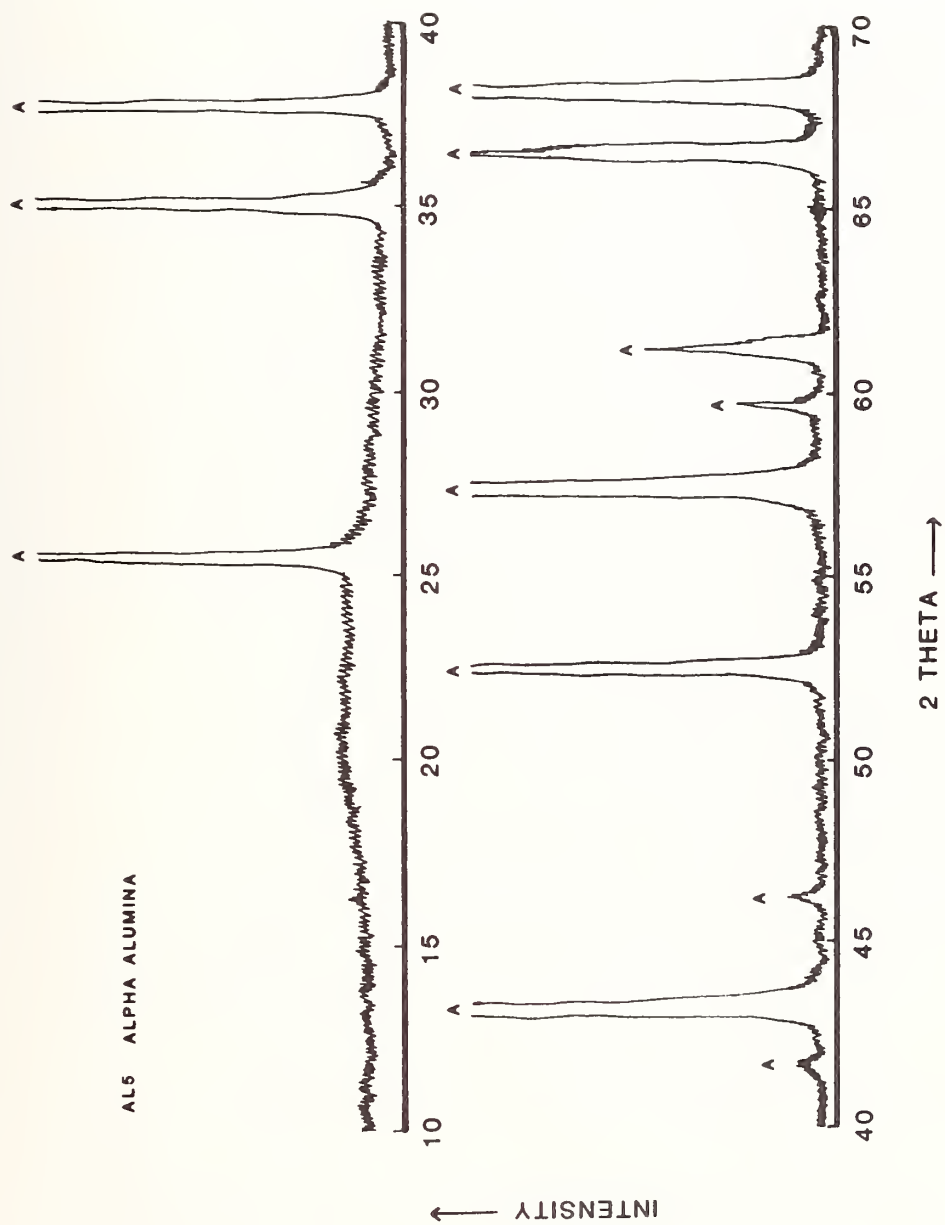
## X-Ray Powder Diffraction Patterns for Reference Powders AL1 through AL6

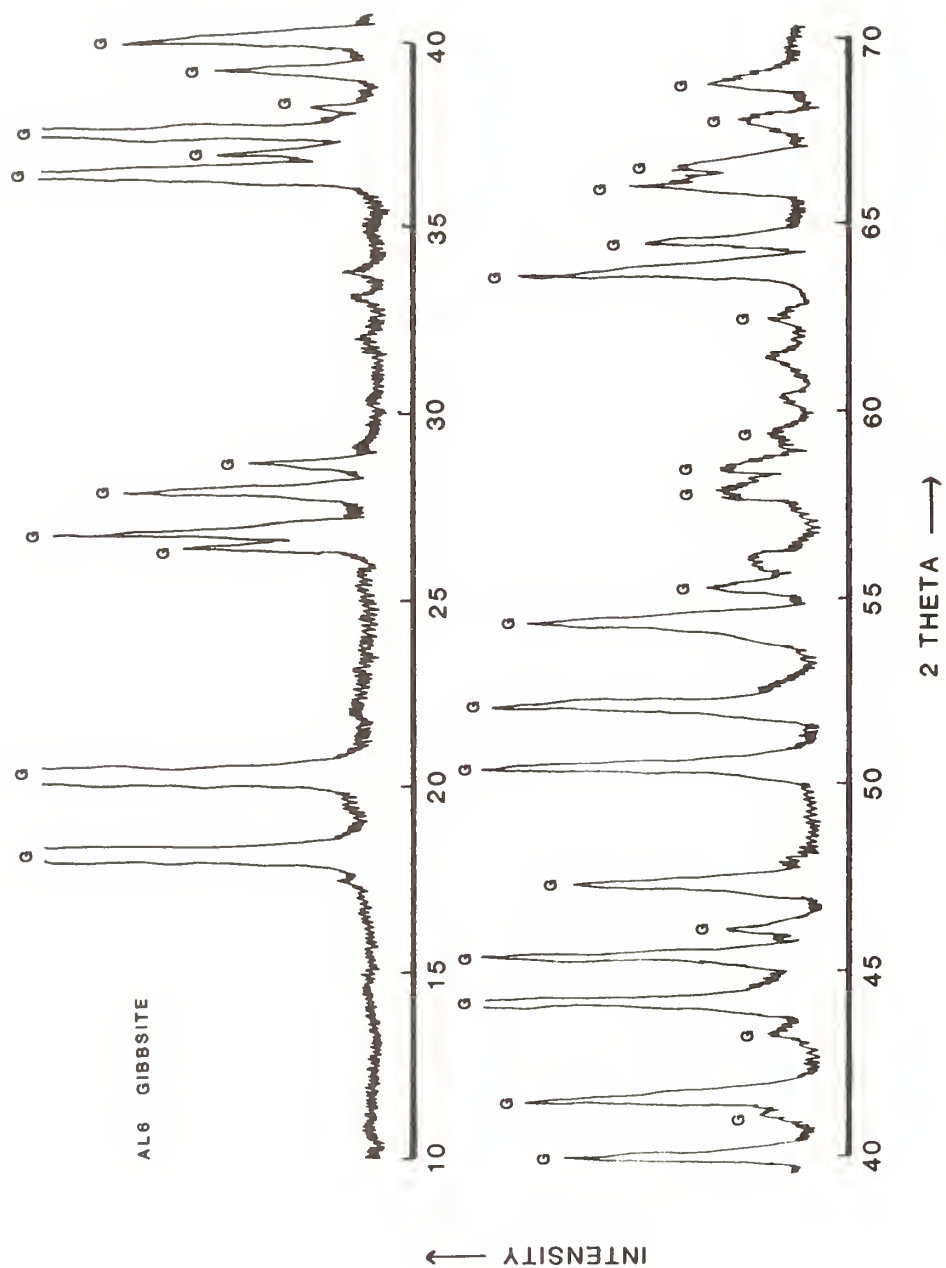




AL<sub>3</sub> BOEHMITE







## APPENDIX G

Interplanar Spacings, 2 Thetas, and Relative  
Line Intensities for X-Ray Powder Diffraction  
Patterns of Alumina's, Aluminum Oxide Hydroxides  
and Aluminum Trihydroxides

$\alpha$			$\gamma$			$\delta$			$\theta$		
JCPDS File # 10-173			JCPDS File # 10-425			JCPDS File # 16-394			JCPDS File # 23-1009		
dÅ	2 $\theta$	I/I <sub>0</sub>	dÅ	2 $\theta$	I/I <sub>0</sub>	dÅ	2 $\theta$	I/I <sub>0</sub>	dÅ	2 $\theta$	I/I <sub>0</sub>
3.479	25.58	75	4.56	19.45	40	7.6	11.63	4	5.70	15.53	2
2.552	35.13	90	2.80	31.93	20	6.4	13.82	4	5.45	16.25	10
2.379	37.78	40	2.39	37.60	80	5.53	16.01	4	4.54	19.54	18
2.165	41.68	< 1	2.28	39.49	50	5.10	17.37	8	2.837	31.51	80
2.085	43.36	100	1.977	45.86	100	4.57	19.41	12	2.730	32.78	65
1.964	46.18	1	1.520	60.89	30	4.07	21.82	12	2.566	34.94	14
1.740	52.55	45	1.395	67.03	100	3.61	24.64	4	2.444	36.74	60
1.601	57.52	80				3.23	27.59	4	2.315	38.87	45
1.546	59.77	3		Cubic		3.05	29.26	4	2.257	39.91	35
1.514	61.16	5				2.881	31.01	8	2.019	44.85	45
1.510	61.34	7				2.728	32.80	30	1.9544	46.42	8
1.404	66.54	30				2.601	34.45	25	1.9094	47.58	30
1.374	68.19	50				2.460	36.49	60	1.7998	50.68	14
1.337	70.35	1				2.402	37.41	16	1.7765	51.39	6
1.276	74.26	3				2.315	38.87	8	1.7376	52.63	4
						2.279	39.51	40	1.6807	54.55	2
						2.160	41.78	4	1.6216	56.72	6
						1.986	45.64	75	1.5715	58.70	2
						1.953	46.46	40	1.5426	59.91	25
						1.914	47.46	12	1.5120	61.25	6
						1.827	49.87	4	1.4883	62.33	25
						1.810	50.37	8	1.4526	64.05	25
						1.628	56.48	8	1.4264	65.37	10
						1.604	57.40	4	1.3883	67.40	100
						1.538	60.11	8			
						1.517	61.03	16			
						1.456	63.88	8			
						1.407	66.38	50			
						1.396	66.98	100			

<sup>(1)</sup>Based on Cu K<sub>α1</sub> radiation.



Boehmite JCPDS File # 21-1307			Diaspore JCPDS File # 5-0355			Akdalaitite JCPDS File # 25-17		
dÅ	2θ	I/I <sub>0</sub>	dÅ	2θ	I/I <sub>0</sub>	dÅ	2θ	I/I <sub>0</sub>
6.11	14.48	100	4.71	18.82	13	4.61	19.24	10
3.164	28.18	65	3.99	22.26	100	4.38	20.26	60
2.346	38.33	55	3.214	27.73	10	4.23	20.98	20
1.980	45.79	6	2.558	35.05	30	3.24	27.51	70
1.860	48.93	30	2.434	36.90	3	3.15	28.13	20
1.850	49.21	25	2.386	37.67	5	2.781	32.16	30
1.770	51.59	6	2.356	38.17	8	2.530	35.45	10
1.662	55.22	14	2.317	38.83	56	2.494	35.98	90
1.527	60.59	6	2.131	42.38	52	2.406	37.34	20
1.453	64.03	16	2.077	43.54	49	2.35	38.27	90
1.434	64.98	10	1.901	47.81	3	2.32	38.78	80
1.412	66.12	2	1.815	50.22	8	2.19	41.18	20
1.396	66.98	2	1.733	52.78	3	2.16	41.78	10
1.383	67.69	6	1.712	53.48	15	2.11	42.82	100
1.369	68.48	2	1.678	54.65	3	2.07	43.69	10
1.312	71.90	16	1.633	56.29	43	1.925	47.17	10
1.302	72.48	4	1.608	57.24	12	1.905	47.70	10
Orthorhombic			1.570	58.76	4	1.859	48.96	70
			1.522	60.81	6	1.684	54.44	30
			1.480	62.72	20	1.667	55.04	10
			1.431	65.13	7	1.647	55.77	10
			1.423	65.54	12	1.622	56.70	50
			1.400	66.76	6	1.547	59.72	60
			1.376	68.08	16	1.511	61.30	30
			1.340	70.17	5	1.471	63.15	10
			1.329	70.84	6	1.461	63.63	20
			1.289	73.39	6	1.418	65.80	100
			1.279	74.06	1	1.393	67.14	100
			Orthorhombic			1.334	70.54	10
						1.328	70.90	20
						1.288	73.46	10
						1.280	73.99	25
						1.264	75.09	20
						Hexagonal		

<sup>(1)</sup> Based on Cu K<sub>α1</sub> radiation.

Gibbsite			Gibbsite			Bayerite			Nordstrandite			II Phase		
JCPDS File #			JCPDS File #			JCPDS File #			JCPDS File #			JCPDS File #		
29-41			33-18			20-11			24-6			26-25		
dÅ	2θ	I/I <sub>0</sub>	dÅ	2θ	I/I <sub>0</sub>	dÅ	2θ	I/I <sub>0</sub>	dÅ	2θ	I/I <sub>0</sub>	dÅ	2θ	I/I <sub>0</sub>
4.853	18.26	100	4.8486	18.28	100	4.71	18.82	90	4.79	18.51	100	3.58	24.85	100
4.380	20.26	36	4.3711	20.30	70	4.35	20.40	70	4.32	20.54	25	2.549	35.18	10
4.328	20.50	18	4.3187	20.55	50	3.20	27.86	30	4.21	21.08	18	2.407	37.33	10
3.365	26.46	5	3.3590	26.51	17	2.699	33.16	4	4.16	21.34	12	2.259	39.87	30
3.318	26.85	9	3.3122	26.89	30	2.464	36.43	2	3.89	22.84	12	2.171	41.56	60
3.189	27.95	7	3.1829	28.01	25	2.356	38.17	4	3.61	24.64	8	2.067	43.76	5
3.110	28.68	3	3.1054	28.72	13	2.274	39.60	2	3.43	25.95	6	1.998	45.35	10
2.471	36.33	7	2.4658	36.40	25	2.222	40.57	100	3.03	29.45	4	1.926	47.15	15
2.456	36.56	12	2.4522	36.61	40	2.156	41.86	2	2.848	31.38	4	1.796	50.79	35
2.426	37.02	4	2.4224	37.08	15	2.073	43.62	2	2.710	33.03	2	1.751	52.19	5
2.389	37.62	16	2.3851	37.68	55	1.983	45.71	4	2.501	35.87	2	1.613	57.05	60
2.294	39.24	4	2.3471	38.32	4	1.969	46.06	2	2.480	36.19	12	1.469	63.25	25
2.250	40.04	6	2.2899	39.31	15	1.917	47.38	2	2.455	36.57	8	1.334	70.54	5
2.243	40.17	4	2.2464	40.11	20	1.835	49.64	2	2.393	37.55	25	1.275	74.33	10
2.169	41.60	7	2.1924	41.14	2	1.826	49.90	2	2.333	38.56	6	Cubic		
2.159	41.80	5	2.1647	41.69	27	1.723	53.11	40	2.271	39.65	30			
2.052	44.09	12	2.0845	43.37	4	1.895	54.06	2	2.217	40.66	4			
2.037	44.44	8	2.0489	44.16	40	1.688	54.30	2	2.146	42.07	4			
1.9973	45.37	8	2.0239	44.75	3	1.656	55.44	2	2.113	42.76	2			
1.9909	45.42	6	1.9944	45.44	28	1.646	55.80	2	2.074	43.60	4			
1.9669	46.11	2	1.9637	46.19	6	1.641	55.99	2	2.016	44.92	25			
1.9196	47.31	5	1.8042	50.54	30	1.600	57.55	10	1.991	45.52	2			
1.8074	50.45	10	1.7517	52.17	30	1.572	58.68	2	1.975	45.91	2			
1.7966	50.77	6	1.7365	52.66	4	1.554	59.43	8	1.945	46.66	6			
1.7542	52.09	9	1.6974	53.97	4	1.492	62.16	2	1.902	47.78	20			
1.6871	54.33	7	1.6845	54.42	30	1.478	62.82	2	1.877	48.46	2			
1.6826	54.49	5	1.6576	55.38	9	1.457	63.83	12	1.821	50.05	2			

(continued)

Gibbsite JCPDS File # 29-41			Gibbsite JCPDS File # 33-18			Bayerite JCPDS File # 20-11			Nordstrandite JCPDS File # 24-6			II Phase JCPDS File # 26-25		
dÅ	2θ	I/I <sub>0</sub>	dÅ	2θ	I/I <sub>0</sub>	dÅ	2θ	I/I <sub>0</sub>	dÅ	2θ	I/I <sub>0</sub>	dÅ	2θ	I/I <sub>0</sub>
1.6591	55.32	2	1.5926	57.85	7	1.445	64.42	8	1.804	50.55	4			
1.5943	57.98	2	1.5865	58.09	7	1.392	67.19	6	1.784	51.16	14			
1.5891	57.99	2	1.5739	58.60	8	1.381	67.80	2	1.715	53.38	2			
1.5764	58.50	2	1.5525	59.49	3	1.348	69.70	2	1.704	53.75	2			
1.4600	63.68	5	1.4846	62.51	4	1.333	70.60	18	1.668	55.00	4			
1.4428	64.53	3	1.4577	63.80	30	1.277	74.20	2	1.653	55.55	4			
1.4138	66.02	4	1.4405	64.65	18	Monoclinic			1.632	56.32	2			
1.4078	66.34	2	1.4115	66.14	19				1.616	56.93	2			
1.4042	66.53	4	1.4021	66.65	13				1.598	57.63	6			
1.3971	66.92	2	1.3808	67.81	6				1.572	58.68	4			
1.3643	68.75	2	1.3620	68.88	10				1.560	59.18	2			
1.3611	68.93	2	1.3311	70.71	7				1.547	59.72	6			
Monoclinic			1.3247	71.11	4				Triclinic					
			1.2999	72.68	3									
			Monoclinic											

(1) Based on Cu K<sub>α1</sub> radiation.

## Appendix H

An Estimate of the Hertizan Contact Diameter,  
Mean Pressure and Maximum Pressure for 52100 Steel  
and Alumina Specimens in the Four-Ball Apparatus

Hertzian Contact Diameter

The Hertz equation for the radius of the contact area formed between two elastic spherical surfaces under static load is as follows<sup>1</sup>

$$\text{radius } a = \left( \frac{3\pi N (k_1 + k_2) R_1 R_2}{4(R_1 + R_2)} \right)^{1/3} \quad [1]$$

where  $R_1 = R_2 = 0.6350 \text{ cm}$  (0.25 inches)

$$N = 0.408L$$

where  $L$  = the applied machine load in  $\text{kg}_f$

$$k_1 = k_2 = \frac{1 - \nu^2}{\pi E} \quad [2]$$

where  $\nu$  = Poissons Ratio = 0.30 for 52100 steel

$$E = \text{Young's Modulus} = 2.10 \times 10^6 \frac{\text{kg}_f}{\text{cm}^2} \text{ for 52100 steel}$$

Using these values  $k = 1.379 \times 10^{-7}$

$$a = \left( \frac{3\pi (0.408) (L) (2.758 \times 10^{-7}) (0.403)}{(4) 1.270} \right)^{1/3} \quad [3]$$

$$a = 4.382 \times 10^{-3} \quad [L]^{1/3} \quad (\text{cm}) \quad [4]$$

$$d = 8.764 \times 10^{-3} \quad [L]^{1/3} \quad (\text{cm}) \quad [5]$$

$d = 8.76 \times 10^{-2} \quad [L]^{1/3} \quad (\text{mm})$	[52100 steel] [6]
---	-------------------

For alumina, values of Poisson's Ratio and Young's Modulus for alumina were obtained from reference 2 for fully dense polycrystalline alumina

$$E = 403.45 \quad \frac{\text{GN}}{\text{m}^2}$$

$$\nu = 0.236$$

$$E = \left( 403.45 \frac{\text{GN}}{\text{m}^2} \right) \left( \frac{1\text{m}^2}{10^4 \text{cm}^2} \right) \left( \frac{1\text{kg}_f}{9.8\text{N}} \right) = 4.12 \times 10^6 \quad \frac{\text{kg}_f}{\text{cm}^2}$$

Substituting into equation [1]

$d_H = 7.09 \times 10^{-2} \quad [L]^{1/3}$	[Alumina]	[7]
---	-----------	-----

<sup>1</sup>Klaus, E.E., "Wear and Lubrication Characteristics of Some Mineral Oil and Synthetic Lubricants," Ph.D. Thesis, The Pennsylvania State University, 1952, p. 111.

<sup>2</sup>Alumina, Processing, Properties, and Applications, E. Dorre and H. Hubner, Springer-Verlag Berlin, Heidelberg, 1984, p. 76.

### Mean Pressure in a Contact Junction

$$P_{\text{mean}} = \frac{\text{Force}}{\text{Area}}$$

where Force = load applied in the 4-ball contact geometry = N

Area = area of the wear scar

for a uniform wear scar  $\text{Area} = \pi r^2 = \frac{\pi d^2}{4}$

For an area in  $\text{cm}^2$

if d is given in mm,  $\text{Area} = \frac{\pi d^2}{4(100)}$

For the 4-ball contact geometry:

$$\text{Force} = N = 0.408L$$

where L = the applied load in  $\text{kg}_f$

$$P_{\text{mean}} \left( \frac{\text{kg}_f}{\text{cm}^2} \right) = \frac{N}{\pi d^2 / 4(100)} = \frac{(400) (0.408)L}{\pi d^2}$$

$$P_{\text{mean}} \left( \frac{\text{kg}}{\text{cm}^2} \right) = \frac{(51.9)L}{d^2}$$

$$P_{\text{mean}}(\text{kpsi}) = P_{\text{mean}} \left( \frac{\text{kg}}{\text{cm}^2} \right) (0.014223) = \frac{(0.73817)L}{d^2}$$

$$P_{\text{mean}}(\text{MPa}) = P_{\text{mean}} \left( \frac{\text{kg}}{\text{cm}^2} \right) (0.09807) = \frac{(5.09)L}{d^2}$$

$$1 \text{ kpsi} = 6.895 \text{ MPa}$$

### Wear Scar Diameters and Pressures in a Hertzian Contact

#### 52100 Steel

Applied Load, kg <sub>f</sub>	d <sub>H</sub> , mm	P <sub>mean</sub>		P <sub>max</sub>	
		MPa	kpsi	MPa	kpsi
5	0.149	1,147	166.3	1,720	249.4
10	0.188	1,440	208.9	2,160	313.3
20	0.237	1,812	262.8	2,719	394.3
40	0.299	2,277	330.3	3,416	495.4
100	0.405	3,103	450.0	4,655	675.1
200	0.511	3,898	565.4	5,847	848.1
300	0.584	4,477	649.3	6,716	974.0



## Alumina

Applied Load, kg <sub>f</sub>	d <sub>H</sub> , mm	P <sub>mean</sub>		P <sub>max</sub>	
		MPa	kpsi	MPa	kpsi
5	0.121	1,738	252.1	2,607	378.1
10	0.153	2,174	315.3	3,261	473.0
20	0.192	2,761	400.5	4,142	600.7
40	0.242	3,476	504.2	5,215	756.3
100	0.329	4,702	682.0	7,053	1,023.0
200	0.415	5,910	857.2	8,865	1,285.8
300	0.475	6,767	981.5	10,151	1,472.3

$P_{\max} = 1.5 P_{\text{mean}}$  for hemispherical load distribution.

## Appendix I

Derivation of a Pseudo First Order Dependence for the  
Gamma Alumina/Water Reaction at 194°C

The reaction we are considering is the reaction between water and  $\gamma$ -alumina to form boehmite [the alumina monohydrate or aluminum oxide hydroxide  $\text{AlO}(\text{OH})$ ]



this can be generalized as



If we assume mass action kinetics and a homogeneous reaction model in which mass and heat transfer is not limiting

$$r = - \frac{dC_A}{dt} = k_1 C_A C_B - k_{-1} C_C^2 \quad [3]$$

if 1)  $C_B \approx \text{Constant}$  (i.e., excess B)

2) Either  $C_C$  is very small (low conversion) or  $k_{-1}$  is very small  
(reaction not very reversible)

such that

$$k_{-1} C_C^2 \ll k_1 C_A C_B$$

then

$$r = - \frac{dC_A}{dt} = k_1' C_A \quad [4]$$

where  $k_1' = k_1 C_B$

$$\frac{dC_A}{dt} = - k_1' C_A$$

$$\int_0^{C_A} \frac{dC_A}{C_A} = - \int_0^t k_1' dt$$

subject to conditions: @  $t = 0$

$$C_A = C_{A_0}$$

$$\ln C_A \Big|_{C_{A_0}}^{C_A} = - k_1' t \Big|_0^t$$

$$\ln \frac{C_A}{C_{A_0}} = - k_1' t \quad [5]$$

or

$$C_A = C_{A_0} e^{-k_1' t} \quad [6]$$

in terms of fractional conversion

$$C_A = C_A(1 - f)$$

or

$$\frac{C_A}{C_A} = 1 - f$$

Substituting into eq [5]

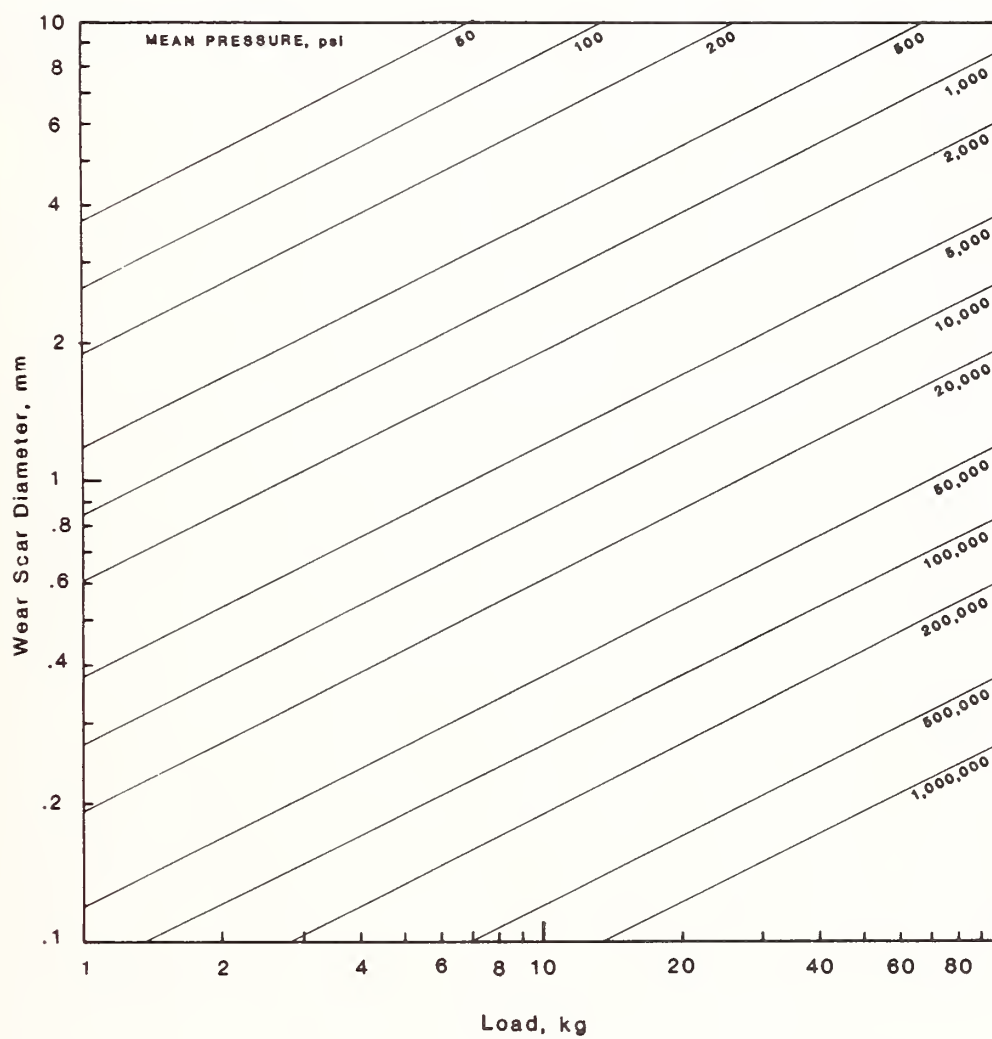
$$\ln(1 - f) = -kt$$

[7]

therefore a plot of  $\ln(1 - f)$  versus  $t$  will produce a straight line of slope  $-k$  if this reaction is pseudo first order.

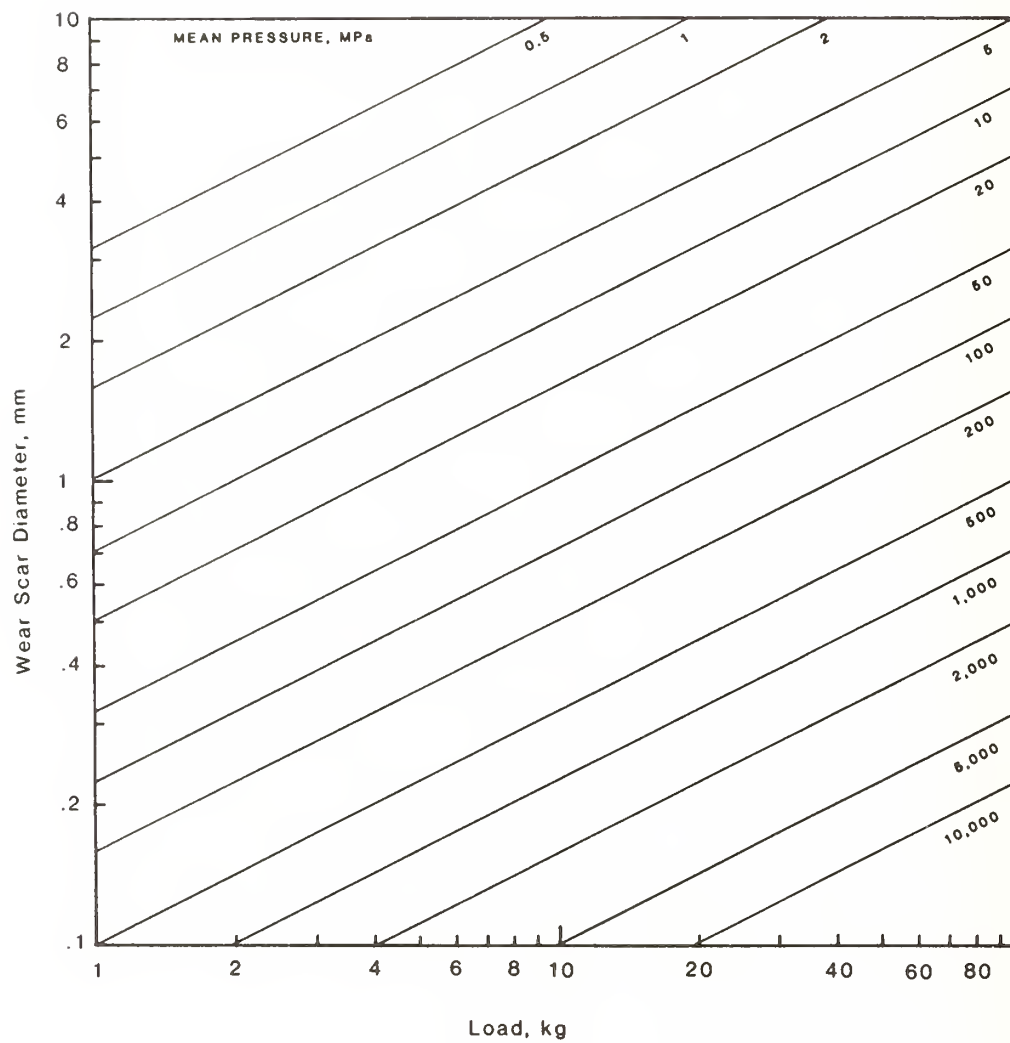
## APPENDIX J

Mean Pressure Test Severity Plot for Wear Scar  
Diameter vs Load (psi)



## APPENDIX K

Mean Pressure Test Severity Plot for Wear Scar  
Diameter vs Load (MPa)



U.S. DEPT. OF COMM. <b>BIBLIOGRAPHIC DATA SHEET</b> <i>(See instructions)</i>	<b>1. PUBLICATION OR REPORT NO.</b> NIST/SP-758	<b>2. Performing Organ. Report No.</b>	<b>3. Publication Date</b> September 1988
<b>4. TITLE AND SUBTITLE</b> CERAMIC TRIBOLOGY: METHODOLOGY AND MECHANISMS OF ALUMINA WEAR			
<b>5. AUTHOR(S)</b> Richard S. Gates, Stephen M. Hsu, and E. Erwin Klaus			
<b>6. PERFORMING ORGANIZATION</b> <i>(If joint or other than NBS, see instructions)</i> NATIONAL INSTITUTE OF STANDARDS AND TECHNOLOGY (formerly NATIONAL BUREAU OF STANDARDS) U.S. DEPARTMENT OF COMMERCE GAITHERSBURG, MD 20899			<b>7. Contract/Grant No.</b>  <b>8. Type of Report &amp; Period Covered</b> Final
<b>9. SPONSORING ORGANIZATION NAME AND COMPLETE ADDRESS</b> <i>(Street, City, State, ZIP)</i> SAME AS ITEM #6 ABOVE.			
<b>10. SUPPLEMENTARY NOTES</b> Library of Congress Catalog Card Number: 88-600582 <input type="checkbox"/> Document describes a computer program; SF-185, FIPS Software Summary, is attached.			
<b>11. ABSTRACT</b> <i>(A 200-word or less factual summary of most significant information. If document includes a significant bibliography or literature survey, mention it here)</i> <p>This report describes a systematic study that has been conducted to develop methods for measuring the tribological properties of ceramic materials under concentrated contacts. Step-loading four-ball and ball-on-three-flat wear tests were developed to provide friction and wear characteristics of ceramic/lubricant combinations under various lubrication conditions. These measurement techniques now enable one to study the effect of different materials processing parameters, material microstructures, and different lubricants on the friction and wear performance of ceramics.</p> <p>Water was found to react with alumina in a wearing contact to produce lubricous products. A combination of x-ray diffraction and thermogravimetric analysis techniques were used to investigate the kinetics of alumina-water reactions. These experiments determined that transition (gamma) alumina reacts with water at <math>\approx 200^{\circ}\text{C}</math> to form aluminum oxide hydroxide (boehmite - <math>\text{AlO}(\text{OH})</math>), while reactions at <math>\approx 100^{\circ}\text{C}</math> produce aluminum trihydroxide (bayerite - <math>\text{Al}(\text{OH})_3</math>). A mechanism for lubrication of alumina with water is proposed whereby stresses in the contact junction cause a phase transformation from alpha to gamma alumina. The gamma alumina subsequently reacts with water to form a lubricous, layer lattice, hydroxide.</p>			
<b>12. KEY WORDS</b> <i>(Six to twelve entries; alphabetical order; capitalize only proper names; and separate key words by semicolons)</i> alumina, aluminum hydroxides, ceramic, four-ball, friction, lubrication, paraffin oil, transition alumina, tribochemistry, tribology, water, wear			
<b>13. AVAILABILITY</b> <input checked="" type="checkbox"/> Unlimited <input type="checkbox"/> For Official Distribution. Do Not Release to NTIS <input checked="" type="checkbox"/> Order From Superintendent of Documents, U.S. Government Printing Office, Washington, D.C. 20402. <input checked="" type="checkbox"/> Order From National Technical Information Service (NTIS), Springfield, VA. 22161			<b>14. NO. OF PRINTED PAGES</b> 229 <b>15. Price</b>











NATIONAL INSTITUTE OF STANDARDS AND TECHNOLOGY  
(formerly NATIONAL BUREAU OF STANDARDS)  
U.S. DEPARTMENT OF COMMERCE  
GAITHERSBURG, MD 20899

Official Business  
Penalty for Private Use \$300



Stimulating America's Progress  
1913-1988